De Ilii Coloribus: A Photometric Study of the Largest Jupiter Trojan Asteroids

by

Joseph P. Chatelain

Under the Direction of Todd J. Henry, PhD

ABSTRACT

The Jupiter Trojan asteroids are minor bodies that orbit 60 degrees before and 60 degrees behind Jupiter. Because these orbits are stable over the lifetime of the Solar System, the properties of these objects may inform us about the conditions under which the Solar System formed. We present $BVRI$ photometry for 110 of the intrinsically brightest and presumably largest members of the L4 and L5 Jupiter Trojans. We use a new principal color component derived by Chatelain et al. (2016) that is indicative of taxonomic types relevant to the Jupiter Trojan asteroids. We find that 83% of the largest Jupiter Trojans are consistent with a D-type classification, while 17% show shallower slopes more consistent with X-type and C-type classifications. We show the L4 and L5 populations to be taxonomically indistinguishable at large sizes, as well as include findings about certain objects that have resulted from these data. Specifically, multi-filter light curves for twelve objects show signs of $V - I$ color variation in as many as two thirds of these objects, and our richest datasets allow for the

determination of phase curves and shapes for some asteroids including a new shape model and pole solution for 1173 Anchises. Our goal is to use this study to shed light on these fascinating objects and to place the Trojans in context in the larger Solar System.

INDEX WORDS: Asteroids, Trojan Asteroids, Photometry, Rotation Properties

De Ilii Coloribus: A Photometric Study of the Largest Jupiter Trojan Asteroids

by

Joseph P. Chatelain

A Dissertation Submitted in Partial Fulfillment of Requirements for the Degree of

Doctor of Philosophy

in the College of Arts and Sciences

Georgia State University
2017

De Ilii Coloribus: A Photometric Study of the Largest Jupiter Trojan Asteroids

by

Joseph P. Chatelain

Committee Chair:	Todd J. Henry
Committee:	Russel J. White
	David E. Trilling
	Linda M. French
	Steven T. Manson

Electronic Version Approved:

Office of Graduate Studies

College of Arts & Sciences

Georgia State University

August 2017

Acknowledgments

This work has been supported by NOAO, SMARTS, and NSF grant AST-1212115 to Linda French. This work would not have been possible without the support of Dr. David Trilling, Dr. Todd Henry, and Dr. Linda French who have each contributed in vital ways to my productivity and success. Students at Georgia State who managed to help by dedicating some of their observing time to this project were also incredibly important to the robust nature of the data presented here. Finally, I also thank NAU and Lowell for use of their facilities; Michael Mommert, Will Grundy, and Nicholas Moskovitz for insightful advice; and friends and family for their support.

This research has made use of data and/or services provided by the International Astronomical Union's Minor Planet Center.

Contents

List of Tables

List of Figures

– 1 –
Introduction

1.1 Asteroids: Minor Bodies in the Solar System

Minor bodies exist scattered throughout the Solar System as debris left over from when the Sun and major planets were formed. The minor bodies that remain in the Solar System today contain only a tiny fraction of the Solar System's mass, but a huge percentage of its surface area. They are responsible for shaping the surfaces of the terrestrial planets in fundamental and lasting ways and are possibly even responsible for the current orbits of the giant planets. As technology and our understanding of the Solar System improves, these objects have become an increasingly important source of inquiry and exploration as they play not only a vital role in our past, but, perhaps, our future.

Minor bodies can range in size from worlds a thousand kilometers across to mountains in space, a few dozens of kilometers in size, to boulders only a few meters in diameter. The largest of these objects, like (1) Ceres and (134340) Pluto, are known as dwarf planets, while the rest may be comets, asteroids, or both. Here we will largely avoid discussion of comets, but instead focus on non-active minor bodies found across the Solar System. The primary focus of this work is on the Jupiter Trojan population that is co-orbital with Jupiter at 5.2 AU from the Sun, but first we will give a brief introduction to the locations, names, and descriptions of populations of minor bodies at a variety of heliocentric distances.

Groups and subgroups of minor bodies are discussed here in order of generally increasing semi-major axis. Jupiter Trojans are saved for Section 1.2 to be discussed in more detail. All population numbers given in this chapter are determined using either the JPL Small-Body

Database Search Engine[1] or the lists provided by the International Astronomical Union's Minor Planet Center[2] as of April, 2017. The spatial distributions of the various populations are shown in Figure 1.1 and Figure 1.3, and detailed descriptions of the orbital elements discussed in this chapter are given in Appendix A.

1.1.1 NEOs

The population of Near Earth Objects (NEOs) includes over sixteen thousand asteroids that come within 1.3 AU of the Sun. As a group, these objects are of particular interest as they tend to be the most accessible minor bodies in the Solar System. This means that they pose the greatest threat of impact, as well as the greatest potential benefit in terms of resources. Understanding the dynamics, composition, and distribution of these objects is critical as humanity begins its efforts to build infrastructure that might facilitate future space exploration and exploitation.

It is generally believed that NEOs are sourced from instability regions in the Main Belt. As small objects, likely the result of collisions, slowly migrate into resonant orbits with Jupiter, their eccentricities are ramped up until they begin to interact with the rocky planets of the inner Solar System. Eventually these objects enter orbits that bring them close enough to Earth to be considered NEOs where they tend to survive for about 10 Myrs (Bottke et al. 2002). The time it takes an individual object to reach such an orbit is determined by the part of the Main Belt in which it originated.

[1] https://ssd.jpl.nasa.gov/sbdb_query.cgi
[2] http://www.minorplanetcenter.net/iau/lists/MPLists.html

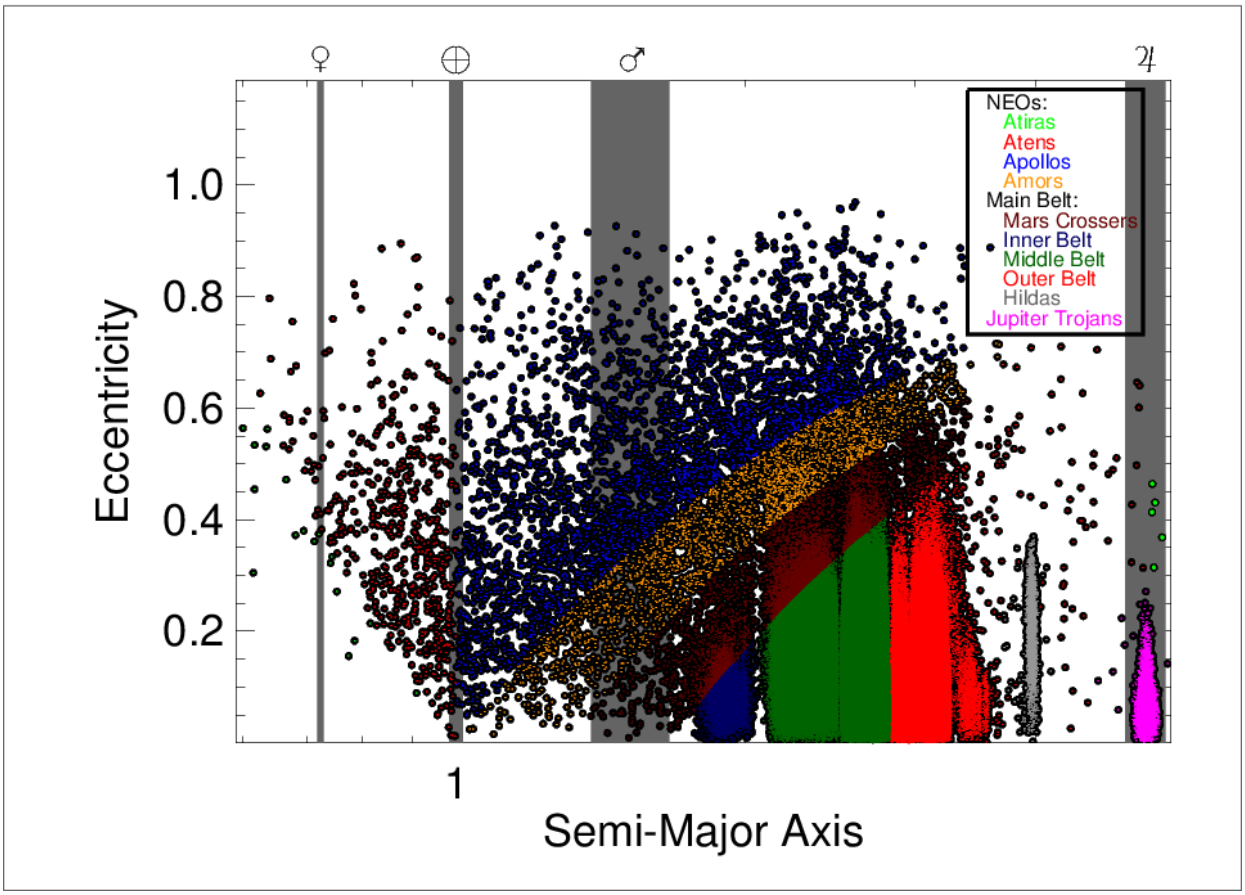

Figure 1.1: A plot of semi-major axis vs. eccentricity for the dynamical groups of the inner Solar System and Jupiter Trojans. Descriptions of the individual dynamical groups are given in Subsection 1.1.1 and Subsection 1.1.2. The specific Main Belt boundaries used here are the 4:1 resonance at 2.06 AU for the Inner Main Belt and the 5:2 resonance at 2.89 AU for the Outer Main Belt. Gray bars show the orbital ranges of the planets from aphelion to perihelion. Note the relative width of the orbits of Mars (♂) and Jupiter (♃). All data presented here are from the International Astronomical Union's Minor Planet Center (`http://www.minorplanetcenter.net/data`.)

NEOs are further divided into dynamical subclasses based on the particular circumstances of their orbits and their proximity to the orbit of Earth. Here we discuss four major subgroups.

Atiras

Named for (163693) Atira, these NEOs have orbits entirely with Earth's orbit. The sunward direction of these objects makes them exceptionally difficult to detect, and though we only know of a few (fewer than twenty have been discovered so far) it is likely that many more exist. These objects can be seen to the far left in Figure 1.1.

Atens

This dynamical subgroup is named for its exemplar, (2062) Aten, which has an Earth-crossing orbit and semi-major axis within Earth's orbit. So far, 1,170 objects have been discovered with similar Earth-crossing orbits. These objects are generally more mission accessible than Atiras or Amors, and could also pose impact threats if they have low enough inclinations.

Apollos

More than 8,700 objects have semi-major axes outside Earth's orbit and perihelia inside 1 AU. This second group of Earth-crossing asteroids is named for (1862) Apollo. Similarly to the Atens, these objects pose a threat to Earth if their inclinations are low, and are generally better mission targets than Atiras and Amors.

Amors

Any asteroid with a perihelion between 1 AU and 1.3 AU is considered an Amor. This group is named after (1221) Amor, which has a semi-major axis of 1.9 AU and an eccentricity (e) of 0.44, resulting in a perihelion distance (q) of 1.08 AU. There are 6,138 known asteroids that belong to this classification. Along with Apollos, Amors with a semi-major axis greater

than 2.0 AU spend most of their time among Main Belt objects, but their high eccentricities bring them much closer to the Sun compared to other Main Belt objects.

1.1.2 Main Belt

The vast majority of Solar System small bodies that have been discovered so far exist in the space between Mars and Jupiter, a region referred to as the "Main Belt." To date, nearly 700,000 objects have been discovered in this region. With such vast numbers of relatively nearby objects, it is no wonder that this dynamical group has seen the most comprehensive study since the discovery of its first and largest member, (1) Ceres by Giuseppe Piazzi on January 1st, 1801 (Piazzi 1801). As the largest reservoir of known asteroids, and as the likely source region for NEOs, the Main Belt has proven scientifically interesting in its own right. It has also been the target of several space missions, including flybys of certain objects from craft heading to the outer Solar System. Recently, the *Dawn* spacecraft has visited (4) Vesta and (1) Ceres, orbiting Vesta for over a year before heading to Ceres in 2015 where it is planned to remain indefinitely. Additionally, a mission to (16) Psyche has been approved by NASA and should launch in 2022. The mission, which shares a name with its target, will orbit Psyche for at least 21 months collecting data.

This intense scrutiny has lead to the discovery of collisional families within the larger Main Belt population. Generally speaking, these families are named for their largest members and share similar compositions and orbital elements. Several of these families can be readily seen in Figure 1.2 from Parker et al. (2008). Though interlopers are possible through normal asteroid migration, it is suspected that the majority of each family's members are the result of a massive collisional event in the past that largely disrupted a parent body and resulted

in a large number of objects with similar properties and orbits. The age of the family (or date of the collision) can be estimated by measuring the spread of family members in orbital space vs. their sizes, as smaller objects will be more susceptible to effects such as Yarkovsky drift[3] than larger members. Though first investigated and most obvious in the Main Belt, collisional families exist in many of the large dynamical groups throughout the Solar System, including Jupiter Trojans and Trans-Neptunian Objects.

Similarly to NEOs, the Main Belt can also be subdivided into dynamical subgroups based on their orbital elements; here we outline five subgroups.

[3]The Yarkovsky effect is a phenomenon, first described by Ivan Yarkovsky around 1900, that causes a change in the orbits of relatively small asteroids (D $<$ 40 km) over time. This change is due to the unequal emission of thermal radiation from the surface of the body, which results in a steady change in orbital energy that depends on the object's rotation period and pole orientation. Bottke et al. (2006) discuss the Yarkovsky effect in detail.

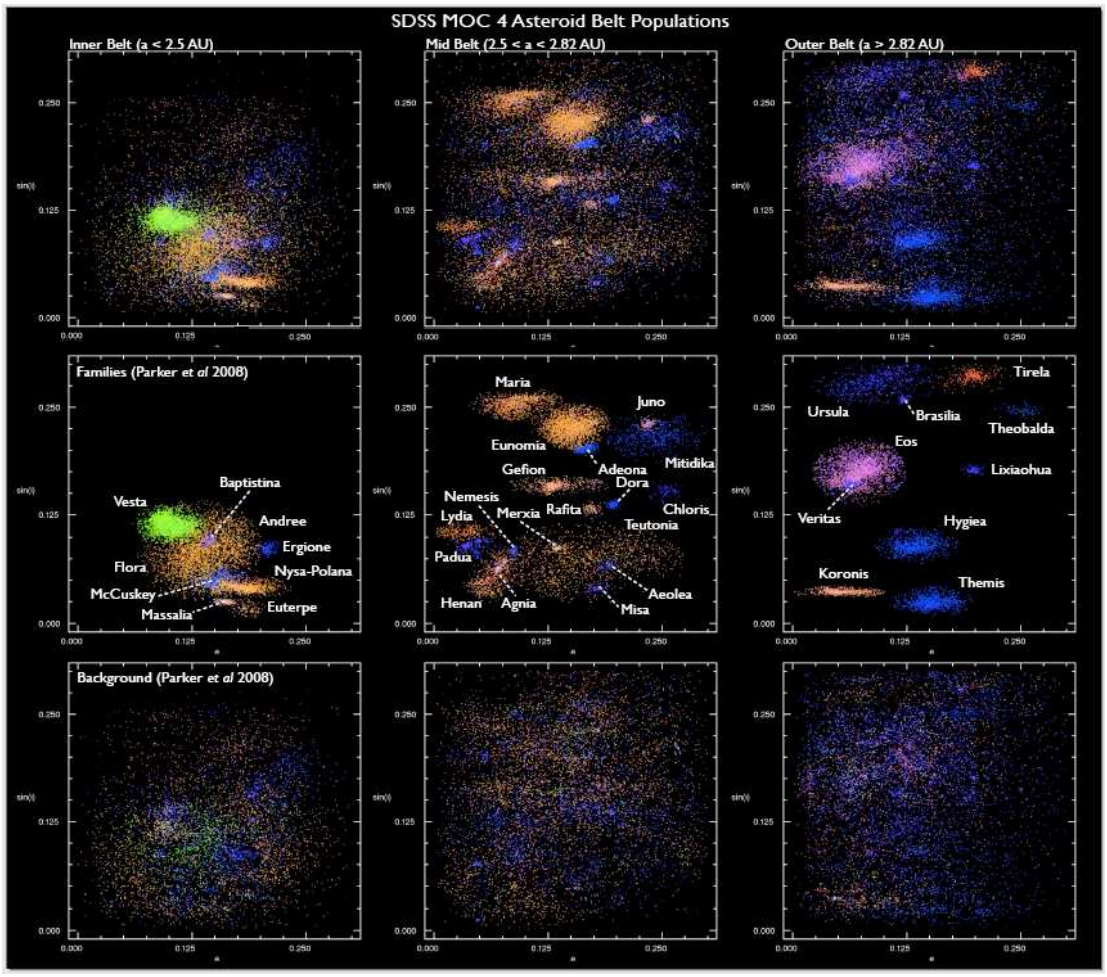

Figure 1.2: *Figure from described by Parker et al. (2008)*[a] . Sloan Digital Sky Survey Moving Object Catalog 4 data for Main Belt Asteroids. Each plot shows eccentricity vs. sine of the inclination for objects in the Inner Main Belt ($a < 2.5$ AU, left), Middle Main Belt (2.5 AU $< a <$ 2.82 AU, center), and Outer Main Belt (2.82 AU $< a <$ 3.5 AU, right). The top row is all of the MOC4 data colored by the principal component a^*, the middle row is only families, and the bottom row is background objects with collisional families removed.

[a] http://www.astro.washington.edu/users/ivezic/r_solarsystem.html

Mars-Crossers

Ultimately, there are as many as 29,600 known objects with an orbit that crosses the orbit of Mars. However, 47% of these are considered NEOs as they also come within 1.3 AU of the Sun, including the vast majority of the Apollo and Amor subgroups discussed above. The

remaining 15,400 Main Belt Mars-Crossers have a perihelion between 1.3 AU and 1.666 AU, or roughly the width of the Martian orbit.

Inner Main Belt

The exact boundaries of the Inner, Middle, and Outer Main belt are poorly defined and somewhat dependent on the region an author is keen to discuss. In most cases, however, the Kirkwood gaps are used as boundaries. These "gaps" are the result of certain resonances with Jupiter that have resulted in few objects surviving with the corresponding semi-major axes. The Inner Main belt is often defined as objects with a semi-major axis less than either that associated with the 4:1 or 3:1 resonance with Jupiter (about 2.06 AU and 2.50 AU, respectively.) This categorization may or may not exclude Mars-Crossers with a perihelion less than 1.666 AU. Depending on the region examined, the population of this group ranges from as few as 14,800 objects to as many as 230,000 objects. DeMeo & Carry (2013) give a taxonomic breakdown for Main Belt asteroids in each dynamical group and found that the Inner Main Belt is mostly populated by S- and V-type asteroids, with only 6% of resident objects being of the C- or D-type[4].

Outer Main Belt

The resonances that mark the inner boundary of the Outer Main Belt are typically the 5:2 resonance at 2.82 AU or the 2:1 resonance at 3.27 AU. The outer extent of this region is usually taken as the orbit of Jupiter, but excludes the Jupiter Trojans in the 1:1 resonance. The Outer Main Belt population can range from just over 7600 objects to nearly 214,000

[4]Asteroid Taxonomy is discussed in much more detail in Section 5.1, but is ultimately a way of categorizing objects based on spectral and photometric observations which are ultimately linked to an object's composition. Classification schema vary, but tend to rely on a single or double letter notation that implies a certain spectral or photometric signature.

objects, depending on whether one uses the inner or outer resonance. DeMeo & Carry (2013) found a very diverse population in the Outer Main Belt. They estimate that 52% of this population is C-type and only 6% S-type objects. The remaining population is made up of a variety of different types.

Middle Main Belt

The Middle Main Belt is vaguely defined as the region between the Inner and Outer Main Belts. This is the most densely populated part of the Main Belt, with a population ranging from 247,000 within the most conservative boundaries to 669,000 objects at the most generous. Taxonomically, this group is dominated by C-Type asteroids (70%), with only 8% of the population consisting of S-types (DeMeo & Carry 2013). Demographics of the remaining population are complex and made up of many different taxonomic types.

Hildas

The Hilda population consists of about 3000 known objects in a stable 3:2 resonance (a = 4.0 AU) with Jupiter. The largest member and namesake of this population is (153) Hilda, which also has its own collisional family within the dynamical group of resonant objects. The orbits of these objects are stable because members of this group reach aphelion only in opposition to Jupiter or at the L4 and L5 Lagrange points discussed in Section 1.2. Over three successive orbits, each individual Hilda will visit each of these three locations, mapping out an equilateral triangular orbit in Jupiter's rotational reference frame. As these objects are some of the only asteroids whose orbits both cross the Outer Main Belt and enter the L4 and L5 Jupiter Trojan clouds, their composition is of great interest. DeMeo & Carry (2013)

estimate 71% of Hildas to be P-type (a classification included in the X-complex classification found in Subsection 2.5.1). The remaining 29% of objects are fairly evenly split between D- and C-type objects. These demographics show a stark contrast to those seen in the Trojan clouds discussed in Section 1.2.

1.1.3 Centaurs

Transient objects with lifetimes of at most a few million years (Horner et al. 2004), Centaurs orbit among the major planets of the outer Solar System. They have semi-major axes between the orbits of Jupiter and Neptune, and they generally cross the path of at least one of the four giant planets. There are 219 known Centaurs, and these objects occasionally show cometary activity implying an outer Solar System origin for at least some members. Centaurs tend to be dark and red (Tegler et al. 2016), with a clear bimodality in their color distribution (see Subsection 5.1.3). As can be seen in Figure 1.3, Centaurs are evenly distributed in eccentricity as they are scattered by the giant planets.

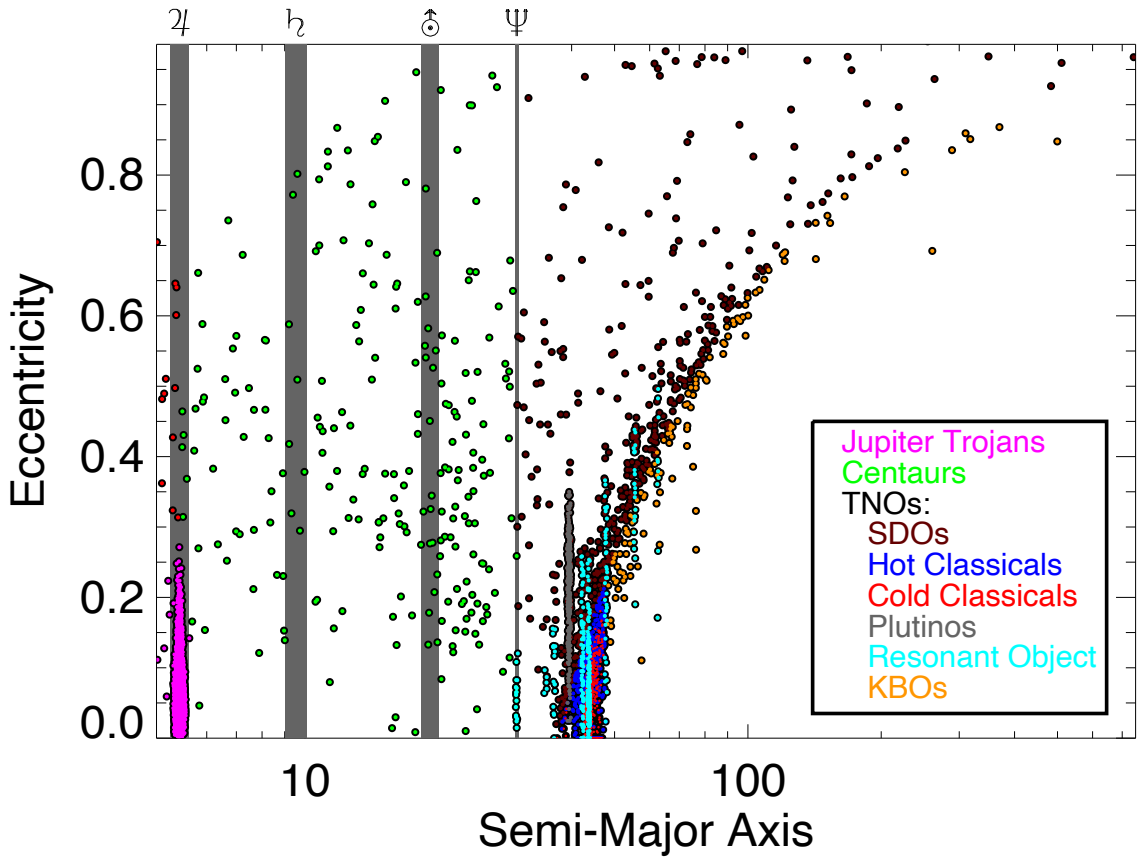

Figure 1.3: A plot of semi-major axis vs. eccentricity for the dynamical groups of the outer Solar System and Jupiter Trojans. Descriptions of the individual dynamical groups are given in Subsection 1.1.3 and Subsection 1.1.4. Resonant objects are plotted separately in gray (Plutinos) and light blue. The orange points to the upper right are detached or scattered KBOs that don't fall into the classical populations (Cold Classical: bright red; Hot Classical: blue). Gray bars once again represent the orbital widths of the planets, but due to the log scale on the x axis, relative widths between planets might be misleading. All data presented here is from the International Astronomical Union's Minor Planet Center [5].

1.1.4 Trans-Neptunian Objects

Trans-Neptunian Objects (TNOs) comprise a large population of minor bodies that have semi-major axes beyond the orbit of Neptune. To date, 2,326 minor bodies have been discovered with orbits beyond that of Neptune. As many of these objects are quite large

and bright, they have been fairly well studied despite their large distances from the Sun. Most recently, (134340) Pluto and its cadre of moons were visited by the *New Horizons* spacecraft for the first detailed surface study of any of these objects. TNO modelling efforts have predicted that there are massive numbers of objects and a primordial TNO mass of nearly 10 $M_{\oplus}$. These models are primarily based on how much material would be required to build the largest TNOs that we see today in the low energy environment of the early outer Solar System. However, more recent deep surveys have found significantly fewer objects than are predicted by these models. The survey performed by Bernstein et al. (2004) not only suggests a significant decrease in TNO sizes beyond 40 AU, but also a mass for the current TNO population of less than 10 times the mass of Pluto or $\sim$ 0.02 $M_{\oplus}$. Like the Main Belt and NEO populations, TNOs are often divided into various dynamical groupings. Most of the these groupings tend to be based on the energetics of their orbits rather than their semi-major axes, with high inclination objects being separated from objects with lower energy orbits. Additionally, there are many mean motion resonances (MMRs) with Neptune that provide zones of stability and show overpopulations relative to the background TNO distribution. As with previous populations, here we provide general parameters for five of these subgroups. Different studies divide up this population in different ways depending on what aspects of it are to be explored. We attempt to describe in general terms what objects are usually meant when these subgroups are referenced.

Resonant Objects

There are hundreds of objects that have been discovered in resonant orbits with Neptune. A mean motion resonance (MMR) is described in terms of the integer number of orbits it

takes for the two bodies to return to the same relative positions. This is usually denoted as $M : N$ where M gives the number of orbits made by the inner body and N is the number of orbits made by the outer body. These resonances vary in strength, with stronger resonances tending to be those with the least difference between between M and N. There are 17 TNOs at the 1:1 resonance at 30.1 AU. Thirteen of these Neptune Trojans have been discovered at the L4 point and four at the L5 point. It is generally believed that these objects were captured into various stable resonances as Neptune migrated during the early Solar System. These objects are plotted in light blue in Figure 1.3 and can be seen to form thin vertical lines in that figure.

Plutinos

The best populated resonant group is that of the 3:2 resonance (39.46 AU). These objects are named for their first discovered (and most popular with the general public) member as a consolation prize for Pluto's "demotion" by the International Astronomical Union (IAU) from planet to dwarf planet[6]. About a third of the total resonant TNO population is at the 3:2 resonance, accounting for over 300 objects.

Kuiper Belt Objects

Kuiper Belt Objects (KBOs) are those that reside within the Kuiper belt or (Edgeworth-Kuiper belt) that extends from the orbit of Neptune to about 50 AU or so. This group of objects includes most of the TNOs so far discovered as well as most of the dynamical groupings described here, with the occasional exception of Scattered Disk Objects (SDOs).

[6]In actuality, the name "Plutino" was used to describe this population by Jewitt & Luu (1996) a decade before the IAU defined Pluto as a minor planet in 2006.

Usage of terms in the literature is inconsistent at best with TNO and KBO sometimes being used interchangeably and sometimes being used to refer to very specific populations, which themselves can vary between publications. In the most general terms, however, KBOs are objects that reside in a disk of objects that exists past Neptune, but does not typically include objects in the scattered disk, or the hypothesized Oort cloud.

Hot and Cold Classical Objects

These objects are the ones that largely make up the Kuiper belt. They have a perihelion outside of Neptune's orbit and are separated by inclination: the Cold Classical objects typically have inclinations less than 5° and Hot Classical objects have $i > 5^\circ$. The outer boundary of the classical region is somewhat poorly defined, but it is expected to be at about 50 AU. More than 1,800 objects have been discovered in the classical region, with about 750 considered Cold Classical and 1,050 Hot Classical.

Scattered Disk Objects

Scattered Disk Objects (SDOs) are often highly eccentric objects with semi-major axes beyond Neptune, but they will often have orbits that cross Neptune's orbit. As these objects cross Neptune's orbit, but are not in a stable resonance, they are likely to have relatively short lifetimes and high probabilities of being scattered. (136199) Eris is the largest of the 476 known members of this population and of the TNO population in general.

1.2 Jupiter Trojans

Jupiter Trojans are minor bodies that are co-orbital with Jupiter in a 1:1 MMR, held stable near the L4 and L5 Lagrange points. There are 6510 known asteroids in these special

orbits with Jupiter. Jupiter Trojans are of particular interest because they represent a large number of potentially primordial objects that have experienced little mixing with other asteroid populations since capture into their present orbits. The glimpse that these objects provide into the composition and evolution of the early Solar System make Jupiter Trojans important objects for observation and study. Additionally, they are located at an important location between the inner and outer Solar System. Jupiter Trojans are plotted in magenta in both Figure 1.1 and Figure 1.3.

1.2.1 History

Lagrange (1772) first proposed the existence of stable regions 60° to each side of an orbiting body as part of his analysis of the three-body problem. These regions of stability within the gravitational potential of an orbiting body later became known as the 4th and 5th Lagrange points, typically referred to as L4 and L5 respectively. It wasn't until February, 1906, however, that any objects were discovered in an orbit that placed it within one of these points. Wolf (1906) discovered asteroid 1906 TG (Berberich 1906), eventually named (588) Achilles, near the L4 point of Jupiter. (617) Patroclus was discovered near the L5 point later that year, and Jupiter Trojans would continue to be sporadically discovered for the next several decades. Eventually, a naming convention was established such that objects discovered near the L4 point were named for Greek warriors described in the *Iliad*, *Odyssey*, and *Aeneid* as present during the Trojan war, while asteroids discovered on the other side of Jupiter were named for heroes of Troy and her allies. This left a few members discovered earlier, namely (617) Patroclus and (624) Hektor, as spies within the enemy camps. Thus, generally, objects at the Lagrange points of a planet became known as Trojan

asteroids, and Jupiter Trojans could be described as L4 Greeks if present in the leading camp, and L5 Trojans if found in the trailing camp. Discoveries began to speed up when van Houten et al. (1970b) published 19 objects discovered during the Palomar-Leiden survey, which inspired a dedicated examination of the L4 camp that revealed an additional 45 objects (van Houten et al. 1970a). Since then, thousands of Jupiter Trojans have been discovered in each camp, and these populations have become widely studied both due to their nature as an intermediate population between the very different asteroid demographics of the inner and outer Solar System as well as the role they play as a litmus test for various Solar System formation models.

1.2.2 Solar System Formation

The Nice Model was first proposed in three papers in 2005. Specifically, Tsiganis et al. (2005) used numerical simulations to show that the current Solar System configuration can be reproduced using relatively large scale migration of the giant planets. Such a migration could have been caused by the destruction of a large asteroid belt extending out to about 35 AU and containing as much as $35M_{\oplus}$ of material. Eventually, energy exchange between the asteroids and Jupiter would bring Jupiter into a 2:1 resonance with Saturn that would shake the Solar System. In some simulations, such as that shown in Figure 1.4, this even caused the two outermost giant planets to swap places. Such a process is shown to result in orbital eccentricities and inclinations for the giant planets that are similar to what we see now and that are difficult to produce through normal planet formation models that suggest much more circularized orbits. Additionally, Gomes et al. (2005) suggest that this period of instability could have resulted in a large number of planetesimals being flung into the

inner Solar System, creating the Late Heavy Bombardment (LHB). The LHB is an event hypothesised to have occurred around 700 million years after the planets formed because of a large increase in the cratering rate of terrestrial planets and the Moon around this time period (Hartmann et al. 2000). In the last of the initial Nice Model papers, Morbidelli et al. (2005) dealt with the fate of Jupiter Trojans during the 2:1 resonance between Jupiter and Saturn. Though it is likely that Trojan asteroids were captured into Trojan orbits near the L4 and L5 Lagrange points during initial Solar System formation as Jupiter's mass increased, such a massive disruption as a resonance between the two largest planets in the Solar System would have caused most of these primordial Jupiter Trojans to be lost. Morbidelli et al. (2005) show that with a large enough flux of objects from the outer Solar System crossing Jupiter's orbit just as the two gas giants left their mutual resonance, sufficient numbers of objects could be recaptured in the Jupiter Trojan camps. Furthermore, being populated by scattered objects in this way could reproduce the observed inclination distribution of the two camps that will be discussed in more detail in Subsection 2.5.2 and Section 5.3.

Since its proposal, the Nice Model has become quite popular as a means of explaining the current configuration of the outer Solar System. Many other tweaks (Morbidelli et al. 2007; Levison et al. 2011), as well as more extensive modifications, have since been proposed to the Nice Model in an effort to shore up its failings. For example, the Grand Tack model proposed by Walsh et al. (2011) attempts to explain the relatively small size of Mars by having Jupiter and Saturn travel as far inward as 1.5 AU before turning around and finding themselves in their present orbits. Additionally, the Jumping Jupiter model, first proposed by Morbidelli et al. (2009) abandons the idea of a smooth transition across the 2:1 resonance ($\sim$ 1Myr) in favor of a rapid one (10,000 to 100,000 years) due to the scattering of an ice

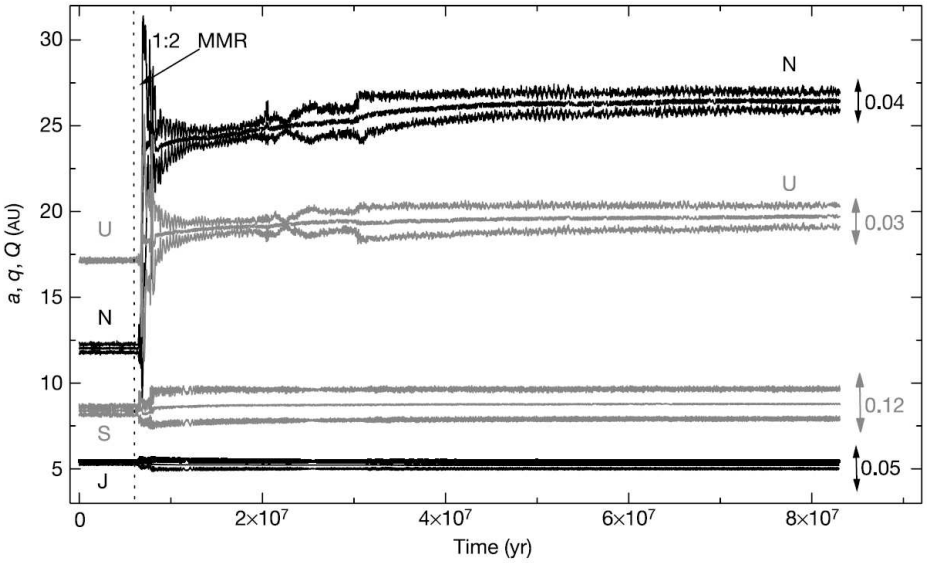

Figure 1.4: *Figure from Tsiganis et al. (2005). A full description can be found in the original text.* Semi-major axis (a), perihelion (q), and aphelion (Q) for the four giant Solar System planets with time for an example simulation using the Nice Model scenario. The maximum eccentricities for the final 2 million years of the simulation are given to the right of each orbit, and the dotted line shows the time of 2:1 resonance between Jupiter and Saturn. Note the circular nature of pre-resonance orbits and the relative positions of Uranus and Neptune before and after the 1:2 MMR.

giant by Jupiter. Nesvorný et al. (2013) show that a rapid shift in the L4 and L5 positions as Jupiter "jumps" across the 2:1 resonance could result in the capture of objects that were previously formed near 5 AU. Additionally, as will be discussed in Section 5.3, this model could account for the asymmetry seen in the number of objects between the two camps.

Reproducing the numbers, orbits, and compositional distributions of the current Jupiter Trojan populations is of paramount importance for any of these models. Thus, improving our knowledge the Trojan populations leads to additional constraints on the formation of not just the surrounding minor bodies, but the evolution of the entire early Solar System. It is with this ultimate goal in mind that we seek to examine the Jupiter Trojan color distribution for the largest, and presumably most pristine, objects. A comparison of these objects between

camps, as well as to various other Solar System populations, could give us a clue to their origins, and help us discriminate between various formation models.

1.3 My Dissertation Research

Here I describe my effort to characterize the colors and attributes of the largest Jupiter Trojans. The largest Jupiter Trojans were chosen for study due to their accessibility on 1-meter class telescopes, the fact that all of the largest objects in the Trojan camps have been discovered to a high degree of certainty, and that these objects likely represent a relatively undisrupted population compared to smaller Trojans whose existence is likely the result of catastrophic collisions that have not been experienced by the large objects in the population. For all aspects of this project, we use optical $BVRI$ Johnson-Kron-Cousins filters on telescopes in both the Northern and Southern Hemispheres. Observations were made over six years from 2010 to 2016, and targets were found using ephemerides calculated by the IAU MPC Minor Planet & Comet Ephemeris Service.

1.3.1 Photometry

Compositional characterization is necessary to determine the ultimate source or sources of these minor bodies and to help confirm or constrain simulations such as those described above. Emery et al. (2011), for example, show a potential bimodality present in the near-infrared spectra of Trojans that might imply the clouds were sourced from two disparate regions of the Solar System.

In Chapter 2 we discuss our program for obtaining and analysing photometric colors for 110 of the brightest L4 (Greek) and L5 (Trojan) Jupiter Trojans. Due to the featureless spectra observed for Trojans (Emery et al. 2011), we can use these broadband photometric

data to create a method for further taxonomic classification of this intermediate population that bridges the gap between the small bodies of the inner and outer Solar System by performing comparisons in both directions. Ultimately, through visible color comparisons of the largest objects in the Greek and Trojan camps, we hope to achieve a greater understanding of the relationship between the two Jupiter swarms and their evolutionary place in the Solar System.

1.3.2 Light Curve Analysis

In addition to photometric colors, the rotational properties and shapes of Jupiter Trojan asteroids can be important indicators of collisional history and overall stability of the Jupiter Trojan clouds, as well as internal structure and bulk composition of individual objects. Unfortunately, such information requires extensive observations that take place over a significant portion of the target's orbit, resulting in programs that are observationally expensive and long in character, as Jupiter Trojans have roughly twelve year orbital periods. For this reason, while most large Jupiter Trojans have fairly well defined rotation periods (e.g. Mottola et al. 2011) that can be determined over nights or weeks, relatively few have good shape models or pole orientation estimates that take several years to secure.

In Chapter 3 we not only present additions to the light curve coverage for a dozen large Jupiter Trojans, but also search for the presence of color variations on the surfaces of these objects. These data contribute to an understanding of the collisional history of the large Jupiter Trojans and also provide a check on the precision of the mean color values determined in Chapter 2. Furthermore, we explore the rotational properties of (1173) Anchises in significantly more depth in Chapter 4, in which we present a very precise rotation period,

pole orientation, and axial ratios for this particular object. These efforts serve as an example to the kind of results that can be obtained when one dedicates significant resources to light curve observations of Jupiter Trojans.

– 2 –

Trojan Photometry

2.1 Trojan Photometry in the Literature

Several Jupiter Trojan[1] photometric surveys that span a range of wavelengths and sample sizes exist in the literature. Such efforts provide vital context upon which this work expands.

Karlsson et al. (2009) present $(U)BVRI$ photometry for 27 Jupiter Trojans (H ranging from 9.8 to 12.8)[2] in an effort to examine a size-slope ratio for these objects compared to previous work on outer Main Belt objects. Two of these objects, (4791) Iphidamas and (5130) Ilioneus, are also in the dataset presented in this work.

The most recent Sloan Digital Sky Survey (SDSS) Moving Object Catalogue (MOC) (Abazajian et al. 2009; Ivezić et al. 2002) contains some data on as many as five hundred unique Greeks and Trojans. Hasselmann et al. (2011) have used these data to determine possible taxonomies for 343 Greeks and Trojans. However, due to incomplete spatial and temporal coverage, only 16 and 13 of these objects overlap with the largest 68 L4 Greeks and 42 L5 Trojans examined in this work, respectively.

The Wide-field Infrared Survey Explorer (WISE) observed large portions of the Trojan clouds at 3.4, 4.6, 12, and 22 μm. 988 known objects from the L4 camp and 754 objects from the L5 camp have enough data for thermal fits (Grav et al. 2011) which are important for determining albedos and sizes for these objects. While geometric albedos have been

[1] As discussed in Section 1.2, in general, the term Trojan is used to refer to any minor body orbiting near either the L4 or L5 Lagrange point of a planet. Jupiter Trojans are Trojan asteroids that co-orbit with Jupiter. Throughout this chapter and the chapters that follow, individual camps will be referred to as L4 Greeks or L5 Trojans.

[2] H is the absolute magnitude of a Solar System object corresponding to the apparent V magnitude an object would have if it were located at one AU from both the observer and the Sun and viewed at a 0 degree phase angle. This parameter is effectively a combined measure of size and albedo.

shown to be unrelated to taxonomic type (Emery et al. 2011), Grav et al. (2012) are able to differentiate between redder D-types and less-red Trojans using the 3.4 μm albedo due to the difference in spectral slopes in the vis-NIR. Updated thermal models for the 110 objects discussed here are also presented by Grav et al. (2012).

Most of the largest Jupiter Greeks and Trojans have published rotation periods (Mottola et al. 2011), with concerted efforts ongoing to extend that dataset to fainter objects (French et al. 2015). These surveys also provide separate data on the origins and evolution of the Trojan swarms by providing information regarding collisional histories for these objects.

2.2 Survey of Jupiter Greeks and Trojans - The Sample

The data presented here are part of a project to characterize members of both of Jupiter's Lagrangian camps with optical photometry. In addition to the $BVRI$ photometric colors presented by Chatelain et al. (2016) for the L5 Trojans, in this dissertation we update the L5 photometry and include photometry obtained for the L4 Greek population. This work, in addition to the light curves discussed in Chapter 3 and Chapter 4, is part of an initiative to better characterize the observable properties of the Greek and Trojan asteroids so that connections between the inner and outer Solar System, as well as Solar System formation processes, might be better understood.

For our complete photometric sample, we obtained $BVRI$ colors for 110 Jupiter Greeks and Trojans with an absolute magnitude H $\lesssim$ 10, which corresponds to an effective diameter of about 60 km. The original sample included 113 objects; 71 are in the L4 Greek camp and the remaining 42 are in the L5 Trojan camp. This initial cut-off of $H \leqslant 10$ was chosen for two primary reasons: (1) The known sample should be complete down to this limit (Szabó et al.

2007; Karlsson 2010), so we can be sure that our sample is unbiased and readily compared to other samples of similarly sized objects in other populations. (2) $H = 10$ results in a V apparent magnitude between 17 and 18 for Jupiter Trojans. This is well within the faint limits (mag $\sim$ 20) of the 1 meter class telescopes (Table 2.1) to which we have ready access, thus making a good sample for this project. This sample was chosen in early 2010, meaning that some objects have updated values for H. Thus, 16 objects are now thought to be slightly fainter than $H = 10.0$, with the faintest having an H of 10.4. The most recent values are given in Table 2.3 and Table 2.4.

2.3 Observations and Data Reduction

2.3.1 Observations

A total of 162 photometric observations have been made in Johnson-Kron-Cousins (hereafter $BVRI$) filters for 42 different L5 Trojans, while 155 observations have been made for 68 different L4 Greeks. As outlined in Table 2.1, many of these observations (137) were made at the Cerro Tololo Inter-American Observatory (CTIO) 1.0-m telescope in Chile. Ninety-four of the remaining observations were made at the CTIO 0.9-m, and the final 86 were acquired with the Lowell 42-in. telescope in the Northern Hemisphere. These data were gathered over thirteen observing runs from July 2010 to November 2013. Individual observations are given in the Appendix in Section B.

Standard stars from Landolt's equatorial sample (Landolt 2009) and Graham's E-fields (Graham 1982) were used to calibrate the photometry. Standard stars were chosen that were of sufficiently faint magnitude to minimize errors due to shutter speed, and calibration images were taken at a range of airmasses similar to those at which our targets were observed

Table 2.1: Telescopes Used for Observing Jupiter Trojans

Telescope	Site	Instrument	Filters	Number of Observations	
				L4 Greeks	L5 Trojans
1.0-m	CTIO	Y4KCam CCD	BVR_CI_C	23	114
0.9-m	CTIO	Tek2K CCD	BVR_CI_C	65	29
42-in.	Lowell	NASA42 CCD	BVR_CI_C	67	19

to correct for atmospheric extinction. Integration times were less than 600 seconds for most targets, so non-sidereal tracking was unnecessary because these objects have an apparent motion of about $0\farcs3$/min. Targets were specifically observed at times during which crowding by background stars could be best avoided. All observations reported here were made on photometric nights using $BVRI$ filters with typical seeing of $2''$ or better, with individual exposure times ranging from 60 to 900 seconds.

2.3.1.1 CTIO/SMARTS 1.0-m

Observations were made using the Cerro Tololo Inter-American Observatory (CTIO) Small and Moderate Aperture Research Telescope System (SMARTS) 1.0-m through time allocated by the National Optical Astronomy Observatory (NOAO). Photometry was obtained with this telescope during 15 nights between June and November 2011.

Images taken using the Y4KCam on the CTIO/SMARTS 1.0-m were typically binned in 2×2 pixels (to $0\farcs578$/pixel) to reduce readout time. Images were taken in the $BVRI$ filters. Details about the transmission curves for these filters can be seen in Figure 2.7. In the I band, fringing could be readily observed for some long integration frames. The fringe pattern was removed during the data reduction process by median combining the worst affected images. This pattern was scaled to be at the same level as the background fringes and then subtracted from the corresponding image.

2.3.1.2 CTIO/SMARTS 0.9-m

Photometric observations of Greeks and Trojans using the CTIO/SMARTS 0.9-m telescope were made on sixteen nights between July 2010 and March 2013. Some of these observations were made using time on nights primarily dedicated to the REsearch Consortium On Nearby Stars (RECONS[3]) effort to discover and characterize stars within 25 pc (Henry et al. 2006). Thus, for several targets taken using the 0.9-m, the B filter was neglected (leaving VRI) because it did not fit into the larger RECONS observing plan, and significant time would be lost on B standards for relatively few frames. No binning was used for frames taken using the 0.9-m Tek2k camera, which has a 0.″401/pixel scale. At the 0.9m, observations were made both in full chip mode (13.7′ on a side) and using the central quarter of the chip (6.8′ on a side).

2.3.1.3 Lowell 42-in.

The Lowell 42-in. Hall Telescope was used for observing Jupiter Trojans on six nights between November 2010 and November 2013. These observations were made possible through Georgia State University's partnership with Lowell Observatory. NASACam was used with $BVRI$ filters. This instrument is also subject to fringing in the I filter, which was easily removed by subtracting a scaled fringe map made from median combining the worst affected frames. We used 3×3 binning (0.″981/pixel) for these observations.

[3] *www.recons.org*

2.3.2 Data Reduction

On most nights, sky flats were taken. On nights when the CTIO 0.9-m was used, dome flats were usually also acquired. These flats, in conjunction with nightly bias frames, were used to process the data. As mentioned, for some I images on the 1.0-m and the 42-in. fringe removal was necessary. Aperture photometry was used to calculate instrumental magnitudes. These instrumental magnitudes were converted into apparent magnitudes using transformation equations created using the standards discussed above. The pipeline and methodology are described in detail in Jao et al. (2005) and Winters et al. (2011).

The primary sources of error in the photometry are the Poisson noise in calculating the fluxes and the error in calculating nightly extinction curves using the standard star observations. At the telescope, a signal to noise (S/N) ratio of about 150 was considered ideal because this generally results in a magnitude error of about ~ 0.03 magnitudes. This level of precision is essential to being able to differentiate taxonomies at visible wavelengths. Unfortunately, this quality of data was not always achieved, particularly for faint targets when the sky background was high. Figure 2.1 shows that when combined, these sources of error translate into a typical uncertainty of ~ 0.03 mag for V, R, and I filters with slightly higher errors of ~ 0.05 mag in B due to the faintness of objects in this filter. The resulting errors in color are characterized in Table 2.2.

Phase effects were found to be negligible for this sample due to the small phase angles for Trojans in general and these observations specifically. Jupiter Trojans are never observed from Earth at phase angles more than about 12°. The phase angle for each observation is listed in Section B, and no correlation between phase and color is detectable for this sample.

Table 2.2: Comparison of Errors for Photometric Observations

Color	Poisson Error Max	Poisson Error Median	Extinction Error Max	Extinction Error Median	Rotational Error Max	Rotational Error Median	Total Error Median
$B-V$	0.16	0.05	0.11	0.03	0.18	0.02	0.06
$B-R$	0.15	0.05	0.12	0.02	0.23	0.04	0.08
$B-I$	0.22	0.06	0.13	0.03	0.29	0.06	0.09
$V-R$	0.12	0.03	0.08	0.02	0.09	0.02	0.04
$V-I$	0.22	0.04	0.09	0.03	0.19	0.03	0.06
$R-I$	0.22	0.03	0.10	0.03	0.15	0.02	0.04

This table gives a breakdown of the maximum and median values calculated for each individual source of error considered for all photometric color calculations as well as the median total error for each color. All values are in magnitudes.

For comparison, Szabó et al. (2007) calculate an offset of $\sim 0.005 \pm 0.001 \frac{mag}{deg}$ for $g-r$ and $r-i$ colors.

We also examined color variation due to phase effects for Jupiter Trojans using observations from the SDSS MOC. We calculated the slope of color versus phase for each of the 226 known Jupiter Trojans that had more than a single observation in the MOC. We then calculated a weighted mean of these slope values to find the average phase reddening for a Trojan body. We found a value of $-0.001 \pm 0.004 \frac{mag}{deg}$ for $g-r$ and $0.003 \pm 0.004 \frac{mag}{deg}$ for $r-i$. Both of these corrections are consistent with $0 \frac{mag}{deg}$, a finding consistent with lab results for dark asteroids (French & Veverka 1983), and were thus ignored for this sample.

An additional source of error present in the color calculations is the variation in the reflected flux of the asteroids due to their rotations. Thus, when calculating colors based on observations taken at different times through two different filters, an additional, unknown error is present. Table 2.2 shows that for some objects with either relatively fast rotation periods or particularly large lightcurve amplitudes, this error could be as much as that of the Poisson and extinction errors. A comparison of photometric errors with and without

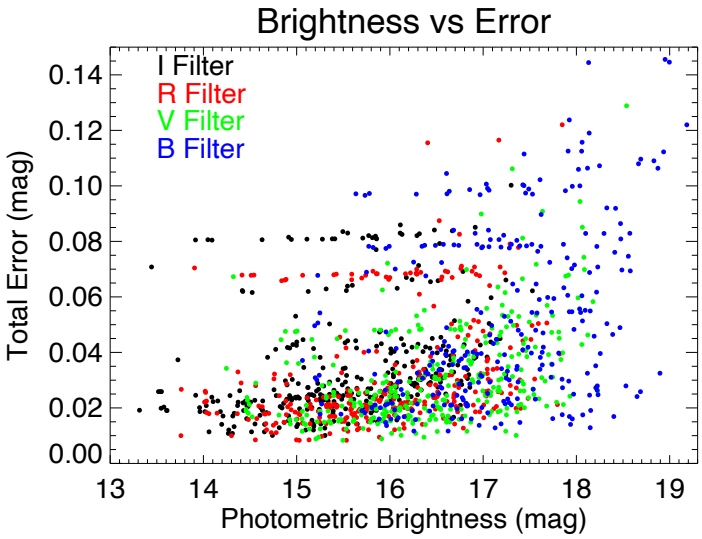

Figure 2.1: Calculated photometric brightnesses versus total calculated errors for both L4 and L5 observations. In general, increased errors for faint objects are somewhat reduced by longer exposure times. However, increased exposure time will eventually increase the error due to ever increasing sky background, especially for moving objects. The observations in the R and I filters at about 0.06 mag error are primarily the result of poorer than normal standard star correction for the night of November 10, 2012.

rotational errors in each color can be seen in Figure 2.2. For each observation, the worst case of this error has been estimated by using the largest amplitude and best period reported for each object in the NASA PDS Lightcurve Database (Harris et al. 2012) to estimate the largest possible variation in color due to the time between exposures with different filters. An estimated period and amplitude, based on the statistics for other Trojans of similar size, were used for objects that had none available in the database. These error estimates were calculated by assuming that photometric observations were made during the period of highest change in bolometric brightness due to rotation as well as during a viewing geometry coinciding with the largest amplitude ever observed for that particular object. Thus, such errors will typically be much smaller than those estimated here. A summary of the results is shown in Table 2.2. Additionally, in Chapter 3 we show that

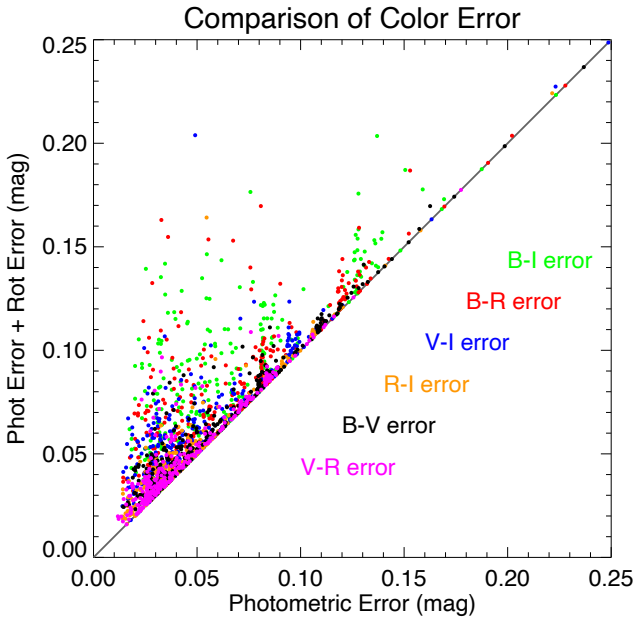

Figure 2.2: Errors in color measurements from purely photometric sources (Poisson noise and atmospheric extinction corrections) versus total error including potential rotational variation as described in Subsection 2.3.2. The time between filters is the primary contribution to this error due to rotation. Thus, because most observations were made in $IRVB$ order, $B - I$ colors on average show the largest increase in error due to rotation. The gray line shows a one-to-one correspondence representative of no increase in error due to rotation.

the color for individual objects may vary by more than 0.05 mag from the mean over the course of a single rotation. Observational procedure was changed to account for this effect by including additional observations to track changes in brightness independent of color for runs in February and November of 2013.

2.4 Results

The photometry presented here represents the most complete sample to date of $BVRI$ photometry for the L4 and L5 Jupiter Trojans with $H \lesssim 10$. Most objects were observed at least twice. Figure 2.3 (L4 Greeks) and Figure 2.4 (L5 Trojans) show each color calculated for each observation reported in Table B.1 and Table B.2. Figure 2.5 and Figure 2.6 show

the clustering of individual observations around a single weighted mean, which was calculated for each color for each object with results for each object given in Table 2.3 and Table 2.4. Certain objects such as 3317 (Paris) and 2357 (Phereclos) were observed with significantly higher frequency (13 and 9 observations, respectively) as part of an effort to more completely characterize these objects through light curve and phase curve examinations; all photometric observations for these objects are included here for completeness. Light curve and color curve analysis of these objects, as well as several other targets of interest are presented in Section 3.4. Furthermore, these targets with a high frequency of visits offer an independent test of the consistency of our methods over time and over varying telescopes and instruments. The general uniformity in the measurements for these targets can be seen by the relatively low errors (0.012 to 0.010 mag for Paris and 0.016 to 0.012 mag for Phereclos) for the mean color values given in Table 2.4. Because these values include standard deviations, these data assure us of consistent measurements in all conditions.

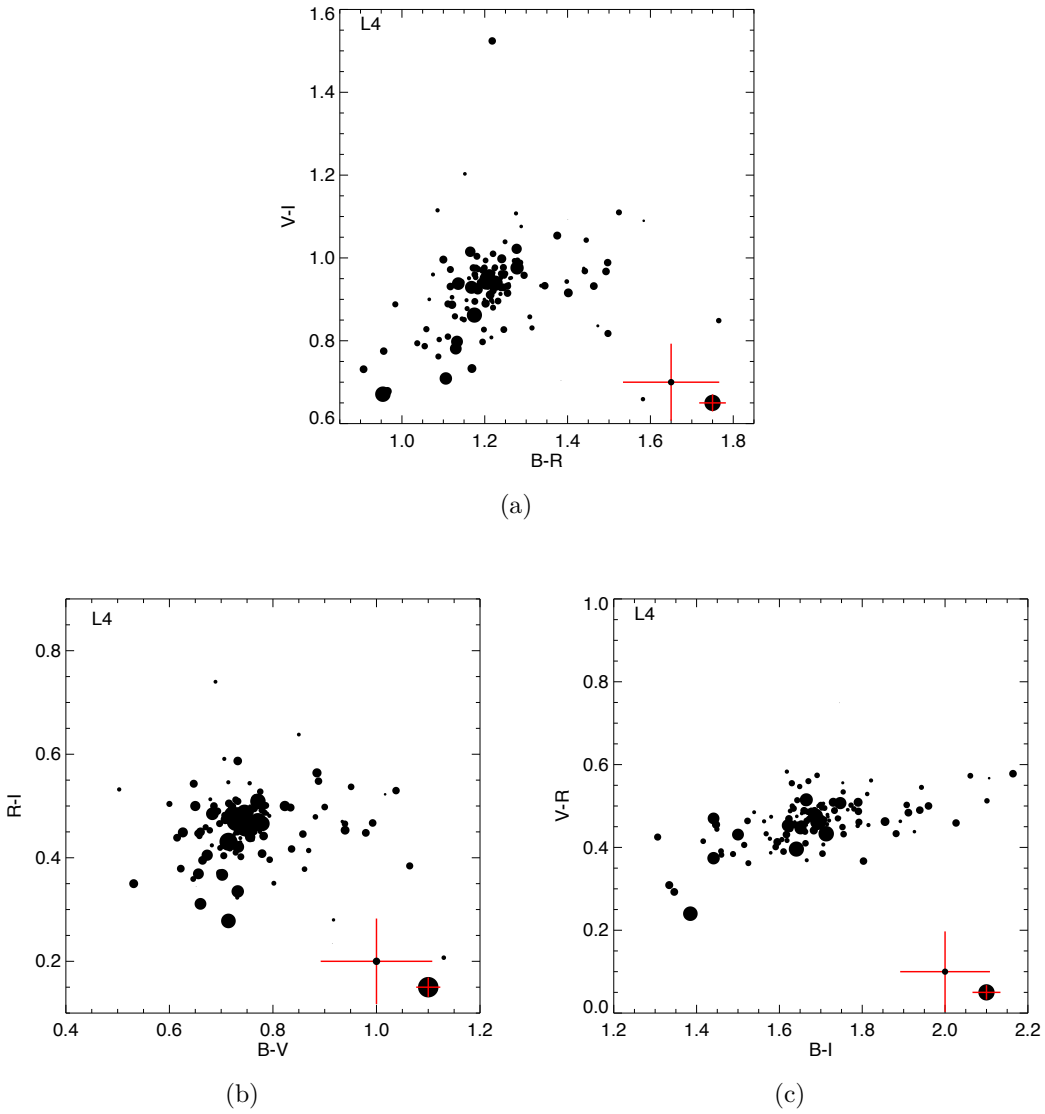

Figure 2.3: L4 Greek Photometric Colors. Symbol size is inversely proportional to the error for each data point. Both the smallest error and the mean error are shown in the lower right corner of each plot. The data shown in 2.3(a) are also shown in Figure 2.5, in addition to the mean values for individual L4 Greeks. Data for these plots can be found in Table B.1.

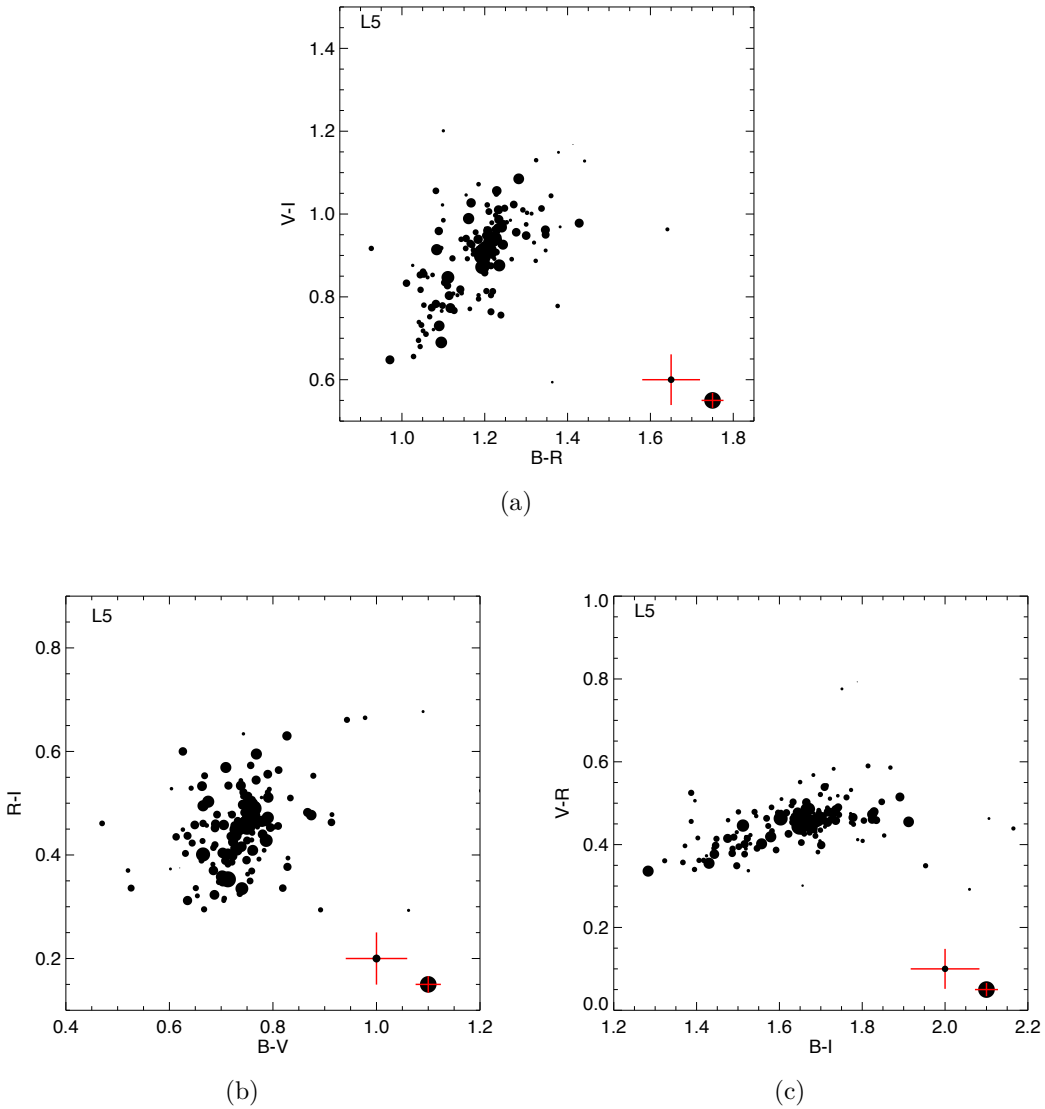

Figure 2.4: L5 Jupiter Trojan Photometric Colors. Symbol size is inversely proportional to the error for each data point. Both the smallest error and the mean error are shown in the lower right corner of each plot. The data shown in 2.4(a) are also shown in Figure 2.6, in addition to the mean values for individual Jupiter Trojans. Data for these plots can be found in Table B.2.

Table 2.3: Individual Object Data for 68 L4 Greeks

Object	Number of obs.	H[a] (mag)	$\overline{B-R}$ (mag)	$\overline{V-I}$ (mag)	a_T^* (mag)	Tax. (Lit.)	Tax. (Here)
(588) Achilles	4	8.67	1.34 ± 0.038	0.94 ± 0.019	0.12 ± 0.038	D[b]	D
(624) Hektor	3	7.20	1.31 ± 0.049	0.93 ± 0.034	0.11 ± 0.049	D[b]	D
(659) Nestor	2	8.99	1.41 ± 0.068	0.79 ± 0.039	−0.01 ± 0.068	XC[b]	DX
(911) Agamemnon	2	7.89	1.42 ± 0.064	0.98 ± 0.038	0.17 ± 0.063	D[b]	D
(1143) Odysseus	6	7.93	1.22 ± 0.029	0.86 ± 0.015	0.03 ± 0.028	D[b]	D
(1404) Ajax	2	9.30	1.18 ± 0.088	0.96 ± 0.032	0.11 ± 0.087	–	D
(1437) Diomedes	4	8.30	1.21 ± 0.041	0.81 ± 0.025	−0.03 ± 0.040	DP[b]	X
(1583) Antilochus	1	8.60	1.22 ± 0.109	0.95 ± 0.043	0.11 ± 0.108	D[b]	D
(1749) Telamon	2	9.20	1.14 ± 0.051	0.97 ± 0.030	0.12 ± 0.050	D[c]	D
(1868) Thersites	2	9.30	1.21 ± 0.044	0.96 ± 0.034	0.12 ± 0.044	–	D
(2260) Neoptolemus	2	9.31	1.27 ± 0.037	0.95 ± 0.024	0.12 ± 0.036	D[bc]	D
(2456) Palamedes	2	9.40	1.17 ± 0.035	0.92 ± 0.024	0.07 ± 0.035	–	D
(2759) Idomeneus	2	9.80	1.35 ± 0.090	0.91 ± 0.054	0.09 ± 0.089	D[c]	D
(2797) Teucer	2	8.40	1.24 ± 0.059	0.92 ± 0.045	0.09 ± 0.058	D[c]	D
(2920) Automedon	6	8.80	1.17 ± 0.029	0.95 ± 0.015	0.11 ± 0.029	D[b]	D
(3063) Makhaon	5	8.60	1.23 ± 0.033	0.83 ± 0.022	−0.01 ± 0.032	D[b]	DX
(3540) Protesilaos	2	9.30	1.22 ± 0.052	0.94 ± 0.040	0.10 ± 0.052	–	D
(3548) Eurybates	2	9.80	0.99 ± 0.060	0.73 ± 0.040	−0.14 ± 0.059	–	C
(3564) Talthybius	1	9.30	1.20 ± 0.102	0.90 ± 0.087	0.06 ± 0.102	D[c]	D
(3596) Meriones	2	9.30	1.26 ± 0.134	0.83 ± 0.057	0.01 ± 0.133	–	DX
(3709) Polypoites	3	9.00	1.22 ± 0.055	1.00 ± 0.034	0.17 ± 0.055	D[b]	D
(3793) Leonteus	3	8.70	1.11 ± 0.037	0.78 ± 0.031	−0.07 ± 0.037	D[bc]	X
(3794) Sthenelos	2	9.90	1.43 ± 0.077	1.07 ± 0.048	0.26 ± 0.077	–	D
(4035)	3	9.60	1.31 ± 0.028	0.97 ± 0.031	0.15 ± 0.028	–	D
(4057) Demophon	2	10.10	1.19 ± 0.049	1.06 ± 0.037	0.22 ± 0.049	–	D
(4060) Deipylos	4	9.40	1.08 ± 0.025	0.76 ± 0.018	−0.09 ± 0.025	C[b]	X
(4063) Euforbo	4	8.60	1.23 ± 0.024	0.95 ± 0.014	0.11 ± 0.024	D[b]	D
(4068) Menestheus	3	9.40	1.24 ± 0.032	0.95 ± 0.027	0.12 ± 0.031	D[b]	D
(4086) Podalirius	2	9.10	1.22 ± 0.082	0.87 ± 0.056	0.04 ± 0.081	–	D
(4138) Kalchas	2	10.00	0.96 ± 0.069	0.81 ± 0.038	−0.06 ± 0.068	–	X

Continued on next page

Table 2.3 – continued from previous page

Object	Number of obs.	H (mag)	$\overline{B-R}$ (mag)	$\overline{V-I}$ (mag)	a_T^* (mag)	Tax. (Lit.)	Tax. (Here)
(4489)	3	9.10	1.15 ± 0.059	0.95 ± 0.037	0.10 ± 0.059	D[b]	D
(4543) Phoinix	2	9.70	1.70 ± 0.094	1.20 ± 0.078	0.43 ± 0.094	–	D
(4833) Meges	2	9.10	1.19 ± 0.033	0.94 ± 0.022	0.10 ± 0.033	D[b]	D
(4834) Thoas	2	9.20	1.25 ± 0.056	0.95 ± 0.033	0.12 ± 0.055	–	D
(4835)	2	10.40	1.22 ± 0.085	0.85 ± 0.051	0.01 ± 0.084	D[b]	DX
(4836) Medon	1	9.40	1.22 ± 0.049	0.92 ± 0.039	0.09 ± 0.049	–	D
(4902) Thessandrus	2	9.80	1.29 ± 0.075	0.96 ± 0.044	0.13 ± 0.075	D[bc]	D
(4946) Askalaphus	2	10.10	1.17 ± 0.059	0.94 ± 0.038	0.10 ± 0.059	D[c]	D
(5023) Agapenor	3	10.30	0.96 ± 0.032	0.70 ± 0.025	−0.17 ± 0.031	X[c]	C
(5025)	2	10.30	1.17 ± 0.052	0.83 ± 0.042	−0.01 ± 0.052	CX[c]	DX
(5027) Androgeos	1	9.60	1.21 ± 0.040	0.91 ± 0.033	0.07 ± 0.040	D[c]	D
(5028) Halaesus	1	9.90	1.16 ± 0.089	0.90 ± 0.069	0.05 ± 0.088	D[c]	D
(5123)	2	10.10	1.17 ± 0.067	0.91 ± 0.038	0.06 ± 0.067	–	D
(5254) Ulysses	2	9.20	1.20 ± 0.057	0.97 ± 0.042	0.13 ± 0.057	–	D
(5258)	2	10.20	1.34 ± 0.080	1.01 ± 0.050	0.19 ± 0.079	–	D
(5264) Telephus	2	9.30	1.24 ± 0.045	0.97 ± 0.034	0.14 ± 0.045	D[bc]	D
(5283) Pyrrhus	2	9.30	1.27 ± 0.066	0.95 ± 0.042	0.13 ± 0.066	–	D
(5284) Orsilocus	1	10.00	1.22 ± 0.066	0.97 ± 0.047	0.14 ± 0.065	D[c]	D
(5285) Krethon	2	9.90	1.38 ± 0.067	1.09 ± 0.044	0.27 ± 0.067	–	D
(5652) Amphimachus	2	10.00	1.28 ± 0.132	1.05 ± 0.058	0.22 ± 0.131	–	D
(6090)	2	9.40	1.44 ± 0.089	0.98 ± 0.051	0.18 ± 0.089	–	D
(6545)	2	10.00	1.22 ± 0.066	0.91 ± 0.064	0.08 ± 0.066	D[c]	D
(7119) Hiera	2	9.80	1.26 ± 0.137	0.95 ± 0.107	0.12 ± 0.136	–	D
(7152) Euneus	2	10.20	1.24 ± 0.086	0.91 ± 0.041	0.08 ± 0.085	–	D
(7641)	2	9.30	1.24 ± 0.084	0.98 ± 0.035	0.14 ± 0.084	D[c]	D
(9799)	2	9.50	1.18 ± 0.086	0.91 ± 0.055	0.07 ± 0.086	–	D
(11397)	1	10.00	—	1.09 ± 0.057	—	–	—
(15436)	2	9.20	1.24 ± 0.061	0.87 ± 0.052	0.03 ± 0.060	–	D
(15440)	2	9.50	1.27 ± 0.082	0.97 ± 0.041	0.14 ± 0.081	–	D
(15539)	3	10.20	1.14 ± 0.070	0.89 ± 0.048	0.04 ± 0.070	–	D
(16974)	2	9.80	1.25 ± 0.071	0.96 ± 0.035	0.13 ± 0.071	–	D
(20729)	2	10.30	1.26 ± 0.131	1.00 ± 0.060	0.17 ± 0.130	–	D

Continued on next page

Table 2.3 – continued from previous page

Object	Number of obs.	H (mag)	$\overline{B-R}$ (mag)	$\overline{V-I}$ (mag)	a_T^* (mag)	Tax. (Lit.)	Tax. (Here)
(21601)	2	9.90	1.21 ± 0.052	0.97 ± 0.039	0.13 ± 0.052	–	D
(21900) Orus	2	9.90	1.27 ± 0.080	0.95 ± 0.040	0.12 ± 0.079	–	D
(22149)	1	10.10	1.58 ± 0.161	1.09 ± 0.072	0.31 ± 0.160	–	D
(23135)	1	9.90	1.31 ± 0.078	0.86 ± 0.050	0.04 ± 0.077	–	D
(23958)	3	9.90	1.15 ± 0.041	0.99 ± 0.029	0.14 ± 0.041	–	D
(38050)	2	9.80	1.28 ± 0.096	0.99 ± 0.053	0.17 ± 0.095	–	D

Note: Individual observations can be found in Table B.1.
[a] http://www.minorplanetcenter.net/iau/lists/t_jupitertrojans.html
[b] Neese (2010)
[c] Hasselmann et al. (2011)

Table 2.4: Individual Object Data for 42 L5 Trojans

Object	Number of obs.	H[a] (mag)	$\overline{B-R}$ (mag)	$\overline{V-I}$ (mag)	a_T^* (mag)	Tax. (Lit.)	Tax. (Here)
(617) Patroclus	5	8.19	1.12 ± 0.019	0.84 ± 0.022	−0.01 ± 0.019	P[b]	DX
(884) Priamus	7	8.81	1.20 ± 0.019	0.90 ± 0.017	0.07 ± 0.019	D[bc]	D
(1172) Aneas	4	8.33	1.25 ± 0.029	0.95 ± 0.023	0.12 ± 0.028	D[b]	D
(1173) Anchises	5	8.89	1.09 ± 0.025	0.78 ± 0.021	−0.07 ± 0.025	P[b]	X
(1208) Troilus	4	8.99	1.12 ± 0.027	0.74 ± 0.020	−0.11 ± 0.027	C[b]	X
(1867) Deiphobus	4	8.30	1.22 ± 0.032	0.93 ± 0.027	0.09 ± 0.032	D[bc]	D
(2207) Antenor	4	8.89	1.22 ± 0.027	0.95 ± 0.026	0.12 ± 0.027	D[b]	D
(2223) Sarpedon	3	9.41	1.12 ± 0.043	0.88 ± 0.038	0.03 ± 0.043	D[b]	D
(2241) Alcathous	4	8.64	1.20 ± 0.029	0.94 ± 0.024	0.10 ± 0.028	D[b]	D
(2357) Phereclos	9	8.94	1.22 ± 0.016	0.96 ± 0.012	0.12 ± 0.016	D[bc]	D
(2363) Cebriones	2	9.11	1.22 ± 0.069	0.91 ± 0.054	0.08 ± 0.069	D[b]	D
(2674) Pandarus	2	9.10	1.22 ± 0.048	1.00 ± 0.026	0.17 ± 0.048	D[bc]	D
(2893) Peiroos	3	9.23	1.19 ± 0.021	0.95 ± 0.020	0.11 ± 0.021	D[b]	D
(2895) Memnon	2	9.90	1.06 ± 0.052	0.71 ± 0.049	−0.15 ± 0.052	–	C
(3240) Laocoon	2	10.10	1.11 ± 0.049	0.88 ± 0.046	0.02 ± 0.049	D[c]	D
(3317) Paris	13	8.40	1.22 ± 0.012	0.95 ± 0.010	0.11 ± 0.012	D[b]	D
(3451) Mentor	6	8.40	1.11 ± 0.025	0.77 ± 0.020	−0.08 ± 0.025	X[c]	X
(3708)	2	9.20	1.21 ± 0.035	0.98 ± 0.031	0.14 ± 0.035	–	D
(4348) Poulydamas	2	9.20	1.04 ± 0.041	0.84 ± 0.036	−0.03 ± 0.041	–	X
(4708) Polydoros	3	9.90	1.27 ± 0.045	0.96 ± 0.040	0.13 ± 0.045	D[c]	D
(4709) Ennomos	7	8.60	1.03 ± 0.022	0.69 ± 0.017	−0.17 ± 0.022	–	C
(4715)	2	9.60	1.11 ± 0.041	0.85 ± 0.030	0.00 ± 0.041	–	DX
(4722) Agelaos	2	9.90	1.18 ± 0.057	0.91 ± 0.046	0.07 ± 0.057	–	D
(4791) Iphidamas	3	9.90	1.19 ± 0.052	1.03 ± 0.049	0.19 ± 0.052	–	D
(4792) Lykaon	4	10.00	1.23 ± 0.026	0.96 ± 0.025	0.13 ± 0.026	D[c]	D
(4828) Misenus	2	10.30	1.09 ± 0.065	0.92 ± 0.055	0.06 ± 0.064	–	D
(4832) Palinurus	3	9.80	1.41 ± 0.025	1.00 ± 0.038	0.19 ± 0.025	D[c]	D
(4867) Polites	2	9.60	1.16 ± 0.058	1.01 ± 0.044	0.16 ± 0.058	–	D
(5119)	3	10.10	1.20 ± 0.025	0.97 ± 0.032	0.13 ± 0.025	–	D

Continued on next page

Table 2.4 – continued from previous page

Object	Number of obs.	H (mag)	$\overline{B-R}$ (mag)	$\overline{V-I}$ (mag)	a_T^* (mag)	Tax. (Lit.)	Tax. (Here)
(5120) Bitias	2	9.50	1.23 ± 0.043	0.78 ± 0.037	−0.05 ± 0.043	–	X
(5130) Ilioneus	5	9.60	1.26 ± 0.033	0.96 ± 0.030	0.12 ± 0.033	–	D
(5144) Achates	9	8.90	1.21 ± 0.016	0.92 ± 0.014	0.08 ± 0.016	–	D
(5511) Cloanthus	3	10.10	1.21 ± 0.057	0.89 ± 0.044	0.05 ± 0.057	–	D
(5638) Deikoon	2	10.00	1.19 ± 0.042	0.91 ± 0.041	0.07 ± 0.042	D[c]	D
(5648)	2	9.60	1.20 ± 0.026	0.90 ± 0.032	0.06 ± 0.026	D[b]	D
(7352)	4	9.80	1.17 ± 0.027	0.85 ± 0.027	0.01 ± 0.027	XL[c]	DX
(12929)	4	9.90	1.30 ± 0.049	0.88 ± 0.031	0.06 ± 0.048	–	D
(16070)	3	9.80	1.29 ± 0.043	0.96 ± 0.037	0.14 ± 0.043	D[c]	D
(22180)	3	9.80	1.22 ± 0.021	0.98 ± 0.035	0.14 ± 0.021	–	D
(32496)	4	9.80	1.23 ± 0.039	0.95 ± 0.027	0.12 ± 0.039	–	D
(34746)	2	9.70	1.12 ± 0.036	0.95 ± 0.031	0.10 ± 0.036	–	D
(76867)	5	10.10	1.33 ± 0.027	0.94 ± 0.032	0.12 ± 0.027	–	D

Note: Individual observations can be found in Table B.2.
[a] http://www.minorplanetcenter.net/iau/lists/t_jupitertrojans.html
[b] Neese (2010)
[c] Hasselmann et al. (2011)

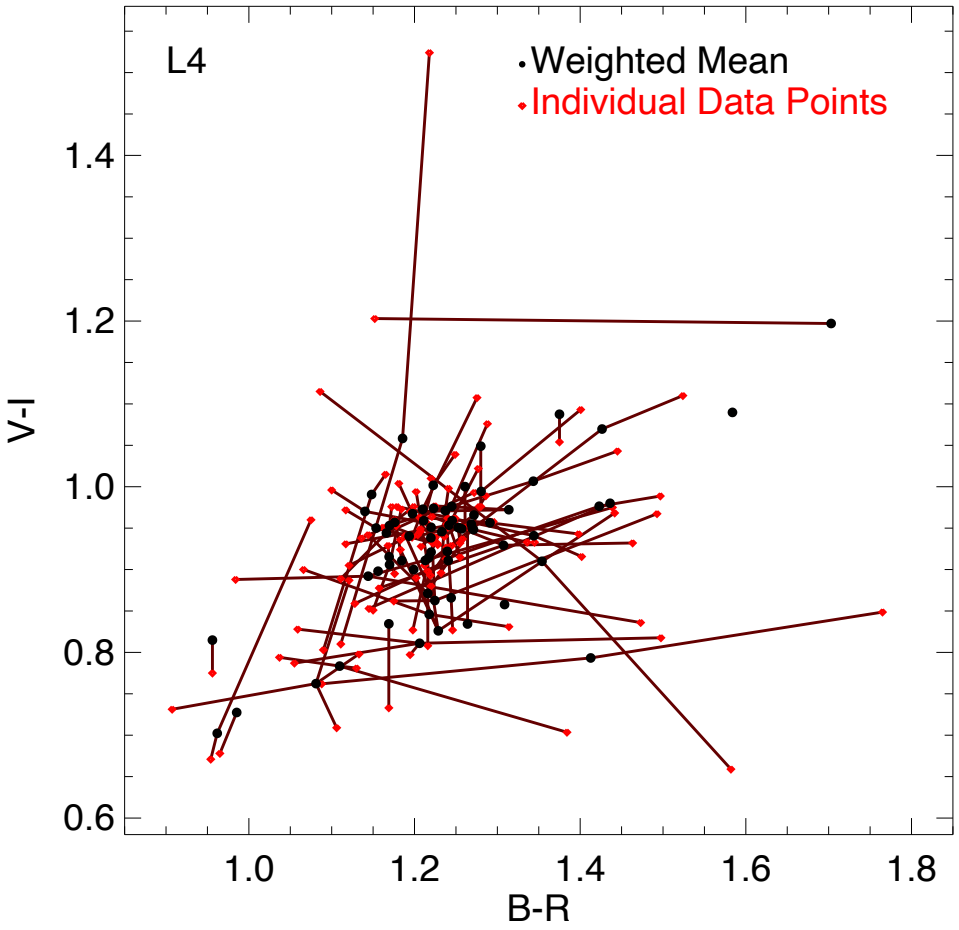

Figure 2.5: Photometry for 68 L4 Greeks. A mean value was calculated for each object, weighted by the individual errors, and plotted in black. Individual observations are plotted in red and connected to their mean values. Significant disparities in error can cause some weighted means to appear to have only one observation.

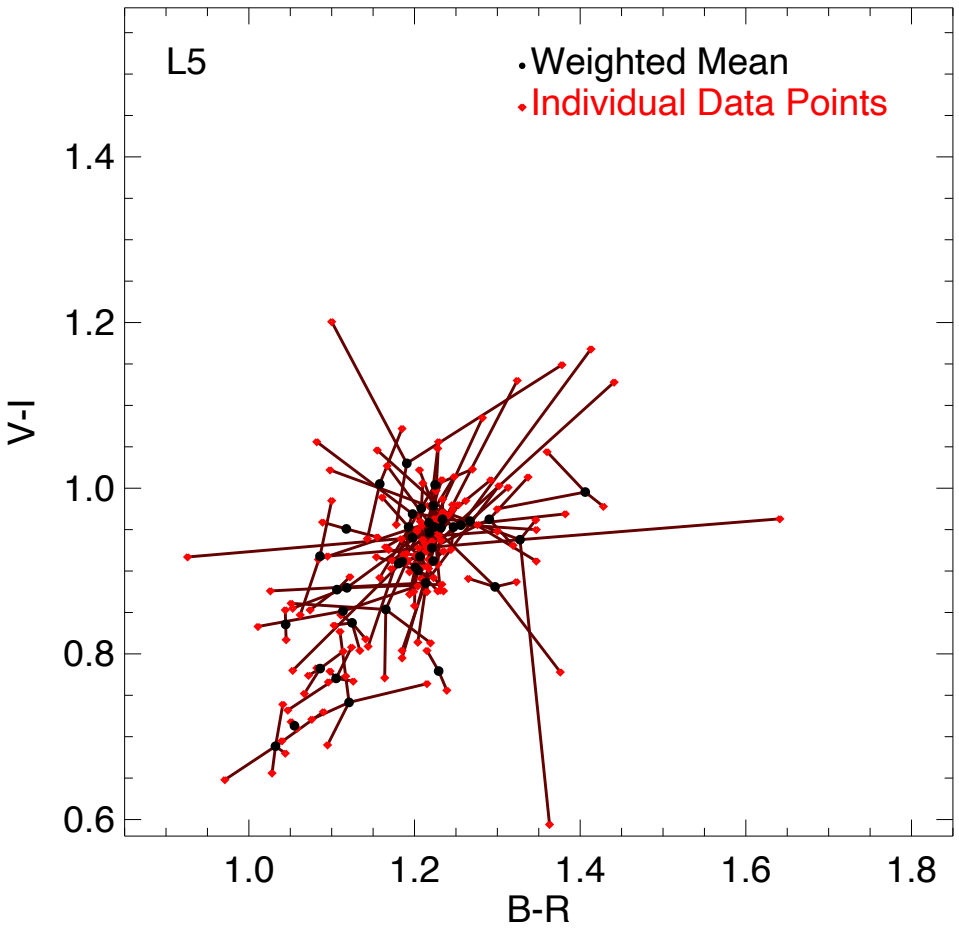

Figure 2.6: Photometry for 42 L5 Trojans. A mean value was calculated for each object, weighted by the individual errors, and plotted in black. Individual observations are plotted in red and connected to their mean values.

2.5 Analysis

2.5.1 A Principal Component for Trojans

For diagnostic and classification purposes, a principal color component[4] such as a^* defined by Ivezić et al. (2001) can prove extremely useful because it combines multiple photometric colors into a single parameter. However, this principal component is ill-suited for this survey for multiple reasons. First, it is defined by Ivezić et al. (2001) using $ugriz$ magnitudes. Fortunately, Moskovitz (2012) provides a conversion to the $BVRI$ filter set used here:

$$a^* = 0.908 \cdot (B - V) + 0.409 \cdot (R_C - I_C) - 0.856 \tag{2.1}$$

However, even with this conversion to the desired filter set, a^* remains less than ideal. Originally, it was designed to create a clear separation of Main Belt objects in color-color space. It is fundamentally a rotation in color space ($g^* - r^*$ versus $r^* - i^*$)[5] to maximize this Main Belt separation, which effectively maximizes the separation between the C and S-Complex asteroids that largely populate this portion of the Solar System. However, because numerous surveys (e.g., DeMeo & Carry 2013) have failed to find any S-Complex objects in either Trojan camp, such a criterion as separating C-type from S-type asteroids is not ideal for this population. Instead, we have calculated a new principal component for the Trojan asteroids (a^*_T) that maximizes the separation between the D-Complex and X-Complex objects that dominate the Trojan swarms.

[4]Principal Component Analysis (PCA) is a method for statistically analysing a dataset through orthogonal transformations. By design the first principal component is defined as the rotation that maximizes the variance along an axis. In other words it is the dimension the combines variables in such a way that it accounts for the most variability within the sample. It is this principal component that we are interested in here.

[5]The 2.5m Sloan Digital Sky Survey reports $ugriz$ photometric values calculated from $u'g'r'i'z'$ filters. Final calibrated magnitudes are given as $u^*g^*r^*i^*z^*$.

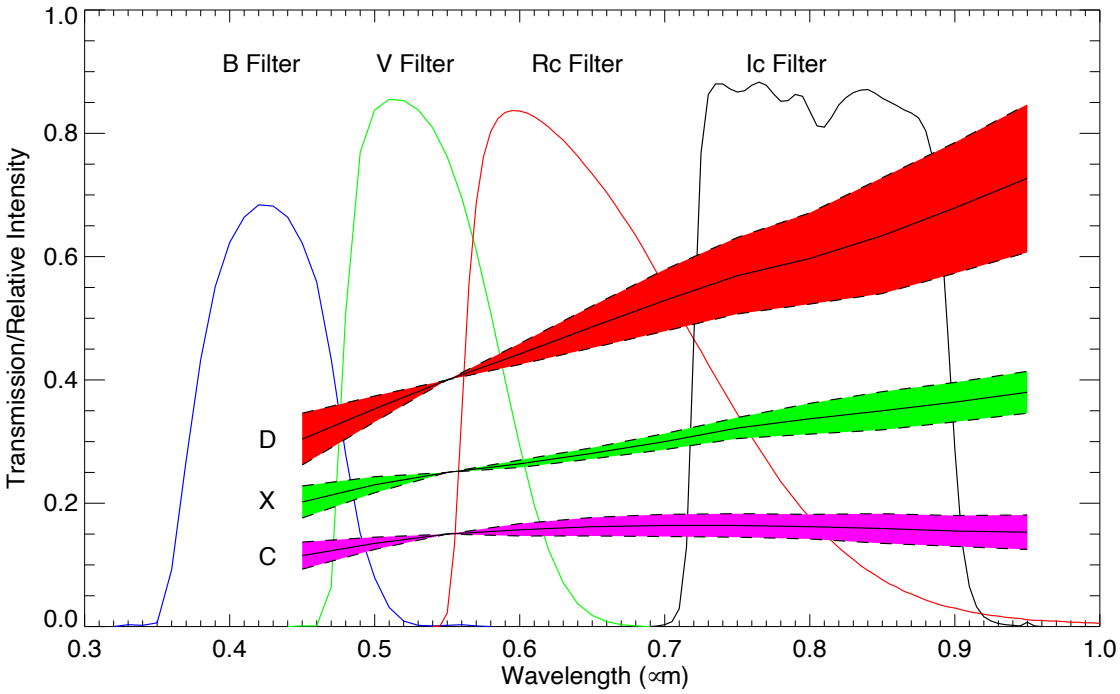

Figure 2.7: Three standard spectra of the Bus-DeMeo taxonomy presented in DeMeo et al. (2009). The standard spectra are normalized at $0.55\mu m$ and offset from each other by an arbitrary amount. The variation in possible spectra that should be considered within each taxonomic group is depicted via the 1σ range shown as a solid colored region associated with each taxonomy. The three spectra shown here were chosen as representative of the Jupiter Greeks and Trojans because numerous surveys (e.g. DeMeo & Carry 2013) have failed to find evidence of other types within the camps. The spectra are restricted to the visible range and overlaid above the transmission curves for the $BVRI$ filters used for this project (specifically as reported for the 1.0-m). The relative slopes and variations of these standard spectra allow us to calculate the regions in color space where such objects would appear.

Here we use the standard spectra for Bus-DeMeo taxonomy (DeMeo et al. 2009) shown in Figure 2.7 to determine photometric regions within which D-type, X-type, and C-type objects should be most concentrated, as shown for our data in Figure 2.8 (L4 Greeks) and Figure 2.9 (L5 Trojans). Comparing these regions to the photometric data gathered in this survey and previous taxonomic classifications in the literature (Neese 2010; Hasselmann et al. 2011), we determined the color space and transformation that result in the clearest taxonomic

separations while also minimizing regional overlap. We found that $B - R$ and $V - I$ colors provide the clearest divisions between classes. With a transformation and shift within this space designed to minimize overlap between the D-type and X-type objects, we calculate a_T^*:

$$a_T^* = 0.152 \cdot (B - R_C) + 0.988 \cdot (V - I_C) - 1.01 \tag{2.2}$$

This principal component is similar to the color index t^* computed by Szabó et al. (2007) in that it maximizes separation of the Trojan population into distinct groups. However, a_T^* also considers Main Belt taxonomy in an attempt to readily extend the scheme into the Trojan population. A comparison between a^* and a_T^* is shown in Figure 2.10 and Figure 2.11 along with the regions determined using the 1-sigma regions for Bus-DeMeo standard taxonomic spectra converted to photometric $BVRI$ colors. The a_T^* values were calculated for the mean photometry of each Trojan and are given, along with the related taxonomy, for the L4 camp in Table 2.3 and for the L5 camp in Table 2.4. The linear shift of a_T^* is conceived to place the majority of D-type objects at an a_T^* greater than 0 while X-type and C-type objects predominantly have negative a_T^* values. C-type objects typically show an a_T^* less than -0.11, which is directly between the Bus-DeMeo 1-sigma values for X-type and C-type asteroids. A "flat," perfectly reflected, solar spectrum (using solar colors presented by Ramírez et al. (2012)) would have an a_T^* of -0.16. This new principal color component shows significantly less overlap in the taxonomies present in the L4 and L5 swarms than a^* and could prove to be a much more precise method of estimating taxonomic classifications for photometric surveys within this region of the Solar System. Though more rigorous taxonomic classification can be done via spectroscopic analysis, the featureless Trojan spectra allow us to differentiate

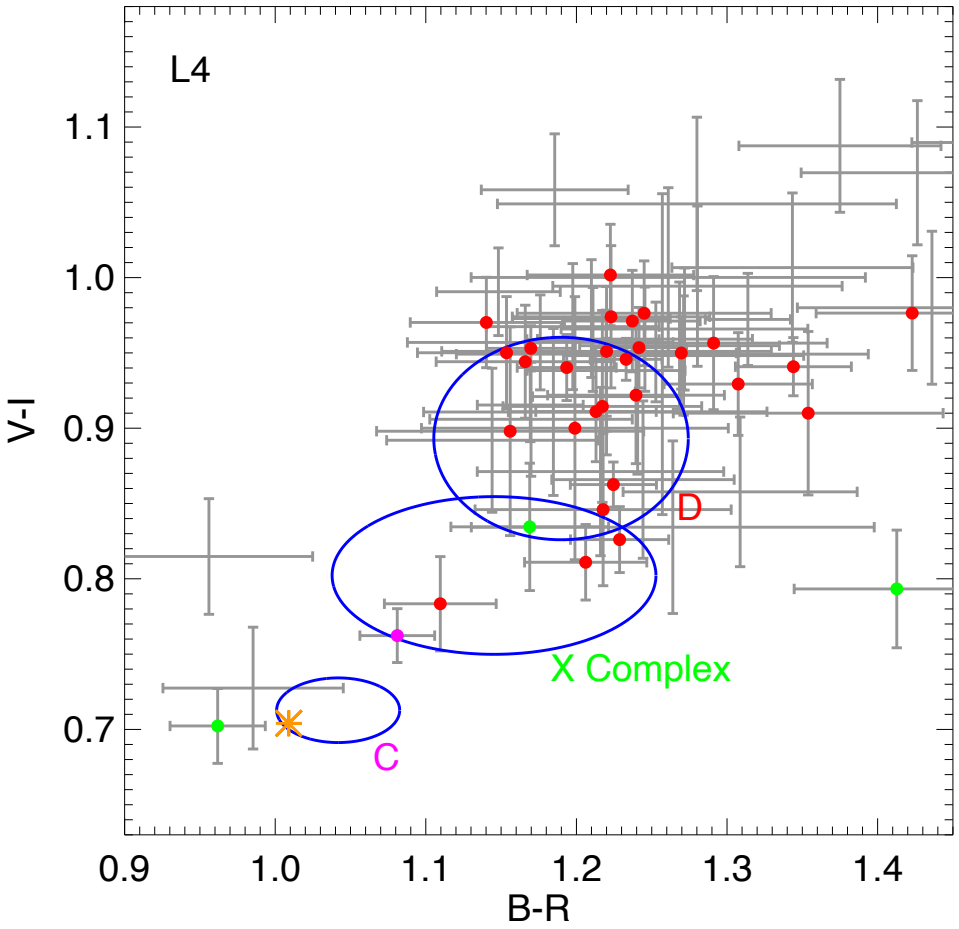

Figure 2.8: The taxonomic classifications for the brightest L4 Greeks are shown here at their mean color values. Red data points correspond to redder, D-type objects, green correspond to X-type and magenta correspond to C-type classifications as defined by Neese (2010) and Hasselmann et al. (2011). Ellipses designate the 1σ definitions for Bus-DeMeo taxonomies converted into $BVRI$ colors. The yellow asterisk shows the position of solar colors (Ramírez et al. 2012), or the equivalent of a flat asteroid spectrum.

D-like objects from X-like and C-like objects by using photometry and the resultant a_T^* as a proxy for the spectral slope.

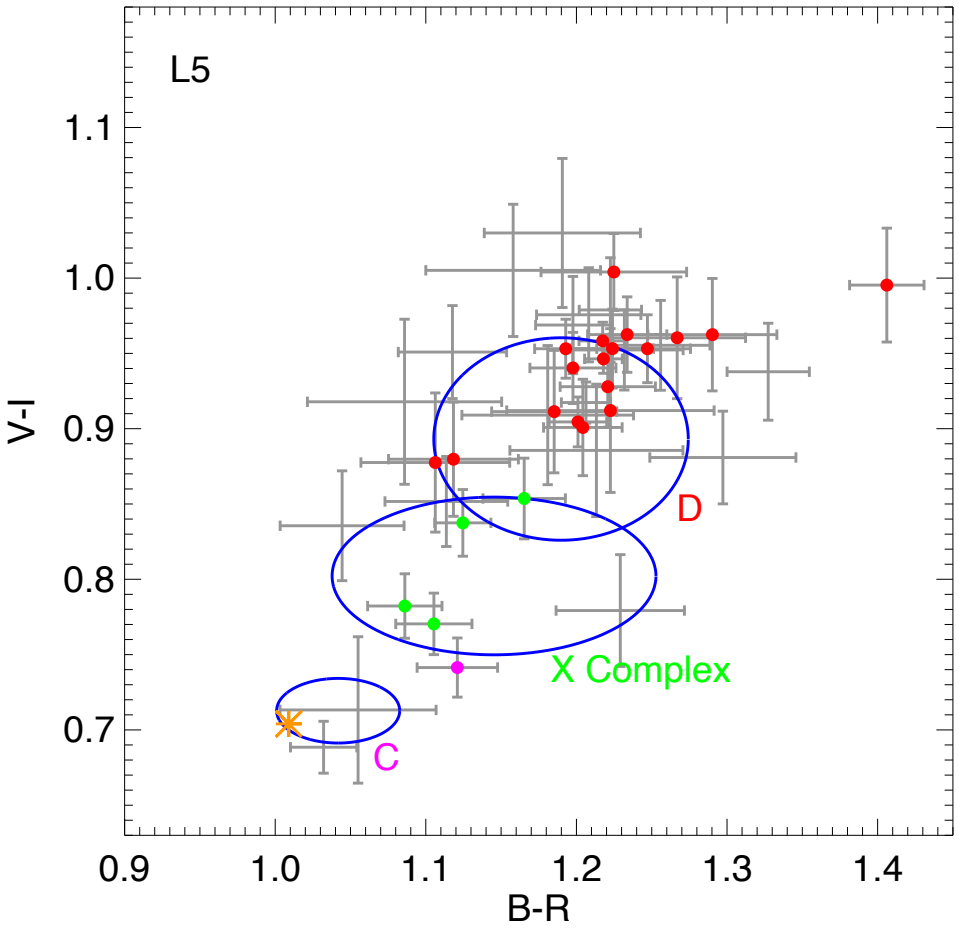

Figure 2.9: The taxonomic classifications for the brightest L5 Trojans are shown here at their mean color values. Red data points correspond to redder, D-type objects, green correspond to X-type and magenta correspond to C-type classifications as defined by Neese (2010) and Hasselmann et al. (2011). Ellipses designate the 1σ definitions for Bus-DeMeo taxonomies converted into $BVRI$ colors. The yellow asterisk shows the position of solar colors (Ramírez et al. 2012), or the equivalent of a flat asteroid spectrum.

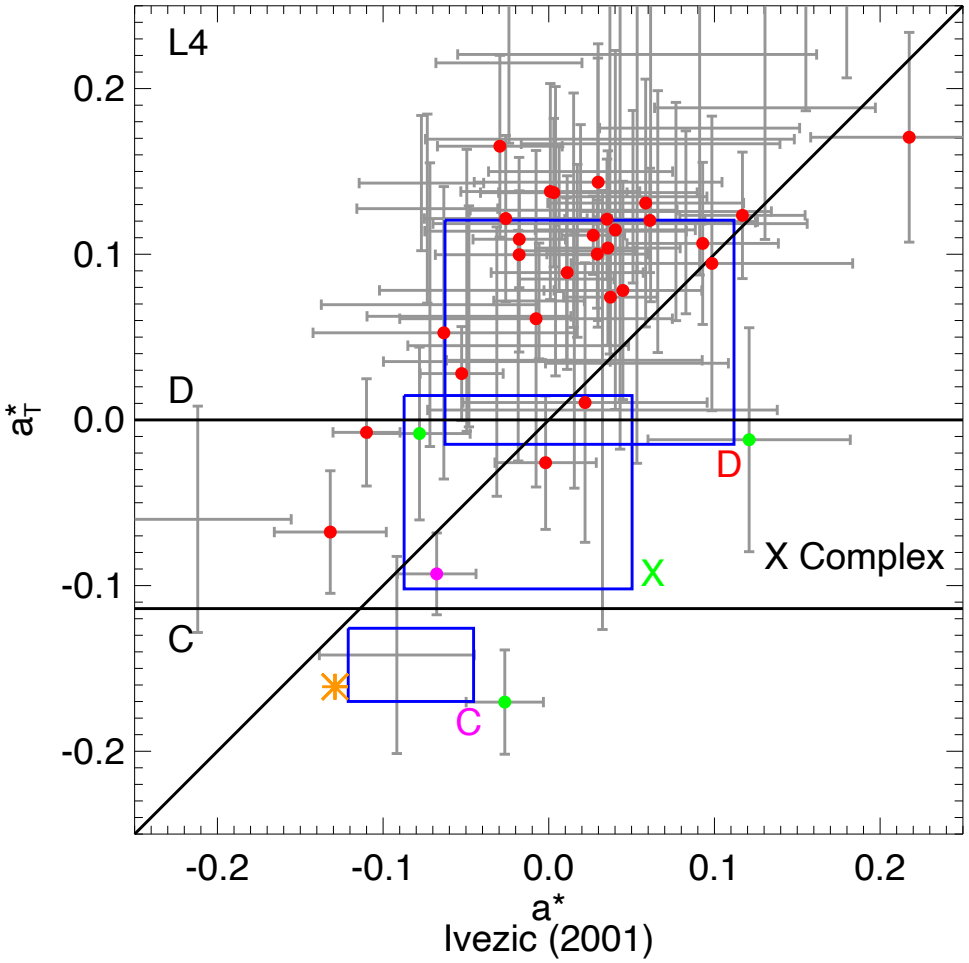

Figure 2.10: Mean photometric values for the L4 objects are plotted, converted into the a^* (Equation 2.1) and a^*_T (Equation 2.2) parameters. The boxes show the regions dictated by the dispersion of the Bus-DeMeo standard spectra, while the colored data show the objects with taxonomies previously determined by Neese (2010) and Hasselmann et al. (2011). Red data points correspond to D-type objects, green correspond to X-type, and magenta correspond to C-type classifications. The a^*_T regional demarcations of taxonomy are shown as horizontal lines with the D/X dividing line being set to 0, and the X/C line near -0.11 to be half way between the X and C regions. The black diagonal line shows a one-to-one relationship between a^* and a^*_T. The yellow asterisk shows the position of the Sun in principal component space, or the equivalent of a flat asteroid spectrum. There are four previously classified objects that lie outside their taxonomic boundaries. The two D types are (1437) Diomedes (which Neese (2010) classify as a borderline DP type) and (3793) Leonteus (which Hasselmann et al. (2011) reports as a D type with only a 32% confidence level.) (5023) Agapenor is reported to be X type by Hasselmann et al. (2011) with 65% confidence, though we show this object to be significantly less red in our a^*_T cross section than most X types. Considering that this target was classified using SDSS photometry and a principal component similar to a^* this may simply be a misclassification. Finally, we show the C type asteroid, 4060 Deipylos significantly more red than would be expected.

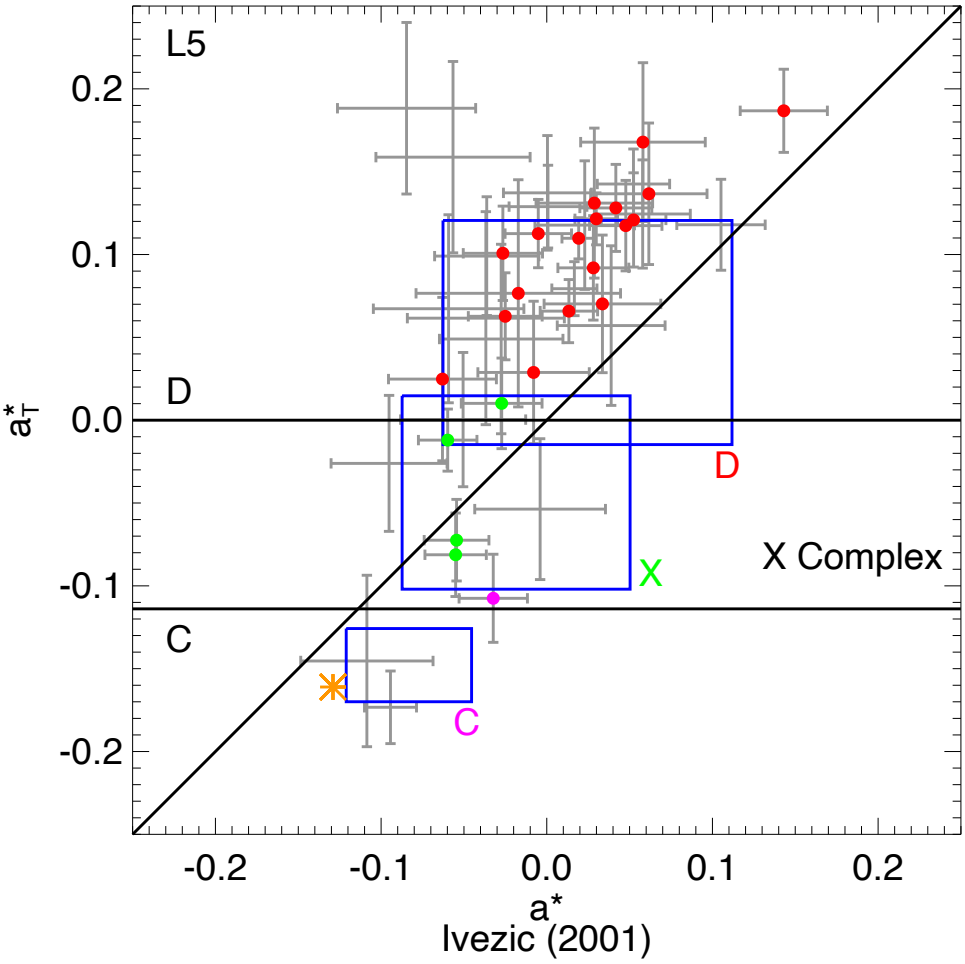

Figure 2.11: Mean photometric values for the L5 objects are plotted, converted into the a^* (Equation 2.1) and a^*_T (Equation 2.2) parameters. The boxes show the regions dictated by the dispersion of the Bus-DeMeo standard spectra, while the colored data show the objects with taxonomies previously determined by Neese (2010) and Hasselmann et al. (2011). Red data points correspond to D-type objects, green correspond to X-type, and magenta correspond to C-type classifications. The a^*_T regional demarcations of taxonomy are shown as horizontal lines with the D/X dividing line being set to 0, and the X/C line near -0.11 to be half way between the X and C regions. The black diagonal line shows a one-to-one relationship between a^* and a^*_T. The yellow asterisk shows the position of the Sun in principal component space, or the equivalent of a flat asteroid spectrum. Only (4709) Ennomos is blue relative to solar. Note: The taxonomy of the outlier green X-type object (7352) with a^*_T above 0 was calculated by Hasselmann et al. (2011) as an XL at a 47% confidence level. This particular object is of interest as an extremely long rotator with a period of 648 hours (Stephens et al. 2014b).

2.5.2 Trends with Inclination

This principal component may now be compared to other physical and orbital parameters associated with these objects in order to explore potential trends that might explain the origin and evolution of the swarms. Roig et al. (2008) found a correlation of inclination, absolute magnitude, and spectral slope among Jupiter Trojans in the SDSS MOC. They claim that both swarms trend towards redder objects being larger and having higher orbital inclinations. As all of the objects in this survey are relatively large compared to most of the objects in the MOC, we examine if this trend holds true for inclination. Figure 2.12 shows a_T^* as a function of inclination for both the L4 Greeks presented here and the MOC4 sample. Only known L4 Jupiter Trojans with quality *griz* photometric data were used for the MOC4 sample, resulting in 167 objects. Figure 2.13 shows the same, but for the L5 camp and with 232 objects from the MOC4. The Lupton (2005) conversion equations (Equation 2.3 through Equation 2.6) from the SDSS website[6] were used to calculate a_T^*.

$$B = g + 0.3130 * (g - r) + 0.2271 \tag{2.3}$$

$$V = g - 0.5784 * (g - r) - 0.0038 \tag{2.4}$$

$$R = r - 0.2936 * (r - i) - 0.1439 \tag{2.5}$$

[6] http://classic.sdss.org/dr4/algorithms/sdssUBVRITransform.html#Lupton2005

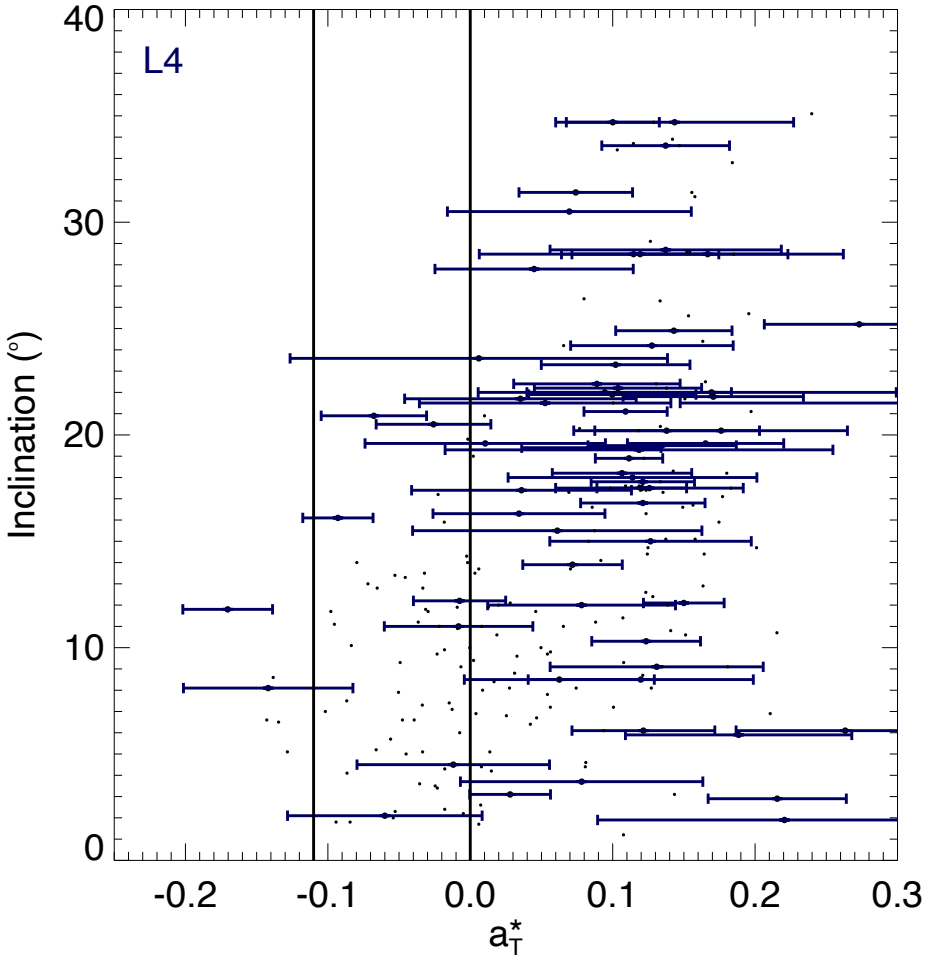

Figure 2.12: Principal component a_T^* (Equation 2.2) plotted for converted SDSS MOC4 L4 Greeks (small black points) as well as the photometric data presented for L4 Greeks in this work (larger dots with blue error bars) against the orbital inclination in degrees for these objects. Unlike the L5 data shown in Figure 2.13, high inclination, less-red X-type and C-type objects with a_T^* less than 0 are not seen in the Greek camp.

$$I = i - 0.3780 * (i - z) - 0.3974 \tag{2.6}$$

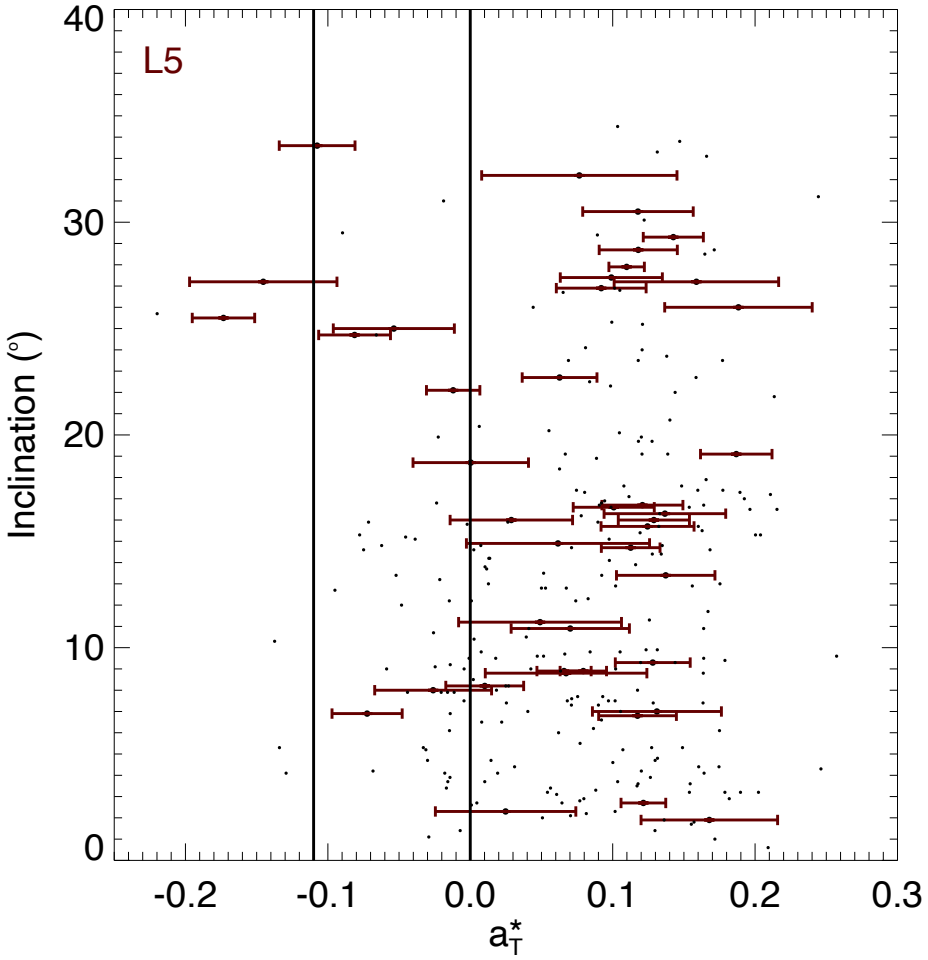

Figure 2.13: Principal component a_T^* (Equation 2.2) plotted for converted SDSS MOC4 L5 Trojans (small black points) as well as the photometric data presented for L5 Trojans in this work (larger dots with red error bars) against the orbital inclination in degrees for these objects. Fewer high inclination, less-red X-type and C-type objects with a_T^* less than 0 are seen among the MOC4 objects than among the Trojans observed here.

The lack of high inclination, less-red[7] objects apparent in the MOC4 sample appears to be present in our L4 Greek population, but is not obvious in the larger L5 objects used for this survey. As can be seen from Figure 2.14, when the two camps are combined less-red

[7]Here we use the terms "less-red" in the style of Emery et al. (2011) to describe the bluer X- and C-type Jupiter Trojans as none of these objects are truly blue and are indeed quite red compared to many other Solar System objects.

X- and C-type objects seem to be lacking in our sample at all inclinations compared to the MOC4 sample (SDSS Trojans in Figure 2.14). A cutoff of 11° was used to separate high inclination objects from low inclination objects because this value cuts the population roughly in half. The two-sample Kolmogorov-Smirnov test (KS test) gives the probability that two samples could be randomly drawn from the same parent sample by evaluating the maximum difference between the cumulative distribution functions of each sample and accounting for sample size. This statistic indicates a small probability[8] (5.4%) that the high and low inclination populations in the L5 MOC4 data are drawn from the same underlying color distribution. We find an even smaller probability for the L4 MOC4 data. However, the same statistical test finds no such distinction for the sample provided in this work (labelled "Large Trojans" in Figure 2.14). Not only is no statistical difference found between the high and low inclination Large Trojan populations, but also there is not any significant difference between the high inclination Large Trojans and the equivalent population from the MOC4 sample. However, when both camps were combined, there is a significant difference (6.2% probability of being drawn from like samples) between the profiles of the MOC4 and Large Trojans at inclinations below 11°. In other words, we show no significant difference between the entire sample of Large Trojans presented here and the high inclination population of somewhat smaller objects in MOC4, but we do see a significant probability that this population of large objects is distinct from the low inclination objects found in MOC4. This might imply two different populations, one that is very red, at high inclinations, and containing most of

[8]The two sample KS test results in a P value representative of the similarity between the two samples. By convention P values less than 0.05 are considered "significant", but there is no quantitative reason for this convention. Since high numbers (here considered to be significantly larger than 5%) are nondiagnostic, we only report P values less than 10%.

the largest objects in the camps, as well as a second, less-red population of smaller objects that is less scattered at low inclinations.

Both Roig et al. (2008) and Wong et al. (2014) tentatively hypothesize that the redder D-types that dominate the higher inclinations in the MOC4 sample are older and therefore less likely to have experienced collisions than the more recently resurfaced or disrupted less-red, X- and C-type objects in the lower inclination Trojan orbits. Szabó et al. (2007) suggest that a dynamical effect could increase weathering effects on the higher inclination objects. The similar color distributions for large high and low inclination Trojans from both camps shown here could support these hypotheses if a lack of disruptive events is what allows these large objects to survive and redden over time. This hypothesis is also supported by fact that more large Jupiter Trojans exist at high inclinations.

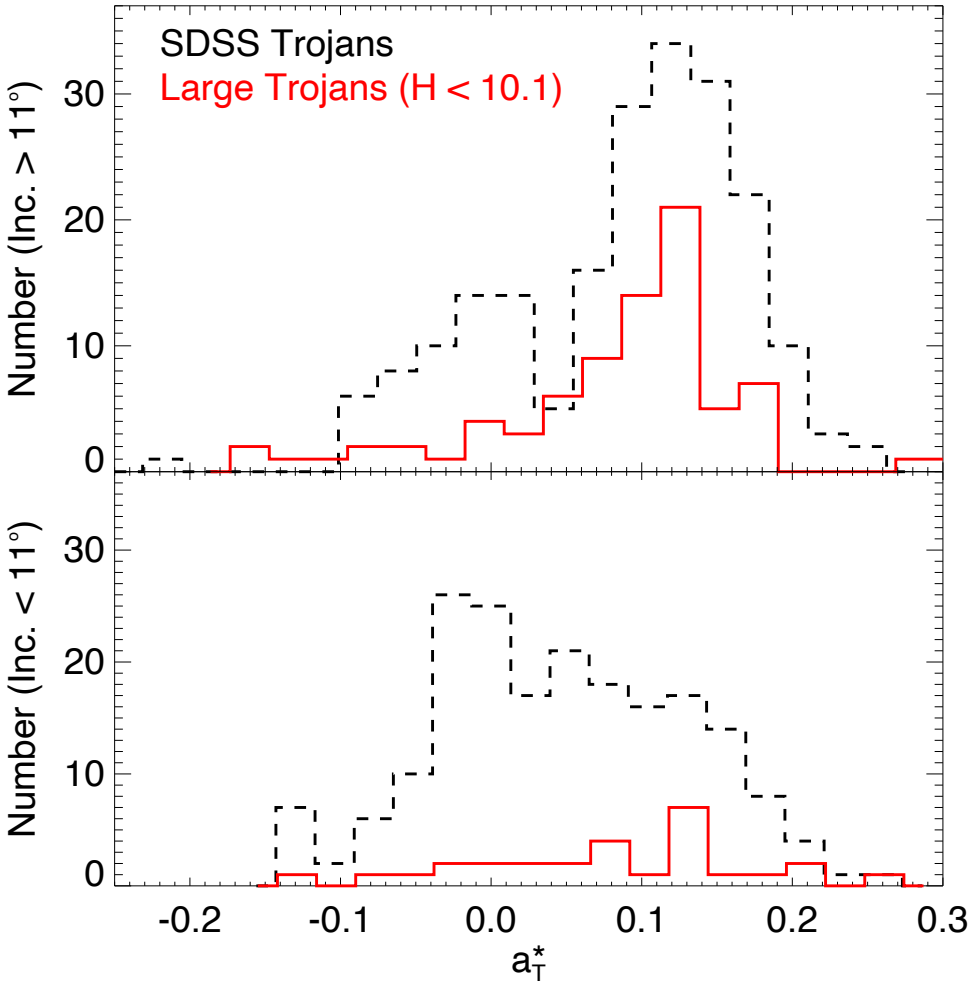

Figure 2.14: Histograms of the SDSS MOC4 Jupiter Trojans (SDSS Trojans) and the larger objects from both camps observed for this work (Large Trojans), both shown in Figure 2.12 and Figure 2.13, divided into roughly equal populations at an inclination of 11°. The SDSS population (black, dashed line) is clearly differentiated, with low inclination objects in the lower frame having a significantly disparate color distribution to that of high inclination objects (upper frame). The low and high inclination Large Trojan populations (solid, red line) are statistically indistinguishable from each other, but we find only a 6.2% probability that the low inclination Large Trojan and SDSS populations are sourced from the same parent population.

2.5.3 Comparing Camps

Even though the Jupiter Trojans in the L4 and L5 Lagrangian points share an orbit, the two camps are perpetually separated by about nine AU. This means that very little communication is possible between camps; therefore, their evolution has been independent from each other since the populations were captured in their current orbits. Signatures of major events could shape the composition or orbital evolution of one camp and leave the other unaffected. Alternatively, differences between the camps could be seen if multiple parent populations were present for the original sourcing of the camps, or if some preferential bias was present during their capture.

However, if such a bias or evolutionary event occurred it left behind no significant signature in the color profiles for the largest Jupiter Trojans (see Figure 2.15). When the relative population sizes are taken into account, we find no significant differences between the taxonomic demographics of the two Trojan camps. We find the largest L4 Greeks to be photometrically consistent with a composition of 87% D types, 10% X types, and 3% C type objects. The largest L5 Trojans are 81% D types, 14% X types, and 5% C types. Additionally, we have listed objects between the overlapping regions of the D and X taxonomic regions as DX on Table 2.3 and Table 2.4. These intermediate objects make up about 7% of each population. A KS test results in no significant difference ($P = 47\%$) between the color profiles of the two camps. With large objects, it is likely that we are probing the original source populations of the two Trojan camps more strongly than evolutionary effects such as collisions or migrations that might change the compositional landscape of these populations. Therefore, from this information we can conclude that it is unlikely that there was any

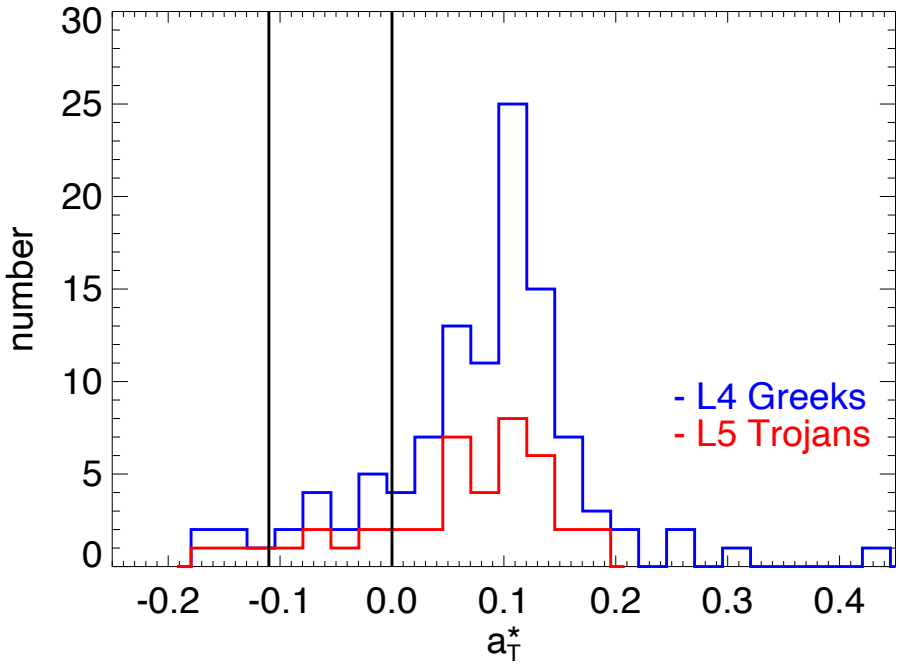

Figure 2.15: Histogram showing the number of objects from this sample according to a_T^* principal component. This figure shows the color profile for both Jupiter Trojan camps. The L4 Greeks are plotted above the L5 Trojans making the Greek line the total number in that bin for both camps, and the difference between lines the number of Greeks in that bin. Redder objects are towards the right of the plot, and less-red objects are located to the left. Black lines have been placed at 0 and -0.11 to separate the region where one could expect to find D like objects from those regions populated by X like and C like objects as described in Subsection 2.5.1.

compositional bias present during the sourcing of the two independent camps. This should be true regardless of the dynamical effects that have resulted in the disparity in numbers between the groups, as the color profiles are indistinguishable.

2.6 Discussion

Using the a_T^* principal component described in the previous section, we have classified 109 of the Jupiter Trojans presented in this sample. Of these large objects, we have found 88 to have a_T^* consistent with D-type asteroids, 9 consistent with X-type objects, and 4 consistent

with C-types. We found 8 objects to be indeterminate between the D and X regions. This leads to a population that is 81% D-type, 8% X-type, 4% C-type, and 7% intermediate DX-type objects. This fractional distribution is similar to the distribution presented by DeMeo & Carry (2013) with a slightly larger ratio of D's to X's.

Emery et al. (2011) and Wong et al. (2014) have shown a lopsided bimodality within the Greek and Trojan populations that they have designated as Red (R) and Less-Red (LR) groups. These two groups have a ratio of about 2.2 to 1 in favor of the R group for objects with $H < 12.3$. When the Wong et al. (2014) sample is limited to include only objects brighter than H of 10, the ratio is in good agreement with the 4.2 to 1 ratio of red D-type asteroids to less-red DX, X, and C-type asteroids we derive here. The demographics represented by the Bus-DeMeo taxonomies for the Main Belt can now be extended into the Greek and Trojan clouds, and it is possible that the bimodality of the Centaur and KBO populations (Peixinho et al. 2012) might have a presence of some form as far in as Jupiter's orbit (see Chapter 5).

– 3 –

Search for Surface Variation on Individual Jupiter Trojans

3.1 Introduction

As discussed in Chapter 5, space weathering and compositional differences are commonly assumed to be the reasons that different asteroids are different colors. Even among Jupiter Trojans, $V - I$ color can vary by as much as 0.45 magnitudes between different objects (see Section 2.4), and these objects experience a very small range of environmental conditions compared to that experienced by other dynamical groups. With such a large variation in color within the Jupiter Trojan populations as a whole, we examine several large Trojans for color inhomogeneities across their surfaces in an effort to determine both the reliability of instantaneous color observations such as those discussed in Chapter 2 and to search for clues as to the source of variety between objects. This is the first study of its kind for Jupiter Trojans, although (4709) Ennomos has garnered much attention for its relatively high albedo of about 0.15 reported by Fernández et al. (2003) (compared to the significantly lower albedo of about 0.07 Grav et al. (2011) found to be typical for large Jupiter Trojans). Additionally, Shevchenko et al. (2014) found a more typical Jupiter Trojan albedo for Ennomos of 0.052, suggesting a possible bright spot on its surface. Near-Infrared spectroscopy presented by Emery et al. (2016) does show evidence of spectral slope variations with rotation for Ennomos.

If the majority of the differences among Trojan colors is caused by the relative age of an object's surface and subsequent space weathering, then recent non-disruptive collisional events could be visible in the form of a relative deviation of $V - I$ color from the mean as the asteroid rotates and these surface features come into and out of view. The strength of this

deviation would depend on the novelty of the event and the strength of the weathering effect, as well as the size of the feature relative to the the visible projected area of the asteroid. For instance, a hypothetical crater that covered 10% of an asteroid's surface and differed from the predominate surface color by ~ 0.3 mag could have a signature of about 0.03 magnitudes deviation from the rest of the color curve. The width of the deviation is dependent on the size of the feature, its latitude, and the current aspect angle of the body. However, due to the low signal to noise ratio of these detections, several epochs of data spanning a variety of aspect angles are necessary to truly map any complex surface features on an unresolved asteroid. We attempt this with (1173) Anchises in Subsection 4.3.4, but in this chapter we present more limited findings for partial light curves of twelve different Jupiter Trojans.

3.2 Observations and Reductions

Observations were primarily taken on non-photometric or partially photometric nights during observing runs at CTIO and Lowell Observatory that were otherwise largely dedicated to the Jupiter Trojan photometry discussed in Chapter 2. The specific observing runs are discussed in some detail in Section 4.2 and the three telescopes used for these observations are detailed in Table 2.1.

For these observations, frames were taken in alternating Johnson-Kron-Cousins V and I filters. For some datasets intermittent R frames were taken as well. These latter frames were primarily used to check the general shape of the light curve in case there were any errors present in one of the two primary filters. Taking the V and I images nearly simultaneously allows us to calculate the $V - I$ color of the target over time as the projected aspect and surface of the body rotate into and out of view.

Table 3.1: Partial Light Curve Summaries

Asteroid	Camp	H (mag)	P_{rot} (hours)	Date (UT)	λ (deg)	β (deg)	α (deg)	r (AU)	Δ (AU)	Observed Amplitude	Telescope
(884) Priamus	L5	8.81	6.8505	2011 Nov 16	343.01	7.72	10.84	4.96	4.54	$\geqslant 0.16$	1.0m
(911) Agamemnon	L4	7.89	6.592	2013 Feb 24	151.48	2.94	0.94	5.26	4.27	$\geqslant 0.07$	0.9m
(1143) Odysseus	L4	7.93	10.111	2010 Oct 22	58.17	−0.73	5.79	4.89	4.00	$\geqslant 0.14$	1.0m
(2207) Antenor	L5	8.89	7.965	2011 Nov 16	328.30	0.00	10.99	5.17	4.99	$\geqslant 0.11$	1.0m
				2012 Sept 29	5.83	−3.80	0.75	5.13	4.13	$\geqslant 0.22$	0.9m
(2357) Phereclos	L5	8.94	14.394	2011 Sept 08	339.05	1.09	1.18	5.17	4.17	–	42in
				2012 Oct 03	12.67	−0.73	0.49	5.30	4.30	–	0.9m
				2013 Nov 08	43.13	−2.28	0.64	5.40	4.41	$\geqslant 0.16$	42in
(2920) Automedon	L4	8.9	10.212	2011 Dec 13	96.35	−17.88	4.55	4.98	4.06	–	1.0m
				2013 Feb 23	128.26	−25.38	6.61	5.04	4.21	–	0.9m
				2013 Feb 24	128.14	−25.35	6.73	5.04	4.21	–	0.9m
(3317) Paris	L5	8.4	7.048	2011 June 27	348.51	-11.38	11.83	4.76	4.38	$\geqslant 0.09$	1.0m
				2011 Aug 09	346.69	−15.06	6.75	4.80	3.92	$\geqslant 0.13$	1.0m
(3451) Mentor	L5	8.4	7.730	2011 Aug 14	354.86	6.59	6.87	4.80	3.93	$\geqslant 0.63$	1.0m
				2012 Sept 30	27.35	−12.76	4.63	4.99	4.05	–	0.9m
				2012 Oct 03	26.95	−12.93	4.14	4.99	4.04	–	0.9m
(3793) Leonteus	L4	8.7	5.622	2011 Nov 15	118.09	−23.25	11.17	4.73	4.27	–	1.0m
				2011 Dec 11	117.06	−25.09	8.44	4.73	3.98	$\geqslant 0.38$	0.9m
				2013 Feb 23	154.07	−19.38	3.86	4.87	3.93	$\geqslant 0.31$	1.0m
(4709) Ennomos	L5	8.6	12.275	2011 Sept 05	349.55	31.25	6.02	5.10	4.22	$\geqslant 0.15$	42in
(4833) Meges	L4	8.9	14.250	2015 Feb 08	194.90	38.37	8.94	5.71	5.20	0.17	42in
				2015 Feb 09	194.86	38.47	8.89	5.71	5.19	–	42in
				2015 Feb 16	194.46	39.11	8.48	5.71	5.13	–	42in
				2015 Feb 17	194.39	39.20	8.42	5.71	5.12	–	42in
(5144) Achates	L5	9.0	5.958	2011 June 26	326.09	−1.72	12.06	3.84	3.13	0.14	1.0m

The three telescopes used to acquire these data were the CTIO/SMARTS 0.9-m and 1.0-m as well as the Lowell 42-in.

H is the predicted absolute V magnitude that a Solar System object would have at 0° phase angle and 1 AU from both the Sun and observer.

H and P_{rot} were taken from the JPL Small Body Database: https://ssd.jpl.nasa.gov/sbdb_query.cgi

λ and β are the mean Ecliptic Longitude and Latitude respectively of each object in a geocentric reference frame over the course of observations for that epoch.

α is the mean phase angle of the observations in degrees.

r is the distance of each Jupiter Trojan from the Sun while Δ is its distance from Earth.

Ephemerides were all calculated using JPL HORIZONS system: http://ssd.jpl.nasa.gov/horizons.cgi

The data were bias and flat corrected using standard IRAF reduction procedures and fringe removal was applied to I frames taken at the CTIO 1.0m and Lowell 42in as needed. Once processed, the frames were split according to filter and run through the *MPO Canopus* software (Bdw Publishing). This software was used to track the object through the fields and to select five comparison stars with which the brightness variation of the asteroid was determined. The relative magnitude of the target in each filter was then output and used for further analysis. Details about individual objects and observations are given in Table 3.1 while a full list of observed and calculated values for each target at each epoch can be found in Section C.

3.3 Analysis

3.3.1 Light Curves

Once the data were processed and reduced, a light curve was created for each filter. Due to the non-photometric nature of most nights, these light curves were uncalibrated to any absolute value and represent only the relative change in brightness for the object over the period of observation. The light curves were then phased to an appropriate rotational period as given in the literature, usually the asteroid Lightcurve Database (LCDB, Harris et al. 2012). In some cases enough of the phase was observed to calculate a minimum amplitude during the observed epoch, while for several epochs, either insufficient coverage was achieved or no change was observed. For two objects, (4833) Meges and (5144) Achates, we observed the entire rotation phase within a single apparition. Where possible, the amplitudes for these observations were calculated by subtracting the average of the two minima from that of the two maxima so as to mitigate some of the discrepancy between the actual asteroid shape

and that of a tri-axial ellipsoid. Unfortunately, this is not a universally used method, as many authors publish amplitudes that are simply the difference between observed maximum and minimum values, and some do not explicitly state how their values are calculated. This lack of a standard method means that without examining the published light curves directly, published amplitudes cannot necessarily be directly compared. In general, the amplitudes given here will be equal to or less than the amplitudes that would have been calculated for the same object at the same epoch by other authors. All of these calculated values are given in Table 3.1. Amplitudes, even lower limits, of an asteroid at different epochs can be used to calculate the pole orientation and shape of the object. For most of the objects listed here we have either too little of the full rotation at each epoch, or too little orbital coverage, to perform these calculations with any certainty. For a much more in-depth discussion of this process as applied to (1173) Anchises, see Section 4.3.

Plots of these color light curve data are given in Section 3.4. For each object, the relative magnitude (of both brightness and color) about the mean for that apparition is given, with apparitions on different dates denoted by different symbols. The symbol color denotes the filter in which the observation was made, and a gray line is shown at the mean value for that apparition. If an epoch is shifted in magnitude it will be noted in the caption. In many cases a fourth order Fourier fit is applied to all or a portion of the data. This trend line is plotted in black and is meant primarily to lead the eye, rather than suggest an actual shape for the light curve. In each Figure, the relative magnitude is plotted such that brighter values are on top and fainter values are below, while the $V - I$ color curve is plotted such that redder values are towards the top and bluer values are towards the bottom.

3.3.2 Color Curves

The color curve for each object is created by interpolating the I magnitudes to the light corrected times of the V filter observations. This method accounts for the changing slope of the I light curve in order to simulate truly simultaneous (rather than "nearly simultaneous") observations in each filter. The error for each interpolated I datum is then calculated based on the errors of I data that were used in the interpolation. Once this is accomplished, the new I values are subtracted from the V values and a color curve is produced for the same phased time as the original light curve. We then examine each of these color curves for variation and scatter to determine which objects might be of interest for future examination.

A second plot is then created for each object to examine any possible color variation. These too can be found in Section 3.4. We created a toy model of a circular spot on a spherical, rotating object in order to create a first order approximation of the strength and duration of the signature produced by a colored surface feature. For this model, the color difference between the feature and surrounding material was assumed to be a factor of two. This corresponds well with the range of $V-I$ colors seen in the Trojan camps (see 2.3(a) and 2.4(a)). Furthermore changes to the model due to changing the relative color of the feature could be replicated by changing the size of the feature, and was therefore a degenerate variable. Keeping this value constant, the important unknown variables for this model are the aspect angle of the object, the latitude of the feature, and the size of the feature. Varying these parameters changes the width and strength of of the model signature. This model is then fit to any variations seen in the color curve for each object. For this model we assume that the base material of the object is either bluer or redder than any features by a factor

of two, and set the zero point for the color curve to the best fit to the flattest part of the curve at either the top or bottom of the $V - I$ color curve. Then, the shapes of any features are compared to that provided by the model discussed above, and the best-fit orientation (representing either blue or red features) is used. For each object presented here, features were better fit when the base material was redder and the surface features were bluer.

To calculate the probability of a variation in color representing a real feature on the surface of an object rather than photometric error, we first calculate the probability that an individual data point is consistent with zero. A relative $V - I$ value of zero, in this case, is consistent with a flat color curve representing no color change over the portion of the rotation period examined. The probability that an individual datum is consistent with a value of zero is determined by the 1σ error calculated for a particular observation and plotted as error bars in the appropriate Figures. This probability is plotted for each observation for each object in Section 3.4. In cases where features are suspected, the net probability that all of the data points with the phase space of the feature are consistent with zero is calculated and then normalized to form a confidence level[1] for the feature itself. This confidence level is given as a percent probability that the entire variation differs from the rest of the color curve. In general a confidence level above 95% is considered highly likely to represent a real colored feature or crater on the surface of the object.

[1]This feature confidence level is determined by calculating the product of individual probabilities of data points that make up a feature. This value is normalized by setting it to the power of 1/n where n is the number of data points making up the feature and then adjusted for the average error of the entire light curve segment.

3.4 Results for Individual Objects

The following sections describe results for 12 Jupiter Trojans observed in the V and I filters, ordered by identification number.

(884) Priamus

Priamus was observed about every three minutes for three hours and fifteen minutes on November 16th, 2011. This accounts for roughly half of the rotational phase. The period of Priamus has been well determined and is listed as 6.8605 hours in the asteroid Lightcurve Database (LCDB, Harris et al. 2012). This is the period to which we phased the data in Figure 3.1. The object was also observed by Mottola et al. (2011), French et al. (2011b), Shevchenko et al. (2012a), Stephens et al. (2015), and Stephens et al. (2016c). All of these observations found nearly identical rotation periods and amplitudes ranging from 0.24 to 0.40 mag.

None of these sources published any color information, though a mean $V-I$ color of 0.91 was found by Chatelain et al. (2016), who averaged six individual photometric observations that had a $V-I$ range of 0.14 mag. In Figure 3.2 we see a $V-I$ color change of about 0.06 mag from phase 0 to 0.2 as well as between phase 0.2 and 0.35. The shapes of these features fits our model well and produces a high confidence level for each feature of 96.4% and 97.0%. Therefore, we consider (884) Priamus to be be a strong candidate for surface variation, although further observations at varying aspect angles are required to determine more information about the nature of any features. A full data table can be found in Table C.1.

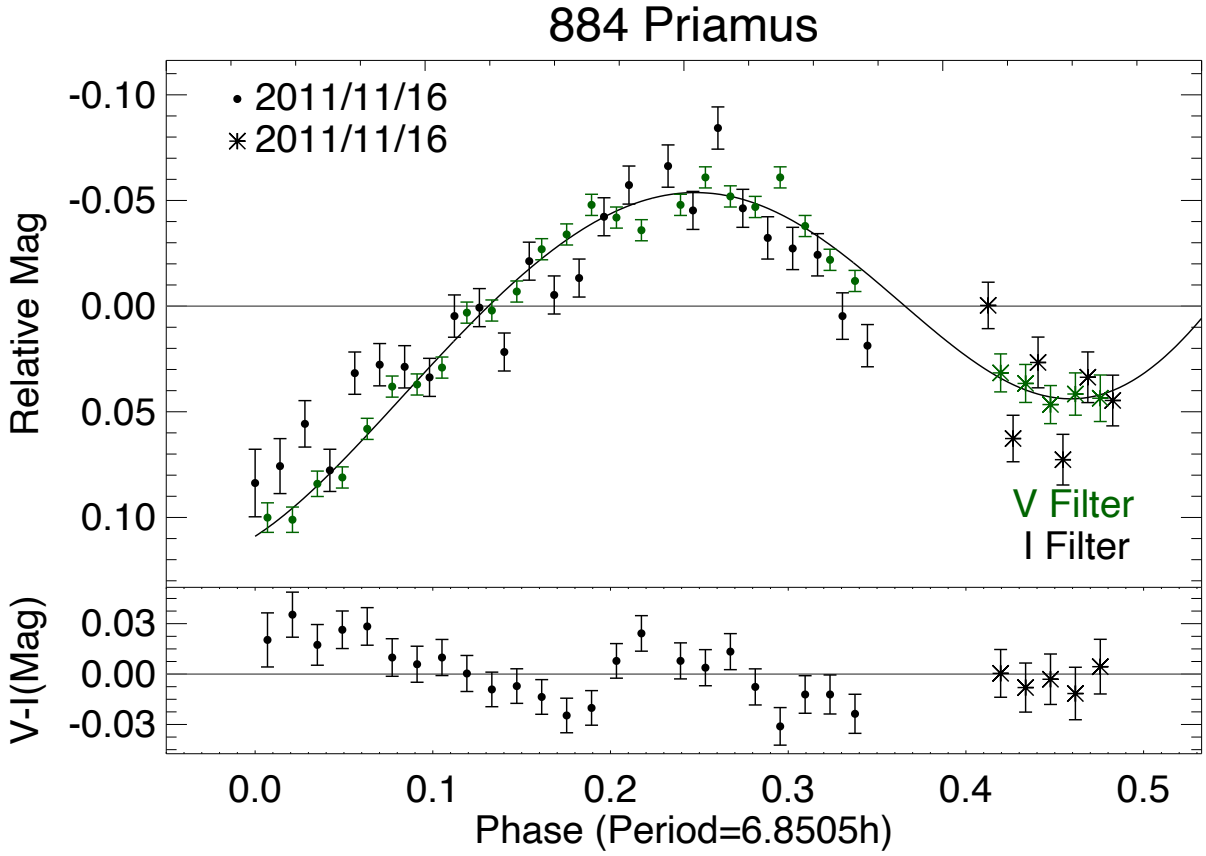

Figure 3.1: Light curve (top) and $V - I$ color curve (bottom) for (884) Priamus during November 2011. The second dataset has been shifted by 0.05 mag to better fit the presumed light curve.

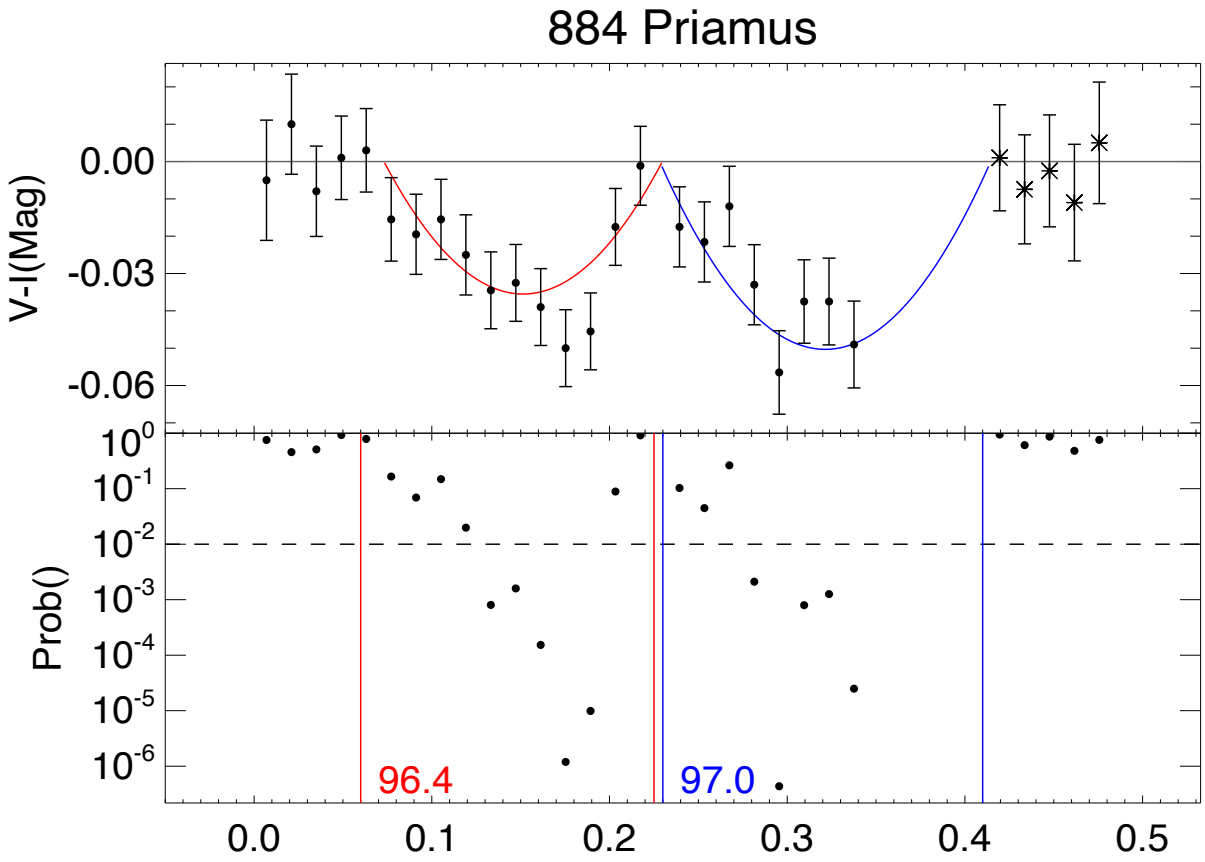

Figure 3.2: Color curve (top) and Individual Probability curve (bottom) for (884) Priamus during November 2011. We model two potential features (as described in Subsection 3.3.2) centered at phase 0.15 and 0.32 with a confidence level of 96.4% and 97.0% respectively. The dashed line shows a 99% probability that a data point represents color change. The symbols used in the color curve are the same as those used in Figure 3.1.

(911) Agamemnon

Agamemnon was observed about once every two minutes for five hours and forty-eight minutes on February 24th, 2013. This results in a very densely sampled light curve that covers most of the object's rotational phase. The rotation period of Agamemnon has been well determined, and is listed as 6.592 hours in the LCDB (Harris et al. 2012). This is the period to which we phased the data in Figure 3.3. The object was also observed by Stephens (2009), Mottola et al. (2011), French et al. (2012), and Stephens et al. (2014a). All of these observations found nearly identical rotation periods. Howerver, they did find amplitudes ranging from 0.04 mag with an uneven single peaked light curve (French et al. 2012) to 0.29 mag with a much more standard double peaked light curve (Mottola et al. 2011). Our data set from 2013 much more closely resembles the shape and amplitude of the French et al. (2012) light curve rather than those observed before or after.

None of these sources published any color information, though we find a mean $V - I$ color of 0.98 in Table 2.3 where we averaged 2 individual photometric observations that had a $V-I$ range of 0.08 mag. We find no sign of color variation in Figure 3.4 that would indicate an unevenly weathered surface. However, due to the relatively flat nature of Agamemnon's light curve at this apparition compared to the amplitude it has been seen to have at other parts of its orbit, it is very likely that the object has a very high obliquity and we happen to be looking mostly at the pole during this particular epoch. If this is indeed the case, then color variation would not be expected, as most of the projected surface stays in view for the entire rotation and features would not be visible relative to the rest of the surface since they would never go below the horizon. A full data table can be found in Table C.2.

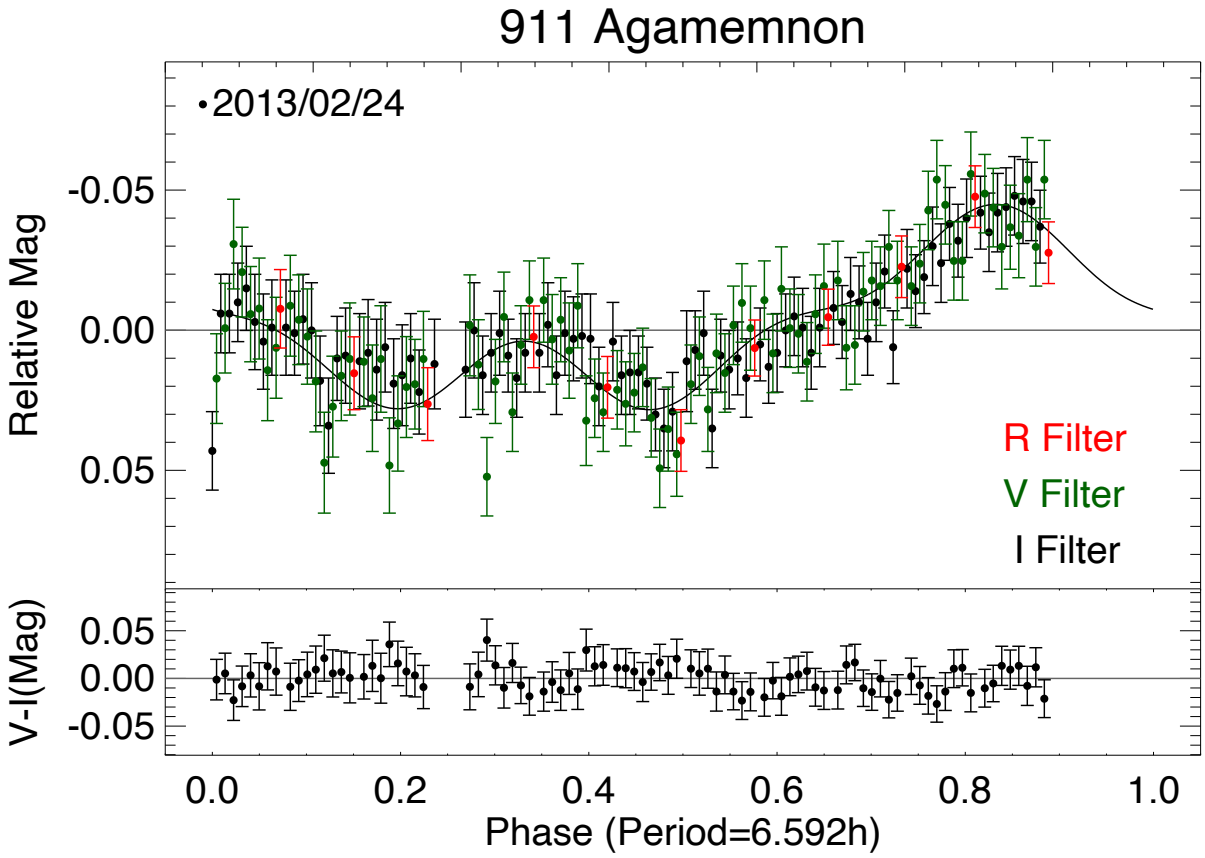

Figure 3.3: Light curve (top) and $V-I$ color curve (bottom) for (911) Agamemnon during February 2013.

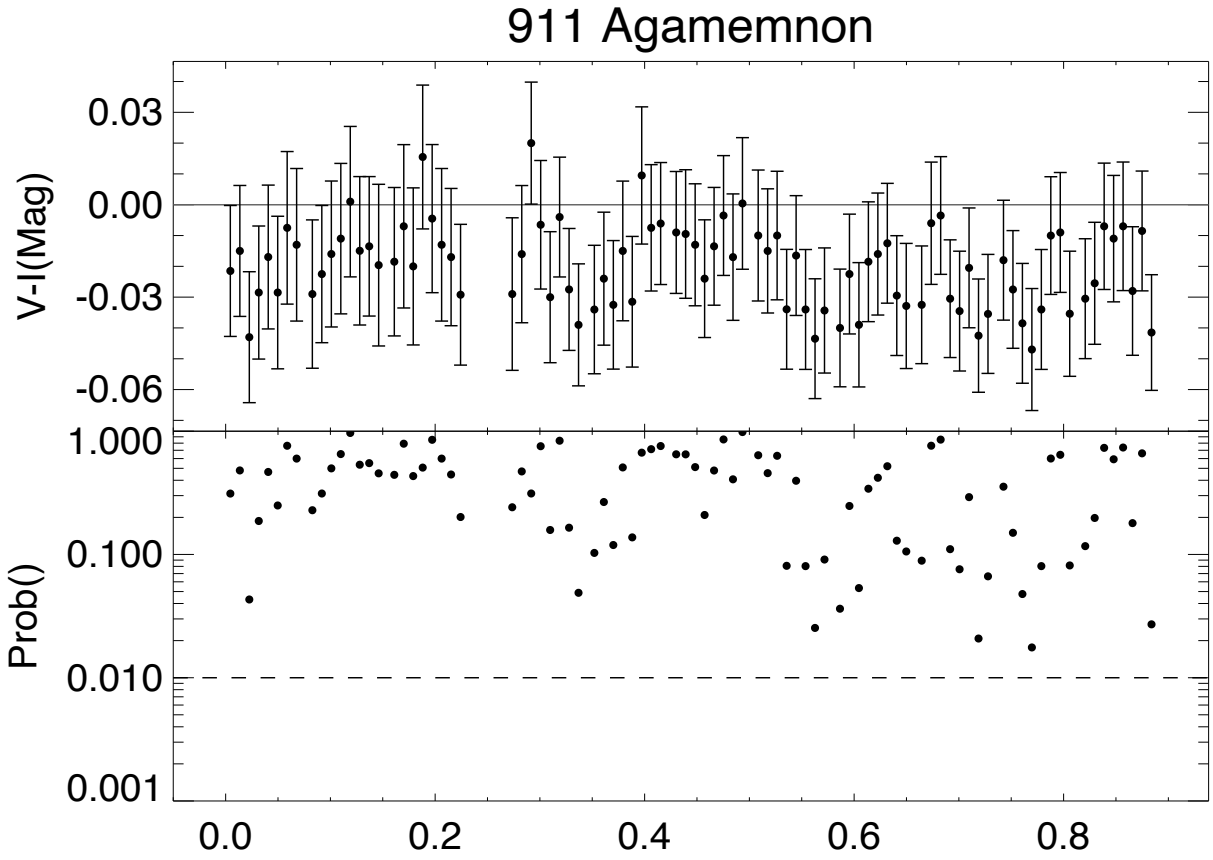

Figure 3.4: Color curve (top) and Individual Probability curve (bottom) for (911) Agamemnon during February 2013. We found no notable features that might be modelled (as described in Subsection 3.3.2). The dashed line shows a 99% probability that a data point represents color change. The symbols used in the color curve are the same as those used in Figure 3.3.

(1143) Odysseus

Odysseus was observed every minute or so for three hours and twenty minutes on October 22nd, 2010. This results in a well-sampled partial light curve covering about 40% of the object's rotational phase. The rotation period of Odysseus has been well determined to be 10.111 hours as cited in the LCDB (Harris et al. 2012). This is the period to which we phased the data in Figure 3.5. Light curves of Odysseus were also gathered by Molnar et al. (2008), Mottola et al. (2011), Shevchenko et al. (2012a), and Stephens et al. (2014a). All of these observations found rotation periods that were in good agreement and amplitudes ranging from 0.15 to 0.22 mag. Many of these sources show a complex light curve that has a small dip in brightness near the secondary maximum. Though our partial coverage does not fully capture either maxima, it is likely that part of this dip is visible near a phase of 0.38.

None of these sources published any color information, though we find a mean $V-I$ color of 0.86 in Table 2.3 where we averaged six individual photometric observations that had a $V-I$ range of 0.11 mag. We find two potential features in Figure 3.6 that might indicate an unevenly weathered surface. The first feature from phase 0.05 to 0.2 shows a net color change of 0.07 magnitudes and has a confidence level of 93.4%, while the second feature from phase 0.25 to 0.4 has about the same color change and a confidence level of 93.5%. A full data table can be found in Table C.3.

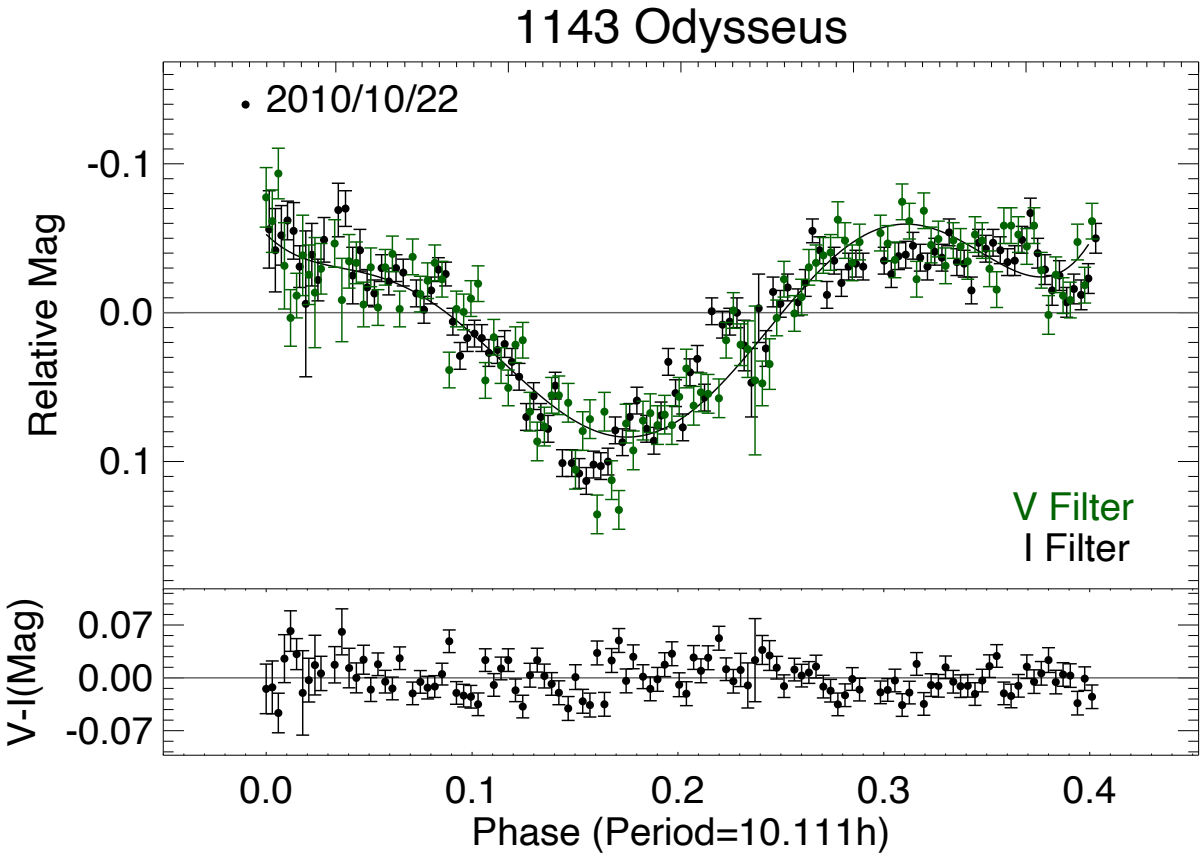

Figure 3.5: Light curve (top) and $V - I$ color curve (bottom) for (1143) Odysseus during October 2010.

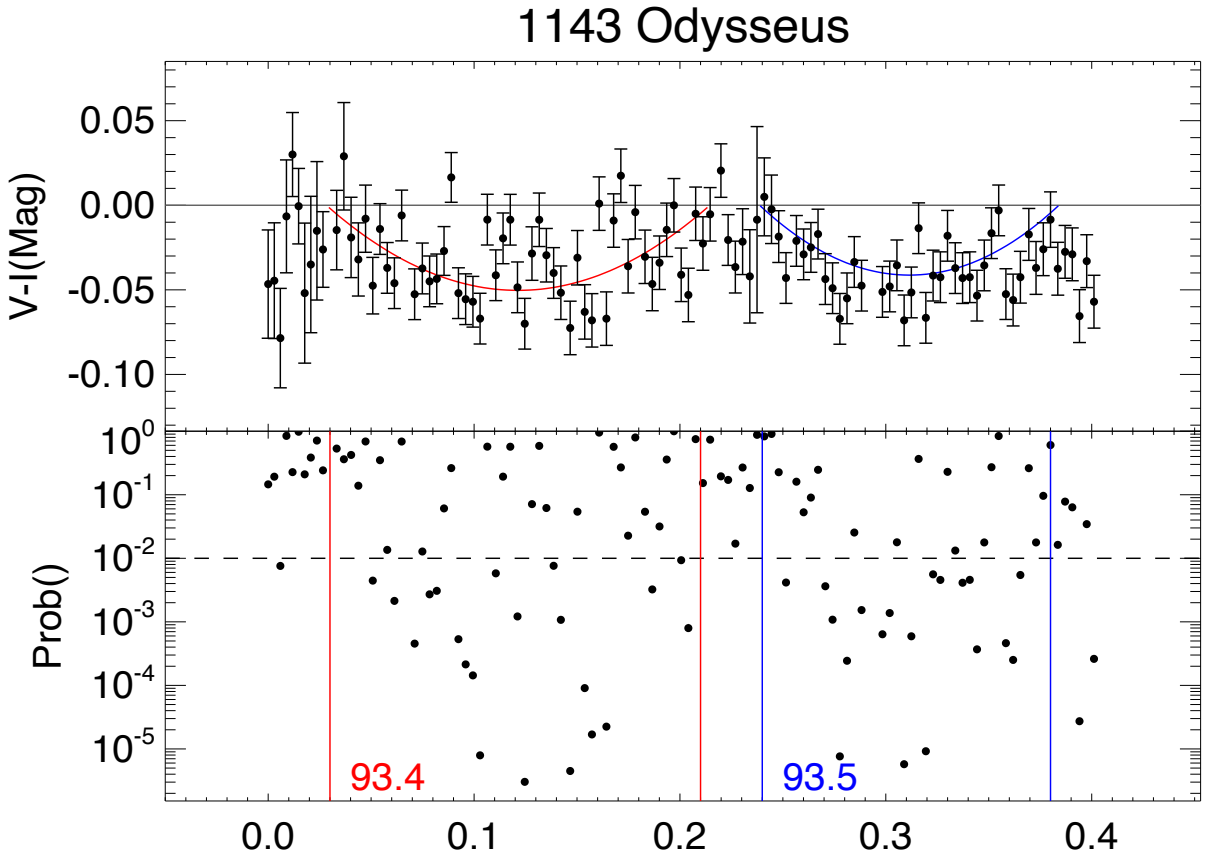

Figure 3.6: Color curve (top) and Individual Probability curve (bottom) for (1143) Odysseus during October 2010. We model two potential features (as described in Subsection 3.3.2) centered at phase 0.11 and 0.31 with a confidence level of 93.4% and 93.5% respectively. The dashed line shows a 99% probability that a data point represents color change. The symbols used in the color curve are the same as those used in Figure 3.5.

(2207) Antenor

Antenor was observed every 3 minutes for three hours on November 17th, 2011 and four hours and fifty minutes on September 29th, 2012. Combining these two epochs results in nearly total phase coverage if we assume the rotation period to be precisely the 7.965 hours listed in the the LCDB (Harris et al. 2012). Even though this is the period to which we phased the data in Figure 3.7, the time between the two epochs means that without a more precise period, the phase of each apparition could shift by as much as 0.6 relative to the other, making this placement effectively arbitrary. This is caused by the accumulation of at least an 18 second uncertainty in the object's rotational period over many thousands of rotations between epochs. Light curves of Antenor were also gathered by Gonano et al. (1991), Mottola et al. (2011), and Stephens et al. (2016b). All of these observations found rotation periods in relatively good agreement, but with a deviation between them of about four minutes. They also found amplitudes ranging from 0.09 on a nearly featureless light curve (Stephens et al. 2016b) to 0.19 mag with a complex light curve showing many sharp peaks and valleys much more closely resembling our 2012 data (Mottola et al. 2011). This particular progression from complex features and large amplitude in 1989 to featureless and small amplitudes in 2016 implies a large axial tilt, and a near equatorial viewing geometry in both 1989 and 2012 (two dates almost exactly two orbits apart).

None of these sources published any color information, though we find a mean $V-I$ color of 0.92 in Chatelain et al. (2016) where we averaged four individual photometric observations that had a $V-I$ range of 0.25 mag. Even though the likely equatorial viewing geometry is ideal for spotting surface inhomogeneities, the potential features modelled in Figure 3.8 are

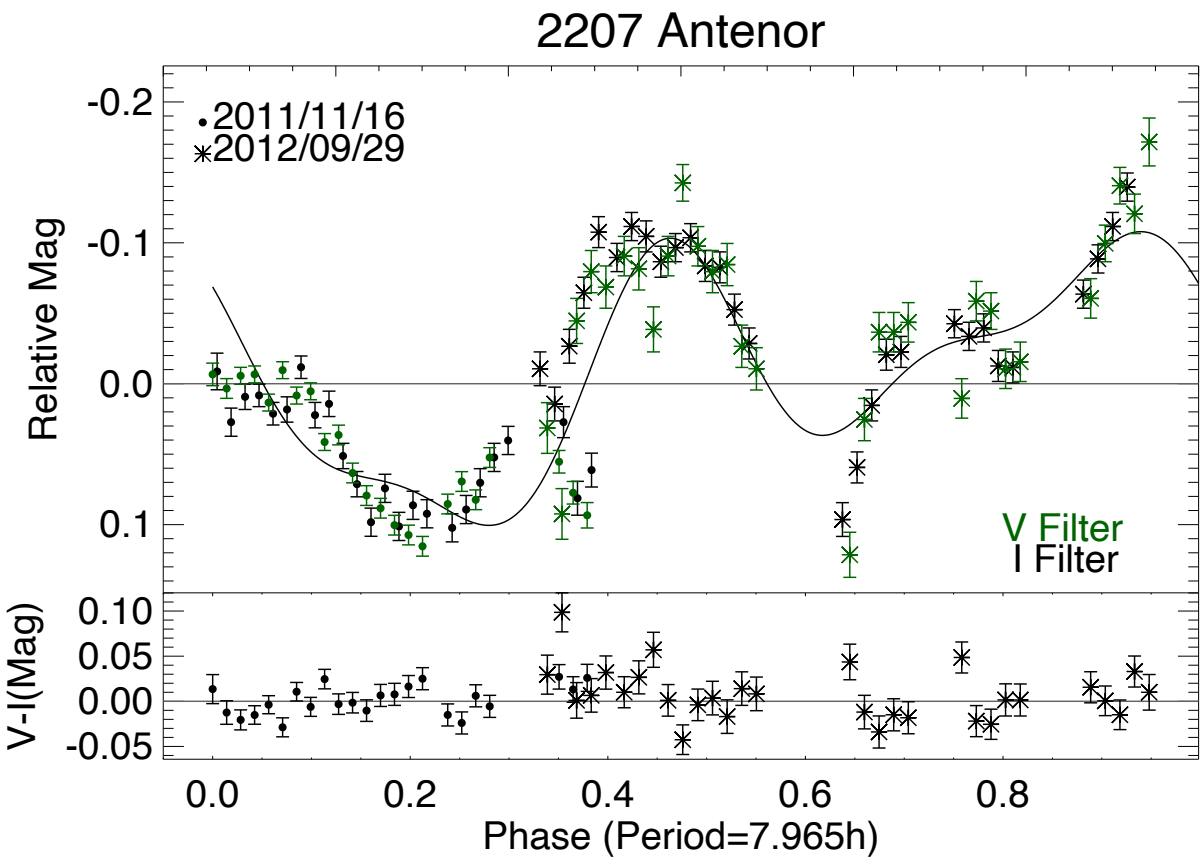

Figure 3.7: Light curve (top) and $V - I$ color curve (bottom) for (2207) Antenor during November 2011 and September 2012. The 2011 data have been shifted by 0.5 mag to provide a better visual fit to the 2012 light curve.

relatively weak and at lower confidence levels of 78.4% and 88.0%. However, both features appear quite broad, which is consistent with an aspect angle of nearly 90° that would result in the expected viewing geometry. A full data table can be found in Table C.4.

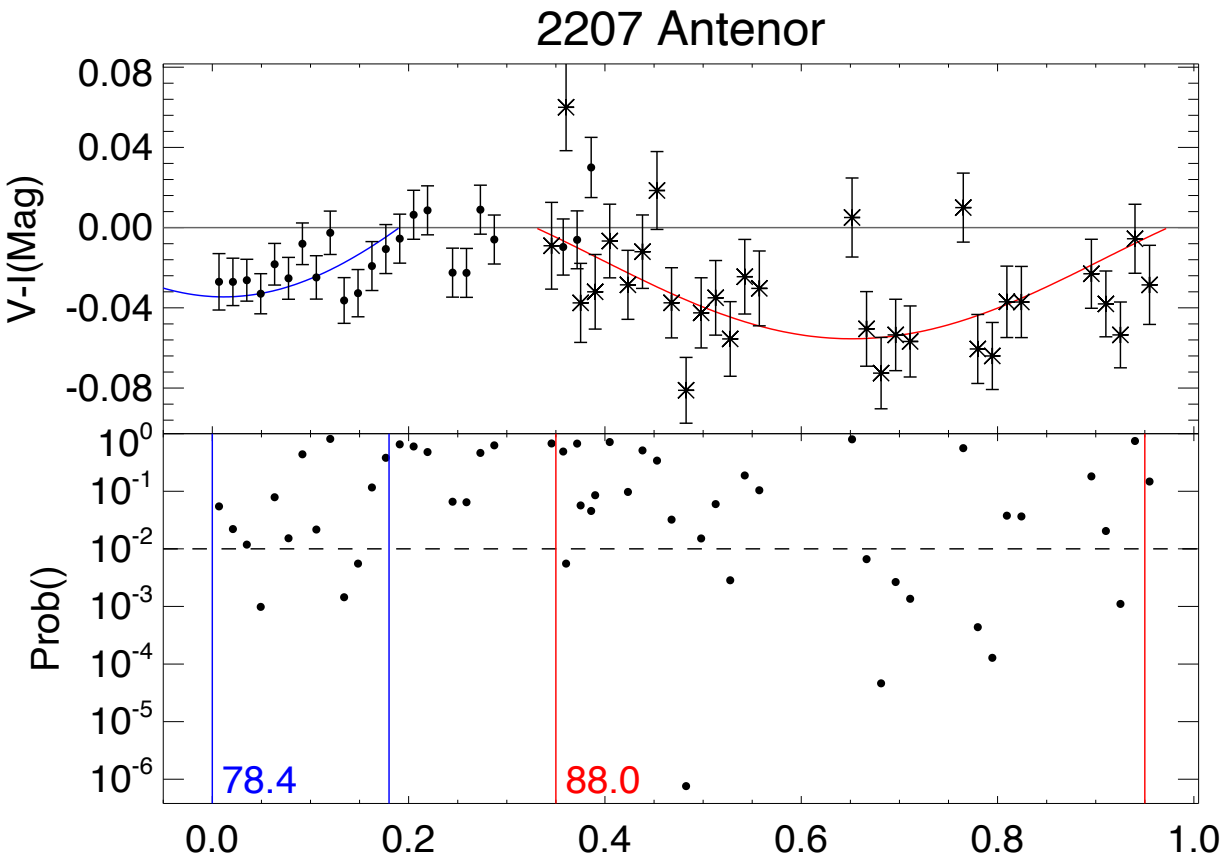

Figure 3.8: Color curve (top) and Individual Probability curve (bottom) for (2207) Antenor during November 2011 and September 2012. We model two potential features (as described in Subsection 3.3.2) centered at phase 0.0 and 0.65 with a confidence level of 78.4% and 88.0% respectively. However, due to the time between these two epochs and the lack of a highly precise period, these features could possibly be the same feature, partially sampled on two different dates. The dashed line shows a 99% probability that a data point represents color change. The symbols used in the color curve are the same as those used in Figure 3.7.

(2357) Phereclos

Phereclos was observed once every 4.5 minutes for about three hours on September 8th, 2011; every three minutes for five and a half hours on October 12th, 2012; and every ten minutes for about eight and a half hours on November 8th, 2013. Though we phased the data to the 14.394 hour rotation period given by the LCDB (Harris et al. 2012), due to

the long periods of time between epochs, the relative phases of each dataset are effectively arbitrary. Figure 3.9 displays the data from the three epochs offset from one another so as to avoid confusion. For the partial light curves we have acquired, we show a large change in amplitude between apparitions. Something similar can be seen in the light curves of Phereclos gathered by Mottola et al. (2011) and Stephens et al. (2016b). Both of these sources found similar rotation periods, but the light curve shape and amplitude varied significantly between observations. Mottola et al. (2011) observed Phereclos at two different epochs and saw an increase in amplitude from 0.06 to 0.09 mag between their observations in 1994 and 2010, while Stephens et al. (2016b) found an amplitude of 0.18 in 2015. Considering that we find a minimum amplitude of 0.16 in 2013, it is likely that this apparition was coincidentally near an equatorial projection, and the other two datasets simply did not cover enough of the phase to provide accurate amplitude estimates.

Chatelain et al. (2016) found a mean $V - I$ color of 0.96, which is shown in Table 2.4. This value was the weighted average of seven individual photometric observations that had a $V - I$ range of 0.1 mag. Unfortunately, only V and R filter data were usable for the 2013 epoch, meaning that a $V - I$ color curve was not available for this date. The data were included regardless, due to the amplitude information they contained. For the two prior datasets, we see no variation in Figure 3.10 that is statistically different from the random scatter of the data. A full data table can be found in Table C.5.

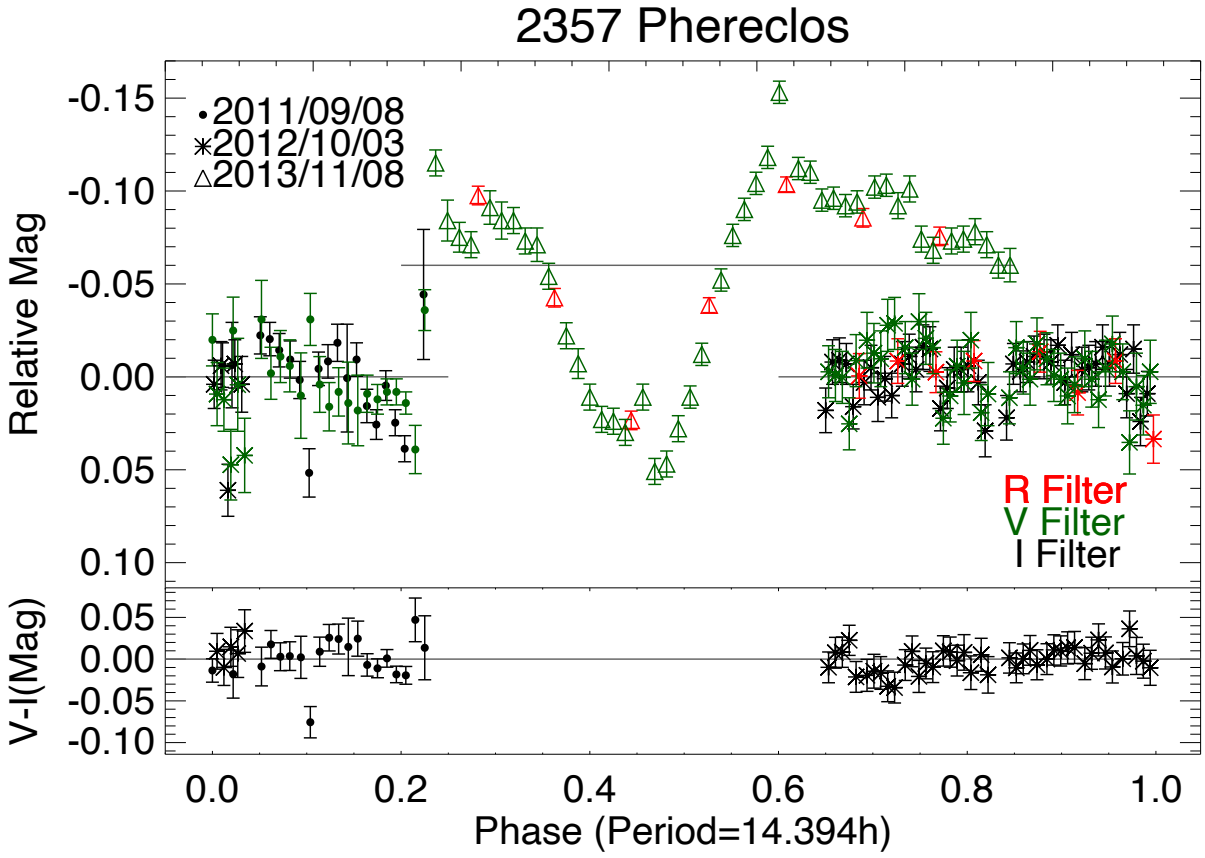

Figure 3.9: Light curve (top) and $V - I$ color curve (bottom) for (2357) Phereclos during September 2011, October 2012, and November 2013. Due to the large variation in light curve shape and amplitude between epochs, individual datasets have been offset from one another. The 2013 data are in V and R only, so no $V - I$ points are shown.

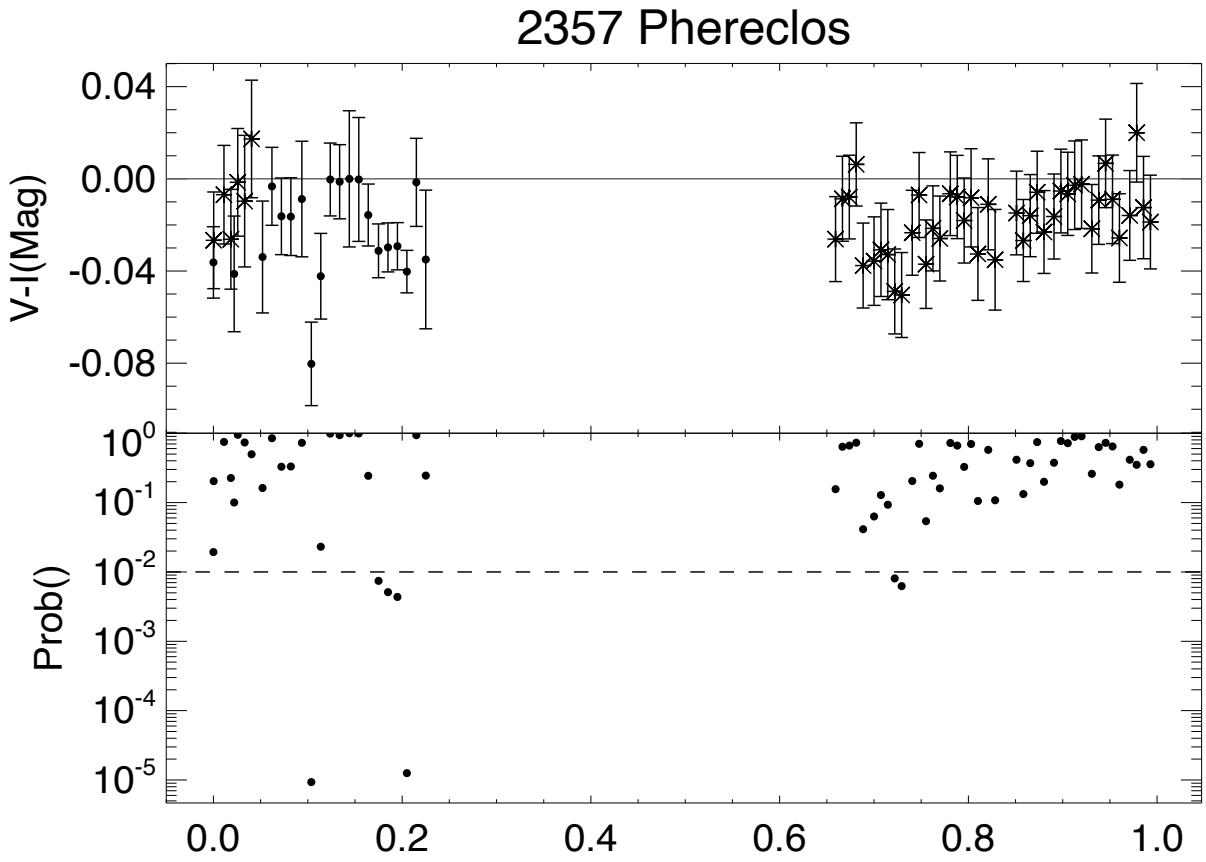

Figure 3.10: Color curve (top) and Individual Probability curve (bottom) for (2357) Phereclos during September 2011 and October 2012. We found no notable features that might be modelled (as described in Subsection 3.3.2). The dashed line shows a 99% probability that a data point represents color change. The symbols used in the color curve are the same as those used in Figure 3.9.

(2920) Automedon

Automedon was observed once a minute for one and a half hours each night on December 13th, 2011 and February 23rd, 2013; and once every two minutes for another thirty minutes on February 24th, 2013. These data were phased to a 10.212 hour rotation period (LCDB, Harris et al. 2012) in Figure 3.11. The two 2013 datasets will be properly placed with respect to each other in phase space, but the relative position between these two datsets and the 2011 data is effectively arbitrary due to the accumulation of uncertainty in the period over two years. The data have been offset from one another so as to avoid confusion. We have too little phase coverage to approximate any kind of useful amplitude, but Molnar et al. (2008) and Mottola et al. (2011) have obtained light curves for Automedon. Both of these sources found similar rotation periods and fairly standard double-peaked light curves. They observed amplitudes of 0.17 and 0.12 mag respectively. Though we do see some slope to the 2011 data, it is impossible to place this piece of the light curve into context without a significantly more refined and precise estimate of the period.

We show a mean $V-I$ color of 0.95 in Table 2.3 calculated from six individual photometric observations with a $V-I$ range of 0.05 mag. During the 2011 data (at a phase of about 0.15 in Figure 3.12) there is a small feature that could potentially be attributed to a surface color variation. However, as this candidate feature has a relatively low confidence level of 84.0%, and is uncorroborated by any overlapping data from a different night, it would require more observations to determine if it is real. Additionally, these observations would be difficult to plan due to the limited amplitude knowledge for this particular object. A full data table can be found in Table C.6.

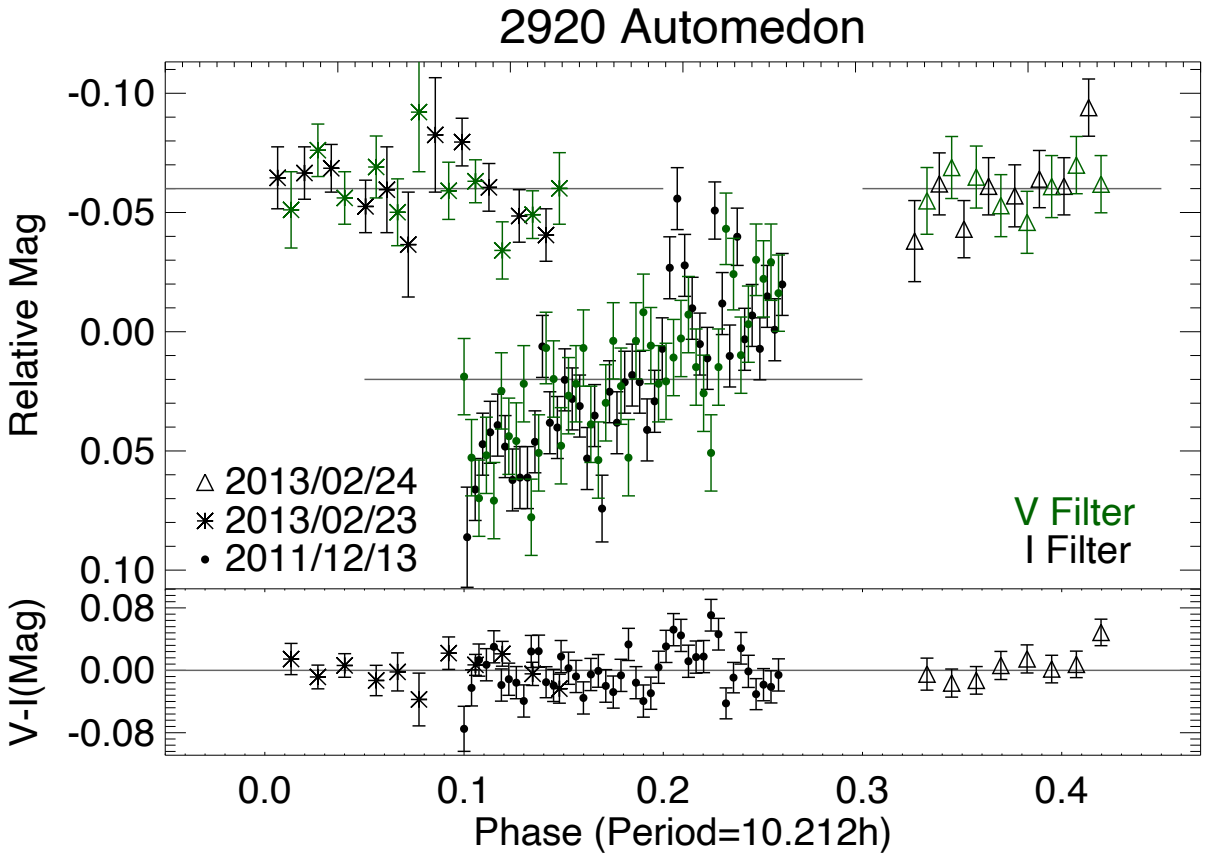

Figure 3.11: Light curve (top) and $V - I$ color curve (bottom) for (2920) Automedon during December 2011 and February 2013. The data have been offset to avoid confusion.

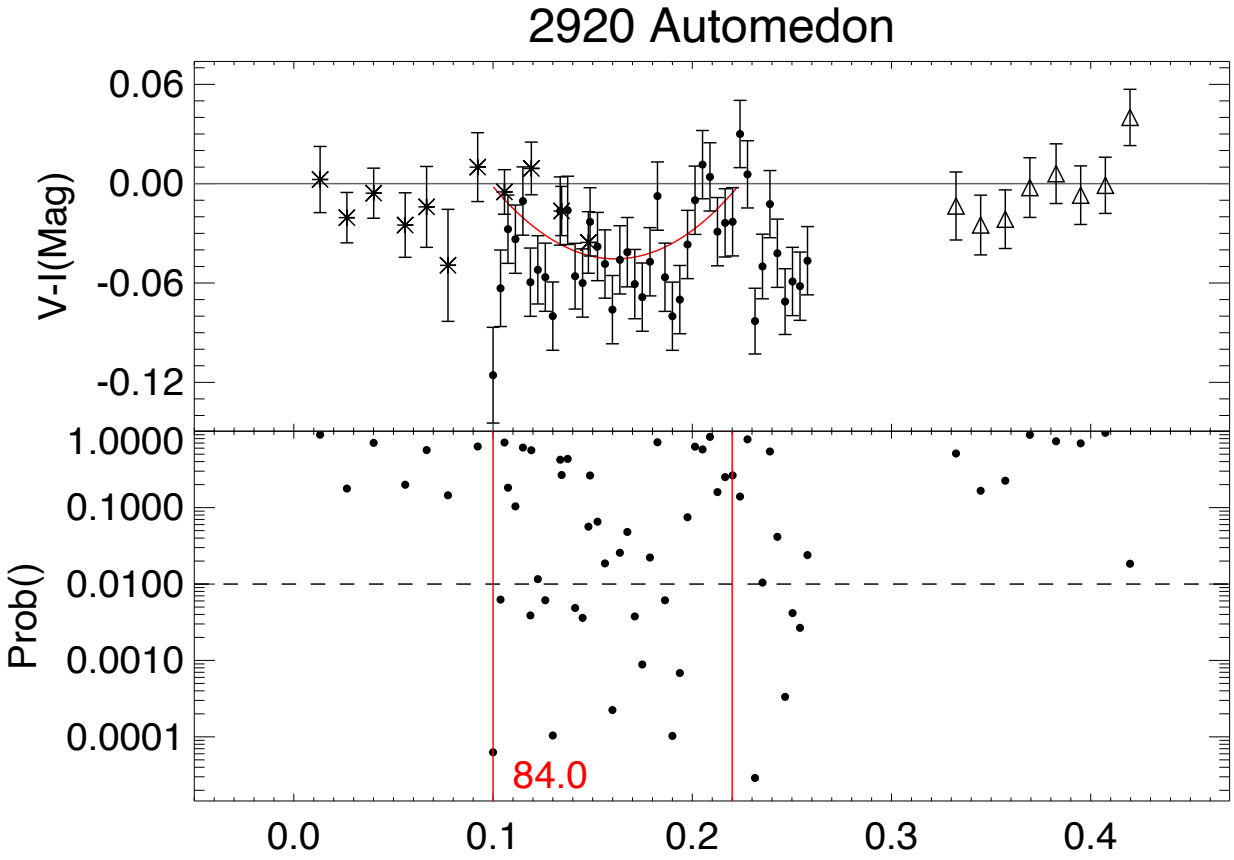

Figure 3.12: Color curve (top) and Individual Probability curve (bottom) for (2920) Automedon during December 2011 and February 2013. We model one potential feature (as described in Subsection 3.3.2) centered at phase 0.16 with a confidence level of 84.0%. The dashed line shows a 99% probability that a data point represents color change. The symbols used in the color curve are the same as those used in Figure 3.11.

(3317) Paris

Paris was observed every two minutes for about three hours on June 27th, 2011 and about two hours on August 9th, 2011. In Figure 3.13 these data were phased to a rotation period of 7.048 hours as listed in the LCDB (Harris et al. 2012). The 43 days between the two datasets only correspond to about 150 rotations for Paris. The relatively small amount of time between epochs translates into a more reliable phasing of the two datasets, which should not be off by more than 0.1 phase from their given positions. Additionally, because Paris will not have travelled far along its orbit during the elapsed time, the overall shape and amplitude of the light curve should be relatively consistent between the two apparitions. Behrend (2009), Mottola et al. (2011), and Stephens et al. (2016b) each provide light curves for Paris. They found very similar rotation periods and a complex, multi-peaked lightcurve when at low amplitude (0.08 mag) replaced by an off-center double-peaked light curve at high amplitude (0.11). Figure 3.13 shows a still fairly complex light curve with a minimum amplitude higher than those seen in the literature (0.13).

Chatelain et al. (2016) provide the mean $V - I$ color of 0.95 shown in Table 2.4 that is calculated using 13 individual photometric observations with a $V - I$ range of 0.21 mag. Variation in Figure 3.14 is small, and seems well within the expected noise. No single feature is significant enough to model, and the surface seems markedly consistent throughout the rotation. A full data table can be found in Table C.7.

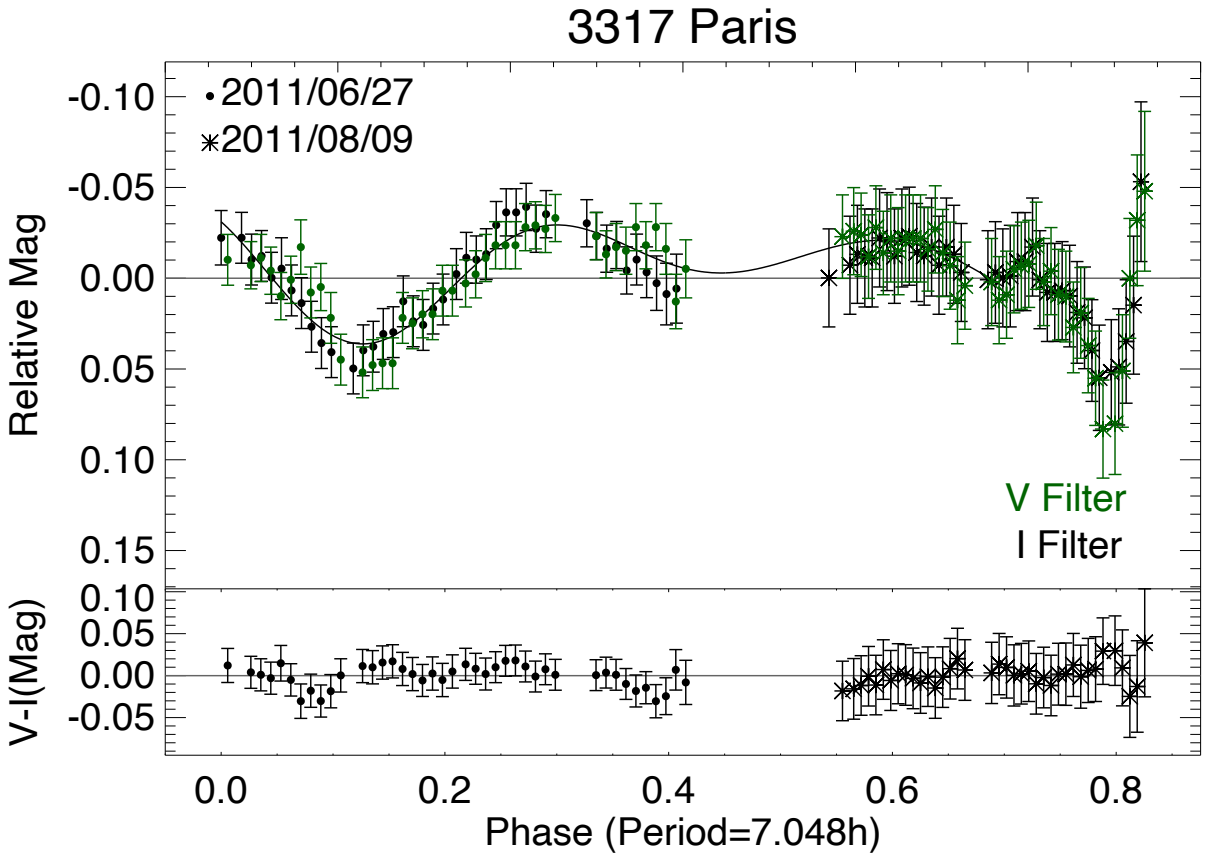

Figure 3.13: Light curve (top) and $V - I$ color curve (bottom) for (3317) Paris during June and August 2011.

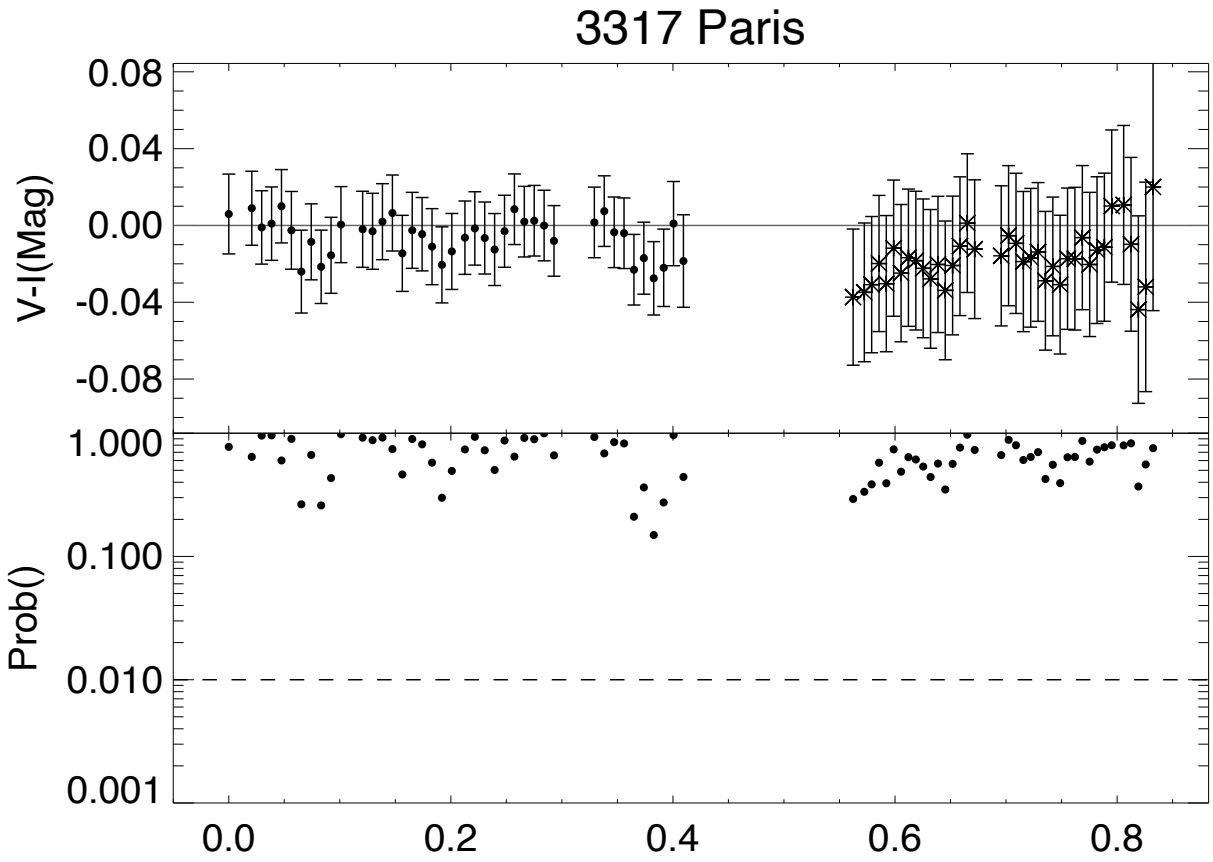

Figure 3.14: Color curve (top) and Individual Probability curve (bottom) for (3317) Paris during June and August 2011. We found no notable features that might be modelled (as described in Subsection 3.3.2). The dashed line shows a 99% probability that a data point represents color change. The symbols used in the color curve are the same as those used in Figure 3.13.

(3451) Mentor

Mentor was observed every 1.5 minutes for about five hours on August 14th, 2011; two and a half hours on September 30th, 2012; and another hour the night of October 3rd, 2012. These observations are plotted in Figure 3.15, where they are phased to the 7.730 hour rotation period provided by the LCDB (Harris et al. 2012). With over a year between the two observation epochs of 2011 and 2012, the phase of the 2011 dataset is more or less arbitrary relative to the 2012 datasets. The 2012 data were offset from the 2011 data to prevent confusion. Mentor's rotational properties have been well studied. Behrend (2009), Sauppe et al. (2007), Duffard et al. (2008), Mottola et al. (2011), French et al. (2011a), Stephens et al. (2014b), and Stephens et al. (2016b) have all collected light curves for Mentor. They found similar rotation periods and a well behaved two-peaked light curve. In amplitude, however, these sources are divided between low amplitudes (below 0.2 mag) and very high amplitudes around 0.6 mag. This disparity suggests that Mentor is a highly elongated body with a large obliquity. Our 2011 data clearly fall near an equatorial viewing geometry similar to that seen by Behrend (2009), Sauppe et al. (2007) and, and Duffard et al. (2008). The 2012 epoch does not have enough phase coverage to reasonably determine an amplitude, but based on the 2011 epoch and the amplitudes in the literature, we can assume it would not have been above 0.4 mag.

Chatelain et al. (2016) calculate 0.78 mag for the mean $V-I$ color of Mentor. This is also shown in Table 2.4, and the value is calculated using six individual photometric observations with a total $V-I$ range of 0.08 mag. There is a signature in Figure 3.16 for the 2011 data around phase 0.4 that has a confidence level of 95.9%. There is also a fairly strong signature

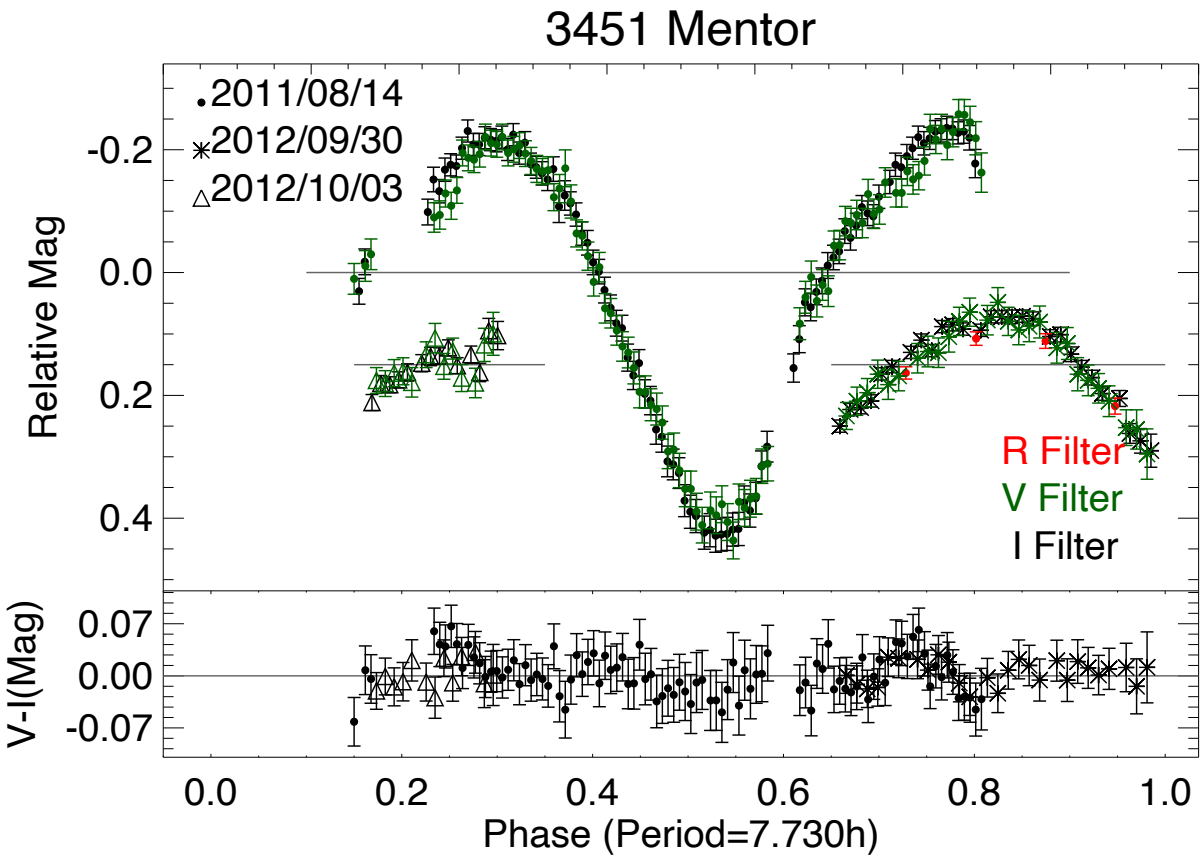

Figure 3.15: Light curve (top) and $V - I$ color curve (bottom) for (3451) Mentor during August 2011 as well as September and October of 2012. The 2012 datasets have been offset to avoid confusion.

in the 2011 data at a phase of 0.8, but we did not get enough data to fit a model. It is also possible that there is a corresponding signature in the September 2012 data at this same phase, but the feature is so small that it would need to be at a much higher obliquity to be the same feature a year later. A full data table can be found in Table C.8.

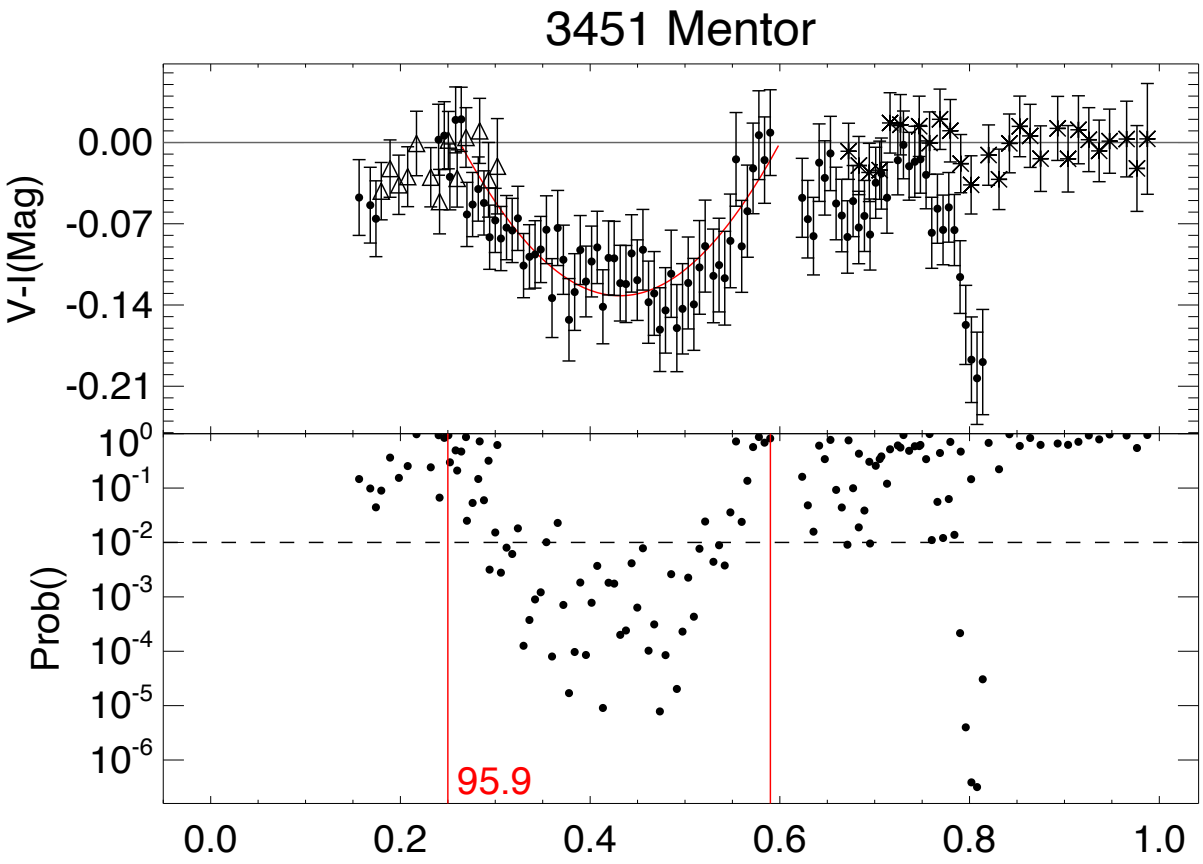

Figure 3.16: Color curve (top) and Individual Probability curve (bottom) for (3451) Mentor during August 2011 as well as September and October of 2012. We model one potential feature (as described in Subsection 3.3.2) in the 2011 data, centered at phase 0.46 with a confidence level of 95.9%. We see no features in either of the 2012 data sets, but we see another high confidence color change in the 2011 data around a phase of 0.8. More data would be needed to reasonably model this feature. The dashed line shows a 99% probability that a data point represents color change. The symbols used in the color curve are the same as those used in Figure 3.15.

(3793) Leonteus

Leonteus was observed for just thirty minutes on November 15th, 2011 but was followed up with an observation each minute for nearly two hours of observations on December 11th, 2011 and once every four minutes for another four and a half hours on February 23rd, 2013.

These observations are plotted in Figure 3.17, phased to a 5.622 hour rotation period from the LCDB (Harris et al. 2012). With only a month between the two 2011 datasets, the uncertainty in the period is unlikely to change their phase relative to each other. The 2013 data, however, has no phase relationship with the other two datasets due to the several years between epochs. For this reason, the 2013 data were offset from the 2011 data to prevent confusion. Additionally, a sizeable (two hour) gap is present in the middle of the 2013 data; however, due to the short period, the two halves of the night have phased together. Light curves for Leonteus have previously been produced by Mottola et al. (2011), Stephens et al. (2016a), and Stephens et al. (2016c). These sources found similar rotation periods once the high obliquity was taken into account. For many of these observations Leonteus presented a nearly pole-on view with a nearly featureless light curve and an amplitude as low as 0.06 mag. Intermediate amplitudes of 0.11 mag were seen by Stephens et al. (2016a) and Stephens et al. (2016c), while a typical double-peaked light curve with a 0.21 mag amplitude was observed by Mottola et al. (2011) in 1994. Our data are likely taken closer to an equatorial apparition, as we show an amplitude of at least 0.38 mag, which is significantly larger than any amplitude reported to date. We believe Leonteus is a moderately elongated object with a pole orientation of nearly 90°.

We calculate a mean $V - I$ color for Leonteus of 0.78 mag using three individual photometric observations with a total $V - I$ range of 0.01 mag (Table 2.3). All variation in color in Figure 3.18 appears to be well within the general scatter and smaller than the average error. A full data table can be found in Table C.9.

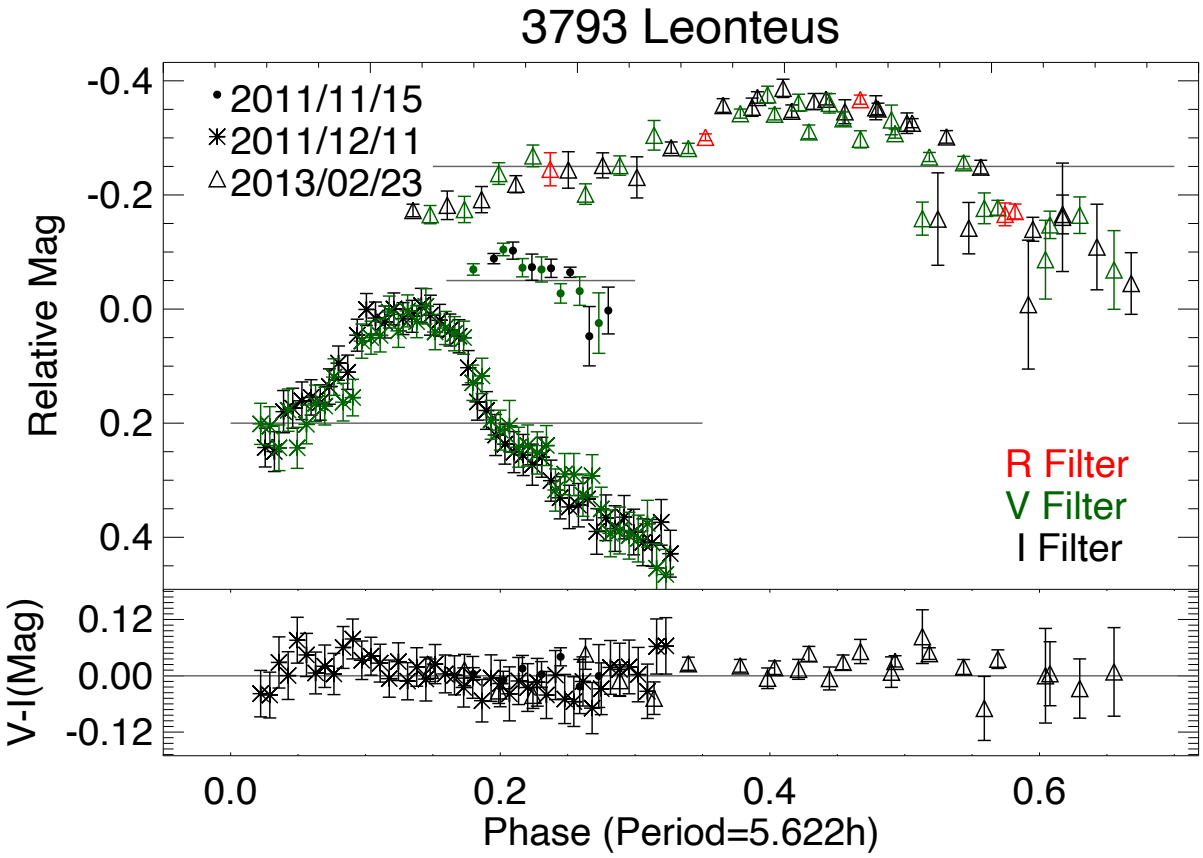

Figure 3.17: Light curve (top) and $V - I$ color curve (bottom) for (3793) Leonteus during 2011 and 2013. Due to the large variation in light curve shape and amplitude, individual datasets have been offset from one another.

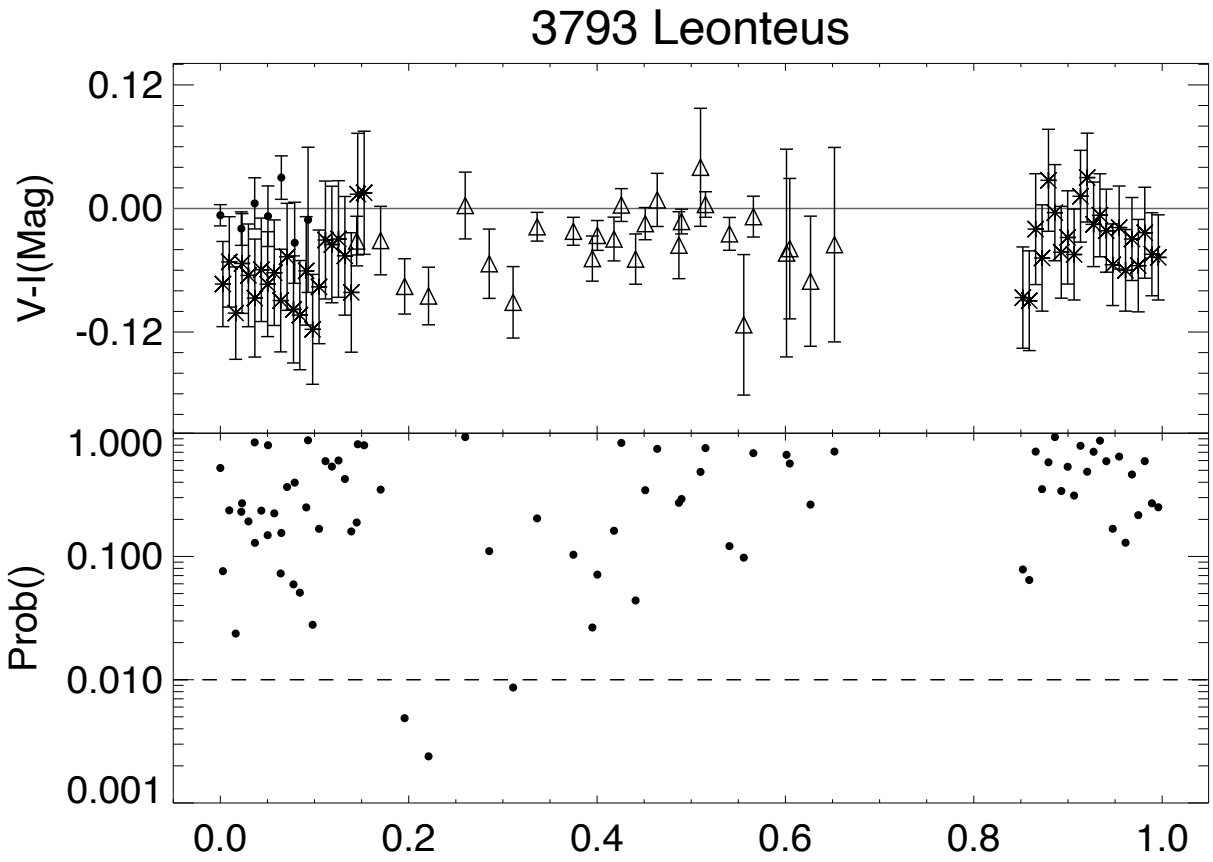

Figure 3.18: Color curve (top) and Individual Probability curve (bottom) for (3793) Leonteus during 2011 and 2013. We found no notable features that might be modelled (as described in Subsection 3.3.2). The dashed line shows a 99% probability that a data point represents color change. The symbols used in the color curve are the same as those used in Figure 3.17.

(4709) Ennomos

Ennomos was observed every two minutes for two and a half hours on September 5th, 2011. It was also observed in November 2013 for two and a half hours on the both 7th and 8th. The resulting light curve is plotted in Figure 3.19, phased to the 12.269 hour best fit rotation period found by R. Stephens (personal communication, June 5, 2017). With only a fraction of the full rotation period covered, it is difficult to get an accurate sense of global properties, such as light curve amplitude. However, Mottola et al. (2011), Stephens et al. (2016a), and Stephens et al. (2016b) did manage full phase coverage for Ennomos. The sources that calculated rotation periods largely agreed in their findings, and showed a light curve with a very large disparity between the two maxima with consistent amplitudes between observations ranging from 0.45 to 0.46. Unfortunately, without more data we cannot add useful amplitude information to this earlier collection.

A mean $V-I$ color for Ennomos is reported by Chatelain et al. (2016) to be 0.69 mag and is calculated using seven individual photometric observations with a total $V-I$ range of 0.09 mag (Table 2.4). Importantly, it has been hypothesized by Shevchenko et al. (2012b) that the significant difference between the maxima is the result of a bright albedo spot covering up to 30% of the surface of Ennomos. Such a large change in albedo should be visible as a change in color from the bright maximum to the fainter maximum. This albedo change may be visible in our data during the 2013 apparition from phase 0.1 to 0.3 in Figure 3.20. The steep slope of the V data appears to capture part of the large peak, and shows a sharp contrast to the behavior of the I data over the same period. This results in a large swing in relative color for both nights. This likely shows the results of a significant feature on the

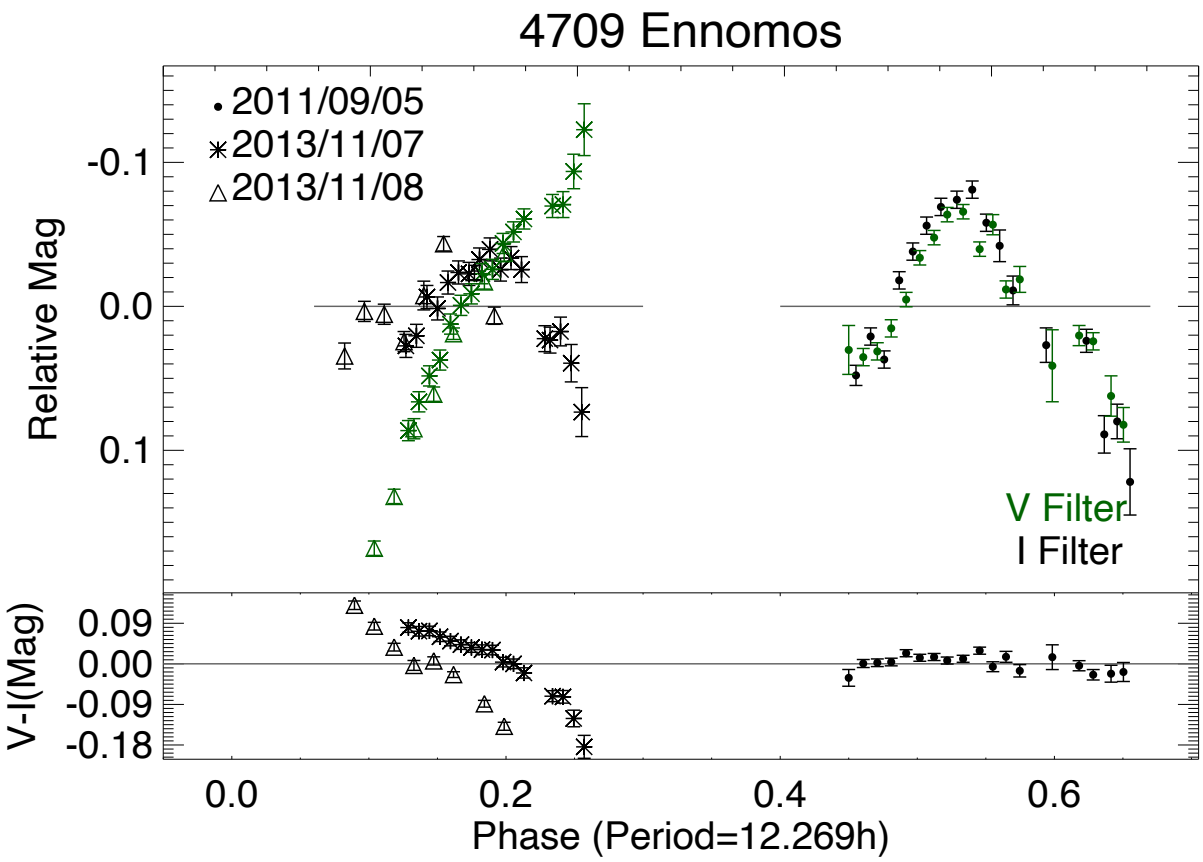

Figure 3.19: Light curve (top) and $V - I$ color curve (bottom) for (4709) Ennomos during September 2011 and November 2013. The 2013 data are only one night apart, they have been shifted in Relative Magnitude so that the nights better align.

surface of Ennomos that corresponds to the asteroid's primary peak. A color curve over the full rotation period is needed to model this feature more precisely. A full data table can be found in Table C.10.

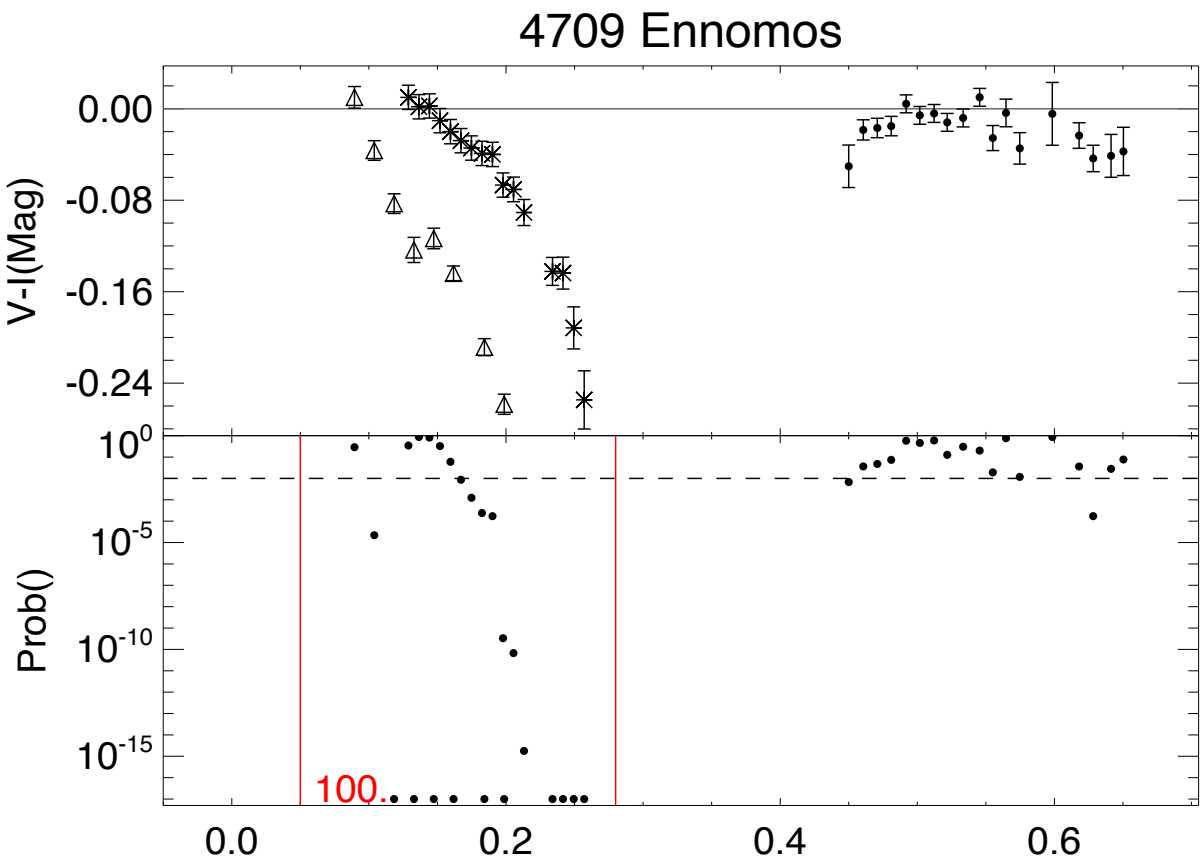

Figure 3.20: Color curve (top) and Individual Probability curve (bottom) for (4709) Ennomos during September 2011 and November 2013. We found indications of very large color change in the 2013 data near phase 0.2, but no signs of variation in the 2011 data. There is not enough data to reasonably model this change as a feature (as described in Subsection 3.3.2), but the confidence level in this feature is effectively 100%. Additionally, it is likely that the color change shown between the two nights in 2013 is cumulative, making the net variation even greater. The dashed line shows a 99% probability that a data point represents color change. The symbols used in the color curve are the same as those used in Figure 3.19. Note: The software used to calculate the probability that an individual data point is consistent with 0 (no net change) fails beyond 10^{-17}.

(4833) Meges

Meges was observed once every ten minutes for about five hours each night on February 8th, 9th, 16th, and 17th, 2015. These four epochs create a full composite light curve that was

phased to the 14.250 hour rotation period as is reported in the LCDB (Harris et al. 2012). The full light curve and resulting color curve are shown in Figure 3.21. Due to the proximity of the nights that went into this composite, the uncertainty in the period will not have a large effect on the phase of the individual epochs. Light curves of Meges were also gathered by Mottola et al. (2011) and Stephens et al. (2016c). Both of these observations found similar rotation periods and light curve shapes. The amplitudes found in these sources, ranging from 0.13 to 0.27, encompass the 0.17 amplitude we see.

Neither of these sources published any color information, though we provide a mean $V-I$ color of 0.94 in Table 2.3 which was averaged from two individual photometric observations that had a $V-I$ range of 0.04 mag. With over twenty hours of coverage of a 14.25 hour rotation period we have significant overlap in what turns out to be some very interesting parts of the light curve. Specifically, in Figure 3.22, we see what appear to be periodic features in the color curve that are present with similar slopes on multiple nights. This behavior is consistent with a large, fresh crater that takes up a significant portion of the projected surface area of the asteroid. We model features that together cover most longitudes of Meges and have confidence levels of 99.9%, 99.9%, and 95.3%. A full data table can be found in Table C.11.

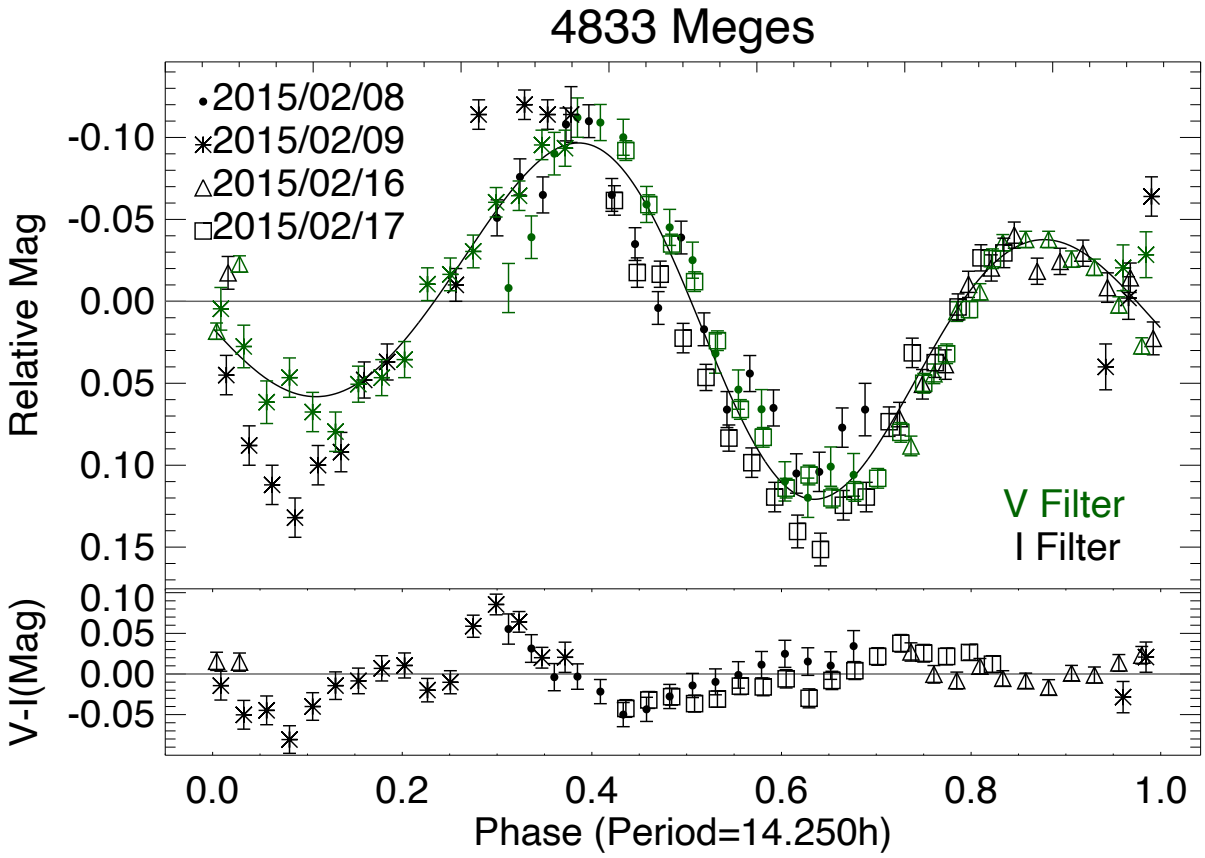

Figure 3.21: Light curve (top) and $V - I$ color curve (bottom) for (4833) Meges during February 2015.

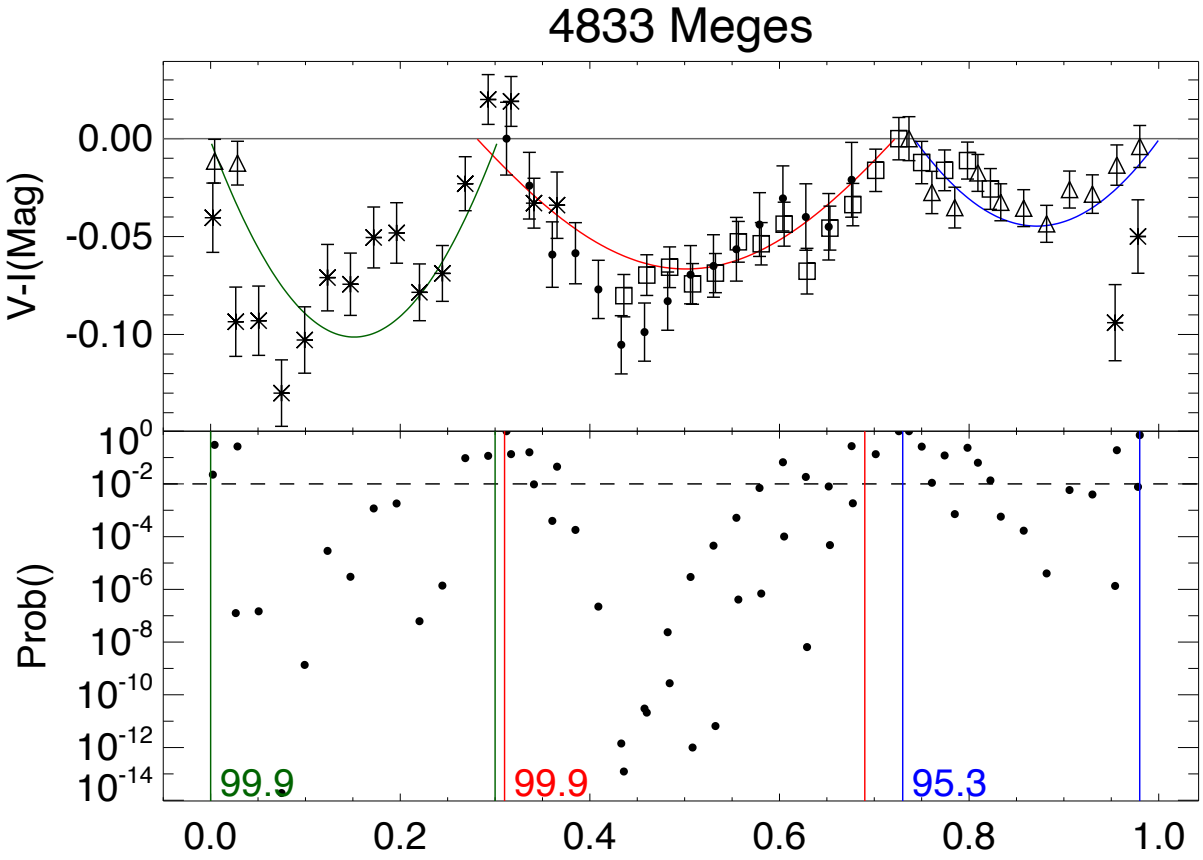

Figure 3.22: Color curve (top) and Individual Probability curve (bottom) for (4833) Meges during February 2015. We model three potential features (as described in Subsection 3.3.2) centered at phase 0.15, 0.5, and 0.87 with a confidence level of 99.9%, 99.9%, and 95.3% respectively. The dashed line shows a 99% probability that a data point represents color change. The symbols used in the color curve are the same as those used in Figure 3.21.

(5144) Achates

Achates was observed every 2.5 minutes for six hours and ten minutes on June 26th, 2011. With these observations we manage complete phase coverage for the entire 5.958 hour rotation period reported by the LCDB (Harris et al. 2012). The resulting full light curve is plotted in Figure 3.23. Previously, Molnar et al. (2008), Mottola et al. (2011), and Stephens et al. (2015) published light curves for Achates. They largely agreed on the period and show a fairly simple double-peaked light curve. Molnar et al. (2008) shows a bit more of the complexity that we see near the secondary minimum. Published amplitudes vary from 0.20 to 0.35 mag, making the observed amplitude of 0.14 presented here the smallest yet seen.

A mean $V - I$ color for Achates of 0.92 mag is reported by Chatelain et al. (2016) using nine individual photometric observations with a total $V-I$ range of 0.09 mag (Table 2.4). There are two large outliers near phase 0.05 and 0.65 in the color curve for Achates (Figure 3.24). For our analysis, we assume these outliers are artefacts and ignore them when fitting the models to the rest of the data. Once this is done we see two possible features that dominate the color curve with confidence levels of a moderate 91.5% and a low 77.9%. A future color curve when Achates shows a larger light curve amplitude might confirm the existence of these potential features. A full data table can be found in Table C.12.

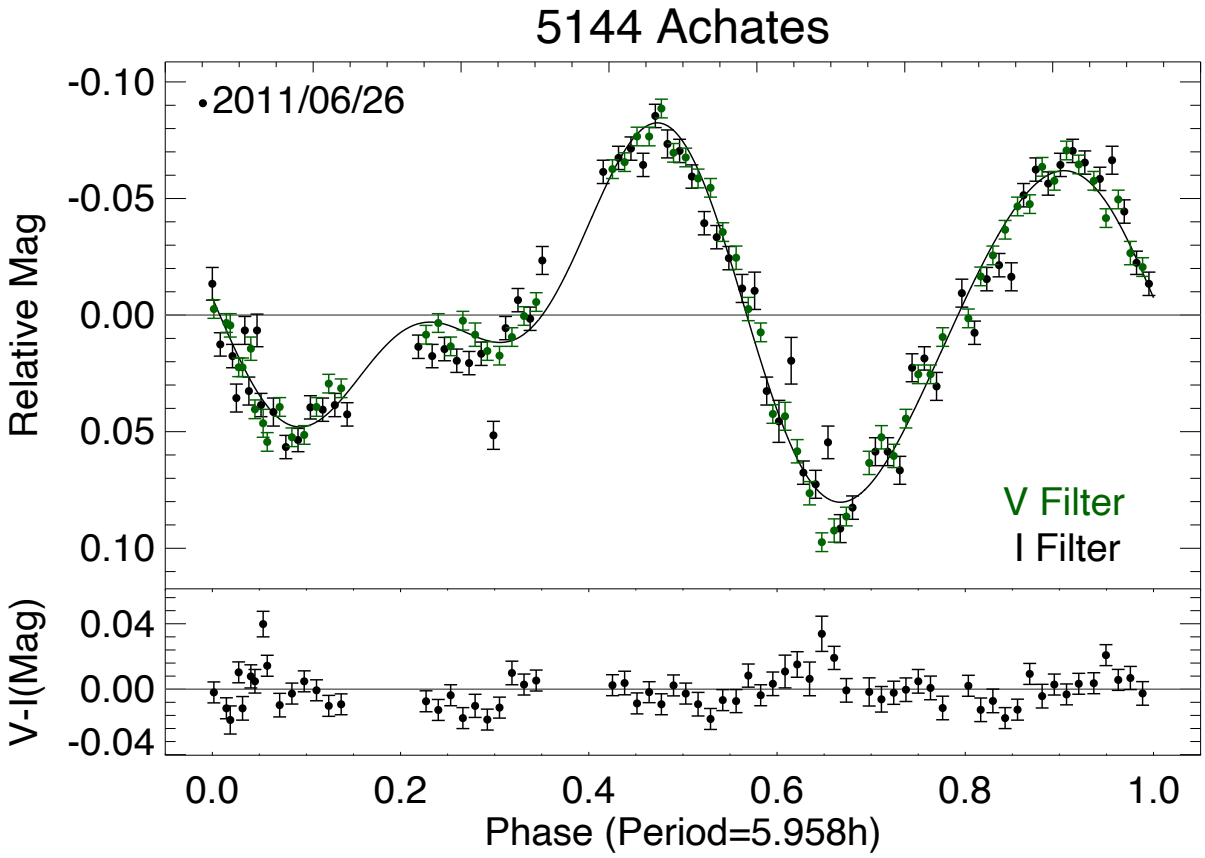

Figure 3.23: Light curve (top) and $V - I$ color curve (bottom) for (5144) Achates during June 2011.

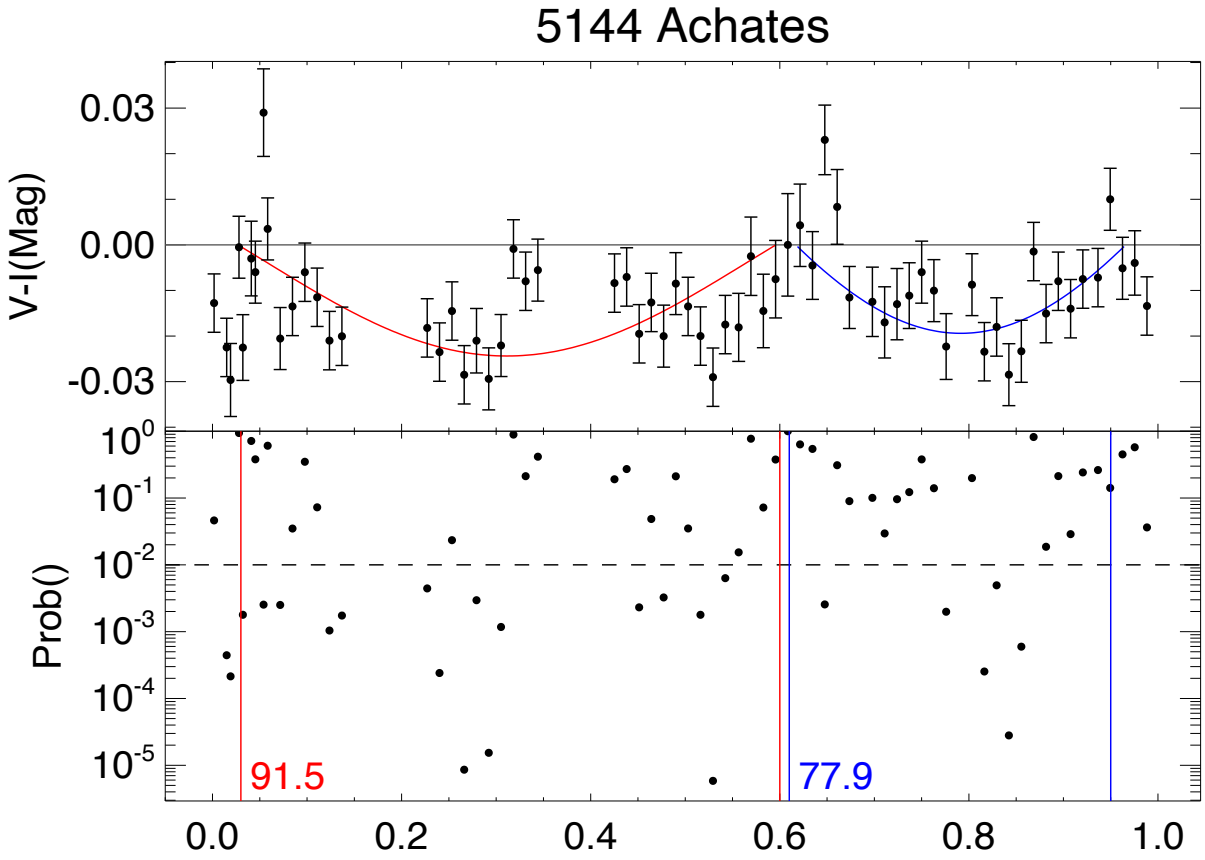

Figure 3.24: Color curve (top) and Individual Probability curve (bottom) for (5144) Achates during June 2011. We model two potential features (as described in Subsection 3.3.2) centered at phase 0.33 and 0.8 with a confidence level of 91.5% and 77.9% respectively. The dashed line shows a 99% probability that a data point represents color change. The symbols used in the color curve are the same as those used in Figure 3.23.

3.5 Summary

We summarize the color curve study of the twelve objects listed here in Table 3.2. Of these objects, we find one object, (4833) Meges, with confirmed signs of color variation over its surfaces that are highly indicative of a surface feature. The fact that the variations seen on this object are present over multiple nights rules out any statistical or photometric anomalies. Another object, (4709) Ennomos, shows very strange color behavior that is likely indicative of a massive surface feature with a highly different color profile to that of the surrounding material. Two additional objects, (884) Priamus and (3451) Mentor, display the signatures for surface features at a confidence level over 95%. (1143) Odysseus and (5144) Achates each show signs of at least one feature with a confidence level of 90% or more, while (2207) Antenor and (2920) Automedon display even weaker signals. The remaining four targets show no significant signs of variation, though additional light curves with more complete coverage at a variety of aspect angles could prove that these objects also possess surface variation. overall, we conclude that at least seven of the twelve asteroids studied certainly or almost certainly show color variation over their surface. This implies that cratered or mottled surfaces are common among Jupiter Trojans, suggesting a more active collisional history and/or a slower weathering process than previously suspected. Without more data, the model used for this work is extremely limited in its predictive capabilities, as there are several variable combinations capable of producing identical shape profiles. Specifically, we would need a precise measurement of the aspect angle during a given apparition and observations of the same feature at a variety of epochs. With more data, models could be developed to more precisely calculate the relative surface areas, latitudes, and colors of

these large surface features, which in turn would lead us closer to an understanding of the individual histories of these select objects.

Additionally, this study has important implications for our work in Trojan photometry, specifically as it applies to Chapter 2. For these twelve objects, we find an average spread of nearly 0.1 mag in $V - I$ color over the course of an object's rotation. This spread may be caused by either coherent variation as is seen in 4833 Meges (Figure 3.21) or a more random scattering as seen in 2357 Phereclos (Figure 3.9). This means that a single epoch of photometry is unreliable for determining an object's true mean color to a precision better than 0.05 mag, as the intrinsic variability of the asteroid may be larger than this. This additional source of error, which is not known *a priori*, is of the same order of magnitude as the total median photometric errors calculated for Jupiter Trojans in Table 2.2. However, this error for a mean color rapidly diminishes with additional data that sample a range of points along the asteroid's rotational phase.

Table 3.2: Potential Color Features

	$V-I$			Potential Features				
Asteroid	Mean (Mag)	Min (Mag)	Max (Mag)	Epoch (MM/YY)	Center (Phase)	Depth (Mag)	Width (Phase)	Confidence Level (Percent)
(884) Priamus	0.90	0.86	1.00	11/11	0.15	0.036	0.17	96.5
				11/11	0.32	0.049	0.18	97.0
(911) Agamemnon	0.98	0.91	0.99	–	–	–	–	–
(1143) Odysseus	0.86	0.86	0.97	10/10	0.12	0.050	0.18	93.4
				10/10	0.31	0.040	0.14	93.5
(2207) Antenor	0.95	0.81	1.06	11/11	0.01	0.035	0.36	78.4
				09/12	0.65	0.060	0.60	88.0
(2357) Phereclos	0.96	0.90	1.05	–	–	–	–	–
(2920) Automedon	0.95	0.93	0.98	12/11	0.16	0.050	0.12	84.0
(3317) Paris	0.95	0.90	1.11	–	–	–	–	–
(3451) Mentor	0.77	0.73	0.81	08/11	0.43	0.130	0.34	95.9
(3793) Leonteus	0.78	0.70	0.79	–	–	–	–	–
(4709) Ennomos	0.69	0.65	0.74	11/13		> 0.26		~ 100
(4833) Meges	0.94	0.90	0.94	02/15	0.15	0.045	0.30	99.9
				02/15	0.50	0.068	0.38	99.9
				02/15	0.87	0.100	0.25	95.3
(5144) Achates	0.92	0.88	0.97	06/11	0.31	0.024	0.57	91.5
				06/11	0.79	0.020	0.34	77.9

$V-I$ values are discussed in Chapter 2

The width of a feature in phase space is effectively the fraction of the rotation period for which the feature is visible during that epoch.

Features with confidence levels above 95% are considered highly probable and have been highlighted.

– 4 –

1173 Anchises: Rotational Properties

4.1 Introduction

We have acquired several epochs of data for (1173) Anchises[1]. Anchises is a Jupiter Trojan within the L5 swarm 60° behind Jupiter in its orbit. Anchises has been observed several times since its discovery by K. Reinmuth in 1930, with previous amplitude[2] and period estimates by French (1987) (data we incorporate here) as well as a more recent light curve by Stephens et al. (2016b) which we do not include. Several thermal observations were made (Grav et al. 2011; Horner et al. 2012) that have been used for size and albedo estimates. Well-determined orbital and physical properties of Anchises are given in Table 4.1. Anchises is of particular interest due to its large photometric amplitude of over 0.6 magnitudes as well as its similar size and taxonomic type to some of the targets that the *Lucy* spacecraft is scheduled to visit in the near future (see Section 6.3). Additionally, French (1987) observed little or no opposition surge, which is unusual for a P-type asteroid like Anchises. here we add to these measurements and present a much more precise rotation period, as well as shape and pole orientation, using data from five epochs spanning over a third of the object's orbital path.

[1]This work was submitted to *Icarus* in March 2017.

[2]An asteroid's amplitude (often written as Δm) is roughly the difference in magnitude between the maximum and minimum brightness of the object over a full rotation period, at a certain aspect angle, once other effects such as phase and a change in distance have been removed. This change of brightness is typically independent of observation filter as it is usually dominated by the projected shape of the object rather than albedo changes.

Table 4.1: Anchises: Orbital and Physical Properties

(1173) Anchises 1930_{UB}

Orbital Elements			Physical Properties		
Semi-Major axis	(a)	5.30 AU	Absolute Magnitude	(H_V)	8.89 mag
Eccentricity	(e)	0.137	Effective Diameter	(D)	99.5 km
Inclination	(i)	6.92°	Geometric Albedo	(p)	0.050
Argument of Perihelion	(ω)	40.8°	Rotation Period	(P_{rot})	11.60 h
			Phase Slope[a]	(G)	0.15
Longitude of the Ascending Node	(Ω)	283.9°	Color[b]	(B-V)	0.691 mag
				(V-I)	0.78 mag
Perihelion Date	(t_p)	2455922.329 JD		(B-R)	1.08 mag
Orbital Period	(P)	12.20 years	Spectral Type[c]		P

Orbital and physical properties of (1173) Anchises are from the JPL Small-Body Database: http://ssd.jpl.nasa.gov/sbdb.cgi?sstr=1173.

[a] Assumed value.

[b] $(V-I)$ and $(B-R)$ are mean color values calculated by Chatelain et al. (2016).

[c] In Chapter 2 we determine Anchises to be an X-type object, which includes objects classified as P-type under earlier taxonomic schemes. (See Section 5.1 for a more in-depth discussion of the history of asteroid taxonomy.)

4.2 Observations and Data Reduction

French (1987) observed Anchises over five nights from July 3rd 1986 through July 10th 1986. These relatively low phase observations represent a baseline period determination for this work. These observations were made using the Cerro Tololo (CTIO) 0.9m telescope. French (1987) found a period of 11.6095 ± 0.0036 h and an amplitude (Δm) of about 0.57 mag.

From 2011 to 2015, four epochs of light curve observations of Anchises were made. Details of these observations, as well as the 1986 observations made by French (1987) are summarized in Table 4.2. Our first observations were obtained on a single night on August 8th 2011 on the CTIO/Yale 1.0m telescope. Data were taken in both the V and I filters with the purpose of searching for signs of color variation over a rotation. We found a rotation period consistent with that found by French (1987) and a Δm of about 0.45 mag. The October, 2012 epoch consists of data taken over two nights approximately a week apart on September 30th and October 7th. Observations were made on the CTIO 0.9m telescope in both V and I filters.

Anchises was observed again in September, 2013 on the 20th and 25th using the Lowell 31in robotic telescope. Unfortunately, the I frames from these observations have a larger than normal error due to significant amounts of fringing. The Lowell 42in telescope was used for four nights (the 7th, 8th, 16th, and 17th) of observations in February, 2015. Alternating images in V and I were once again taken.

The data from August 2011 through February 2015 were processed using IRAF CCD reduction procedures described by Jao et al. (2005) and Winters et al. (2011). The bias-subtracted, flat-fielded images were further reduced using the *MPO Canopus* software (Bdw Publishing). This software was used to construct relative photometry of Anchises by removing airmass and sky variations by means of in-field calibration stars. All of the photometry was light-travel corrected[3] and then used for more extensive analysis. These data can be found in Section D.

[3]Due to the changing distance between the Earth and the object, the light travel time between the two is subtracted from the observation times so that the observations correspond to local time at the object and are independent of the observer's relative location.

Table 4.2: Anchises: Light Curve Epochs

Epoch	July 1986[a]	Aug. 2011	Oct. 2012	Sept. 2013	Feb. 2015
Telescope	CTIO 0.9m	CTIO 1.0m	CTIO 0.9m	Lowell 31in	Lowell 42in
Dates	03,04,05,10	08	09/30,10/07	20,25	07,08,16,17
Hours Observed	23.72	9	11.25	16.75	18.65
α (°)[b]	1.196	1.915	4.617	7.247	10.32
λ_A (°)[b]	289.6	307.8	350.2	37.06	62.48
β_A (°)[b]	0.703	3.817	8.191	8.016	3.783
r (AU) [b]	4.667	4.593	4.646	4.913	5.425
Δ (AU)[b]	3.655	3.588	3.704	4.084	5.175
Δm (mag)	0.5305	0.4524	0.1452	0.10	0.29
Δm error (mag)	0.0087	0.0048	0.0064	0.01	0.01

α is the mean phase angle over the observation nights in degrees.
λ_A and β_A are the mean Ecliptic Longitude and Latitude respectively of Anchises in a geocentric reference frame over the course of observations for that epoch.
r is the distance of Anchises from the Sun, while Δ is the distance of Anchises from Earth.
Δm is the amplitude calculated from the best 4th-order Fourier fit to the reduced light curve data.
[a] from French (1987)
[b] Calculated using JPL HORIZONS system: `http://ssd.jpl.nasa.gov/horizons.cgi`

4.3 Analysis and Results

A fourth order Fourier series was fit to the light curves (shown in Figure 4.1) output by *Canopus*. A fourth order fit was found to provide the best fit to the data without any unreasonable, artificial wiggles in the light curve, and was also the order used by French (1987). These fits were used to calculate amplitudes by taking the mean of the two maxima and subtracting the mean of the two minima. This method minimizes discrepancies between the true, bulk shape of the asteroid and a smooth ellipsoid model. Amplitude errors were calculated using a Monte-Carlo simulation that found the range of possible amplitudes at each epoch when individual data points were varied randomly within a Gaussian distribution calibrated to their 1σ error bars. Results for both the amplitude (Δm) and its error (Δm error) are given for each epoch in Table 4.2. As Anchises travels around the Sun, a different orientation is presented to Earth, resulting in changes in the amplitudes of the observed light

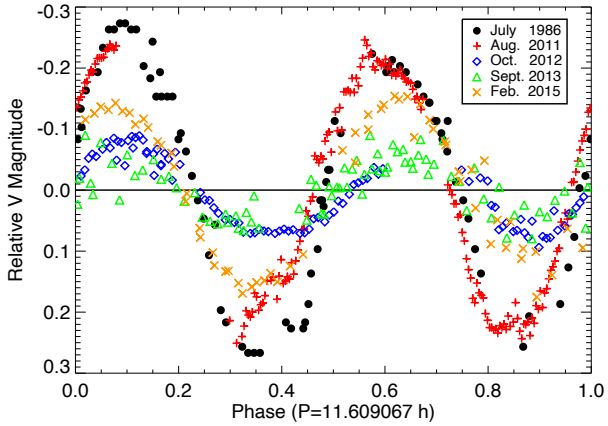

Figure 4.1: The relative V filter light curves for each epoch shown in Table 4.2 phased to the best fit period. Note the change in amplitude with time. July 1986 data are from French (1987).

curves. These changes are shown in Figure 4.2 along with the geocentric, ecliptic longitudinal position of Anchises.

4.3.1 Rotation Period

In an iterative process, the Fourier fits were used to calculate a sidereal rotation period for Anchises. Rotation periods at each epoch were individually consistent with the 11.6 hour period found by French (1987) each with errors ranging from 0.05 to 0.008 hours. They also showed a strong signal at the half-period of about 5.8 hours. To be compatible with each other, data from each epoch were corrected for light travel time and adjusted to account for the changing position of Anchises and Earth. To calculate this rotation period, Fourier fits were found for each epoch and then phased. The best fit period to all of the data was then calculated and used for all future fits. When combined, all five epochs cover a nearly 30 year baseline, and have been used to calculate a very precise sidereal rotation period for Anchises of 11.609067 ± 0.000002 hours or $11h36m32.644s \pm 0.007s$. This precision is

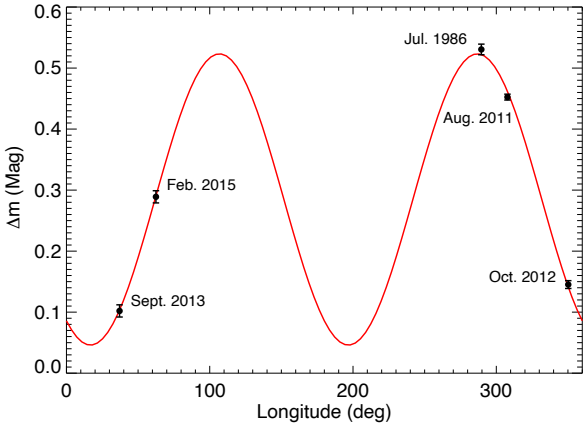

Figure 4.2: A sinusoidal fit for the change of Anchises' amplitude with geocentric ecliptic longitude based on the data from five epochs given in Table 4.2. This is a basic, rudimentary model from which some rough pole and axis information can be extracted. It serves as a good check for our more complex amplitude-aspect model.

possible because of the slight difference between the two light curve maxima (Figure 4.1) that allows for a differentiation of otherwise degenerate rotation periods. Error in the rotation period was calculated using a Monte-Carlo simulation where the individual data points were varied within a Gaussian distribution with a width equal to the 1σ error of the data points. It should be noted that any short term change in the rotation period over the thirty years covered by these observations is negligible compared to the several minutes to tens of seconds error on the periods found for individual light curves.

4.3.2 Pole Position and Axis Ratios

In order to find the pole position and axis ratios, we used the amplitude variation model described in Magnusson (1986)

$$\Delta m(\psi_i, \alpha_i) = 1.25 log[\frac{(b/c)^2 cos^2\psi_i + sin^2\psi_i}{(b/c)^2 cos^2\psi_i + (b/a)^2 sin^2\psi_i}] + \beta_A \alpha_i \tag{4.1}$$

where ψ_i is the aspect angle (the angle between the asteroid's c-axis and line of sight to Earth) for observation i, a/b and b/c are axial ratios greater than or equal to 1, β_A is the amplitude phase coefficient described below, and α_i is the phase angle of the asteroid at the time of observation i.

The aspect angle ψ_i can be defined for each epoch as

$$\psi_i = 90 - arcsin[sin\beta_{\oplus,i} sin\beta_p + cos\beta_{\oplus,i} cos\beta_p cos(\lambda_{\oplus,i} - \lambda_p)] \tag{4.2}$$

where λ_p and β_p are the heliocentric ecliptic longitude and latitude of the pole of Anchises, and $\lambda_{\oplus,i}$ and $\beta_{\oplus,i}$ are the ecliptic longitude and latitude for Earth at observation i, all in a reference frame centered at Anchises.

We used a grid search to simultaneously fit the pole position and axial ratios by minimizing the difference between the observed amplitudes and the model for a tri-axial ellipsoid with axes $a \geqslant b \geqslant c$. The results of this grid search can be seen in Figure 4.3. There is a 4-fold degeneracy in the pole orientation with this model, but the axis ratios were found to be consistent for all pole solutions.

When no bounds were placed on the minimization function we found axial ratios of $a/b = 1.62 \pm 0.02$ and $b/c = 0.91 \pm 0.1$. This is consistent with a b/c value of 1. When a lower bound of 1 is placed on the b/c ratio, a best fit for a/b of 1.61 is found. This is well within the error determined by a 10% level above the best fit χ^2.

We found the pole position to be best fit at ecliptic longitude and latitude (198, -29) and (18, 29), with 1 sigma errors of about $\pm 1.5^\circ$ in longitude and $\pm 5^\circ$ in latitude. The two values are mirrors of each other and therefore indistinguishable with the amplitude method.

The pole coordinates (198, 6) and (18, −6) are also well fit, but have a best fit χ^2 more than 10% higher than the pole solution given above. It should be noted that Horner et al. (2012) found that a retrograde rotation was best fit to their infrared (IR) models, perhaps leaving the solutions with north pole positions at negative latitudes as more probable options, thus leaving us with a preferred orientation of (198, −29) ecliptic longitude and latitude.

The amplitude phase coefficient β_A, a linear correction factor to the amplitude model, was calculated simultaneously as part of the fit parameters. This value accounts for variation of the object's amplitude with solar phase angle[4] and was found to be best fit at about 0.002 mag/deg. The amplitude phase coefficient found here is similar to values found in the literature for other objects. For example, Magnusson (1986) found values for this phase coefficient for 18 main belt objects with results ranging between 0.01 and 0 mag/deg with an average value of about 0.003 mag/deg.

These well-defined pole orientation and axial ratio results found using this amplitude-aspect model agree well with the first-order approximations that can be determined from the simple Δm-longitude model shown in Figure 4.2.

[4] β_A is a low-phase linear approximation of the non-linear effect that a changing phase angle has on an object's photometric amplitude. Phase angle affects the apparent amplitude of an object because the ratio of the projected surface area of the visible, gibbous portion of the object to the full projected area of the facing side is not a constant, but instead depends on the size of the full projected area. The concept is explored in much more detail by Zappala et al. (1990).

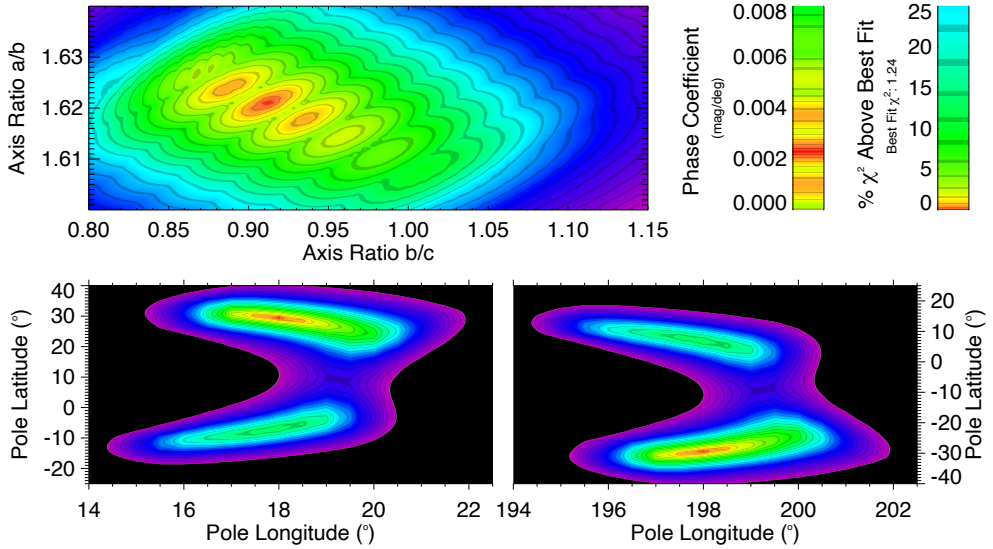

Figure 4.3: Results of a grid search for parameters in Equation 4.1 for an amplitude model with red indicating preferred results and green representing a χ^2 about 10% higher than the best fit value (top right). We find Anchises' axis ratios a/b and b/c (top left) to be best fit at 1.62 ± 0.002 and 0.91 ± 0.1 respectively. A preferred phase coefficient of 0.002 mag/deg is indicated by the top middle plot. Pole longitude and latitude (bottom) were found to be (198,−29) or (18,29) with errors of $\pm 1.5^\circ$ in longitude and $\pm 5^\circ$ in latitude. The two bottom frames are clipped to show only the best fit regions, which are reflections of each other (180° in longitude and about the ecliptic in latitude.)

4.3.3 Density

A minimum density can be found using the axial ratios and rotation period calculated above. Chandrasekhar (1969) shows the minimum density for a Jacobi ellipsoid composed of a fluid or a strengthless rubble pile in hydrostatic equilibrium. This is the density Anchises would have if it were pulled into its current shape due to rotational forces and ultimately represents a minimum density for a realistic asteroid. Such an object's angular spin frequency (ω) and its density (ρ) are related to its shape via the following:

$$\frac{\omega^2}{\pi G \rho} = 2\beta\delta \int_0^\infty \frac{u}{(1+u)(\beta^2+u)\Delta}\,\mathrm{d}u, \tag{4.3}$$

where G is the gravitational constant, the axial ratios are expressed as $\beta = b/a$ and $\delta = c/a$, and $\Delta = \sqrt{(1+u)(\beta^2+u)(\delta^2+u)}$ where u is a variable substitution for $c^2 tan^2\theta$. Solving Equation 4.3 with the axial ratios determined above, we find a minimum density of about $0.35\,g/cm^3$. This density is significantly below densities calculated for the only two Jupiter Trojans with well determined densities of $1.08\pm0.33\,g/cm^3$ and $2.480^{+0.292}_{-0.08}\,g/cm^3$ for (617) Patroclus (Mueller et al. 2010) and (624) Hektor (Lacerda & Jewitt 2007), respectively. Thus, as it is unlikely that we are probing the actual density of Anchises, we can assume that this particular object was not pulled into its elongated shape by rotational forces alone.

4.3.4 Color

Color variation is rarely observed on asteroid surfaces, but we show in Chapter 3 that some level of variability may be common among Trojans. Additionally, it is known that collisions can uncover pristine, unweathered material that differs in color from the surrounding, more weathered surface. Thus, a light curve that shows color variation can be an important indicator of recent collisional activity.

To estimate the color variation for Anchises we observed the asteroid in alternating V and I filters. The I magnitudes were interpolated between the original values to be simultaneous with the V magnitudes and then subtracted from the V values to calculate $V-I$ colors for the entire night of observations (see Table E.1 for results.) This results in color curves for the majority of the phase for each epoch for which we have data. As seen in Figure 4.4 we detect a possible reddening of a few percent at the same phase (~ 0.8 in Figure 4.4) in both the 2011 and 2012 data. The noisy nature of the 2013 I data (due to the fringing mentioned in Section 4.2) makes detection of such a subtle feature difficult for this epoch. The 2015

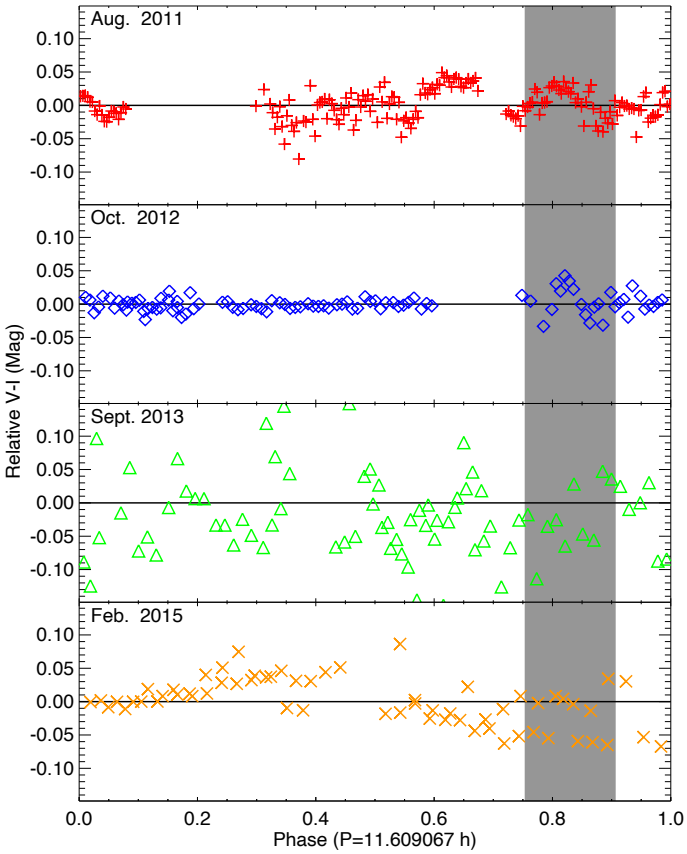

Figure 4.4: Relative $V-I$ color for each recent epoch, redder values are positive. The gray bar near phase = 0.8 is the region of interest. Possible variations can be seen in 2011 and 2012, but there is nothing obvious in 2013 and 2015. As can be seen from Figure 4.2, the viewing geometry is changing over these observations from a nearly equatorial sub-observer latitude in August 2011 to a nearly pole on orientation in October 2012 and September 2013. By February 2015, the sub-observer latitude is once again approaching the equatorial zone. It is surprising then that we do not see any features during this epoch. All data are phased in the same way as shown in Figure 4.1.

data also show no obvious sign of the feature that was observed in 2011 and 2012, though the overall scatter of these data is 50% and 100% larger than that of the 2011 and 2012 data, respectively. This could potentially hide such a small signal.

4.4 Discussion

We have characterized several physical and rotational properties of 1173 Anchises, summarized as follows:

- We find best fit amplitudes for four new epochs of data from 2011 to 2015. These amplitudes show a definite change with time, decreasing from 0.45 mag in August 2011 to 0.10 mag in September 2013 and increasing again to 0.29 mag in February 2015. These observations cover about a third of the asteroid's orbit, meaning that we have significant coverage of possible aspect angles.

- We calculate a highly precise sidereal rotation period of $11h36m32.644s \pm 0.007s$ by combining five epochs of light curves over a 30 year baseline. This precision is critical for putting past and future observations into the appropriate context of Anchises' highly variable light curve. Without the ability to determine the precise light curve phase and magnitude, direct comparisons cannot be made between different epochs of instantaneous photometric data.

- We confirm that Anchises is a highly elongated body with an $a/b = 1.62 \pm 0.02$ and $b/c \approx 1$ using an amplitude-aspect model and a grid search of relevant parameter space. Additionally, through the same process, we find an amplitude phase coefficient of 0.002 mag/degree, which indicates a small, but fairly typical, correlation between the object's light curve amplitude and the phase angle at which it was observed.

- Using five epochs of data, including the 1986 data presented in French (1987), we find that Anchises has a significantly tilted pole orientation. Considering that Horner et al.

(2012) predict a retrograde rotation, we present (198, −29) as our preferred solution, though we cannot entirely rule out either the degenerate orientation of (18, 29) or the more poorly fit values of (198,6) and (18,−6) using our models alone.

- We calculate a minimum density for Anchises of 0.35 g/cm^3 assuming a strengthless rubble pile pulled into its elongated shape through rotational forces. Such a low density suggests some cause other than rotation for the asteroid's highly elongated shape.

- Using simultaneous V and I filter light curve observations, we searched for color variation over the visible surface of the object at four different epochs. We see some signs of a coherent color variation signalling a possible change in surface weathering or a potential impact crater at that location. This variation is only present, however, in the 2011 and 2012 epochs and is not visible in the later epochs, although data from those epochs are of lower quality. More high-fidelity observations are required to confirm this feature.

– 5 –

Trojans in Context

5.1 Solar System Taxonomy

Several different taxonomic systems have been used to classify minor bodies over the years. Additionally, methods vary depending on which population one is interested in and where that population resides in the Solar System. Definitions and descriptions of these populations are provided in Section 1.1. Methods of classification for several different broad populations, as well as analysis for several different specific surveys are discussed in this chapter. These discussions are not meant to represent an exhaustive examination for these populations, but rather to provide a broad overview of the current classification schemes in order to place my work with Jupiter Trojans in proper context. The individual surveys that were chosen for further analysis were selected primarily based on sizes of the datasets, publication dates, and availability of broadband visible photometry that could be readily converted to a_T^*. These surveys are meant to give a general idea of the color distributions present in these populations as compared to that of the Jupiter Trojan clouds.

5.1.1 NEOs

Near Earth Objects (NEOs) are in the unique position of being the link between extremely well-measured and well-studied meteorites and the large number of moderately well-studied Main Belt objects. Meteorites tend to be classified based on their composition and internal structure (see Weisberg et al. 2006). Much effort is being made to tie this very detailed analysis to that of the much more difficult to observe space rocks we refer to as NEOs.

Likewise, significant research is also being done to source the NEO population to various regions in the Main Belt. Dandy et al. (2003) provide $BVRIZ$ photometric observations for 56 NEOs ranging in H magnitude from 13.8 to 21.6 mag. They attempt to connect the taxonomic types of these objects to regions of orbital space that evolutionary models predict would have required different amounts of time to populate with objects removed from the Main Belt.

5.1.2 Main Belt

Taxonomy of the Main Belt goes back to Wood & Kuiper (1963) and Chapman et al. (1971), who first began grouping objects into categories based on their colors and spectra. This taxonomy received a degree of formalism with Tholen (1984), who introduced 13 or 14 distinct classes and subclasses using principal component and cluster analysis. Several other competing schema have been used since, sharing similar naming conventions as those found in Tholen (1984). Here we use the taxonomic methods described by DeMeo et al. (2009) as it has been applied to many more objects and is well defined across both visible and infrared wavelengths. "Key" spectra from DeMeo et al. (2009) are shown in Figure 5.1.

Many large and robust visible light surveys have been done for Main Belt objects, and over 700,000 asteroids have been discovered to date[1]. Thus, we limit ourselves to the massive database provided by the Sloan Digital Sky Survey (SDSS) and the objects collected in their Moving Object Catalogue (MOC) (Abazajian et al. 2009; Ivezić et al. 2002). Figure 5.2, Figure 5.3, and Figure 5.4 show 1054 objects from this sample that had good photometry, and H < 12.5 mag. This cut in magnitude was made to make the sample size manageable and

[1]As of March 12th, 2017. http://www.minorplanetcenter.net/iau/lists/ArchiveStatistics.html

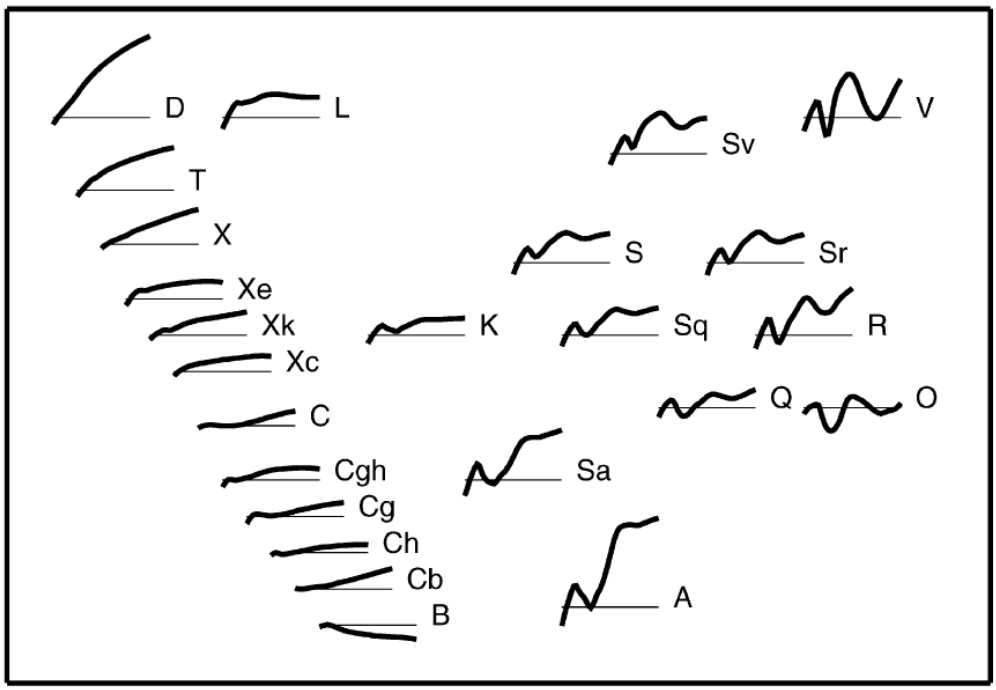

Figure 5.1: *Figure credit: DeMeo et al. (2009).* Taxonomic classes as defined by DeMeo et al. (2009) over $0.45 - 2.45\mu m$. These sample spectra show the wide variety in features and slopes present in asteroid spectra. The D, X complex, and C types shown here were used to calculate a_T^* in Section 2.5.

more comparable to the Jupiter Trojan sample without sacrificing the spatial distribution of the asteroids. From this sample, we highlight 52 resonant objects of the Hilda population (displayed in light green in the Figures).

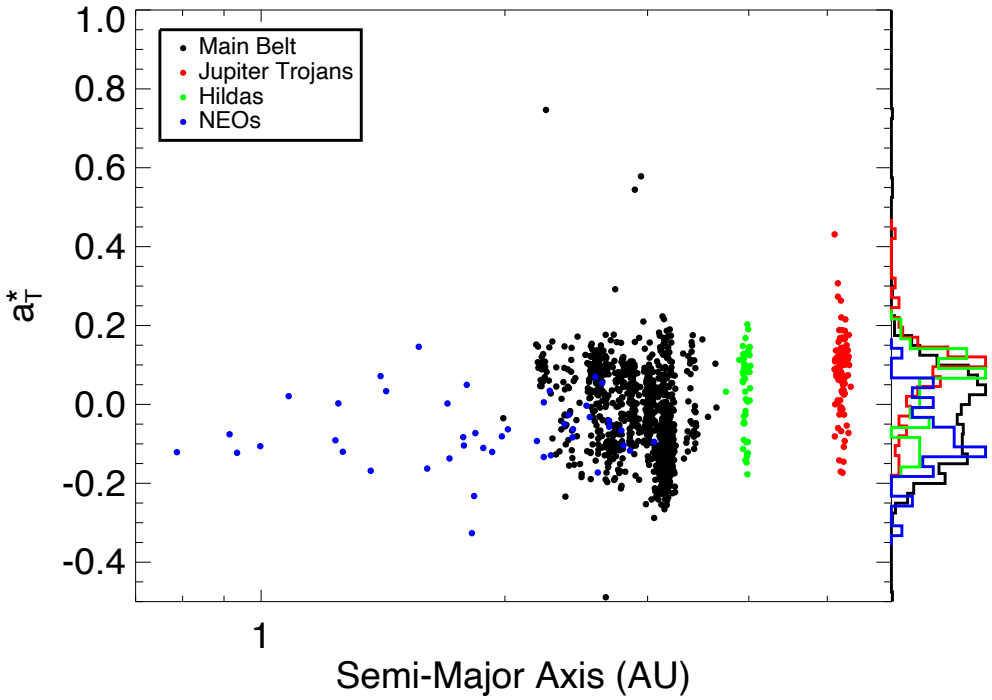

Figure 5.2: A plot of semi-major axis (a) vs a^*_T for objects in the inner Solar System. The NEOs are from a survey performed by Dandy et al. (2003), the Main Belt and Hilda data are from the SDSS MOC (Abazajian et al. 2009; Ivezić et al. 2002), and the Trojan data are from this work as described in Chapter 2. All orbital elements are from the Minor planet Center (`http://www.minorplanetcenter.net`). To the right of the plot are normalized histograms showing the color distribution for the dynamical classes shown. These histograms can be seen in more detail in Figure 5.4.

5.1.3 Centaurs

Centaurs are relatively difficult to study compared to some of the other Solar System populations due to their distances, dark surfaces, and small numbers. Taxonomic classifications for Centaurs depart from the systems used for the inner Solar System and tend to be descriptive in nature. For instance, Tegler et al. (2016) describe two groups of Centaurs that they call "gray" and "red." Wong & Brown (2017) and Wong & Brown (2016) find "Less Red" (LR), "Red" (R), and "Very Red" (VR) objects throughout the Trojan, Centaur, and TNO

populations. It should be noted that, generally speaking, the gray population of Tegler et al. (2016) corresponds to the R population from Wong & Brown (2017) and the D-type Jupiter Trojans discussed here in Section 2.6.

Though Tegler et al. (2016) present excellent color photometry for 35 Centaurs, they do not include I band observations necessary for calculating a_T^* (see Equation 2.2). Thus, for comparison purposes we used the dataset found in Peixinho et al. (2015b) and described by Peixinho et al. (2015a) that contains 33 Centaurs, ranging in H from 5.9 to 12.3 mag. We included these objects in Figure 5.3 and Figure 5.4. Figure 5.4 clearly shows the bimodal color distribution of this population as well as the apparent similarity between the Centaurs with lower a_T^* and the Jupiter Trojan color distribution.

5.1.4 TNOs

Trans-Neptunian Objects are generally grouped into dynamical families rather than taxonomic types, though both Tegler et al. (2016) and Wong & Brown (2017) extend their taxonomies into the TNO populations. The myriad dynamical families of the TNOs are determined by mean motion resonances (MMR) with Neptune as well as various orbital parameters with a primary focus on relative orbital energetics, separating high and low inclination/eccentricity objects from each other. The specifics of these distinctions are discussed in Section 1.1.

We again pull data from Peixinho et al. (2015b) for Figure 5.3 and Figure 5.4. Due to the large number of objects (326 in total), we were able to break them into their dynamical families for this analysis and retain significant color distribution information for individual subsets of the TNO population. Specifically, we note that the Cold Classical objects are too

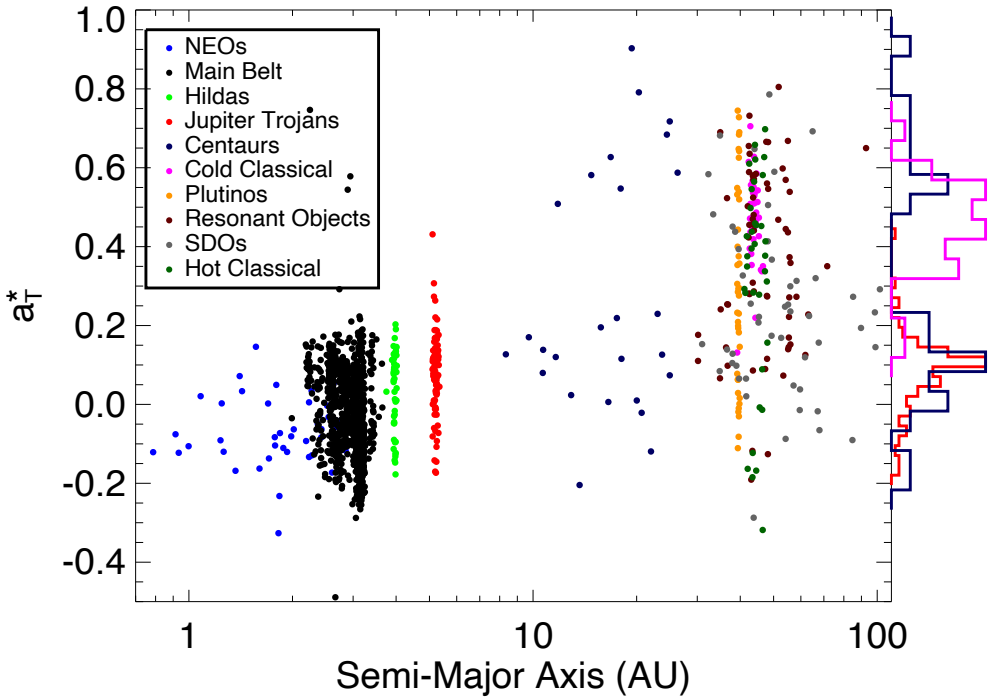

Figure 5.3: A plot of semi-major axis (a) vs a_T^* for objects in the Solar System. Objects with a semi-major axis less than 5.5 AU are shown in Figure 5.2. Data for the outer Solar System are from Peixinho et al. (2015b). To the right of the plot are normalized histograms showing the color distribution for some of the dynamical classes shown. These histograms can be seen in more detail in Figure 5.4.

red to match the Jupiter Trojan colors, but they seem quite similar to the high a_T^* Centaurs discussed above. The remaining dynamical families experience a wide distribution of colors spanning much of the possible a_T^* range. The objects in this sample range from $H = -1.1$ mag (136199 Eris) to $H = 9.2$ mag.

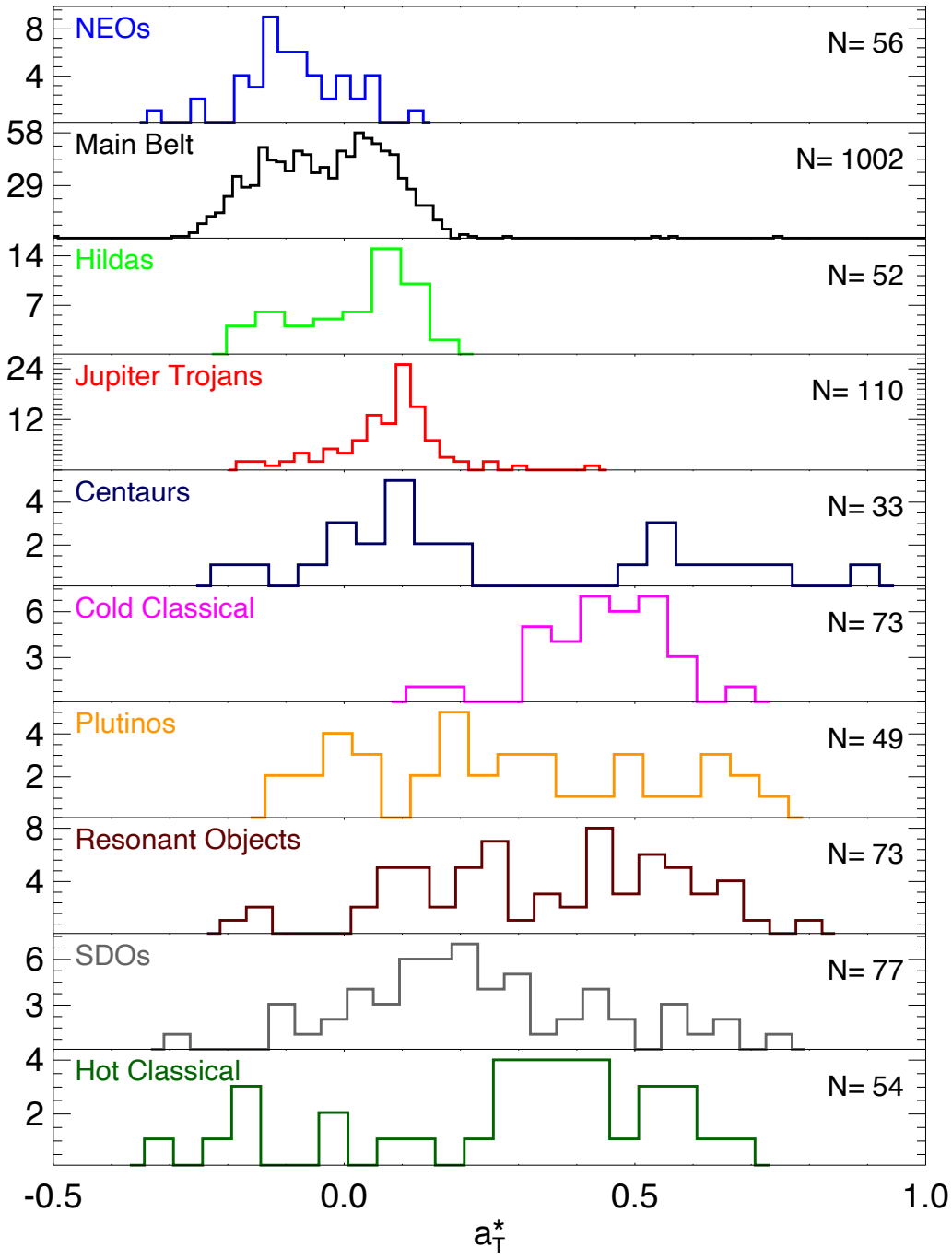

Figure 5.4: Histograms showing the color distributions for a_T^* for several populations throughout the Solar System. The individual datasets used are discussed in Section 5.1 and the Jupiter Trojan data are from Chapter 2. The populations generally increase in average semi-major axis from top to bottom. The plotted colors match those used in Figure 5.2 and Figure 5.3 and the total number of objects in each sample is given in the upper right corner of each plot. It should be noted that while a_T^* value of 0 divides the D and X taxonomic regimes for the Trojan asteroids, taxonomy of the Main Belt and NEO populations is much more complex, while outer SS objects are classified in a different way altogether.

5.2 Space Weathering and Surface Evolution

It is generally accepted that the surfaces of asteroids change with time. The exact cause and precise effect of this evolution depends on the composition of the surface, local conditions, and exactly whom you ask. Commonly cited sources of weathering include solar irradiation, particle bombardment, and micrometeorite impact. The relative strengths and time scales for these operations are still a matter of some debate and almost certainly a function of distance from the Sun. Surface composition also plays a major role in the strength of space weathering effects, but precise asteroid compositions remain unknown for the vast majority of objects. This is especially true for Jupiter Trojans with their largely featureless spectra. When combined, these facts mean that weathering effects, including even the direction of color change for some objects, are still a matter of speculation within the community. In some cases, surface composition is believed to be the primary culprit in taxonomic differences, and in others it is related to the amount of weathering experienced by the object. For example, Wong & Brown (2016) speculate that a mix of objects from both sides of the hydrogen sulfide (H_2S) sublimation line (Figure 5.5) is responsible for the different color populations from the Trojans outwards, while Dandy et al. (2003) suggest that Q-type NEOs are simply unweathered S-type objects that have spent less time closer to the Sun than the Main Belt.

In addition to space weathering that acts on the surface expression of asteroids, it is believed that collisional activity has the tendency to erase these effects through either minor gardening or more catastrophic events. Both of these effects resurface the asteroid, placing pristine material once more on the surface and resetting the weathering process. Again, the rates of these events depend on the local environment and orbital energetics of the individual object. All of this means smaller objects are generally less weathered than large objects as (if

we assume they were created through collisional grinding) they more recently experienced a resurfacing event. This is one possible explanation for the difference in color and inclination distribution between large and small Jupiter Trojans discussed in Subsection 2.5.2. Finally, it is generally assumed that an individual object conforms to a single taxonomic type, and experiences relatively uniform weathering across its surface. However, in Chapter 3 we show that color variation can, indeed, be present for some objects at a statistically significant level. It is likely that these variations contribute in some way to the width of color distributions for various populations. This may be especially true for populations like the Trojans and other resonant objects that share a nearly identical semi-major axis, as they experience similar amounts of solar radiation, and therefore, presumably similar amounts of weathering.

5.3 Source Regions for the Jupiter Trojans

The Jupiter Trojan clouds are populated by a massive number of objects, possibly even rivalling the number of Main Belt objects (Yoshida & Nakamura 2005). Understanding such a large population of objects that has experienced relatively little outside contamination and consistent internal evolution is necessary to understanding the formation of the Solar System. However, as a population, Jupiter Trojans offer some unique difficulties to study and inherent mysteries that must be explained by any models attempting to describe their origin. Specifically, unlike most Main Belt objects, Jupiter Trojans have no good meteorite analogues or strong spectral features that can lend support to a specific compositional theory. Additionally, Trojans have a broad distribution of inclinations (up to about about 40°) compared to the vast majority of Main Belt objects, which have inclinations less than 20°. Populating this orbital space is dynamically difficult, and it would involve more than simple

migration of nearby objects. Finally, there is a significant number discrepancy between the L4 and L5 clouds. Karlsson (2010) found that the L4 leading cloud contains 29% more objects than the L5 trailing cloud down to the completeness limit of H = 11.5 mag, while Szabó et al. (2007) estimates as many as 60% more L4 objects than L5 objects for the smaller bodies. Recreating these different sized populations is a necessary challenge when attempting to model Jupiter Trojan origins.

5.3.1 *In Situ*

One possible source region for Jupiter Trojans is the local area surrounding Jupiter as it formed. It has been shown by Marzari & Scholl (1998a) and Fleming & Hamilton (2000) that analytic and numerical models can reproduce the capture of large numbers of objects at the L4 and L5 Lagrange points of Jupiter during the gas giant's mass accretion phase. Indeed, these models find that gas drag and a growing Jupiter may be critical to stabilizing the orbits of Jupiter Trojans into those we see today. Marzari & Scholl (1998b) suggest that the correct rate of increase for Jupiter's mass could result in a secular resonance that converts high eccentricity, low inclination orbits into high inclination, low eccentricity orbits like those seen in today's Trojan populations. However, Marzari & Scholl (1998a) also find that nebular gas drag could create an asymmetry in the capture probabilities for the two clouds, but with the opposite result than we see, i.e., in their simulations more objects were captured in the L5 cloud than the L4 due to this aspect. Ultimately, it is quite likely that large, primordial Trojan clouds were formed simultaneous to the formation of Jupiter, but whether these primordial objects survived until the present is another matter.

5.3.2 Outer Solar System

The Nice Model (described by Tsiganis et al. 2005) shows through numerical simulation that significant migration of the giant planets in the outer Solar System could have been possible during the first few million years of Solar System formation to result in the current orbital elements of these planets. One major obstacle with this hypothesis is that the Lagrange regions of Jupiter, which can otherwise be shown to be mostly stable over the lifetime of the Solar System (Levison et al. 1997), become completely chaotic when Jupiter and Saturn enter a disruptive 2:1 MMR. It is during the time shortly after this period that Morbidelli et al. (2005) show capture of a new Trojan population is possible. Their simulation suggests that it would be possible for the large numbers of outer Solar System objects disrupted during the Jovian/Saturnian resonance to be captured in sufficient numbers to produce the current Jupiter Trojan clouds at their present range of inclinations. Marzari & Scholl (2007) go further to suggest that secondary resonances in addition to the 2:1 resonance with Saturn would have begun to destabilize any original Jupiter Trojans before even reaching that point, ending in the removal of over 90% of any original population prior to the L4 and L5 regions' resettlement by captured interlopers from the outer Solar System. Wong & Brown (2016) even suggest a more precise outer Solar System origin, as shown in Figure 5.5, based on the color differences present within the clouds. Though the idea of a progenitor population for the Jupiter Trojans coming from the outer Solar System has an easier time explaining the increased inclinations of the camps, it struggles to reproduce the number discrepancy between the two camps.

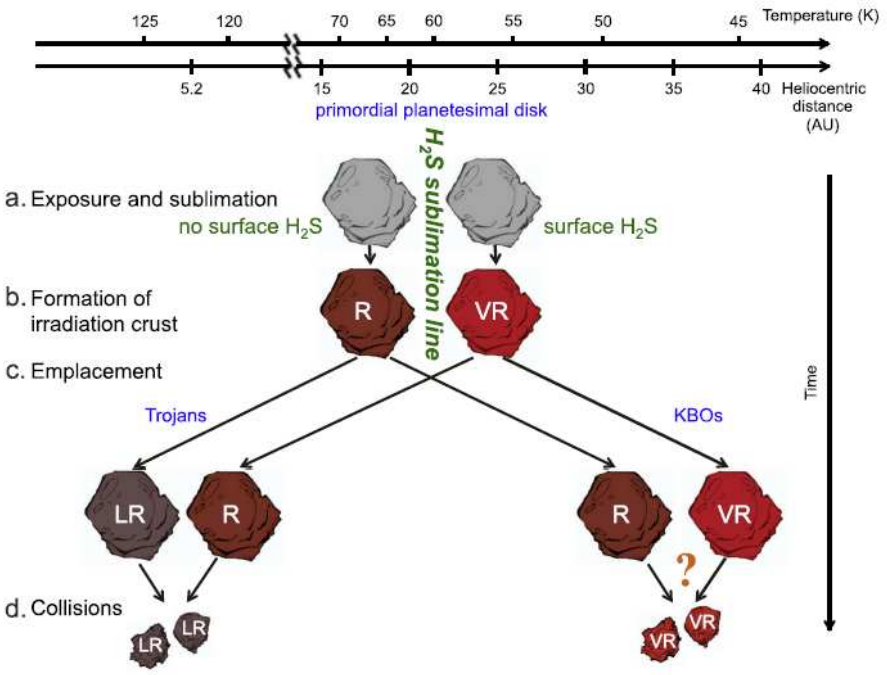

Figure 5.5: *Figure credit: Wong & Brown (2016).* A full figure description can be found in the original source. The hypothetical source region for the Trojans suggested by Wong & Brown (2016) is from a primordial population straddling the H_2S sublimation line at around 20 AU from the Sun.

5.4 Conclusions

We can see from Figure 5.2 and Figure 5.3 that Jupiter Trojans are an integral part to understanding the Solar System. They bridge and define the boundary between the inner and outer Solar System. The color distribution of these populations suggests an interesting relationship to both the inner and outer Solar System, as can be seen in Figure 5.4, as the Trojans share aspects with both the Main Belt and the icy objects of the Centaurs and TNOs. All of this brings into question the origins of these objects, and we see that answering this question could inform our understanding of the formation of the entire Solar System. An accurate assessment of the color distribution of this population and the reason for that distribution brings us one step closer to resolving the conundrum of their origins.

– 6 –

Conclusions and Future Work

6.1 Summary of Results

6.1.1 Photometry

In Chapter 2 we present photometric observations for 110 of the largest Jupiter Trojans, each at multiple epochs. Using measured $BVRI$ colors we define a new principal component a_T^*. We use this parameter to classify these objects by means of a proxy for the Bus-DeMeo taxonomic scheme. We find 84% of the largest Jupiter Trojans to be consistent with D-type classification and that 16% have less-red slopes more consistent with X-type and C-type classifications. We also look for color trends with inclination similar to those found by Roig et al. (2008). For the largest members of the Jupiter Trojan clouds, we find no appreciable difference in color distributions between either high and low inclination objects, or the L4 Greek and L5 Trojan camps. The portion of this work describing the L5 Trojan camp is published in Chatelain et al. (2016).

6.1.2 Light Curve Analysis

In Chapter 3 we examine twelve objects for color variations in $V-I$ and amplitude using light curves with partial rotational coverage. We discover that two thirds of the objects observed have at least some suggestion of color variation and one third have highly convincing signs of large surface features. We show that for a proper examination of photometric colors for Jupiter Trojans, such as that done in Chapter 2, surface variations must be taken into account, as intrinsic color variability may result in a difference of over 0.05 mag between a single epoch color measurement and a true mean value.

Additionally, in Chapter 4 we perform extensive analysis of (1173) Anchises. Observed over 5 epochs, with a total baseline of nearly 30 years, we calculate a very precise rotation period, pole orientation, and axial ratios for Anchises. We also find some evidence of $V - I$ color variation for this object at a level of $\sim$ 0.1 mag. This specific target serves as an example of the type of analysis that can be done with extensive observations of Jupiter Trojan light curves.

What We Have Learned

- The largest L4 Greeks and L5 Trojans have nearly identical color profiles implying that they were sourced from the same region and experienced similar weathering and evolutionary processes.

- The largest L4 Greeks and L5 Trojans do not show the same color gradation with inclination as smaller Jupiter Trojans. The fact that most of the largest Jupiter Trojans and redder small Jupiter Trojans both have relatively high inclinations could imply that collision rates are decreased at high inclinations.

- Many large Jupiter Trojans from both camps show signs of color variation over their rotation period consistent with less red cratering features on their surfaces. This implies either a high collision rate or an exceptionally slow weathering process for these objects.

- Surface color variation also implies a complex history and surface composition for many of these objects that needs to be taken into account when performing photometric and spectroscopic analyses.

- We calculated a newly precise rotational period for (1173) Anchises along with a pole orientation and shape model for this object. Similar methods could be used to understand other Jupiter Trojans as well.

- We find additional evidence of color variation for (1173) Anchises which, with additional calibration and analysis, could lead to a detailed understanding of this object's surface features and the recent collision rates in the Jupiter Trojan clouds.

- The largest Jupiter Trojans seem to fit a color profile trend with other minor body populations that are relatively close to them in semi-major axis. This likely means that though they are dynamically very different from these populations, weathering is likely the primary driving force in their coloration and most of these objects were sourced from the same parent population.

6.2 Future Work

As a continuation of the photometry project, smaller Jupiter Greeks and Trojans can be examined for population bimodality, such as that seen by Emery et al. (2011) and Wong et al. (2014), and taxonomic distribution using methods similar to Hasselmann et al. (2011) and DeMeo & Carry (2013). This will extend these examinations to smaller objects and expand the overall completeness within the Trojan clouds. This examination should help us to understand what role the Greeks and Trojans play in Solar System formation as a whole. If the bimodality seen by Emery et al. (2011) is real, and represents two distinct parent populations as suggested in Wong & Brown (2016), understanding the origins of these populations and their eventual fates could be vital to fully understanding the taxonomic, and presumably

compositional, gradient that exists in the Main Belt (DeMeo & Carry 2013). A thorough understanding of Jupiter's Greek and Trojan asteroids is necessary to understanding the formation of this region of the Solar System.

Continuation of the light curve project (as always) requires additional data. Many more light curves with full phase coverage at different orbital longitudes are necessary to describe the objects discussed in Chapter 3 to the same level we describe (1173) Anchises in Chapter 4. With additional coverage from future observations and from the literature, accurate pole orientations and axial ratios, as well as more precise shape models will be possible. If these observations include multiple filters, the color variation that we find for several of these objects could be connected to physical features on their surfaces, with latitudes, shapes, and true colors of the features able to be derived. Additionally, a more advanced shape model for these features is required that takes into account asteroid shape, feature shape, and more complicated lighting features such as phase effects and scattering. After the fact calibration using background stars, or additional light curves on photometric nights would allow for absolute color measurements that would make it possible to determine exactly what color the surface features we detect are. Furthermore, the models could be tested and calibrated using an object with more detailed surface observations and known color variation such as Mars' moon Phobos.

The next step for (1173) Anchises is to calibrate these data to allow us to derive accurate estimates for the absolute brightness at each epoch. This will require calibrations using either new observations or measured brightnesses in trustworthy catalogs of background stars. Once absolute calibrations have been made, we can calculate a robust phase curve, a reliable absolute magnitude, and (with an albedo estimate) physical dimensions for (1173)

Anchises. Additionally, using the period, shape model, and pole orientation presented in this work, along with infrared data from IRAS, Akari, and WISE (Horner et al. 2012), a more precise thermal inertia and albedo could be determined for this object.

Further observations of Anchises' amplitude over the next few years, such as those being done by Robert Stephens (Stephens et al. 2016b), could help constrain the pole latitude and eliminate some of the degeneracies in the pole determination. Such observations would provide additional longitudinal coverage and allow more detailed shape models to be constructed as we get a better view of both poles. With simultaneous color data, such observations could also confirm the color variation seen in the 2011 and 2012 epochs.

6.3 *Lucy* and the Future of Trojan Exploration

Lucy is a spacecraft mission that was approved by NASA on January 4th, 2017. The mission will fly past five Jupiter Trojans and one Main Belt object between 2025 and 2033. The predicted flight path and encounters are shown in Figure 6.1. It is currently planned that the spacecraft will launch in October, 2021 and reach its first Jupiter Trojan, (3548) Eurybates, in August, 2027. Over the next year or so, *Lucy* will fly by (15094) Polymele, (11351) Leucus, and (21900) Orus. In order, these objects are listed by their discovery designations, 1999 WB_2, 1997 TS_{25}, and 1999 VQ_{10} in Figure 6.1. At this point, *Lucy* will leave the L4 cloud and head to (617) Patroclus and its companion Menoetius in the L5 camp. It should arrive at this Trojan binary system by March, 2033. We present photometric colors for (3548) Eurybates, (21900) Orus, and (617) Patroclus in Chapter 2. In addition to the first high resolution images of any Jupiter Trojans, the *Lucy* mission will be able to gather unique data on the physical characteristics of these primitive objects. These visitations will no doubt

revolutionize our understanding of Jupiter Trojans, but more ground based research, such as that described here, will be necessary to interpret the observations of *Lucy* for the larger Trojan populations. For example, light curve analysis such as that performed in Chapter 3 and Chapter 4 for the Lucy targets would allow researchers not only to know what to expect from their *in situ* observations, but would also allow them to know what physical reality might explain such observations with much more detail. A highly precise rotation period is necessary for planning the mission flyby of an object, and with the much larger range of phases that will be visible from the spacecraft, understanding Trojan phase properties will also be invaluable for properly calibrating the data. Observations such as those done here are necessary for these calculations. These data combined should allow us to estimate cratering rates within the Jupiter Trojan swarms, which in turn will tell us about the evolutionary history of both these objects and ultimately the Solar System.

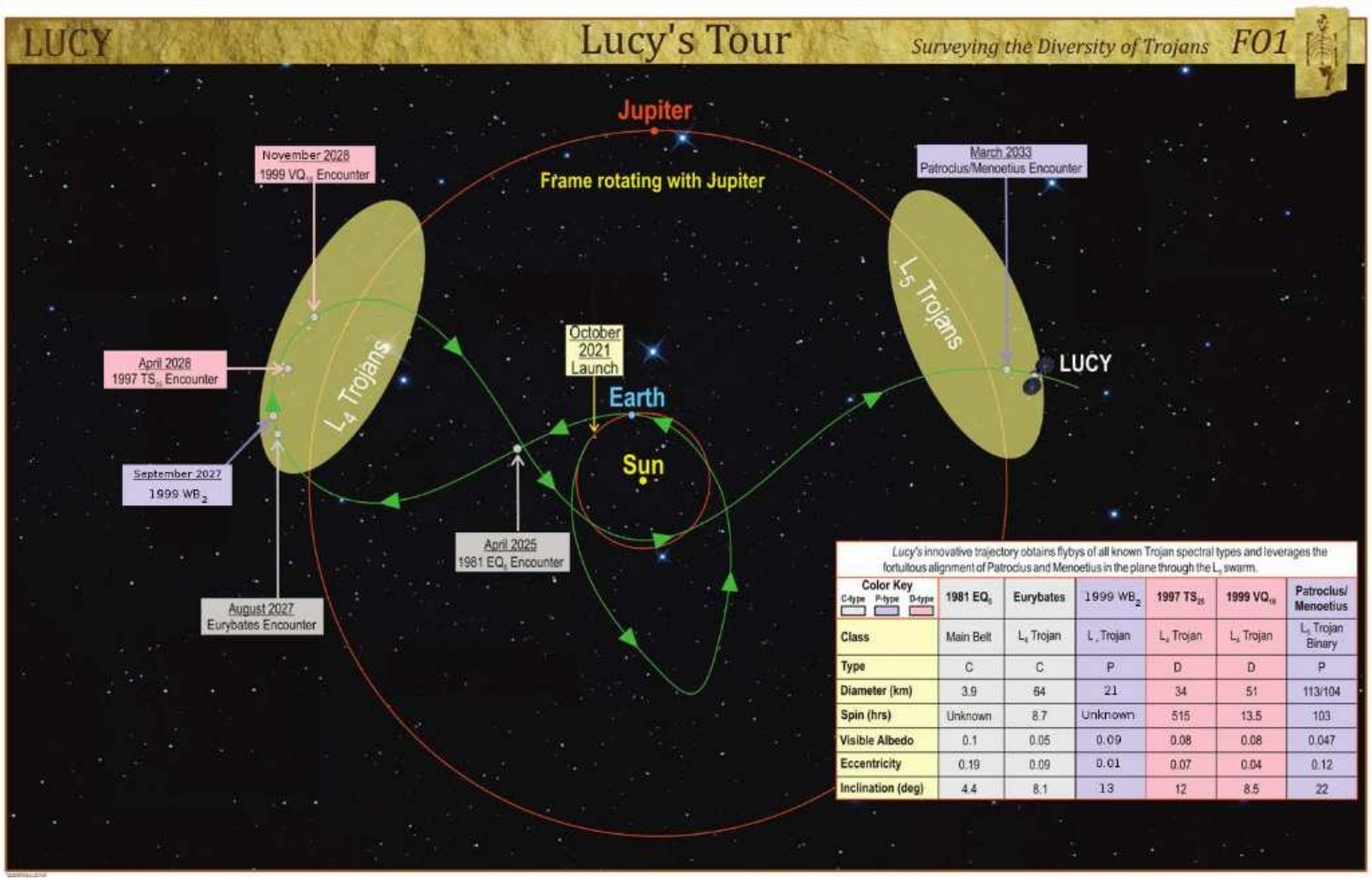

Figure 6.1: *Figure credit: Levison & Lucy Science Team (2016). A full figure description can be found in the original source.* The spacecraft is scheduled to visit members of every known taxonomic type (P-types fall within the X-complex discussed in Chapter 2) present in the Jupiter Trojan clouds.

References

Abazajian, K. N., Adelman-McCarthy, J. K., Agüeros, M. A., Allam, S. S., Allende Prieto, C., An, D., Anderson, K. S. J., Anderson, S. F., Annis, J., Bahcall, N. A., & et al. 2009, ApJS, 182, 543

Behrend, R. 2009, Observatoire de Geneve Web site, http://obswww.unige.ch/~behrend/page_cou.html (accessed 2017-03-30)

Berberich, A. 1906, Astronomische Nachrichten, 171, 11

Bernstein, G. M., Trilling, D. E., Allen, R. L., Brown, M. E., Holman, M., & Malhotra, R. 2004, AJ, 128, 1364

Bottke, Jr., W. F., Vokrouhlický, D., Rubincam, D. P., & Broz, M. 2002, The Effect of Yarkovsky Thermal Forces on the Dynamical Evolution of Asteroids and Meteoroids, ed. W. F. Bottke, Jr., A. Cellino, P. Paolicchi, & R. P. Binzel, 395–408

Bottke, Jr., W. F., Vokrouhlický, D., Rubincam, D. P., & Nesvorný, D. 2006, Annual Review of Earth and Planetary Sciences, 34, 157

Chandrasekhar, S. 1969, Ellipsoidal figures of equilibrium (New Haven: Yale University Press)

Chapman, C. R., Johnson, T. V., & McCord, T. B. 1971, NASA Special Publication, 267, 51

Chatelain, J. P., Henry, T. J., French, L. M., Winters, J. G., & Trilling, D. E. 2016, Icarus, 271, 158

Dandy, C. L., Fitzsimmons, A., & Collander-Brown, S. J. 2003, Icarus, 163, 363

DeMeo, F. E., Binzel, R. P., Slivan, S. M., & Bus, S. J. 2009, Icarus, 202, 160

DeMeo, F. E., & Carry, B. 2013, Icarus, 226, 723

Duffard, R. D., Melita, M., Ortiz, J. L., Licandro, J., Williams, I. P., & Jones, D. 2008, in LPI Contributions, Vol. 1405, Asteroids, Comets, Meteors 2008, 8187

Emery, J. P., Burr, D. M., & Cruikshank, D. P. 2011, AJ, 141, 25

Emery, J. P., Stamper, N., Cartwright, R. J., & Lucas, M. P. 2016, in AAS/Division for Planetary Sciences Meeting Abstracts, Vol. 48, AAS/Division for Planetary Sciences Meeting Abstracts, 221.04

Fernández, Y. R., Sheppard, S. S., & Jewitt, D. C. 2003, AJ, 126, 1563

Fleming, H. J., & Hamilton, D. P. 2000, Icarus, 148, 479

French, L. M. 1987, Icarus, 72, 325

French, L. M., Stephens, R. D., Coley, D., Wasserman, L. H., & Sieben, J. 2015, Icarus, 254, 1

French, L. M., Stephens, R. D., Coley, D. R., Megna, R., & Wasserman, L. H. 2012, Minor Planet Bulletin, 39, 183

French, L. M., Stephens, R. D., Lederer, S. M., Coley, D. R., & Rohl, D. A. 2011a, Minor Planet Bulletin, 38, 116

French, L. M., Stephens, R. D., Lederer, S. M., & Rohl, D. A. 2011b, Minor Planet Bulletin, 38, 2

French, L. M., & Veverka, J. 1983, Icarus, 54, 38

Gomes, R., Levison, H. F., Tsiganis, K., & Morbidelli, A. 2005, Nature, 435, 466

Gonano, M., Mottola, S., Neukum, G., & di Martino, M. 1991, Advances in Space Research, 11, 197

Graham, J. A. 1982, PASP, 94, 244

Grav, T., Mainzer, A. K., Bauer, J., Masiero, J., Spahr, T., McMillan, R. S., Walker, R., Cutri, R., Wright, E., Eisenhardt, P. R. M., Blauvelt, E., DeBaun, E., Elsbury, D., Gautier, IV, T., Gomillion, S., Hand, E., & Wilkins, A. 2011, ApJ, 742, 40

Grav, T., Mainzer, A. K., Bauer, J. M., Masiero, J. R., & Nugent, C. R. 2012, ApJ, 759, 49

Harris, A. W., Warner, B. D., & Pravec, P. 2012, NASA Planetary Data System, 187

Hartmann, W. K., Ryder, G., Dones, L., & Grinspoon, D. 2000, The Time-Dependent Intense Bombardment of the Primordial Earth/Moon System, ed. R. M. Canup, K. Righter, & et al., 493–512

Hasselmann, P. H., Carvano, J. M., & Lazzaro, D. 2011, NASA Planetary Data System, 145

Henry, T. J., Jao, W.-C., Subasavage, J. P., Beaulieu, T. D., Ianna, P. A., Costa, E., & Méndez, R. A. 2006, AJ, 132, 2360

Horner, J., Evans, N. W., & Bailey, M. E. 2004, MNRAS, 354, 798

Horner, J., Müller, T. G., & Lykawka, P. S. 2012, MNRAS, 423, 2587

Ivezić, Ž., Juric, M., Lupton, R. H., Tabachnik, S., & Quinn, T. 2002, in Society of Photo-Optical Instrumentation Engineers (SPIE) Conference Series, Vol. 4836, Survey and Other Telescope Technologies and Discoveries, ed. J. A. Tyson & S. Wolff, 98–103

Ivezić, Ž., Tabachnik, S., Rafikov, R., Lupton, R. H., Quinn, T., Hammergren, M., Eyer, L., Chu, J., Armstrong, J. C., Fan, X., Finlator, K., Geballe, T. R., Gunn, J. E., Hennessy, G. S., Knapp, G. R., Leggett, S. K., Munn, J. A., Pier, J. R., Rockosi, C. M., Schneider, D. P., Strauss, M. A., Yanny, B., Brinkmann, J., Csabai, I., Hindsley, R. B., Kent, S., Lamb, D. Q., Margon, B., McKay, T. A., Smith, J. A., Waddel, P., York, D. G., & SDSS Collaboration. 2001, AJ, 122, 2749

Jao, W.-C., Henry, T. J., Subasavage, J. P., Brown, M. A., Ianna, P. A., Bartlett, J. L., Costa, E., & Méndez, R. A. 2005, AJ, 129, 1954

Jewitt, D., & Luu, J. 1996, in Astronomical Society of the Pacific Conference Series, Vol. 107, Completing the Inventory of the Solar System, ed. T. Rettig & J. M. Hahn, 255–258

Karlsson, O. 2010, A&A, 516, A22

Karlsson, O., Lagerkvist, C.-I., & Davidsson, B. 2009, Icarus, 199, 106

Lacerda, P., & Jewitt, D. C. 2007, AJ, 133, 1393

Lagrange, J.-L. 1772, Prix de l'Académie Royale des Sciences de Paris, IX

Landolt, A. U. 2009, AJ, 137, 4186

Levison, H. F., & Lucy Science Team. 2016, in Lunar and Planetary Science Conference, Vol. 47, Lunar and Planetary Science Conference, 2061

Levison, H. F., Morbidelli, A., Tsiganis, K., Nesvorný, D., & Gomes, R. 2011, AJ, 142, 152

Levison, H. F., Shoemaker, E. M., & Shoemaker, C. S. 1997, Nature, 385, 42

Magnusson, P. 1986, Icarus, 68, 1

Marzari, F., & Scholl, H. 1998a, Icarus, 131, 41

—. 1998b, A&A, 339, 278

—. 2007, MNRAS, 380, 479

Molnar, L. A., Haegert, J., M., & Hoogeboom, K. M. 2008, Minor Planet Bulletin, 35, 82

Morbidelli, A., Brasser, R., Tsiganis, K., Gomes, R., & Levison, H. F. 2009, A&A, 507, 1041

Morbidelli, A., Levison, H. F., Tsiganis, K., & Gomes, R. 2005, Nature, 435, 462

Morbidelli, A., Tsiganis, K., Crida, A., Levison, H. F., & Gomes, R. 2007, AJ, 134, 1790

Moskovitz, N. A. 2012, Icarus, 221, 63

Mottola, S., Di Martino, M., Erikson, A., Gonano-Beurer, M., Carbognani, A., Carsenty, U., Hahn, G., Schober, H.-J., Lahulla, F., Delbò, M., & Lagerkvist, C.-I. 2011, AJ, 141, 170

Mueller, M., Marchis, F., Emery, J. P., Harris, A. W., Mottola, S., Hestroffer, D., Berthier, J., & di Martino, M. 2010, Icarus, 205, 505

Neese, C. 2010, NASA Planetary Data System, 123

Nesvorný, D., Vokrouhlický, D., & Morbidelli, A. 2013, ApJ, 768, 45

Parker, A., Ivezić, Ž., Jurić, M., Lupton, R., Sekora, M. D., & Kowalski, A. 2008, Icarus, 198, 138

Peixinho, N., Delsanti, A., & Doressoundiram, A. 2015a, A&A, 577, A35

—. 2015b, VizieR Online Data Catalog, 357

Peixinho, N., Delsanti, A., Guilbert-Lepoutre, A., Gafeira, R., & Lacerda, P. 2012, A&A, 546, A86

Piazzi, G. 1801, Risultati delle osservazioni della nuova stella scoperta il di' 1. Gennaio all'Osservatorio Reale di Palermo

Ramírez, I., Michel, R., Sefako, R., Tucci Maia, M., Schuster, W. J., van Wyk, F., Meléndez, J., Casagrande, L., & Castilho, B. V. 2012, ApJ, 752, 5

Roig, F., Ribeiro, A. O., & Gil-Hutton, R. 2008, A&A, 483, 911

Sauppe, J., Torno, S., Lemke-Oliver, R., & Ditteon, R. 2007, Minor Planet Bulletin, 34, 119

Shevchenko, V. G., Belskaya, I. N., Slyusarev, I. G., Krugly, Y. N., Chiorny, V. G., Gaftonyuk, N. M., Donchev, Z., Ivanova, V., Ibrahimov, M. A., Ehgamberdiev, S. A., & Molotov, I. E. 2012a, Icarus, 217, 202

Shevchenko, V. G., Slyusarev, I. G., & Belskaya, I. N. 2012b, in LPI Contributions, Vol. 1667, Asteroids, Comets, Meteors 2012, 6105

Shevchenko, V. G., Slyusarev, I. G., & Belskaya, I. N. 2014, Meteoritics and Planetary Science, 49, 103

Stephens, R. D. 2009, Minor Planet Bulletin, 36, 59

Stephens, R. D., Coley, R., D., & French, L. M. 2016a, Minor Planet Bulletin, 43, 15

Stephens, R. D., Coley, D. R., & French, L. M. 2014a, Minor Planet Bulletin, 41, 210

—. 2015, Minor Planet Bulletin, 42, 216

—. 2016b, Minor Planet Bulletin, 43, 265

Stephens, R. D., Coley, D. R., Warner, B. D., & French, M., L. 2016c, Minor Planet Bulletin, 43, 323

Stephens, R. D., French, L. M., Davitt, C., & Coley, D. R. 2014b, Minor Planet Bulletin, 41, 95

Szabó, G. M., Ivezić, Ž., Jurić, M., & Lupton, R. 2007, MNRAS, 377, 1393

Tegler, S. C., Romanishin, W., Consolmagno, G. J., & J., S. 2016, AJ, 152, 210

Tholen, D. J. 1984, PhD thesis, University of Arizona, Tucson

Tsiganis, K., Gomes, R., Morbidelli, A., & Levison, H. F. 2005, Nature, 435, 459

van Houten, C. J., van Houten-Groeneveld, A., & Gehrels, T. 1970a, AJ, 75, 659

van Houten, C. J., van Houten-Groeneveld, I., Herget, P., & Gehrels, T. 1970b, A&AS, 2, 339

Walsh, K. J., Morbidelli, A., Raymond, S. N., O'Brien, D. P., & Mandell, A. M. 2011, Nature, 475, 206

Weisberg, M. K., McCoy, T. J., & Krot, A. N. 2006, Systematics and Evaluation of Meteorite Classification, ed. D. S. Lauretta & H. Y. McSween, 19–52

Winters, J. G., Henry, T. J., Jao, W.-C., Subasavage, J. P., Finch, C. T., & Hambly, N. C. 2011, AJ, 141, 21

Wolf, M. 1906, Astronomische Nachrichten, 170, 353

Wong, I., & Brown, M. E. 2016, AJ, 152, 90

—. 2017, AJ, 153, 145

Wong, I., Brown, M. E., & Emery, J. P. 2014, AJ, 148, 112

Wood, H. J., & Kuiper, G. P. 1963, Publications of the Goethe Link Observatory, 53, 1279

Yoshida, F., & Nakamura, T. 2005, AJ, 130, 2900

Zappala, V., Cellino, A., Barucci, A. M., Fulchignoni, M., & Lupishko, D. F. 1990, A&A, 231, 548

Appendix

A Orbital Mechanics

Throughout this document we use many terms and discuss many ideas related to the fundamentals of orbital mechanics for Solar System bodies. Here we will define and address some of these terms and ideas.

The standard elements that are required to define an elliptical orbit are as follows:

a **Semi-Major Axis:** This is one half of the major axis distance, where the major axis is the line that crosses the entirety of the ellipse and passes through both the focus and the center of the orbit. This value will typically be given in Astronomical Units (AU), or the distance equal to the semi-major axis of Earth.

e **Eccentricity:** A measure of how much an orbit deviates from circular, eccentricity can be calculated by dividing the distance between the focus and the center of an ellipse by the semi-major axis. For elliptical orbits, this will result in values between 0 and 1 with $e = 0$ being a perfectly circular orbit and with $e = 1$ being an open parabolic orbit.

i **Inclination:** This is the angle that the orbit is inclined with respect to the ecliptic, which is defined as the plane through which the Earth travels as it orbits the Sun.

Ω **Longitude of the Ascending Node:** This is the angular direction of the orbital ascending node with respect to the vernal point in Pisces. The ascending node is the location on an orbital path that the object would cross from below the ecliptic plane to above it.

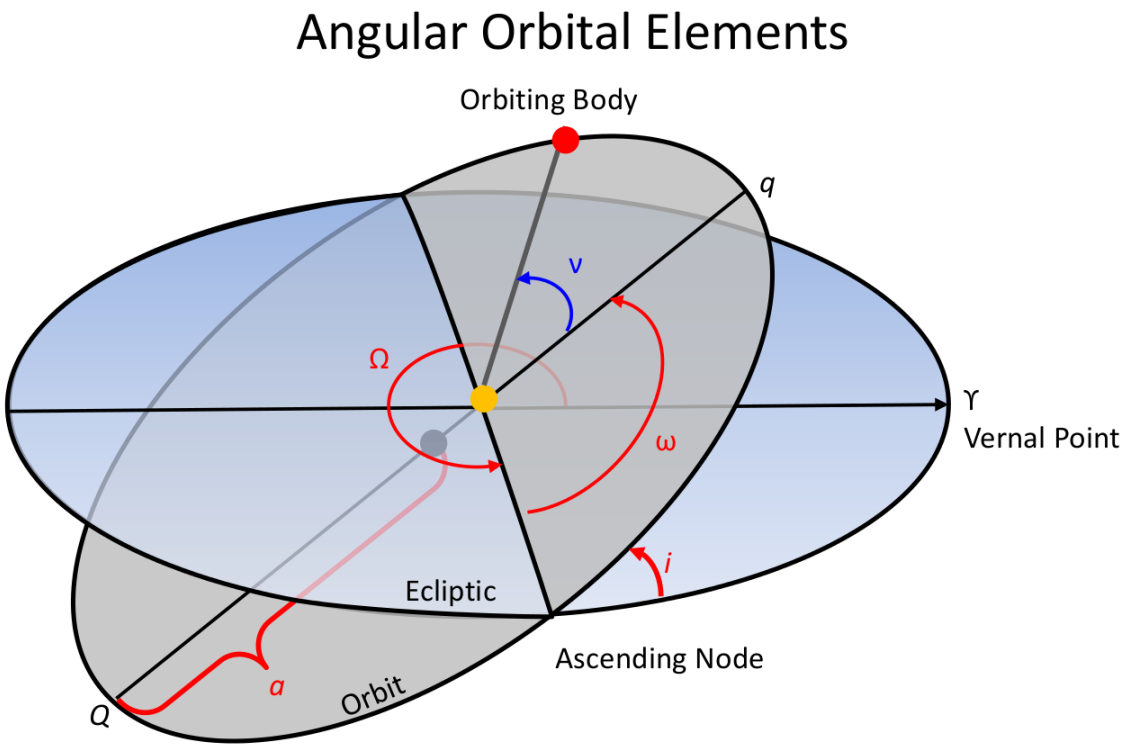

Figure A.1: A graphical depiction of the angular orbital elements described in this section.

ω **Argument of the Perihelion:** This is the angular separation between the periapsis of an object and the ascending node.

With these primary values, any orbit can be defined, but there are other important elements that are often used when describing either an orbit or an object's location along its orbital path. We have listed several of these below. The angular orbital elements are depicted in Figure A.1.

P **Orbital Period:** This is the time it takes an object to complete one orbit. This value is typically given in years for objects that orbit the Sun, and P(years) can be calculated from Kepler's third law, $P^2 = a^3$ if the object orbits the Sun, and a is given in AU.

q **Perihelion:** This is the distance of closest approach for a Solar System body that orbits the Sun. This value is usually given in AU. Note: The general name for q (for objects not necessarily orbiting the Sun) is "Periapsis".

Q **Aphelion:** This is the distance of furthest extent for an object that orbits the Sun. This value is usually given in AU. Note: The general name for Q (for objects not necessarily orbiting the Sun) is "Apoapsis".

T **Time of Periapsis:** The time that an object passed through perihelion, this value can be any date in the past or future that the object can be found at perihelion. Typically the most recent time in the past is given. This value is important for calculating ν and relates to the actual position of the object rather than simply describing its orbit.

ν **True Anomaly:** This is the actual angular separation between the current location of an object and its previous perihelion passage.

With the exception of ν the above orbital elements are relatively constant with time. Once an accurate orbit has been determined for a Solar System object, its exact location can be reasonably well predicted at any time in the past or future through the calculation of ephemerides. These ephemerides require the computation of the right Ascension (RA), Declination (DEC), and geocentric distance of the Solar System object at the specified time from the orbital elements described above. These are used by astronomers to locate and observe objects with known orbits around the Sun, but the same techniques can be applied to moons and binary stars, or any object with a well defined orbit.

B Full Photometry Data Tables

Table B.1: Photometry Data: L4 Greeks

Object	Telescope[a]	Date (UT)	α (°)	V (mag)	B-V (mag)	V-R (mag)	V-I (mag)
(588) Achilles	0.9m	2011 Dec. 19	6.3	14.99 ± 0.016	· · ·	0.44 ± 0.021	0.93 ± 0.031
(588) Achilles	0.9m	2013 Feb. 27	1.1	14.83 ± 0.045	0.94 ± 0.060	0.46 ± 0.055	0.92 ± 0.051
(588) Achilles	0.9m	2013 Feb. 28	1.3	14.89 ± 0.036	0.86 ± 0.078	0.49 ± 0.046	0.93 ± 0.041
(588) Achilles	42in	2010 Nov. 26	2.8	15.08 ± 0.014	0.69 ± 0.082	0.49 ± 0.030	0.98 ± 0.039
(624) Hektor	0.9m	2013 Feb. 25	1.3	14.32 ± 0.067	0.74 ± 0.077	0.42 ± 0.097	0.88 ± 0.098
(624) Hektor	0.9m	2013 Feb. 28	1.9	14.25 ± 0.034	0.98 ± 0.076	0.48 ± 0.043	0.93 ± 0.039
(624) Hektor	42in	2010 Nov. 25	5.7	14.88 ± 0.048	0.76 ± 0.110	0.47 ± 0.084	0.96 ± 0.097
(659) Nestor	0.9m	2013 Feb. 27	5.2	16.37 ± 0.055	1.25 ± 0.105	0.51 ± 0.068	0.85 ± 0.065
(659) Nestor	42in	2010 Nov. 26	1.8	15.79 ± 0.015	0.70 ± 0.084	0.39 ± 0.033	0.76 ± 0.049
(911) Agamemnon	0.9m	2013 Feb. 28	1.7	15.02 ± 0.036	1.04 ± 0.079	0.46 ± 0.046	0.99 ± 0.042
(911) Agamemnon	42in	2010 Nov. 25	6.3	15.01 ± 0.048	0.77 ± 0.109	0.46 ± 0.083	0.91 ± 0.094
(1143) Odysseus	0.9m	2010 Oct. 23	5.3	15.06 ± 0.016	0.78 ± 0.036	0.40 ± 0.024	0.86 ± 0.021
(1143) Odysseus	0.9m	2011 Dec. 19	1.6	14.93 ± 0.016	· · ·	1.17 ± 0.036	0.19 ± 0.063
(1143) Odysseus	0.9m	2013 Feb. 28	5.7	15.39 ± 0.035	0.99 ± 0.076	0.50 ± 0.046	0.97 ± 0.042
(1143) Odysseus	1.0m	2011 Nov. 16	8.3	15.27 ± 0.028	0.69 ± 0.070	0.46 ± 0.056	0.94 ± 0.041
(1143) Odysseus	42in	2010 Nov. 25	2.0	14.99 ± 0.047	0.75 ± 0.111	0.47 ± 0.086	0.94 ± 0.102
(1143) Odysseus	42in	2010 Nov. 26	2.3	15.10 ± 0.014	0.72 ± 0.081	0.46 ± 0.028	0.94 ± 0.037
(1404) Ajax	0.9m	2013 Feb. 28	3.6	17.02 ± 0.046	· · ·	0.51 ± 0.062	0.95 ± 0.058
(1404) Ajax	42in	2010 Nov. 26	4.8	16.19 ± 0.020	0.73 ± 0.086	0.45 ± 0.033	0.96 ± 0.037
(1437) Diomedes	0.9m	2013 Feb. 28	3.7	15.19 ± 0.038	1.06 ± 0.082	0.43 ± 0.049	0.82 ± 0.044
(1437) Diomedes	0.9m	2013 Mar. 1	3.6	15.16 ± 0.045	0.79 ± 0.089	0.40 ± 0.055	0.80 ± 0.049
(1437) Diomedes	42in	2010 Nov. 26	8.3	15.30 ± 0.015	0.70 ± 0.083	0.36 ± 0.032	0.83 ± 0.047
(1437) Diomedes	42in	2012 Jan. 14	5.3	15.06 ± 0.012	0.67 ± 0.044	0.38 ± 0.036	0.79 ± 0.067
(1583) Antilochus	1.0m	2011 Nov. 14	11.0	16.19 ± 0.025	0.76 ± 0.071	0.46 ± 0.097	0.95 ± 0.061
(1749) Telamon	0.9m	2010 Oct. 22	4.5	16.29 ± 0.042	0.65 ± 0.070	0.45 ± 0.051	1.00 ± 0.050
(1749) Telamon	42in	2010 Nov. 26	4.2	16.25 ± 0.014	0.74 ± 0.081	0.48 ± 0.027	0.96 ± 0.037
(1868) Thersites	0.9m	2013 Feb. 26	3.5	17.22 ± 0.919	· · ·	0.53 ± 1.284	0.91 ± 0.921
(1868) Thersites	42in	2012 Jan. 14	3.6	16.83 ± 0.012	0.73 ± 0.033	0.48 ± 0.023	0.96 ± 0.035
(2260) Neoptolemus	1.0m	2011 Nov. 16	9.2	16.63 ± 0.028	0.78 ± 0.064	0.44 ± 0.059	0.88 ± 0.046
(2260) Neoptolemus	42in	2012 Jan. 14	2.5	16.28 ± 0.011	0.77 ± 0.030	0.51 ± 0.020	0.98 ± 0.028
(2456) Palamedes	42in	2010 Nov. 26	3.7	16.01 ± 0.015	0.73 ± 0.081	0.44 ± 0.029	0.89 ± 0.038
(2456) Palamedes	42in	2012 Jan. 13	3.5	15.93 ± 0.016	0.72 ± 0.031	0.45 ± 0.025	0.93 ± 0.031
(2759) Idomeneus	0.9m	2013 Feb. 27	5.3	17.42 ± 0.067	0.50 ± 0.141	0.58 ± 0.081	1.11 ± 0.073

Continued on next page

Table B.1 – continued from previous page

Object	Telescope[a]	Date (UT)	α (°)	V (mag)	B-V (mag)	V-R (mag)	V-I (mag)
(2759) Idomeneus	1.0m	2011 Nov. 15	9.4	17.74 ± 0.053	1.13 ± 0.121	0.45 ± 0.072	0.66 ± 0.081
(2797) Teucer	0.9m	2010 Oct. 23	5.7	15.84 ± 0.025	0.76 ± 0.054	0.49 ± 0.037	0.93 ± 0.051
(2797) Teucer	42in	2010 Nov. 25	2.4	15.52 ± 0.048	0.76 ± 0.112	0.46 ± 0.086	0.89 ± 0.103
(2920) Automedon	0.9m	2010 Oct. 23	6.2	15.86 ± 0.020	0.68 ± 0.046	0.45 ± 0.026	0.94 ± 0.025
(2920) Automedon	0.9m	2011 Dec. 19	3.8	15.61 ± 0.016	· · ·	0.48 ± 0.022	0.96 ± 0.033
(2920) Automedon	0.9m	2011 Nov. 22	7.5	15.87 ± 0.014	· · ·	0.51 ± 0.024	0.96 ± 0.034
(2920) Automedon	0.9m	2013 Feb. 25	6.9	15.92 ± 0.063	0.68 ± 0.074	0.49 ± 0.073	0.98 ± 0.067
(2920) Automedon	1.0m	2011 Nov. 13	8.8	15.93 ± 0.029	0.76 ± 0.061	0.48 ± 0.044	0.93 ± 0.071
(2920) Automedon	42in	2010 Nov. 26	1.5	15.61 ± 0.015	0.73 ± 0.081	0.47 ± 0.030	0.98 ± 0.040
(3063) Makhaon	0.9m	2011 Dec. 19	5.1	15.48 ± 0.016	· · ·	1.18 ± 0.034	0.17 ± 0.059
(3063) Makhaon	0.9m	2013 Mar. 1	3.5	15.43 ± 0.045	0.94 ± 0.091	0.50 ± 0.055	0.97 ± 0.050
(3063) Makhaon	1.0m	2011 Nov. 13	10.5	15.95 ± 0.032	0.65 ± 0.068	0.55 ± 0.048	0.99 ± 0.075
(3063) Makhaon	42in	2012 Jan. 13	0.6	15.22 ± 0.015	0.73 ± 0.049	0.47 ± 0.028	0.89 ± 0.040
(3063) Makhaon	42in	2012 Jan. 14	0.6	15.23 ± 0.009	0.73 ± 0.027	0.45 ± 0.028	0.92 ± 0.041
(3540) Protesilaos	42in	2010 Nov. 25	3.5	16.34 ± 0.048	0.73 ± 0.113	0.48 ± 0.087	0.93 ± 0.106
(3540) Protesilaos	42in	2012 Jan. 14	6.0	16.12 ± 0.010	0.75 ± 0.039	0.47 ± 0.026	0.94 ± 0.043
(3548) Eurybates	0.9m	2013 Feb. 25	2.5	16.98 ± 0.090	2.28 ± 0.572	0.51 ± 0.106	0.97 ± 0.098
(3548) Eurybates	42in	2012 Jan. 13	4.3	16.50 ± 0.022	0.66 ± 0.050	0.31 ± 0.034	0.68 ± 0.044
(3564) Talthybius	42in	2010 Nov. 25	2.6	16.75 ± 0.048	0.74 ± 0.117	0.46 ± 0.092	0.90 ± 0.124
(3596) Meriones	42in	2010 Nov. 25	6.9	16.06 ± 0.048	0.79 ± 0.115	0.47 ± 0.087	0.95 ± 0.108
(3596) Meriones	42in	2012 Jan. 13	5.2	16.29 ± 0.053	· · ·	0.39 ± 0.059	0.79 ± 0.068
(3709) Polypoites	0.9m	2010 Oct. 23	5.6	16.41 ± 0.019	0.66 ± 0.060	0.56 ± 0.040	1.01 ± 0.058
(3709) Polypoites	1.0m	2011 Nov. 14	8.5	16.48 ± 0.031	0.72 ± 0.067	0.53 ± 0.074	1.04 ± 0.056
(3709) Polypoites	42in	2010 Nov. 26	4.5	16.19 ± 0.016	0.74 ± 0.088	0.47 ± 0.038	0.95 ± 0.062
(3793) Leonteus	0.9m	2010 Oct. 23	8.7	15.80 ± 0.020	0.66 ± 0.042	0.47 ± 0.029	0.78 ± 0.035
(3793) Leonteus	0.9m	2013 Feb. 26	3.9	15.69 ± 0.916	0.91 ± 0.922	0.47 ± 1.276	0.70 ± 0.917
(3793) Leonteus	1.0m	2011 Nov. 13	11.2	16.31 ± 0.030	0.62 ± 0.062	0.41 ± 0.047	0.79 ± 0.071
(3794) Sthenelos	42in	2010 Nov. 25	5.3	17.38 ± 0.053	0.74 ± 0.122	0.48 ± 0.091	0.91 ± 0.108
(3794) Sthenelos	42in	2012 Jan. 13	2.2	17.27 ± 0.035	0.95 ± 0.089	0.57 ± 0.048	1.11 ± 0.053
4035	0.9m	2013 Mar. 1	5.3	16.81 ± 0.045	0.78 ± 0.089	0.45 ± 0.056	0.98 ± 0.053
4035	42in	2010 Nov. 26	0.8	16.37 ± 0.020	0.71 ± 0.083	0.49 ± 0.031	0.97 ± 0.037
4035	42in	2012 Jan. 14	3.2	(No V data)	R (mag)	B-R	R-I
					16.05 ± 0.012	1.34 ± 0.032	0.50 ± 0.021
(4057) Demophon	1.0m	2011 Nov. 15	9.3	16.88 ± 0.037	0.64 ± 0.056	0.58 ± 0.049	1.52 ± 0.063
(4057) Demophon	42in	2010 Nov. 26	2.2	16.60 ± 0.016	0.70 ± 0.082	0.41 ± 0.031	0.81 ± 0.046

Continued on next page

Table B.1 – continued from previous page

Object	Telescope[a]	Date (UT)	α (°)	V (mag)	B-V (mag)	V-R (mag)	V-I (mag)
(4060) Deipylos	0.9m	2010 Oct. 22	4.6	16.19 ± 0.024	0.70 ± 0.047	0.43 ± 0.031	0.80 ± 0.030
(4060) Deipylos	0.9m	2010 Oct. 23	4.5	16.10 ± 0.020	0.73 ± 0.045	0.37 ± 0.027	0.71 ± 0.027
(4060) Deipylos	0.9m	2013 Feb. 27	6.1	16.01 ± 0.048	0.61 ± 0.064	0.29 ± 0.062	0.73 ± 0.059
(4060) Deipylos	1.0m	2011 Nov. 12	9.0	15.96 ± 0.029	0.71 ± 0.051	0.41 ± 0.041	0.89 ± 0.053
(4063) Euforbo	0.9m	2010 Oct. 23	9.9	15.60 ± 0.015	0.75 ± 0.034	0.46 ± 0.021	0.95 ± 0.021
(4063) Euforbo	0.9m	2011 Dec. 19	6.5	15.45 ± 0.016	· · ·	0.45 ± 0.021	0.94 ± 0.031
(4063) Euforbo	0.9m	2013 Feb. 25	3.1	15.97 ± 0.072	1.79 ± 0.199	0.51 ± 0.085	1.02 ± 0.078
(4063) Euforbo	42in	2012 Jan. 14	0.8	15.21 ± 0.009	0.75 ± 0.025	0.48 ± 0.017	0.94 ± 0.025
(4068) Menestheus	0.9m	2010 Oct. 22	3.5	16.68 ± 0.038	0.69 ± 0.073	0.43 ± 0.052	0.93 ± 0.046
(4068) Menestheus	0.9m	2010 Oct. 23	3.4	16.68 ± 0.036	0.89 ± 0.074	0.37 ± 0.049	0.91 ± 0.045
(4068) Menestheus	1.0m	2011 Nov. 14	6.3	16.60 ± 0.032	0.77 ± 0.047	0.51 ± 0.058	1.02 ± 0.048
(4086) Podalirius	42in	2010 Nov. 25	7.9	16.30 ± 0.050	0.73 ± 0.114	0.48 ± 0.087	0.81 ± 0.102
(4086) Podalirius	42in	2010 Nov. 26	7.9	16.33 ± 0.026	0.73 ± 0.095	0.49 ± 0.044	0.90 ± 0.067
(4138) Kalchas	0.9m	2013 Mar. 1	3.7	17.32 ± 0.050	· · ·	0.39 ± 0.067	0.87 ± 0.059
(4138) Kalchas	42in	2012 Jan. 13	0.7	17.11 ± 0.027	0.53 ± 0.060	0.42 ± 0.041	0.77 ± 0.051
4489	0.9m	2010 Oct. 22	4.7	16.36 ± 0.031	0.73 ± 0.064	0.38 ± 0.047	0.97 ± 0.055
4489	1.0m	2011 Nov. 15	5.3	16.06 ± 0.026	0.75 ± 0.084	0.47 ± 0.090	0.93 ± 0.058
4489	42in	2010 Nov. 25	5.7	16.21 ± 0.048	0.76 ± 0.112	0.47 ± 0.086	0.93 ± 0.105
(4543) Phoinix	0.9m	2013 Feb. 25	1.9	17.31 ± 0.106	1.52 ± 0.152	0.64 ± 0.126	1.19 ± 0.115
(4543) Phoinix	42in	2010 Nov. 25	7.1	16.75 ± 0.051	0.69 ± 0.125	0.46 ± 0.089	1.20 ± 0.105
(4833) Meges	0.9m	2010 Oct. 22	9.1	16.20 ± 0.017	0.77 ± 0.036	0.43 ± 0.023	0.94 ± 0.022
(4833) Meges	1.0m	2011 Nov. 13	9.2	16.45 ± 0.035	0.66 ± 0.071	0.46 ± 0.056	0.90 ± 0.102
(4834) Thoas	0.9m	2010 Oct. 23	6.5	15.94 ± 0.017	0.82 ± 0.053	0.43 ± 0.033	0.93 ± 0.054
(4834) Thoas	42in	2010 Nov. 26	3.8	15.91 ± 0.015	0.78 ± 0.084	0.47 ± 0.030	0.96 ± 0.042
4835	0.9m	2010 Oct. 22	6.4	17.56 ± 0.042	0.86 ± 0.102	0.45 ± 0.062	0.83 ± 0.057
4835	42in	2010 Nov. 25	6.4	17.57 ± 0.053	0.68 ± 0.122	0.39 ± 0.092	0.90 ± 0.109
(4836) Medon	42in	2012 Jan. 14	2.7	16.02 ± 0.011	0.75 ± 0.043	0.47 ± 0.033	0.92 ± 0.055
(4902) Thessandrus	1.0m	2011 Nov. 13	9.0	16.84 ± 0.037	0.87 ± 0.090	0.53 ± 0.076	0.94 ± 0.078
(4902) Thessandrus	42in	2010 Nov. 26	2.3	16.45 ± 0.017	0.72 ± 0.089	0.48 ± 0.036	0.96 ± 0.054
(4946) Askalaphus	42in	2010 Nov. 26	1.5	17.63 ± 0.031	0.70 ± 0.099	0.57 ± 0.045	0.99 ± 0.052
(4946) Askalaphus	42in	2012 Jan. 13	4.1	17.75 ± 0.031	0.72 ± 0.064	0.39 ± 0.045	0.89 ± 0.055
(5023) Agapenor	0.9m	2013 Feb. 27	6.7	18.54 ± 0.129	· · ·	0.69 ± 0.177	1.24 ± 0.163
(5023) Agapenor	42in	2010 Nov. 25	3.4	17.25 ± 0.049	0.71 ± 0.112	0.37 ± 0.086	0.96 ± 0.099
(5023) Agapenor	42in	2012 Jan. 14	5.0	17.35 ± 0.010	0.71 ± 0.023	0.24 ± 0.023	0.67 ± 0.026
5025	0.9m	2013 Mar. 1	5.5	17.92 ± 0.068	· · ·	0.56 ± 0.087	1.08 ± 0.079

Continued on next page

Table B.1 – continued from previous page

Object	Telescope[a]	Date (UT)	α (°)	V (mag)	B-V (mag)	V-R (mag)	V-I (mag)
5025	42in	2012 Jan. 14	4.1	17.24 ± 0.012	0.71 ± 0.031	0.45 ± 0.030	0.73 ± 0.050
(5027) Androgeos	42in	2012 Jan. 13	4.1	16.76 ± 0.020	0.77 ± 0.042	0.44 ± 0.034	0.91 ± 0.047
(5028) Halaesus	42in	2010 Nov. 25	3.5	16.75 ± 0.049	0.68 ± 0.113	0.47 ± 0.085	0.90 ± 0.098
5123	0.9m	2010 Oct. 23	5.0	17.19 ± 0.047	0.67 ± 0.092	0.51 ± 0.061	0.97 ± 0.056
5123	42in	2010 Nov. 26	2.8	16.81 ± 0.017	0.72 ± 0.095	0.43 ± 0.032	0.85 ± 0.051
(5254) Ulysses	0.9m	2010 Oct. 23	7.4	16.17 ± 0.021	0.63 ± 0.053	0.55 ± 0.037	1.00 ± 0.059
(5254) Ulysses	42in	2010 Nov. 26	1.8	15.83 ± 0.016	0.75 ± 0.086	0.48 ± 0.035	0.93 ± 0.060
5258	0.9m	2010 Oct. 22	2.5	17.31 ± 0.055	0.76 ± 0.130	0.41 ± 0.078	0.95 ± 0.079
5258	42in	2010 Nov. 26	5.1	16.38 ± 0.014	0.90 ± 0.086	0.55 ± 0.036	1.04 ± 0.064
(5264) Telephus	0.9m	2010 Oct. 22	8.7	17.00 ± 0.032	0.73 ± 0.063	0.51 ± 0.040	1.00 ± 0.039
(5264) Telephus	1.0m	2011 Nov. 13	10.0	16.78 ± 0.042	0.74 ± 0.070	0.49 ± 0.057	0.90 ± 0.066
(5283) Pyrrhus	0.9m	2010 Oct. 23	7.9	16.48 ± 0.031	0.83 ± 0.073	0.46 ± 0.043	0.96 ± 0.046
(5283) Pyrrhus	42in	2010 Nov. 25	0.7	16.32 ± 0.048	0.73 ± 0.116	0.45 ± 0.089	0.94 ± 0.111
(5284) Orsilocus	1.0m	2011 Nov. 16	9.9	17.31 ± 0.038	0.73 ± 0.081	0.49 ± 0.054	0.97 ± 0.067
(5285) Krethon	0.9m	2013 Feb. 27	2.1	18.65 ± 0.236	· · ·	1.48 ± 0.263	2.12 ± 0.249
(5285) Krethon	42in	2012 Jan. 14	4.4	17.18 ± 0.026	0.89 ± 0.062	0.49 ± 0.037	1.05 ± 0.045
(5652) Amphimachus	0.9m	2013 Mar. 1	3.0	17.69 ± 0.057	· · ·	0.61 ± 0.074	1.08 ± 0.069
(5652) Amphimachus	42in	2010 Nov. 25	3.1	16.82 ± 0.050	0.79 ± 0.117	0.49 ± 0.088	0.98 ± 0.105
6090	0.9m	2013 Feb. 28	5.0	17.04 ± 0.056	1.59 ± 0.174	0.60 ± 0.068	1.06 ± 0.065
6090	42in	2012 Jan. 13	3.9	16.65 ± 0.020	0.72 ± 0.070	0.42 ± 0.048	0.85 ± 0.082
6545	42in	2010 Nov. 25	4.8	17.21 ± 0.053	0.85 ± 0.128	0.44 ± 0.092	1.08 ± 0.108
6545	42in	2012 Jan. 14	2.2	17.07 ± 0.018	0.78 ± 0.052	0.42 ± 0.037	0.83 ± 0.079
(7119) Hiera	0.9m	2013 Feb. 26	7.0	17.27 ± 0.922	1.56 ± 0.995	0.53 ± 1.280	0.81 ± 0.923
(7119) Hiera	42in	2010 Nov. 25	5.6	16.76 ± 0.048	0.77 ± 0.115	0.47 ± 0.089	0.95 ± 0.107
(7152) Euneus	0.9m	2013 Feb. 28	5.0	17.57 ± 0.072	1.58 ± 0.269	0.62 ± 0.088	1.06 ± 0.082
(7152) Euneus	1.0m	2011 Nov. 16	9.0	17.54 ± 0.025	0.66 ± 0.057	0.46 ± 0.057	0.86 ± 0.048
7641	0.9m	2013 Feb. 26	9.1	16.58 ± 0.913	· · ·	0.44 ± 1.273	0.51 ± 0.914
7641	42in	2010 Nov. 26	2.0	16.31 ± 0.016	0.76 ± 0.081	0.49 ± 0.028	0.98 ± 0.035
9799	1.0m	2011 Nov. 15	8.4	17.20 ± 0.057	0.66 ± 0.111	0.54 ± 0.109	0.24 ± 0.227
9799	42in	2010 Nov. 26	1.8	16.54 ± 0.020	0.68 ± 0.090	0.50 ± 0.038	0.95 ± 0.057
11397	0.9m	2013 Feb. 28	5.4	17.89 ± 0.068	· · ·	0.51 ± 0.103	1.09 ± 0.080
15436	1.0m	2011 Nov. 13	9.4	16.46 ± 0.034	0.84 ± 0.066	0.41 ± 0.046	0.83 ± 0.063
15436	42in	2010 Nov. 25	0.8	15.90 ± 0.048	0.74 ± 0.110	0.50 ± 0.083	0.95 ± 0.095
15440	0.9m	2010 Oct. 22	8.6	17.17 ± 0.027	0.78 ± 0.089	0.50 ± 0.044	0.99 ± 0.056
15440	1.0m	2011 Nov. 16	8.8	17.23 ± 0.032	0.75 ± 0.092	0.49 ± 0.083	0.94 ± 0.059
15539	0.9m	2010 Oct. 22	6.4	18.02 ± 0.060	0.93 ± 0.159	0.51 ± 0.076	0.98 ± 0.115

Continued on next page

Table B.1 – continued from previous page

Object	Telescope[a]	Date (UT)	α (°)	V (mag)	B-V (mag)	V-R (mag)	V-I (mag)
15539	0.9m	2010 Oct. 23	6.3	17.81 ± 0.047	0.60 ± 0.090	0.38 ± 0.062	0.89 ± 0.061
15539	1.0m	2011 Nov. 13	6.8	18.08 ± 0.074	0.92 ± 0.170	0.56 ± 0.107	0.84 ± 0.104
16974	42in	2010 Nov. 25	0.8	16.65 ± 0.048	0.78 ± 0.114	0.48 ± 0.086	0.94 ± 0.102
16974	42in	2010 Nov. 26	1.1	16.62 ± 0.017	0.74 ± 0.083	0.50 ± 0.029	0.96 ± 0.037
20729	0.9m	2013 Mar. 1	4.0	18.18 ± 0.058	· · ·	0.49 ± 0.077	1.03 ± 0.073
20729	42in	2010 Nov. 25	5.1	17.27 ± 0.053	0.75 ± 0.120	0.51 ± 0.089	0.95 ± 0.102
21601	0.9m	2013 Feb. 25	5.8	17.42 ± 0.081	0.71 ± 0.144	0.56 ± 0.095	1.11 ± 0.087
21601	42in	2012 Jan. 14	6.1	17.04 ± 0.022	0.77 ± 0.050	0.43 ± 0.035	0.94 ± 0.044
(21900) Orus	1.0m	2011 Nov. 15	7.4	17.18 ± 0.039	0.88 ± 0.102	0.45 ± 0.082	0.93 ± 0.066
(21900) Orus	42in	2010 Nov. 26	2.7	16.87 ± 0.015	0.75 ± 0.084	0.50 ± 0.033	0.96 ± 0.050
22149	0.9m	2013 Feb. 27	5.3	17.64 ± 0.091	1.02 ± 0.237	0.57 ± 0.111	1.09 ± 0.102
23135	0.9m	2013 Mar. 1	4.2	17.24 ± 0.062	0.80 ± 0.117	0.51 ± 0.077	0.86 ± 0.070
23958	0.9m	2013 Feb. 28	7.2	17.46 ± 0.041	· · ·	0.55 ± 0.057	1.03 ± 0.050
23958	1.0m	2011 Nov. 12	9.8	17.50 ± 0.051	0.65 ± 0.089	0.44 ± 0.065	0.80 ± 0.080
23958	42in	2012 Jan. 13	6.2	17.09 ± 0.019	0.65 ± 0.044	0.52 ± 0.026	1.02 ± 0.040
38050	0.9m	2013 Feb. 26	8.2	17.48 ± 0.925	0.65 ± 0.936	0.75 ± 1.284	1.09 ± 0.926
38050	42in	2010 Nov. 26	2.7	16.61 ± 0.015	0.79 ± 0.085	0.49 ± 0.035	0.99 ± 0.053

[a] *The three telescopes used to acquire these data were the CTIO/SMARTS 0.9-m and 1.0-m as well as the Lowell 42-in. telescopes.*

Note: Weighted means, a_T^*, and physical parameters for individual objects can be found in Table 2.3.

Table B.2: Photometry Data: L5 Trojans

Object	Telescope[a]	Date (UT)	α (°)	V (mag)	B-V (mag)	V-R (mag)	V-I (mag)
(617) Patroclus	0.9m	2011 Mar. 26	10.5	(No V data)	(No B data)	R (mag)	R-I
						15.35 ± 0.020	0.36 ± 0.034
(617) Patroclus	1.0m	2011 June 24	9.6	15.10 ± 0.021	0.74 ± 0.030	0.40 ± 0.036	0.82 ± 0.059
(617) Patroclus	1.0m	2011 Aug. 10	6.0	14.81 ± 0.017	0.66 ± 0.026	0.45 ± 0.026	0.85 ± 0.029
(617) Patroclus	1.0m	2011 Nov. 13	12.4	15.58 ± 0.023	0.72 ± 0.063	0.42 ± 0.050	0.80 ± 0.088
(617) Patroclus	42in	2013 Nov. 6	0.6	14.56 ± 0.029	0.69 ± 0.061	0.41 ± 0.034	0.83 ± 0.047
(884) Priamus	0.9m	2010 July 4	5.9	15.53 ± 0.012	0.74 ± 0.042	0.47 ± 0.034	0.92 ± 0.056
(884) Priamus	0.9m	2010 Oct. 23	12.3	16.10 ± 0.012	0.76 ± 0.043	0.43 ± 0.030	0.92 ± 0.049
(884) Priamus	42in	2010 Nov. 26	11.0	16.25 ± 0.015	0.74 ± 0.088	0.48 ± 0.029	1.00 ± 0.041
(884) Priamus	1.0m	2011 Aug. 10	6.7	15.69 ± 0.017	0.73 ± 0.043	0.46 ± 0.026	0.87 ± 0.027
(884) Priamus	1.0m	2011 Aug. 11	6.5	15.61 ± 0.021	0.80 ± 0.046	0.40 ± 0.034	0.86 ± 0.046
(884) Priamus	1.0m	2011 June 24	11.9	16.10 ± 0.020	0.73 ± 0.049	0.48 ± 0.039	0.94 ± 0.067
(884) Priamus	1.0m	2011 Nov. 13	10.7	16.06 ± 0.024	0.76 ± 0.052	0.47 ± 0.037	0.88 ± 0.066
(1172) Aneas	0.9m	2010 July 4	6.4	15.25 ± 0.012	0.76 ± 0.031	0.47 ± 0.028	0.94 ± 0.045
(1172) Aneas	1.0m	2011 June 22	12.2	15.58 ± 0.026	0.98 ± 0.097	0.46 ± 0.058	1.13 ± 0.107
(1172) Aneas	1.0m	2011 Aug. 10	7.6	15.11 ± 0.017	0.79 ± 0.032	0.45 ± 0.027	0.93 ± 0.035
(1172) Aneas	1.0m	2011 Nov. 14	11.0	15.48 ± 0.021	0.75 ± 0.050	0.46 ± 0.061	0.98 ± 0.042
(1173) Anchises	0.9m	2011 Mar. 26	10.7	16.41 ± 0.024	· · ·	0.37 ± 0.041	0.76 ± 0.067
(1173) Anchises	1.0m	2011 June 22	8.4	16.06 ± 0.017	0.71 ± 0.036	0.40 ± 0.028	0.80 ± 0.039
(1173) Anchises	1.0m	2011 Aug. 10	2.5	15.25 ± 0.019	0.72 ± 0.040	0.35 ± 0.031	0.77 ± 0.042
(1173) Anchises	1.0m	2011 Aug. 13	3.2	15.25 ± 0.019	0.70 ± 0.041	0.38 ± 0.027	0.78 ± 0.041
(1173) Anchises	1.0m	2011 Nov. 13	12.1	16.61 ± 0.024	0.65 ± 0.046	0.42 ± 0.035	0.75 ± 0.083
(1208) Troilus	0.9m	2010 Oct. 23	11.7	16.51 ± 0.012	0.74 ± 0.034	0.35 ± 0.018	0.69 ± 0.027
(1208) Troilus	1.0m	2011 Aug. 10	8.7	15.96 ± 0.015	0.70 ± 0.045	0.37 ± 0.076	0.72 ± 0.101
(1208) Troilus	1.0m	2011 Nov. 16	11.9	16.54 ± 0.019	0.72 ± 0.049	0.39 ± 0.031	0.83 ± 0.038
(1208) Troilus	0.9m	2012 Sept. 29	5.5	15.76 ± 0.026	0.83 ± 0.055	0.39 ± 0.036	0.76 ± 0.046
(1867) Deiphobus	0.9m	2010 July 4	2.1	15.14 ± 0.012	0.75 ± 0.044	0.47 ± 0.034	0.93 ± 0.056
(1867) Deiphobus	1.0m	2011 June 24	10.2	15.68 ± 0.019	0.78 ± 0.034	0.44 ± 0.028	0.90 ± 0.041
(1867) Deiphobus	1.0m	2011 Aug. 9	4.9	15.40 ± 0.026	0.74 ± 0.047	0.51 ± 0.073	0.98 ± 0.079
(1867) Deiphobus	1.0m	2011 Nov. 14	11.4	16.23 ± 0.022	0.76 ± 0.062	0.44 ± 0.081	0.95 ± 0.056
(2207) Antenor	1.0m	2011 June 24	10.2	16.51 ± 0.020	0.77 ± 0.035	0.46 ± 0.029	1.06 ± 0.040
(2207) Antenor	1.0m	2011 Aug. 9	3.3	16.07 ± 0.024	0.75 ± 0.041	0.48 ± 0.072	0.95 ± 0.072
(2207) Antenor	1.0m	2011 Aug. 11	2.9	16.00 ± 0.024	0.81 ± 0.053	0.42 ± 0.039	0.88 ± 0.053

Continued on next page

Table B.2 – continued from previous page

Object	Telescope[a]	Date (UT)	α (°)	V (mag)	B-V (mag)	V-R (mag)	V-I (mag)
(2207) Antenor	1.0m	2011 Nov. 13	10.9	16.72 ± 0.029	0.76 ± 0.055	0.44 ± 0.039	0.81 ± 0.060
(2223) Sarpedon	42in	2010 Nov. 25	10.1	17.09 ± 0.049	0.79 ± 0.111	0.47 ± 0.086	0.98 ± 0.101
(2223) Sarpedon	1.0m	2011 Aug. 9	6.4	16.42 ± 0.024	0.80 ± 0.047	0.43 ± 0.075	0.88 ± 0.081
(2223) Sarpedon	1.0m	2011 Aug. 11	6.2	16.34 ± 0.031	0.64 ± 0.052	0.42 ± 0.041	0.85 ± 0.047
(2241) Alcathous	1.0m	2011 June 24	8.5	16.06 ± 0.019	0.76 ± 0.036	0.54 ± 0.028	0.95 ± 0.042
(2241) Alcathous	1.0m	2011 Aug. 10	3.0	15.79 ± 0.022	0.75 ± 0.040	0.47 ± 0.031	0.95 ± 0.037
(2241) Alcathous	1.0m	2011 Aug. 13	3.0	15.98 ± 0.046	0.47 ± 0.066	0.46 ± 0.063	0.92 ± 0.073
(2241) Alcathous	1.0m	2011 Nov. 13	10.5	16.57 ± 0.023	· · ·	0.52 ± 0.034	0.93 ± 0.057
(2357) Phereclos	0.9m	2010 Sept. 29	10.4	16.36 ± 0.009	0.76 ± 0.025	0.48 ± 0.020	0.97 ± 0.034
(2357) Phereclos	0.9m	2010 Oct. 22	11.3	16.56 ± 0.017	0.67 ± 0.043	0.42 ± 0.022	0.91 ± 0.022
(2357) Phereclos	1.0m	2011 Aug. 10	4.6	16.02 ± 0.019	0.77 ± 0.036	0.44 ± 0.029	0.90 ± 0.036
(2357) Phereclos	1.0m	2011 Aug. 11	4.4	16.05 ± 0.024	0.69 ± 0.048	0.48 ± 0.036	0.93 ± 0.044
(2357) Phereclos	1.0m	2011 June 24	10.8	16.53 ± 0.020	0.71 ± 0.035	0.46 ± 0.028	1.03 ± 0.039
(2357) Phereclos	1.0m	2011 Nov. 14	10.7	16.59 ± 0.023	0.71 ± 0.047	0.51 ± 0.059	1.05 ± 0.039
(2357) Phereclos	0.9m	2012 Sept. 29	1.3	16.06 ± 0.033	· · ·	0.52 ± 0.043	1.05 ± 0.050
(2357) Phereclos	0.9m	2012 Oct. 4	0.3	16.11 ± 0.020	0.87 ± 0.037	0.47 ± 0.037	0.95 ± 0.058
(2357) Phereclos	42in	2013 Nov. 6	0.4	16.21 ± 0.029	0.77 ± 0.062	0.46 ± 0.035	0.96 ± 0.048
(2363) Cebriones	42in	2010 Nov. 25	10.9	16.70 ± 0.048	0.76 ± 0.110	0.48 ± 0.085	0.92 ± 0.100
(2363) Cebriones	42in	2010 Nov. 26	10.9	16.74 ± 0.016	0.72 ± 0.082	0.49 ± 0.043	0.91 ± 0.065
(2674) Pandarus	0.9m	2010 Oct. 22	11.1	16.95 ± 0.023	0.81 ± 0.064	0.46 ± 0.030	1.02 ± 0.028
(2674) Pandarus	1.0m	2011 Aug. 10	4.0	16.32 ± 0.022	0.73 ± 0.052	0.43 ± 0.043	0.89 ± 0.067
(2893) Peiroos	1.0m	2011 Aug. 10	1.9	15.62 ± 0.022	0.67 ± 0.033	0.49 ± 0.030	0.99 ± 0.032
(2893) Peiroos	1.0m	2011 June 24	8.8	16.11 ± 0.019	0.73 ± 0.048	0.46 ± 0.037	0.92 ± 0.063
(2893) Peiroos	0.9m	2012 Oct. 4	5.2	15.96 ± 0.018	0.76 ± 0.031	0.46 ± 0.022	0.93 ± 0.027
(2895) Memnon	1.0m	2011 Aug. 9	2.4	16.95 ± 0.031	0.65 ± 0.049	0.40 ± 0.075	0.72 ± 0.076
(2895) Memnon	1.0m	2011 Aug. 11	2.1	16.87 ± 0.036	0.70 ± 0.064	0.36 ± 0.049	0.71 ± 0.063
(3240) Laocoon	1.0m	2011 June 27	9.4	17.16 ± 0.019	0.69 ± 0.041	0.43 ± 0.035	0.89 ± 0.059
(3240) Laocoon	1.0m	2011 Aug. 10	0.4	16.43 ± 0.016	0.64 ± 0.055	0.43 ± 0.045	0.85 ± 0.074
(3317) Paris	0.9m	2010 July 2	6.3	14.93 ± 0.014	0.77 ± 0.031	0.45 ± 0.025	0.91 ± 0.035
(3317) Paris	0.9m	2010 Sept. 29	11.5	15.50 ± 0.008	0.76 ± 0.024	0.47 ± 0.020	0.94 ± 0.038
(3317) Paris	0.9m	2010 Oct. 22	12.4	15.71 ± 0.013	0.75 ± 0.028	0.44 ± 0.016	0.90 ± 0.018
(3317) Paris	0.9m	2010 Oct. 23	12.5	15.80 ± 0.016	0.73 ± 0.037	0.49 ± 0.022	0.94 ± 0.022
(3317) Paris	42in	2010 Nov. 25	10.9	15.83 ± 0.048	0.78 ± 0.109	0.41 ± 0.084	0.92 ± 0.096
(3317) Paris	42in	2010 Nov. 26	10.8	15.97 ± 0.022	0.72 ± 0.102	0.49 ± 0.058	0.97 ± 0.204
(3317) Paris	1.0m	2011 June 24	11.9	15.85 ± 0.020	0.73 ± 0.042	0.47 ± 0.034	0.93 ± 0.054

Continued on next page

Table B.2 – continued from previous page

Object	Telescope[a]	Date (UT)	α (°)	V (mag)	B-V (mag)	V-R (mag)	V-I (mag)
(3317) Paris	1.0m	2011 Aug. 9	6.5	15.40 ± 0.024	0.73 ± 0.038	0.52 ± 0.071	0.97 ± 0.069
(3317) Paris	1.0m	2011 Aug. 10	6.3	15.35 ± 0.015	0.74 ± 0.026	0.46 ± 0.024	0.92 ± 0.028
(3317) Paris	1.0m	2011 Aug. 11	6.2	15.34 ± 0.019	0.75 ± 0.041	0.45 ± 0.031	0.95 ± 0.044
(3317) Paris	1.0m	2011 Nov. 13	11.3	15.89 ± 0.026	0.69 ± 0.059	0.55 ± 0.042	0.97 ± 0.074
(3317) Paris	0.9m	2012 Sept. 29	6.1	16.01 ± 0.026	· · ·	0.59 ± 0.034	1.11 ± 0.041
(3317) Paris	0.9m	2012 Oct. 4	5.8	15.70 ± 0.021	0.83 ± 0.039	0.45 ± 0.031	1.09 ± 0.033
(3451) Mentor	0.9m	2010 July 2	8.3	15.37 ± 0.014	0.69 ± 0.044	0.36 ± 0.035	0.73 ± 0.057
(3451) Mentor	1.0m	2011 June 24	12.2	15.94 ± 0.020	0.72 ± 0.079	0.40 ± 0.039	0.81 ± 0.066
(3451) Mentor	1.0m	2011 Aug. 10	7.3	15.45 ± 0.015	0.70 ± 0.030	0.41 ± 0.026	0.77 ± 0.035
(3451) Mentor	1.0m	2011 Aug. 11	7.2	15.68 ± 0.022	0.71 ± 0.047	0.39 ± 0.037	0.78 ± 0.050
(3451) Mentor	1.0m	2011 Nov. 13	10.8	15.67 ± 0.025	0.76 ± 0.088	0.34 ± 0.043	0.77 ± 0.077
(3451) Mentor	0.9m	2012 Sept. 29	4.7	15.32 ± 0.024	0.75 ± 0.053	0.38 ± 0.035	0.77 ± 0.045
3708	1.0m	2011 June 27	9.1	16.22 ± 0.017	0.74 ± 0.037	0.47 ± 0.032	1.01 ± 0.054
3708	1.0m	2011 Aug. 10	1.8	15.82 ± 0.023	0.70 ± 0.040	0.50 ± 0.033	0.96 ± 0.038
(4348) Poulydamas	1.0m	2011 June 22	8.5	17.08 ± 0.024	0.65 ± 0.045	0.40 ± 0.038	0.85 ± 0.051
(4348) Poulydamas	1.0m	2011 Aug. 10	2.3	16.51 ± 0.036	0.63 ± 0.061	0.41 ± 0.050	0.82 ± 0.052
(4708) Polydoros	1.0m	2011 Aug. 13	3.8	17.15 ± 0.043	0.83 ± 0.092	0.52 ± 0.060	0.91 ± 0.087
(4708) Polydoros	1.0m	2011 Aug. 9	3.0	17.18 ± 0.046	0.73 ± 0.080	0.58 ± 0.084	1.00 ± 0.086
(4708) Polydoros	1.0m	2011 June 24	6.2	17.38 ± 0.021	0.76 ± 0.045	0.46 ± 0.034	0.96 ± 0.054
(4709) Ennomos	0.9m	2010 Sept. 29	10.2	15.91 ± 0.009	0.71 ± 0.024	0.38 ± 0.019	0.73 ± 0.034
(4709) Ennomos	1.0m	2011 Aug. 11	7.9	16.01 ± 0.027	0.67 ± 0.074	0.36 ± 0.040	0.66 ± 0.048
(4709) Ennomos	1.0m	2011 Aug. 9	8.1	16.06 ± 0.028	0.68 ± 0.048	0.36 ± 0.074	0.74 ± 0.076
(4709) Ennomos	1.0m	2011 June 22	11.4	15.92 ± 0.018	0.63 ± 0.039	0.34 ± 0.028	0.65 ± 0.047
(4709) Ennomos	1.0m	2011 Nov. 14	10.6	16.03 ± 0.021	0.69 ± 0.036	0.36 ± 0.067	0.68 ± 0.048
(4709) Ennomos	42in	2010 Nov. 26	10.3	16.49 ± 0.016	0.70 ± 0.082	0.34 ± 0.031	0.69 ± 0.042
(4709) Ennomos	42in	2013 Nov. 6	3.4	15.35 ± 0.029	· · ·	0.36 ± 0.034	0.66 ± 0.048
4715	0.9m	2010 Oct. 23	11.0	17.43 ± 0.029	0.61 ± 0.061	0.40 ± 0.038	0.83 ± 0.038
4715	1.0m	2011 Aug. 10	3.3	16.88 ± 0.030	0.75 ± 0.052	0.45 ± 0.043	0.88 ± 0.048
(4722) Agelaos	1.0m	2011 Aug. 13	3.5	17.03 ± 0.043	0.66 ± 0.076	0.49 ± 0.055	0.92 ± 0.056
(4722) Agelaos	1.0m	2011 June 22	7.8	17.41 ± 0.021	0.71 ± 0.061	0.51 ± 0.046	0.89 ± 0.082
(4791) Iphidamas	1.0m	2011 Aug. 11	5.1	18.04 ± 0.094	0.06 ± 0.131	1.04 ± 0.108	1.20 ± 0.119
(4791) Iphidamas	1.0m	2011 Aug. 9	4.9	18.06 ± 0.085	0.60 ± 0.138	0.78 ± 0.116	1.15 ± 0.122
(4791) Iphidamas	1.0m	2011 June 24	7.6	17.79 ± 0.022	0.74 ± 0.048	0.43 ± 0.038	0.96 ± 0.061
(4792) Lykaon	1.0m	2011 Aug. 11	2.4	16.66 ± 0.033	0.94 ± 0.073	0.35 ± 0.048	1.01 ± 0.056
(4792) Lykaon	1.0m	2011 Aug. 9	2.4	15.32 ± 0.023	0.71 ± 0.033	0.48 ± 0.070	0.80 ± 0.067

Continued on next page

Table B.2 – continued from previous page

Object	Telescope[a]	Date (UT)	α (°)	V (mag)	B-V (mag)	V-R (mag)	V-I (mag)
(4792) Lykaon	1.0m	2011 June 27	8.8	17.25 ± 0.017	· · ·	0.47 ± 0.026	0.98 ± 0.040
(4792) Lykaon	42in	2013 Nov. 10	2.6	17.00 ± 0.026	0.75 ± 0.031	0.48 ± 0.037	0.99 ± 0.049
(4828) Misenus	1.0m	2011 Aug. 10	2.2	17.82 ± 0.045	0.67 ± 0.093	0.39 ± 0.068	0.85 ± 0.079
(4828) Misenus	1.0m	2011 June 24	8.0	18.23 ± 0.026	0.67 ± 0.058	0.43 ± 0.046	0.99 ± 0.076
(4832) Palinurus	1.0m	2011 Aug. 11	2.7	16.50 ± 0.031	0.88 ± 0.060	0.42 ± 0.050	0.97 ± 0.086
(4832) Palinurus	1.0m	2011 Aug. 9	3.1	16.59 ± 0.031	0.77 ± 0.047	0.59 ± 0.074	1.04 ± 0.073
(4832) Palinurus	42in	2013 Nov. 10	4.8	17.02 ± 0.025	0.91 ± 0.028	0.51 ± 0.041	0.98 ± 0.052
(4867) Polites	0.9m	2010 Oct. 23	11.2	17.83 ± 0.037	0.64 ± 0.092	0.54 ± 0.053	1.07 ± 0.062
(4867) Polites	1.0m	2011 Aug. 10	3.4	16.97 ± 0.031	0.67 ± 0.059	0.48 ± 0.046	0.94 ± 0.062
5119	1.0m	2011 Aug. 10	2.2	16.89 ± 0.029	0.72 ± 0.063	0.42 ± 0.049	0.81 ± 0.073
5119	1.0m	2011 June 24	10.8	17.60 ± 0.023	0.63 ± 0.047	0.46 ± 0.036	1.06 ± 0.053
5119	42in	2013 Nov. 10	3.9	17.40 ± 0.026	0.75 ± 0.029	0.48 ± 0.037	0.97 ± 0.049
(5120) Bitias	1.0m	2011 Aug. 10	2.9	16.84 ± 0.039	0.74 ± 0.069	0.48 ± 0.051	0.80 ± 0.053
(5120) Bitias	1.0m	2011 June 22	10.1	17.44 ± 0.026	0.82 ± 0.051	0.42 ± 0.038	0.76 ± 0.052
(5130) Ilioneus	0.9m	2012 Oct. 4	7.9	17.18 ± 0.019	0.79 ± 0.037	0.49 ± 0.028	0.96 ± 0.042
(5130) Ilioneus	1.0m	2011 Aug. 11	5.3	16.82 ± 0.070	1.09 ± 0.133	0.29 ± 0.112	0.97 ± 0.106
(5130) Ilioneus	1.0m	2011 Aug. 12	5.4	17.20 ± 0.510	0.62 ± 0.536	0.79 ± 0.523	1.17 ± 0.511
(5130) Ilioneus	1.0m	2011 June 25	5.8	17.16 ± 0.064	0.74 ± 0.099	0.41 ± 0.105	1.05 ± 0.110
(5130) Ilioneus	42in	2013 Nov. 6	7.4	17.17 ± 0.030	0.76 ± 0.062	0.46 ± 0.036	0.93 ± 0.052
(5144) Achates	0.9m	2011 Mar. 27	12.3	15.80 ± 0.030	· · ·	0.45 ± 0.041	0.92 ± 0.055
(5144) Achates	1.0m	2011 Aug. 10	0.9	14.48 ± 0.018	0.79 ± 0.030	0.45 ± 0.026	0.88 ± 0.030
(5144) Achates	1.0m	2011 Aug. 10	0.9	14.52 ± 0.017	0.73 ± 0.030	0.46 ± 0.026	0.91 ± 0.035
(5144) Achates	1.0m	2011 Aug. 11	0.6	14.46 ± 0.019	0.74 ± 0.039	0.44 ± 0.030	0.94 ± 0.037
(5144) Achates	1.0m	2011 Aug. 11	0.6	14.46 ± 0.019	0.76 ± 0.040	0.44 ± 0.031	0.91 ± 0.039
(5144) Achates	1.0m	2011 Aug. 11	0.6	14.49 ± 0.021	0.75 ± 0.042	0.46 ± 0.033	0.95 ± 0.040
(5144) Achates	1.0m	2011 Aug. 14	0.3	14.47 ± 0.023	0.72 ± 0.058	0.45 ± 0.036	0.93 ± 0.038
(5144) Achates	1.0m	2011 Aug. 14	0.3	14.47 ± 0.024	0.76 ± 0.071	0.45 ± 0.049	0.89 ± 0.075
(5144) Achates	1.0m	2011 June 24	12.2	15.06 ± 0.019	0.74 ± 0.045	0.49 ± 0.039	0.97 ± 0.069
(5511) Cloanthus	1.0m	2011 Aug. 11	6.7	17.46 ± 0.045	0.77 ± 0.090	0.41 ± 0.060	0.80 ± 0.074
(5511) Cloanthus	1.0m	2011 Aug. 9	7.0	17.08 ± 0.026	0.77 ± 0.045	0.53 ± 0.073	1.00 ± 0.084
(5511) Cloanthus	1.0m	2011 Nov. 14	10.9	18.06 ± 0.043	0.52 ± 0.098	0.51 ± 0.083	0.88 ± 0.072
(5638) Deikoon	1.0m	2011 Aug. 10	1.2	17.43 ± 0.043	0.66 ± 0.073	0.39 ± 0.058	0.78 ± 0.061
(5638) Deikoon	1.0m	2011 June 27	9.1	17.86 ± 0.021	0.79 ± 0.041	0.46 ± 0.033	1.01 ± 0.054
5648	1.0m	2011 June 22	8.0	16.65 ± 0.015	0.72 ± 0.038	0.48 ± 0.029	0.88 ± 0.053
5648	1.0m	2011 June 27	7.3	16.46 ± 0.017	0.73 ± 0.026	0.48 ± 0.026	0.92 ± 0.040

Continued on next page

Table B.2 – continued from previous page

Object	Telescope[a]	Date (UT)	α (°)	V (mag)	B-V (mag)	V-R (mag)	V-I (mag)
7352	1.0m	2011 Aug. 10	1.4	16.90 ± 0.038	0.53 ± 0.060	0.52 ± 0.051	0.86 ± 0.056
7352	1.0m	2011 June 27	7.5	17.36 ± 0.019	0.79 ± 0.032	0.40 ± 0.029	0.91 ± 0.044
7352	1.0m	2011 Nov. 12	11.1	17.85 ± 0.040	0.70 ± 0.087	0.46 ± 0.051	0.77 ± 0.072
7352	42in	2013 Nov. 6	5.2	17.20 ± 0.031	0.76 ± 0.063	0.46 ± 0.037	0.81 ± 0.052
12929	1.0m	2011 Aug. 11	8.9	17.38 ± 0.039	0.91 ± 0.097	0.41 ± 0.054	0.89 ± 0.063
12929	1.0m	2011 Aug. 9	9.1	17.41 ± 0.034	0.78 ± 0.058	0.48 ± 0.076	0.89 ± 0.075
12929	1.0m	2011 Nov. 14	10.1	17.49 ± 0.024	0.75 ± 0.053	0.48 ± 0.072	0.95 ± 0.053
12929	42in	2010 Nov. 26	11.1	17.68 ± 0.021	0.89 ± 0.090	0.48 ± 0.040	0.78 ± 0.061
16070	1.0m	2011 Aug. 11	5.7	16.44 ± 0.037	0.79 ± 0.073	0.38 ± 0.055	0.90 ± 0.065
16070	1.0m	2011 Aug. 9	6.0	16.53 ± 0.030	0.75 ± 0.054	0.57 ± 0.078	0.93 ± 0.088
16070	42in	2013 Nov. 6	3.9	17.31 ± 0.031	0.83 ± 0.063	0.50 ± 0.038	1.01 ± 0.053
22180	0.9m	2012 Oct. 4	8.3	17.44 ± 0.020	0.78 ± 0.033	0.43 ± 0.041	0.88 ± 0.069
22180	1.0m	2011 June 27	7.5	17.93 ± 0.024	0.76 ± 0.049	0.45 ± 0.042	1.02 ± 0.067
22180	42in	2013 Nov. 10	6.7	17.16 ± 0.026	0.77 ± 0.031	0.47 ± 0.036	1.01 ± 0.050
32496	1.0m	2011 Aug. 11	8.9	17.47 ± 0.038	0.75 ± 0.074	0.43 ± 0.051	0.91 ± 0.054
32496	1.0m	2011 Aug. 9	9.0	17.42 ± 0.030	0.79 ± 0.047	0.45 ± 0.075	0.98 ± 0.079
32496	1.0m	2011 Nov. 12	11.2	17.74 ± 0.047	0.74 ± 0.100	0.59 ± 0.059	1.13 ± 0.067
32496	1.0m	2011 Nov. 16	11.4	17.66 ± 0.030	0.73 ± 0.059	0.50 ± 0.045	0.91 ± 0.038
34746	1.0m	2011 Aug. 10	4.8	16.95 ± 0.032	0.69 ± 0.054	0.46 ± 0.043	0.94 ± 0.046
34746	1.0m	2011 June 22	7.8	17.25 ± 0.020	0.66 ± 0.040	0.43 ± 0.031	0.96 ± 0.042
76867	0.9m	2012 Oct. 4	5.8	17.73 ± 0.036	1.20 ± 0.118	0.44 ± 0.050	0.96 ± 0.066
76867	1.0m	2011 Aug. 11	6.7	18.09 ± 0.070	0.60 ± 0.132	0.49 ± 0.087	1.02 ± 0.090
76867	1.0m	2011 Aug. 9	6.7	17.70 ± 0.039	0.63 ± 0.065	0.47 ± 0.079	0.92 ± 0.081
76867	1.0m	2011 Nov. 12	11.3	18.12 ± 0.046	1.06 ± 0.141	0.30 ± 0.073	0.59 ± 0.123
76867	42in	2013 Nov. 10	4.4	17.53 ± 0.027	0.87 ± 0.032	0.48 ± 0.037	0.96 ± 0.050

[a] *The three telescopes used to acquire these data were the CTIO/SMARTS 0.9-m and 1.0-m as well as the Lowell 42-in. telescopes.*

Note: Weighted means, a_T^*, and physical parameters for individual objects can be found in Table 2.4.

C Trojan Color-Curve Data

Table C.1: 884 Priamus: $V - I$ Color Variation for Partial Light Curve

Date	Time[a] (UT)	V (Relative)	I (Interpolated)	$V - I$
15 Nov 2011	23:39:55	0.100 ± 0.007	0.080 ± 0.015	0.020 ± 0.016
15 Nov 2011	23:45:42	0.101 ± 0.006	0.066 ± 0.012	0.035 ± 0.013
15 Nov 2011	23:51:27	0.084 ± 0.006	0.067 ± 0.011	0.017 ± 0.012
15 Nov 2011	23:57:14	0.081 ± 0.005	0.055 ± 0.010	0.026 ± 0.011
16 Nov 2011	00:02:59	0.058 ± 0.005	0.030 ± 0.010	0.028 ± 0.011
16 Nov 2011	00:08:46	0.038 ± 0.005	0.028 ± 0.010	0.010 ± 0.011
16 Nov 2011	00:14:31	0.037 ± 0.005	0.031 ± 0.009	0.006 ± 0.011
16 Nov 2011	00:20:17	0.029 ± 0.005	0.019 ± 0.009	0.010 ± 0.011
16 Nov 2011	00:26:02	0.003 ± 0.005	0.003 ± 0.010	0.000 ± 0.011
16 Nov 2011	00:31:49	0.002 ± 0.005	0.011 ± 0.009	-0.009 ± 0.010
16 Nov 2011	00:37:35	-0.007 ± 0.005	0.000 ± 0.009	-0.007 ± 0.010
16 Nov 2011	00:43:20	-0.027 ± 0.005	-0.013 ± 0.009	-0.014 ± 0.010
16 Nov 2011	00:49:07	-0.034 ± 0.005	-0.009 ± 0.009	-0.025 ± 0.010
16 Nov 2011	00:54:52	-0.048 ± 0.005	-0.028 ± 0.009	-0.020 ± 0.010
16 Nov 2011	01:00:38	-0.042 ± 0.005	-0.050 ± 0.009	0.008 ± 0.010
16 Nov 2011	01:06:24	-0.036 ± 0.005	-0.060 ± 0.009	0.024 ± 0.011
16 Nov 2011	01:15:27	-0.048 ± 0.005	-0.056 ± 0.009	0.008 ± 0.011
16 Nov 2011	01:21:12	-0.061 ± 0.005	-0.065 ± 0.009	0.004 ± 0.011
16 Nov 2011	01:26:59	-0.052 ± 0.005	-0.065 ± 0.009	0.013 ± 0.011
16 Nov 2011	01:32:45	-0.047 ± 0.005	-0.039 ± 0.009	-0.008 ± 0.011
16 Nov 2011	01:38:30	-0.061 ± 0.005	-0.030 ± 0.010	-0.031 ± 0.011
16 Nov 2011	01:44:17	-0.038 ± 0.005	-0.026 ± 0.010	-0.012 ± 0.011
16 Nov 2011	01:50:02	-0.022 ± 0.005	-0.010 ± 0.010	-0.012 ± 0.012
16 Nov 2011	01:55:49	-0.012 ± 0.005	0.012 ± 0.010	-0.024 ± 0.012
16 Nov 2011	02:29:30	-0.008 ± 0.009	-0.009 ± 0.011	0.000 ± 0.014
16 Nov 2011	02:35:16	-0.003 ± 0.009	0.005 ± 0.012	-0.008 ± 0.015
16 Nov 2011	02:41:02	0.007 ± 0.009	0.010 ± 0.012	-0.003 ± 0.015
16 Nov 2011	02:46:47	0.002 ± 0.010	0.013 ± 0.012	-0.012 ± 0.016
16 Nov 2011	02:52:33	0.004 ± 0.011	-0.001 ± 0.012	0.004 ± 0.016

Note: These data are plotted in Figure 3.1.
[a] Times have been corrected for light travel time between the object and the observer.

Table C.2: 911 Agamemnon: $V - I$ Color Variation for Partial Light Curve

Date	Time[a] (UT)	V (Relative)	I (Interpolated)	$V - I$
24 Feb 2013	00:54:27	0.017 ± 0.016	0.019 ± 0.014	-0.001 ± 0.021
24 Feb 2013	00:58:02	-0.001 ± 0.016	-0.006 ± 0.014	0.005 ± 0.021
24 Feb 2013	01:01:37	-0.031 ± 0.016	-0.008 ± 0.014	-0.023 ± 0.021
24 Feb 2013	01:05:11	-0.021 ± 0.016	-0.012 ± 0.015	-0.008 ± 0.022
24 Feb 2013	01:08:45	-0.006 ± 0.017	-0.009 ± 0.016	0.003 ± 0.023
24 Feb 2013	01:12:20	-0.008 ± 0.018	0.001 ± 0.017	-0.008 ± 0.025
24 Feb 2013	01:15:55	0.014 ± 0.018	0.002 ± 0.017	0.013 ± 0.025
24 Feb 2013	01:19:29	0.006 ± 0.018	-0.001 ± 0.017	0.007 ± 0.025
24 Feb 2013	01:25:26	-0.009 ± 0.018	0.000 ± 0.016	-0.009 ± 0.024
24 Feb 2013	01:29:00	-0.004 ± 0.016	-0.001 ± 0.015	-0.002 ± 0.022
24 Feb 2013	01:32:35	0.002 ± 0.017	-0.002 ± 0.017	0.004 ± 0.024
24 Feb 2013	01:36:09	0.018 ± 0.018	0.009 ± 0.017	0.009 ± 0.024
24 Feb 2013	01:39:44	0.047 ± 0.018	0.026 ± 0.017	0.021 ± 0.024

Continued on next page

Table C.2 – continued from previous page

Date	Time[a] (UT)	V (Relative)	I (Interpolated)	$V-I$
24 Feb 2013	01:43:19	0.027 ± 0.018	0.022 ± 0.016	0.005 ± 0.024
24 Feb 2013	01:46:53	0.016 ± 0.016	0.010 ± 0.016	0.007 ± 0.023
24 Feb 2013	01:50:27	0.010 ± 0.020	0.010 ± 0.017	0.001 ± 0.026
24 Feb 2013	01:56:21	0.011 ± 0.016	0.010 ± 0.018	0.002 ± 0.024
24 Feb 2013	01:59:56	0.024 ± 0.019	0.011 ± 0.018	0.013 ± 0.027
24 Feb 2013	02:03:30	0.010 ± 0.019	0.010 ± 0.017	0.000 ± 0.025
24 Feb 2013	02:07:05	0.048 ± 0.017	0.013 ± 0.016	0.036 ± 0.023
24 Feb 2013	02:10:39	0.033 ± 0.017	0.018 ± 0.017	0.016 ± 0.024
24 Feb 2013	02:14:14	0.020 ± 0.018	0.013 ± 0.017	0.007 ± 0.025
24 Feb 2013	02:17:48	0.019 ± 0.016	0.016 ± 0.016	0.003 ± 0.022
24 Feb 2013	02:21:23	0.010 ± 0.017	0.019 ± 0.015	-0.009 ± 0.023
24 Feb 2013	02:40:54	-0.002 ± 0.018	0.007 ± 0.017	-0.009 ± 0.025
24 Feb 2013	02:44:29	0.012 ± 0.016	0.008 ± 0.015	0.004 ± 0.022
24 Feb 2013	02:48:03	0.052 ± 0.014	0.012 ± 0.014	0.040 ± 0.020
24 Feb 2013	02:51:38	0.018 ± 0.015	0.005 ± 0.015	0.014 ± 0.021
24 Feb 2013	02:55:13	-0.005 ± 0.016	0.005 ± 0.014	-0.010 ± 0.021
24 Feb 2013	02:58:47	0.029 ± 0.014	0.013 ± 0.014	0.016 ± 0.019
24 Feb 2013	03:02:21	0.005 ± 0.014	0.013 ± 0.014	-0.007 ± 0.020
24 Feb 2013	03:05:55	-0.011 ± 0.014	0.008 ± 0.014	-0.019 ± 0.020
24 Feb 2013	03:11:54	-0.011 ± 0.015	0.003 ± 0.014	-0.014 ± 0.021
24 Feb 2013	03:15:29	0.003 ± 0.016	0.007 ± 0.015	-0.004 ± 0.022
24 Feb 2013	03:19:03	-0.004 ± 0.015	0.009 ± 0.014	-0.012 ± 0.021
24 Feb 2013	03:22:38	0.007 ± 0.017	0.002 ± 0.015	0.005 ± 0.023
24 Feb 2013	03:26:13	-0.009 ± 0.015	0.003 ± 0.015	-0.011 ± 0.021
24 Feb 2013	03:29:47	0.032 ± 0.016	0.003 ± 0.016	0.030 ± 0.022
24 Feb 2013	03:33:21	0.024 ± 0.014	0.012 ± 0.015	0.013 ± 0.021
24 Feb 2013	03:36:57	0.029 ± 0.014	0.015 ± 0.014	0.014 ± 0.020
24 Feb 2013	03:42:48	0.021 ± 0.014	0.010 ± 0.014	0.011 ± 0.020
24 Feb 2013	03:46:22	0.026 ± 0.015	0.016 ± 0.014	0.011 ± 0.021
24 Feb 2013	03:49:58	0.022 ± 0.014	0.015 ± 0.014	0.007 ± 0.020
24 Feb 2013	03:53:32	0.013 ± 0.014	0.017 ± 0.013	-0.004 ± 0.019
24 Feb 2013	03:57:06	0.031 ± 0.014	0.025 ± 0.013	0.007 ± 0.019
24 Feb 2013	04:00:40	0.049 ± 0.014	0.033 ± 0.014	0.017 ± 0.019
24 Feb 2013	04:04:15	0.035 ± 0.015	0.032 ± 0.014	0.003 ± 0.021
24 Feb 2013	04:07:50	0.044 ± 0.015	0.024 ± 0.015	0.021 ± 0.021
24 Feb 2013	04:13:47	0.019 ± 0.014	0.009 ± 0.016	0.010 ± 0.021
24 Feb 2013	04:17:21	0.009 ± 0.014	0.004 ± 0.015	0.005 ± 0.020
24 Feb 2013	04:20:55	0.028 ± 0.015	0.018 ± 0.015	0.010 ± 0.021
24 Feb 2013	04:24:30	0.008 ± 0.014	0.022 ± 0.013	-0.014 ± 0.019
24 Feb 2013	04:28:05	0.015 ± 0.014	0.012 ± 0.014	0.004 ± 0.019
24 Feb 2013	04:31:39	-0.002 ± 0.014	0.012 ± 0.014	-0.014 ± 0.019
24 Feb 2013	04:35:13	-0.010 ± 0.014	0.014 ± 0.013	-0.023 ± 0.019
24 Feb 2013	04:38:48	-0.001 ± 0.015	0.013 ± 0.014	-0.014 ± 0.020
24 Feb 2013	04:44:39	-0.011 ± 0.014	0.009 ± 0.013	-0.020 ± 0.019
24 Feb 2013	04:48:13	0.008 ± 0.014	0.011 ± 0.014	-0.002 ± 0.019
24 Feb 2013	04:51:48	-0.015 ± 0.015	0.004 ± 0.013	-0.019 ± 0.020
24 Feb 2013	04:55:23	-0.001 ± 0.014	-0.002 ± 0.014	0.002 ± 0.019
24 Feb 2013	04:58:57	0.001 ± 0.014	-0.003 ± 0.014	0.004 ± 0.020
24 Feb 2013	05:02:32	0.011 ± 0.014	0.004 ± 0.013	0.008 ± 0.019
24 Feb 2013	05:06:06	-0.006 ± 0.014	0.004 ± 0.014	-0.009 ± 0.019
24 Feb 2013	05:09:41	-0.016 ± 0.015	-0.003 ± 0.014	-0.013 ± 0.020
24 Feb 2013	05:15:31	-0.018 ± 0.014	-0.005 ± 0.013	-0.012 ± 0.019
24 Feb 2013	05:19:06	0.006 ± 0.015	-0.008 ± 0.013	0.014 ± 0.020

Continued on next page

Table C.2 – continued from previous page

Date	Time[a] (UT)	V (Relative)	I (Interpolated)	$V-I$
24 Feb 2013	05:22:40	0.005 ± 0.014	-0.011 ± 0.013	0.017 ± 0.019
24 Feb 2013	05:26:14	-0.014 ± 0.014	-0.003 ± 0.013	-0.010 ± 0.019
24 Feb 2013	05:29:49	-0.018 ± 0.014	-0.003 ± 0.013	-0.014 ± 0.019
24 Feb 2013	05:33:24	-0.016 ± 0.014	-0.015 ± 0.014	-0.000 ± 0.019
24 Feb 2013	05:36:58	-0.030 ± 0.013	-0.007 ± 0.013	-0.022 ± 0.018
24 Feb 2013	05:40:32	-0.018 ± 0.014	-0.002 ± 0.013	-0.015 ± 0.019
24 Feb 2013	05:46:23	-0.016 ± 0.014	-0.018 ± 0.014	0.002 ± 0.019
24 Feb 2013	05:49:57	-0.024 ± 0.014	-0.016 ± 0.013	-0.007 ± 0.019
24 Feb 2013	05:53:32	-0.043 ± 0.014	-0.024 ± 0.014	-0.018 ± 0.019
24 Feb 2013	05:57:07	-0.054 ± 0.014	-0.027 ± 0.014	-0.027 ± 0.020
24 Feb 2013	06:00:41	-0.045 ± 0.014	-0.031 ± 0.014	-0.014 ± 0.019
24 Feb 2013	06:04:16	-0.025 ± 0.014	-0.035 ± 0.013	0.010 ± 0.019
24 Feb 2013	06:07:50	-0.025 ± 0.014	-0.036 ± 0.014	0.011 ± 0.019
24 Feb 2013	06:11:25	-0.056 ± 0.015	-0.041 ± 0.014	-0.015 ± 0.020
24 Feb 2013	06:17:15	-0.049 ± 0.014	-0.038 ± 0.014	-0.010 ± 0.019
24 Feb 2013	06:20:50	-0.044 ± 0.014	-0.038 ± 0.014	-0.005 ± 0.020
24 Feb 2013	06:24:24	-0.030 ± 0.015	-0.043 ± 0.014	0.013 ± 0.021
24 Feb 2013	06:27:59	-0.037 ± 0.015	-0.046 ± 0.014	0.009 ± 0.021
24 Feb 2013	06:31:33	-0.034 ± 0.015	-0.047 ± 0.015	0.013 ± 0.021
24 Feb 2013	06:35:08	-0.054 ± 0.015	-0.046 ± 0.015	-0.008 ± 0.021
24 Feb 2013	06:38:43	-0.030 ± 0.014	-0.041 ± 0.013	0.012 ± 0.019
24 Feb 2013	06:42:17	-0.054 ± 0.014	-0.032 ± 0.013	-0.021 ± 0.019

Note: These data are plotted in Figure 3.3.
[a] Times have been corrected for light travel time between the object and the observer.

Table C.3: 1143 Odysseus: $V-I$ Color Variation for Partial Light Curve

Date	Time[a] (UT)	V (Relative)	I (Interpolated)	$V-I$
22 Oct 2010	04:20:03	-0.077 ± 0.020	-0.063 ± 0.025	-0.015 ± 0.033
22 Oct 2010	04:21:51	-0.061 ± 0.021	-0.049 ± 0.027	-0.013 ± 0.035
22 Oct 2010	04:23:38	-0.093 ± 0.017	-0.047 ± 0.024	-0.047 ± 0.026
22 Oct 2010	04:25:26	-0.031 ± 0.029	-0.057 ± 0.017	0.025 ± 0.032
22 Oct 2010	04:27:14	0.004 ± 0.019	-0.058 ± 0.016	0.062 ± 0.027
22 Oct 2010	04:29:02	-0.011 ± 0.015	-0.043 ± 0.016	0.031 ± 0.021
22 Oct 2010	04:30:49	-0.038 ± 0.027	-0.019 ± 0.031	-0.020 ± 0.056
22 Oct 2010	04:32:37	-0.025 ± 0.020	-0.022 ± 0.035	-0.003 ± 0.029
22 Oct 2010	04:34:25	-0.013 ± 0.037	-0.030 ± 0.017	0.017 ± 0.040
22 Oct 2010	04:36:12	-0.029 ± 0.017	-0.035 ± 0.014	0.006 ± 0.023
22 Oct 2010	04:40:14	-0.046 ± 0.016	-0.064 ± 0.017	0.017 ± 0.024
22 Oct 2010	04:42:22	-0.008 ± 0.028	-0.069 ± 0.015	0.061 ± 0.030
22 Oct 2010	04:44:30	-0.034 ± 0.018	-0.047 ± 0.015	0.013 ± 0.026
22 Oct 2010	04:46:37	-0.033 ± 0.014	-0.033 ± 0.016	-0.000 ± 0.020
22 Oct 2010	04:48:44	-0.005 ± 0.015	-0.030 ± 0.013	0.024 ± 0.019
22 Oct 2010	04:50:52	-0.030 ± 0.013	-0.015 ± 0.010	-0.016 ± 0.016
22 Oct 2010	04:53:00	-0.003 ± 0.012	-0.021 ± 0.009	0.018 ± 0.015
22 Oct 2010	04:55:08	-0.030 ± 0.012	-0.025 ± 0.009	-0.005 ± 0.015
22 Oct 2010	04:57:15	-0.039 ± 0.012	-0.025 ± 0.009	-0.014 ± 0.015
22 Oct 2010	04:59:23	-0.002 ± 0.012	-0.028 ± 0.009	0.026 ± 0.015
22 Oct 2010	05:03:13	-0.037 ± 0.012	-0.017 ± 0.009	-0.021 ± 0.015
22 Oct 2010	05:05:29	-0.012 ± 0.012	-0.007 ± 0.009	-0.005 ± 0.015
22 Oct 2010	05:07:37	-0.021 ± 0.012	-0.008 ± 0.009	-0.013 ± 0.015

Continued on next page

Table C.3 – continued from previous page

Date	Time[a] (UT)	V (Relative)	I (Interpolated)	$V-I$
22 Oct 2010	05:09:44	-0.033 ± 0.012	-0.022 ± 0.008	-0.012 ± 0.014
22 Oct 2010	05:11:52	-0.022 ± 0.012	-0.027 ± 0.008	0.005 ± 0.014
22 Oct 2010	05:14:00	0.039 ± 0.012	-0.010 ± 0.008	0.048 ± 0.015
22 Oct 2010	05:16:07	-0.002 ± 0.012	0.017 ± 0.009	-0.020 ± 0.015
22 Oct 2010	05:18:15	-0.000 ± 0.012	0.023 ± 0.009	-0.024 ± 0.015
22 Oct 2010	05:20:23	-0.009 ± 0.012	0.016 ± 0.009	-0.025 ± 0.015
22 Oct 2010	05:22:30	-0.019 ± 0.012	0.016 ± 0.009	-0.035 ± 0.015
22 Oct 2010	05:24:38	0.046 ± 0.012	0.022 ± 0.009	0.024 ± 0.015
22 Oct 2010	05:27:08	0.017 ± 0.012	0.026 ± 0.009	-0.009 ± 0.015
22 Oct 2010	05:29:16	0.036 ± 0.012	0.023 ± 0.009	0.012 ± 0.015
22 Oct 2010	05:31:24	0.051 ± 0.012	0.027 ± 0.009	0.023 ± 0.015
22 Oct 2010	05:33:31	0.022 ± 0.012	0.038 ± 0.009	-0.017 ± 0.015
22 Oct 2010	05:35:39	0.019 ± 0.012	0.057 ± 0.009	-0.038 ± 0.015
22 Oct 2010	05:37:47	0.067 ± 0.013	0.063 ± 0.009	0.003 ± 0.016
22 Oct 2010	05:39:55	0.087 ± 0.013	0.063 ± 0.009	0.023 ± 0.016
22 Oct 2010	05:42:02	0.077 ± 0.013	0.074 ± 0.009	0.002 ± 0.016
22 Oct 2010	05:44:10	0.056 ± 0.012	0.064 ± 0.009	-0.008 ± 0.015
22 Oct 2010	05:46:18	0.056 ± 0.013	0.075 ± 0.009	-0.020 ± 0.016
22 Oct 2010	05:49:03	0.061 ± 0.013	0.101 ± 0.009	-0.041 ± 0.016
22 Oct 2010	05:51:11	0.106 ± 0.013	0.105 ± 0.009	0.001 ± 0.016
22 Oct 2010	05:53:19	0.080 ± 0.013	0.111 ± 0.009	-0.031 ± 0.016
22 Oct 2010	05:55:27	0.072 ± 0.013	0.108 ± 0.009	-0.036 ± 0.016
22 Oct 2010	05:57:34	0.136 ± 0.013	0.103 ± 0.009	0.033 ± 0.016
22 Oct 2010	05:59:43	0.067 ± 0.013	0.102 ± 0.009	-0.035 ± 0.016
22 Oct 2010	06:01:51	0.113 ± 0.013	0.090 ± 0.009	0.023 ± 0.016
22 Oct 2010	06:03:59	0.133 ± 0.013	0.083 ± 0.009	0.049 ± 0.016
22 Oct 2010	06:06:07	0.075 ± 0.013	0.079 ± 0.009	-0.004 ± 0.016
22 Oct 2010	06:08:14	0.093 ± 0.013	0.065 ± 0.009	0.028 ± 0.016
22 Oct 2010	06:11:06	0.073 ± 0.013	0.071 ± 0.009	0.002 ± 0.016
22 Oct 2010	06:13:14	0.068 ± 0.013	0.082 ± 0.009	-0.015 ± 0.016
22 Oct 2010	06:15:22	0.076 ± 0.013	0.077 ± 0.009	-0.002 ± 0.016
22 Oct 2010	06:17:29	0.069 ± 0.013	0.051 ± 0.009	0.017 ± 0.016
22 Oct 2010	06:19:37	0.076 ± 0.013	0.044 ± 0.009	0.032 ± 0.016
22 Oct 2010	06:21:45	0.057 ± 0.013	0.066 ± 0.009	-0.009 ± 0.016
22 Oct 2010	06:23:52	0.038 ± 0.013	0.059 ± 0.009	-0.021 ± 0.016
22 Oct 2010	06:26:01	0.063 ± 0.013	0.036 ± 0.009	0.027 ± 0.016
22 Oct 2010	06:28:09	0.054 ± 0.013	0.044 ± 0.009	0.009 ± 0.016
22 Oct 2010	06:30:17	0.055 ± 0.013	0.028 ± 0.009	0.027 ± 0.016
22 Oct 2010	06:33:27	0.058 ± 0.013	0.005 ± 0.009	0.052 ± 0.016
22 Oct 2010	06:35:35	0.019 ± 0.012	0.007 ± 0.009	0.011 ± 0.015
22 Oct 2010	06:37:43	-0.001 ± 0.012	0.003 ± 0.009	-0.005 ± 0.016
22 Oct 2010	06:39:51	0.022 ± 0.014	0.011 ± 0.014	0.010 ± 0.022
22 Oct 2010	06:41:59	0.025 ± 0.019	0.035 ± 0.020	-0.010 ± 0.030
22 Oct 2010	06:44:07	0.046 ± 0.050	0.022 ± 0.023	0.023 ± 0.055
22 Oct 2010	06:46:15	0.048 ± 0.015	0.011 ± 0.018	0.037 ± 0.019
22 Oct 2010	06:48:23	0.035 ± 0.017	0.005 ± 0.011	0.030 ± 0.020
22 Oct 2010	06:50:30	0.004 ± 0.012	-0.010 ± 0.009	0.013 ± 0.015
22 Oct 2010	06:52:38	-0.022 ± 0.012	-0.011 ± 0.009	-0.011 ± 0.015
22 Oct 2010	06:55:42	0.001 ± 0.012	-0.010 ± 0.009	0.011 ± 0.015
22 Oct 2010	06:57:50	-0.010 ± 0.012	-0.013 ± 0.009	0.003 ± 0.015
22 Oct 2010	06:59:58	-0.030 ± 0.012	-0.038 ± 0.008	0.007 ± 0.014
22 Oct 2010	07:02:05	-0.033 ± 0.012	-0.048 ± 0.008	0.015 ± 0.015
22 Oct 2010	07:04:14	-0.038 ± 0.012	-0.027 ± 0.009	-0.012 ± 0.015

Continued on next page

Table C.3 – continued from previous page

Date	Time[a] (UT)	V (Relative)	I (Interpolated)	$V-I$
22 Oct 2010	07:06:22	-0.040 ± 0.012	-0.023 ± 0.009	-0.017 ± 0.015
22 Oct 2010	07:08:30	-0.062 ± 0.012	-0.027 ± 0.009	-0.035 ± 0.015
22 Oct 2010	07:10:37	-0.048 ± 0.012	-0.025 ± 0.009	-0.023 ± 0.015
22 Oct 2010	07:12:46	-0.033 ± 0.012	-0.032 ± 0.009	-0.002 ± 0.015
22 Oct 2010	07:14:54	-0.047 ± 0.012	-0.032 ± 0.009	-0.016 ± 0.015
22 Oct 2010	07:21:04	-0.053 ± 0.012	-0.034 ± 0.009	-0.019 ± 0.015
22 Oct 2010	07:23:12	-0.046 ± 0.012	-0.030 ± 0.009	-0.016 ± 0.015
22 Oct 2010	07:25:20	-0.035 ± 0.012	-0.032 ± 0.009	-0.004 ± 0.015
22 Oct 2010	07:27:27	-0.074 ± 0.012	-0.038 ± 0.009	-0.036 ± 0.015
22 Oct 2010	07:29:34	-0.061 ± 0.012	-0.042 ± 0.009	-0.020 ± 0.015
22 Oct 2010	07:31:43	-0.022 ± 0.012	-0.041 ± 0.009	0.018 ± 0.015
22 Oct 2010	07:33:51	-0.068 ± 0.012	-0.034 ± 0.009	-0.035 ± 0.015
22 Oct 2010	07:35:59	-0.045 ± 0.012	-0.036 ± 0.009	-0.010 ± 0.015
22 Oct 2010	07:38:08	-0.049 ± 0.012	-0.039 ± 0.009	-0.011 ± 0.015
22 Oct 2010	07:40:15	-0.031 ± 0.012	-0.045 ± 0.009	0.014 ± 0.015
22 Oct 2010	07:42:31	-0.048 ± 0.012	-0.043 ± 0.009	-0.005 ± 0.015
22 Oct 2010	07:44:40	-0.044 ± 0.012	-0.033 ± 0.009	-0.011 ± 0.015
22 Oct 2010	07:46:48	-0.034 ± 0.012	-0.024 ± 0.009	-0.011 ± 0.015
22 Oct 2010	07:48:56	-0.052 ± 0.012	-0.031 ± 0.009	-0.021 ± 0.015
22 Oct 2010	07:51:04	-0.048 ± 0.012	-0.045 ± 0.009	-0.004 ± 0.015
22 Oct 2010	07:53:11	-0.029 ± 0.012	-0.045 ± 0.009	0.015 ± 0.015
22 Oct 2010	07:55:18	-0.015 ± 0.012	-0.044 ± 0.009	0.029 ± 0.015
22 Oct 2010	07:57:26	-0.058 ± 0.012	-0.038 ± 0.009	-0.021 ± 0.015
22 Oct 2010	07:59:34	-0.058 ± 0.012	-0.034 ± 0.009	-0.024 ± 0.016
22 Oct 2010	08:01:42	-0.052 ± 0.012	-0.042 ± 0.009	-0.011 ± 0.015
22 Oct 2010	08:04:12	-0.044 ± 0.012	-0.059 ± 0.010	0.015 ± 0.016
22 Oct 2010	08:06:19	-0.058 ± 0.012	-0.053 ± 0.010	-0.005 ± 0.016
22 Oct 2010	08:08:27	-0.028 ± 0.012	-0.034 ± 0.010	0.006 ± 0.016
22 Oct 2010	08:10:35	0.002 ± 0.013	-0.022 ± 0.010	0.024 ± 0.016
22 Oct 2010	08:12:44	-0.025 ± 0.012	-0.020 ± 0.010	-0.006 ± 0.016
22 Oct 2010	08:14:53	-0.011 ± 0.012	-0.016 ± 0.010	0.004 ± 0.016
22 Oct 2010	08:17:00	-0.008 ± 0.012	-0.011 ± 0.010	0.003 ± 0.016
22 Oct 2010	08:19:07	-0.047 ± 0.012	-0.014 ± 0.010	-0.034 ± 0.016
22 Oct 2010	08:21:15	-0.018 ± 0.012	-0.017 ± 0.010	-0.001 ± 0.016
22 Oct 2010	08:23:24	-0.061 ± 0.012	-0.036 ± 0.010	-0.025 ± 0.016

Note: These data are plotted in Figure 3.5.

[a] Times have been corrected for light travel time between the object and the observer.

Table C.4: 2207 Antenor: $V-I$ Color Variation for Partial Light Curve

Date	Time[a] (UT)	V (Relative)	I (Interpolated)	$V-I$
16 Nov 2011	23:38:31	-0.007 ± 0.008	-0.020 ± 0.014	0.014 ± 0.016
16 Nov 2011	23:45:17	0.003 ± 0.007	0.016 ± 0.011	-0.012 ± 0.013
16 Nov 2011	23:52:03	-0.006 ± 0.006	0.015 ± 0.009	-0.021 ± 0.011
16 Nov 2011	23:58:50	-0.007 ± 0.006	0.009 ± 0.008	-0.015 ± 0.010
17 Nov 2011	00:05:36	0.013 ± 0.006	0.017 ± 0.008	-0.004 ± 0.010
17 Nov 2011	00:12:22	-0.010 ± 0.006	0.019 ± 0.009	-0.029 ± 0.011
17 Nov 2011	00:19:08	0.008 ± 0.006	-0.002 ± 0.008	0.011 ± 0.010
17 Nov 2011	00:25:55	0.005 ± 0.006	0.012 ± 0.009	-0.006 ± 0.011
17 Nov 2011	00:32:41	0.041 ± 0.006	0.017 ± 0.009	0.025 ± 0.011
17 Nov 2011	00:39:26	0.036 ± 0.007	0.040 ± 0.009	-0.003 ± 0.011

Continued on next page

Table C.4 – continued from previous page

Date	Time[a] (UT)	V (Relative)	I (Interpolated)	$V-I$
17 Nov 2011	00:46:12	0.063 ± 0.007	0.065 ± 0.009	-0.002 ± 0.011
17 Nov 2011	00:52:58	0.079 ± 0.007	0.090 ± 0.010	-0.010 ± 0.012
17 Nov 2011	00:59:44	0.088 ± 0.007	0.082 ± 0.010	0.006 ± 0.012
17 Nov 2011	01:06:30	0.100 ± 0.007	0.093 ± 0.010	0.008 ± 0.012
17 Nov 2011	01:13:16	0.107 ± 0.007	0.091 ± 0.010	0.016 ± 0.012
17 Nov 2011	01:20:02	0.115 ± 0.007	0.090 ± 0.010	0.025 ± 0.012
17 Nov 2011	01:32:14	0.085 ± 0.007	0.101 ± 0.010	-0.015 ± 0.012
17 Nov 2011	01:39:00	0.069 ± 0.007	0.093 ± 0.010	-0.024 ± 0.012
17 Nov 2011	01:45:46	0.082 ± 0.007	0.076 ± 0.010	0.006 ± 0.012
17 Nov 2011	01:52:33	0.052 ± 0.007	0.058 ± 0.010	-0.006 ± 0.012
17 Nov 2011	02:26:06	0.055 ± 0.008	0.028 ± 0.011	0.027 ± 0.014
17 Nov 2011	02:32:53	0.077 ± 0.008	0.064 ± 0.012	0.013 ± 0.014
17 Nov 2011	02:39:42	0.093 ± 0.009	0.067 ± 0.012	0.026 ± 0.015
29 Sept 2012	00:54:57	0.031 ± 0.018	0.002 ± 0.012	0.029 ± 0.022
29 Sept 2012	01:02:01	0.092 ± 0.018	-0.006 ± 0.012	0.099 ± 0.022
29 Sept 2012	01:09:05	-0.045 ± 0.016	-0.046 ± 0.012	0.001 ± 0.020
29 Sept 2012	01:16:10	-0.080 ± 0.015	-0.086 ± 0.011	0.007 ± 0.019
29 Sept 2012	01:23:15	-0.069 ± 0.015	-0.100 ± 0.011	0.032 ± 0.018
29 Sept 2012	01:32:07	-0.091 ± 0.014	-0.101 ± 0.010	0.010 ± 0.017
29 Sept 2012	01:39:12	-0.082 ± 0.015	-0.108 ± 0.011	0.027 ± 0.018
29 Sept 2012	01:46:17	-0.039 ± 0.016	-0.096 ± 0.011	0.057 ± 0.019
29 Sept 2012	01:53:22	-0.091 ± 0.014	-0.092 ± 0.010	0.001 ± 0.017
29 Sept 2012	02:00:26	-0.143 ± 0.013	-0.100 ± 0.010	-0.043 ± 0.016
29 Sept 2012	02:07:46	-0.098 ± 0.014	-0.094 ± 0.010	-0.004 ± 0.018
29 Sept 2012	02:14:50	-0.080 ± 0.015	-0.083 ± 0.011	0.004 ± 0.019
29 Sept 2012	02:21:55	-0.085 ± 0.015	-0.068 ± 0.011	-0.017 ± 0.019
29 Sept 2012	02:28:59	-0.027 ± 0.015	-0.041 ± 0.011	0.014 ± 0.019
29 Sept 2012	02:36:04	-0.011 ± 0.015	-0.019 ± 0.011	0.008 ± 0.019
29 Sept 2012	03:21:14	0.121 ± 0.016	0.078 ± 0.011	0.044 ± 0.020
29 Sept 2012	03:28:18	0.025 ± 0.015	0.037 ± 0.011	-0.012 ± 0.019
29 Sept 2012	03:35:22	-0.037 ± 0.014	-0.003 ± 0.011	-0.034 ± 0.018
29 Sept 2012	03:42:27	-0.037 ± 0.014	-0.022 ± 0.011	-0.015 ± 0.018
29 Sept 2012	03:49:32	-0.044 ± 0.014	-0.025 ± 0.011	-0.018 ± 0.018
29 Sept 2012	04:15:23	0.010 ± 0.014	-0.038 ± 0.010	0.049 ± 0.017
29 Sept 2012	04:22:27	-0.059 ± 0.014	-0.037 ± 0.010	-0.022 ± 0.017
29 Sept 2012	04:29:32	-0.052 ± 0.013	-0.026 ± 0.010	-0.025 ± 0.017
29 Sept 2012	04:36:36	-0.011 ± 0.014	-0.012 ± 0.011	0.002 ± 0.018
29 Sept 2012	04:43:41	-0.016 ± 0.014	-0.017 ± 0.011	0.001 ± 0.018
29 Sept 2012	05:17:45	-0.061 ± 0.014	-0.076 ± 0.010	0.016 ± 0.017
29 Sept 2012	05:24:50	-0.100 ± 0.013	-0.100 ± 0.010	0.000 ± 0.016
29 Sept 2012	05:31:55	-0.141 ± 0.013	-0.126 ± 0.010	-0.015 ± 0.016
29 Sept 2012	05:38:59	-0.121 ± 0.014	-0.154 ± 0.010	0.033 ± 0.017
29 Sept 2012	05:46:04	-0.172 ± 0.017	-0.182 ± 0.010	0.010 ± 0.020

Note: These data are plotted in Figure 3.7.

[a] Times have been corrected for light travel time between the object and the observer.

Table C.5: 2357 Phereclos: $V-I$ Color Variation for Partial Light Curve

Date	Time[a] (UT)	V (Relative)	I (Interpolated)	$V-I$
8 Sept 2011	06:23:43	-0.020 ± 0.014	-0.006 ± 0.000	-0.014 ± 0.014
8 Sept 2011	06:42:41	-0.025 ± 0.018	-0.007 ± 0.022	-0.018 ± 0.029

Continued on next page

Table C.5 – continued from previous page

Date	Time[a] (UT)	V (Relative)	I (Interpolated)	$V-I$
8 Sept 2011	07:08:38	-0.031 ± 0.021	-0.022 ± 0.010	-0.009 ± 0.023
8 Sept 2011	07:17:17	-0.002 ± 0.014	-0.020 ± 0.009	0.018 ± 0.017
8 Sept 2011	07:25:55	-0.011 ± 0.014	-0.014 ± 0.009	0.003 ± 0.017
8 Sept 2011	07:34:33	-0.006 ± 0.014	-0.010 ± 0.010	0.004 ± 0.017
8 Sept 2011	07:44:39	0.010 ± 0.023	0.008 ± 0.010	0.002 ± 0.025
8 Sept 2011	07:53:18	-0.031 ± 0.014	0.045 ± 0.013	-0.076 ± 0.019
8 Sept 2011	08:01:57	0.004 ± 0.015	-0.005 ± 0.009	0.009 ± 0.017
8 Sept 2011	08:10:35	0.016 ± 0.013	-0.010 ± 0.009	0.026 ± 0.016
8 Sept 2011	08:19:14	0.008 ± 0.013	-0.016 ± 0.012	0.024 ± 0.018
8 Sept 2011	08:28:06	0.014 ± 0.022	-0.001 ± 0.026	0.015 ± 0.034
8 Sept 2011	08:36:44	0.018 ± 0.019	-0.006 ± 0.009	0.025 ± 0.021
8 Sept 2011	08:45:23	0.009 ± 0.010	0.016 ± 0.009	-0.007 ± 0.013
8 Sept 2011	08:54:48	0.012 ± 0.008	0.023 ± 0.008	-0.011 ± 0.011
8 Sept 2011	09:03:28	0.008 ± 0.007	0.007 ± 0.008	0.001 ± 0.011
8 Sept 2011	09:12:06	0.008 ± 0.007	0.026 ± 0.007	-0.018 ± 0.010
8 Sept 2011	09:20:45	0.014 ± 0.006	0.034 ± 0.009	-0.019 ± 0.011
8 Sept 2011	09:29:24	0.039 ± 0.013	-0.008 ± 0.023	0.047 ± 0.026
8 Sept 2011	09:38:03	-0.036 ± 0.011	-0.049 ± 0.037	0.014 ± 0.038
3 Oct 2012	02:17:19	-0.003 ± 0.014	0.007 ± 0.012	-0.010 ± 0.018
3 Oct 2012	02:23:38	-0.001 ± 0.014	-0.008 ± 0.012	0.008 ± 0.018
3 Oct 2012	02:29:56	0.000 ± 0.014	-0.008 ± 0.012	0.008 ± 0.018
3 Oct 2012	02:36:15	0.025 ± 0.014	0.003 ± 0.011	0.023 ± 0.018
3 Oct 2012	02:42:33	-0.009 ± 0.014	0.013 ± 0.012	-0.021 ± 0.018
3 Oct 2012	02:52:33	-0.020 ± 0.015	-0.000 ± 0.012	-0.019 ± 0.019
3 Oct 2012	02:58:51	-0.013 ± 0.016	0.002 ± 0.012	-0.014 ± 0.020
3 Oct 2012	03:05:10	-0.010 ± 0.015	0.007 ± 0.013	-0.017 ± 0.020
3 Oct 2012	03:11:28	-0.028 ± 0.014	0.005 ± 0.012	-0.033 ± 0.018
3 Oct 2012	03:17:47	-0.029 ± 0.014	0.005 ± 0.012	-0.034 ± 0.018
3 Oct 2012	03:27:31	-0.016 ± 0.014	-0.009 ± 0.012	-0.007 ± 0.018
3 Oct 2012	03:33:49	0.001 ± 0.014	-0.008 ± 0.012	0.009 ± 0.018
3 Oct 2012	03:40:07	-0.030 ± 0.015	-0.009 ± 0.012	-0.021 ± 0.019
3 Oct 2012	03:46:26	-0.021 ± 0.014	-0.016 ± 0.012	-0.005 ± 0.018
3 Oct 2012	03:52:45	-0.016 ± 0.014	-0.006 ± 0.012	-0.010 ± 0.018
3 Oct 2012	04:02:24	0.022 ± 0.014	0.012 ± 0.012	0.010 ± 0.018
3 Oct 2012	04:08:43	0.010 ± 0.014	0.002 ± 0.011	0.008 ± 0.018
3 Oct 2012	04:15:01	-0.006 ± 0.014	-0.004 ± 0.012	-0.002 ± 0.018
3 Oct 2012	04:21:20	0.003 ± 0.017	-0.005 ± 0.013	0.008 ± 0.021
3 Oct 2012	04:27:38	-0.020 ± 0.015	-0.003 ± 0.013	-0.016 ± 0.020
3 Oct 2012	04:37:04	0.019 ± 0.015	0.014 ± 0.013	0.005 ± 0.020
3 Oct 2012	04:43:22	0.009 ± 0.017	0.028 ± 0.014	-0.019 ± 0.022
3 Oct 2012	05:02:54	0.011 ± 0.014	0.010 ± 0.012	0.001 ± 0.018
3 Oct 2012	05:09:12	-0.016 ± 0.014	-0.005 ± 0.011	-0.010 ± 0.018
3 Oct 2012	05:15:31	-0.005 ± 0.014	-0.005 ± 0.011	0.000 ± 0.018
3 Oct 2012	05:21:49	0.001 ± 0.014	-0.009 ± 0.011	0.010 ± 0.018
3 Oct 2012	05:28:07	-0.018 ± 0.014	-0.011 ± 0.011	-0.007 ± 0.018
3 Oct 2012	05:37:14	-0.010 ± 0.014	-0.010 ± 0.012	-0.000 ± 0.018
3 Oct 2012	05:43:33	-0.001 ± 0.014	-0.012 ± 0.012	0.011 ± 0.018
3 Oct 2012	05:49:51	0.001 ± 0.014	-0.009 ± 0.011	0.010 ± 0.018
3 Oct 2012	05:56:10	0.010 ± 0.015	-0.003 ± 0.012	0.014 ± 0.019
3 Oct 2012	06:02:28	0.004 ± 0.015	-0.010 ± 0.012	0.014 ± 0.019
3 Oct 2012	06:11:52	-0.010 ± 0.015	-0.004 ± 0.012	-0.005 ± 0.019
3 Oct 2012	06:18:11	0.001 ± 0.015	-0.006 ± 0.012	0.007 ± 0.019
3 Oct 2012	06:24:30	0.012 ± 0.015	-0.011 ± 0.012	0.023 ± 0.019

Continued on next page

Table C.5 – continued from previous page

Date	Time[a] (UT)	V (Relative)	I (Interpolated)	$V-I$
3 Oct 2012	06:30:48	-0.005 ± 0.015	-0.012 ± 0.012	0.007 ± 0.019
3 Oct 2012	06:37:07	-0.018 ± 0.015	-0.008 ± 0.012	-0.009 ± 0.019
3 Oct 2012	06:46:35	-0.003 ± 0.015	-0.003 ± 0.012	0.000 ± 0.019
3 Oct 2012	06:52:53	0.035 ± 0.017	-0.001 ± 0.013	0.036 ± 0.021
3 Oct 2012	06:59:11	0.005 ± 0.018	0.001 ± 0.013	0.004 ± 0.022
3 Oct 2012	07:05:31	0.015 ± 0.016	0.018 ± 0.013	-0.002 ± 0.020
3 Oct 2012	07:11:49	-0.003 ± 0.017	0.008 ± 0.012	-0.010 ± 0.021
3 Oct 2012	07:21:14	0.009 ± 0.017	-0.000 ± 0.013	0.009 ± 0.021
3 Oct 2012	07:27:33	0.012 ± 0.017	0.022 ± 0.013	-0.010 ± 0.022
3 Oct 2012	07:33:51	0.047 ± 0.019	0.032 ± 0.014	0.015 ± 0.023
3 Oct 2012	07:40:09	0.004 ± 0.025	-0.002 ± 0.014	0.007 ± 0.029
3 Oct 2012	07:46:30	0.042 ± 0.020	0.009 ± 0.016	0.034 ± 0.026
8 Nov 2013	02:03:42	-0.024 ± 0.011	· · ·	· · ·
8 Nov 2013	02:14:34	-0.015 ± 0.008	· · ·	· · ·
8 Nov 2013	02:25:14	-0.011 ± 0.007	· · ·	· · ·
8 Nov 2013	02:42:34	-0.031 ± 0.009	· · ·	· · ·
8 Nov 2013	02:53:13	-0.024 ± 0.010	· · ·	· · ·
8 Nov 2013	03:04:06	-0.024 ± 0.007	· · ·	· · ·
8 Nov 2013	03:14:47	-0.013 ± 0.007	· · ·	· · ·
8 Nov 2013	03:25:38	-0.011 ± 0.009	· · ·	· · ·
8 Nov 2013	03:36:19	0.006 ± 0.007	· · ·	· · ·
8 Nov 2013	03:52:25	0.038 ± 0.007	· · ·	· · ·
8 Nov 2013	04:03:19	0.053 ± 0.008	· · ·	· · ·
8 Nov 2013	04:14:00	0.071 ± 0.007	· · ·	· · ·
8 Nov 2013	04:24:52	0.083 ± 0.007	· · ·	· · ·
8 Nov 2013	04:35:32	0.084 ± 0.007	· · ·	· · ·
8 Nov 2013	04:46:24	0.090 ± 0.007	· · ·	· · ·
8 Nov 2013	05:02:30	0.071 ± 0.007	· · ·	· · ·
8 Nov 2013	05:13:23	0.111 ± 0.007	· · ·	· · ·
8 Nov 2013	05:24:15	0.107 ± 0.007	· · ·	· · ·
8 Nov 2013	05:34:55	0.088 ± 0.007	· · ·	· · ·
8 Nov 2013	05:45:47	0.071 ± 0.006	· · ·	· · ·
8 Nov 2013	05:56:27	0.048 ± 0.006	· · ·	· · ·
8 Nov 2013	06:14:04	0.008 ± 0.006	· · ·	· · ·
8 Nov 2013	06:24:46	-0.016 ± 0.006	· · ·	· · ·
8 Nov 2013	06:35:26	-0.030 ± 0.006	· · ·	· · ·
8 Nov 2013	06:46:06	-0.044 ± 0.006	· · ·	· · ·
8 Nov 2013	06:56:46	-0.058 ± 0.006	· · ·	· · ·
8 Nov 2013	07:07:27	-0.093 ± 0.006	· · ·	· · ·
8 Nov 2013	07:24:52	-0.052 ± 0.006	· · ·	· · ·
8 Nov 2013	07:35:44	-0.050 ± 0.006	· · ·	· · ·
8 Nov 2013	07:46:24	-0.035 ± 0.006	· · ·	· · ·
8 Nov 2013	07:57:05	-0.036 ± 0.006	· · ·	· · ·
8 Nov 2013	08:07:57	-0.032 ± 0.006	· · ·	· · ·
8 Nov 2013	08:18:36	-0.034 ± 0.006	· · ·	· · ·
8 Nov 2013	08:34:42	-0.042 ± 0.006	· · ·	· · ·
8 Nov 2013	08:45:23	-0.043 ± 0.006	· · ·	· · ·
8 Nov 2013	08:56:04	-0.032 ± 0.007	· · ·	· · ·
8 Nov 2013	09:06:44	-0.041 ± 0.007	· · ·	· · ·
8 Nov 2013	09:17:24	-0.014 ± 0.007	· · ·	· · ·
8 Nov 2013	09:28:16	-0.008 ± 0.007	· · ·	· · ·
8 Nov 2013	09:45:04	-0.013 ± 0.007	· · ·	· · ·
8 Nov 2013	09:55:56	-0.014 ± 0.007	· · ·	· · ·

Continued on next page

Table C.5 – continued from previous page

Date	Time[a] (UT)	V (Relative)	I (Interpolated)	$V-I$
8 Nov 2013	10:06:36	-0.018 ± 0.007	· · ·	· · ·
8 Nov 2013	10:17:17	-0.011 ± 0.007	· · ·	· · ·
8 Nov 2013	10:27:57	-0.000 ± 0.007	· · ·	· · ·
8 Nov 2013	10:38:38	-0.000 ± 0.009	· · ·	· · ·

Note: These data are plotted in Figure 3.9.
[a] Times have been corrected for light travel time between the object and the observer.

Table C.6: 2920 Automedon: $V-I$ Color Variation for Partial Light Curve

Date	Time[a] (UT)	V (Relative)	I (Interpolated)	$V-I$
13 Dec 2011	04:45:01	-0.001 ± 0.016	0.074 ± 0.024	-0.075 ± 0.029
13 Dec 2011	04:47:18	0.033 ± 0.016	0.055 ± 0.017	-0.023 ± 0.023
13 Dec 2011	04:49:35	0.050 ± 0.016	0.037 ± 0.013	0.013 ± 0.021
13 Dec 2011	04:51:53	0.032 ± 0.016	0.025 ± 0.013	0.007 ± 0.021
13 Dec 2011	04:54:11	0.051 ± 0.016	0.021 ± 0.013	0.030 ± 0.021
13 Dec 2011	04:56:29	0.005 ± 0.016	0.024 ± 0.013	-0.019 ± 0.021
13 Dec 2011	04:58:47	0.024 ± 0.016	0.035 ± 0.013	-0.011 ± 0.021
13 Dec 2011	05:01:04	0.026 ± 0.016	0.042 ± 0.013	-0.016 ± 0.021
13 Dec 2011	05:03:22	0.002 ± 0.016	0.041 ± 0.013	-0.039 ± 0.021
13 Dec 2011	05:05:40	0.058 ± 0.016	0.034 ± 0.013	0.024 ± 0.021
13 Dec 2011	05:07:57	0.031 ± 0.016	0.006 ± 0.013	0.025 ± 0.021
13 Dec 2011	05:10:14	-0.013 ± 0.015	0.002 ± 0.013	-0.015 ± 0.020
13 Dec 2011	05:12:33	-0.000 ± 0.016	0.019 ± 0.013	-0.019 ± 0.021
13 Dec 2011	05:14:50	0.028 ± 0.016	0.010 ± 0.013	0.018 ± 0.021
13 Dec 2011	05:17:07	0.007 ± 0.016	0.004 ± 0.013	0.003 ± 0.021
13 Dec 2011	05:19:26	0.002 ± 0.016	0.010 ± 0.013	-0.008 ± 0.021
13 Dec 2011	05:21:43	-0.013 ± 0.016	0.022 ± 0.013	-0.035 ± 0.021
13 Dec 2011	05:24:00	0.019 ± 0.016	0.024 ± 0.013	-0.005 ± 0.021
13 Dec 2011	05:26:18	0.034 ± 0.016	0.035 ± 0.013	-0.001 ± 0.021
13 Dec 2011	05:28:35	0.010 ± 0.016	0.030 ± 0.014	-0.020 ± 0.021
13 Dec 2011	05:30:53	-0.016 ± 0.016	0.012 ± 0.013	-0.028 ± 0.021
13 Dec 2011	05:33:16	0.003 ± 0.016	0.009 ± 0.013	-0.006 ± 0.021
13 Dec 2011	05:35:34	0.033 ± 0.016	-0.000 ± 0.013	0.033 ± 0.021
13 Dec 2011	05:37:52	-0.016 ± 0.016	-0.000 ± 0.013	-0.016 ± 0.021
13 Dec 2011	05:40:10	-0.028 ± 0.016	0.011 ± 0.013	-0.039 ± 0.021
13 Dec 2011	05:42:27	-0.014 ± 0.016	0.015 ± 0.013	-0.029 ± 0.021
13 Dec 2011	05:44:49	0.002 ± 0.016	-0.002 ± 0.013	0.004 ± 0.021
13 Dec 2011	05:47:07	0.001 ± 0.016	-0.030 ± 0.013	0.031 ± 0.021
13 Dec 2011	05:49:25	-0.009 ± 0.016	-0.061 ± 0.013	0.052 ± 0.021
13 Dec 2011	05:51:43	-0.017 ± 0.016	-0.062 ± 0.013	0.045 ± 0.021
13 Dec 2011	05:54:01	-0.027 ± 0.016	-0.039 ± 0.013	0.012 ± 0.021
13 Dec 2011	05:56:23	-0.005 ± 0.016	-0.022 ± 0.013	0.017 ± 0.021
13 Dec 2011	05:58:41	0.006 ± 0.016	-0.012 ± 0.013	0.018 ± 0.021
13 Dec 2011	06:00:58	0.031 ± 0.016	-0.040 ± 0.013	0.071 ± 0.020
13 Dec 2011	06:03:16	-0.005 ± 0.016	-0.051 ± 0.012	0.046 ± 0.020
13 Dec 2011	06:05:34	-0.063 ± 0.015	-0.021 ± 0.013	-0.042 ± 0.020
13 Dec 2011	06:07:52	-0.044 ± 0.015	-0.035 ± 0.013	-0.009 ± 0.020
13 Dec 2011	06:10:09	-0.010 ± 0.016	-0.038 ± 0.012	0.028 ± 0.020
13 Dec 2011	06:12:27	-0.023 ± 0.016	-0.022 ± 0.013	-0.001 ± 0.021
13 Dec 2011	06:14:49	-0.050 ± 0.015	-0.020 ± 0.013	-0.031 ± 0.020
13 Dec 2011	06:17:07	-0.042 ± 0.016	-0.024 ± 0.013	-0.018 ± 0.021

Continued on next page

Table C.6 – continued from previous page

Date	Time[a] (UT)	V (Relative)	I (Interpolated)	$V-I$
13 Dec 2011	06:19:24	-0.049 ± 0.016	-0.028 ± 0.013	-0.021 ± 0.021
13 Dec 2011	06:21:42	-0.036 ± 0.016	-0.030 ± 0.013	-0.006 ± 0.021
23 Feb 2013	00:00:41	0.009 ± 0.016	-0.006 ± 0.012	0.014 ± 0.020
23 Feb 2013	00:08:55	-0.016 ± 0.011	-0.008 ± 0.010	-0.009 ± 0.015
23 Feb 2013	00:17:09	0.004 ± 0.011	-0.002 ± 0.010	0.006 ± 0.015
23 Feb 2013	00:26:52	-0.009 ± 0.013	0.004 ± 0.014	-0.013 ± 0.019
23 Feb 2013	00:33:27	0.010 ± 0.014	0.012 ± 0.020	-0.002 ± 0.024
23 Feb 2013	00:40:01	-0.032 ± 0.025	0.005 ± 0.023	-0.037 ± 0.034
23 Feb 2013	00:49:09	0.001 ± 0.012	-0.021 ± 0.017	0.022 ± 0.021
23 Feb 2013	00:57:23	-0.003 ± 0.009	-0.010 ± 0.010	0.007 ± 0.013
23 Feb 2013	01:05:38	0.026 ± 0.012	0.005 ± 0.010	0.021 ± 0.016
23 Feb 2013	01:14:58	0.011 ± 0.010	0.015 ± 0.011	-0.005 ± 0.015
23 Feb 2013	01:23:13	-0.000 ± 0.015	0.023 ± 0.011	-0.024 ± 0.019
23 Feb 2013	23:41:41	0.035 ± 0.014	0.040 ± 0.015	-0.005 ± 0.021
23 Feb 2013	23:49:17	0.021 ± 0.013	0.037 ± 0.013	-0.016 ± 0.018
23 Feb 2013	23:56:51	0.025 ± 0.013	0.038 ± 0.012	-0.013 ± 0.018
24 Feb 2013	00:04:26	0.037 ± 0.013	0.031 ± 0.012	0.006 ± 0.018
24 Feb 2013	00:12:29	0.044 ± 0.013	0.029 ± 0.013	0.015 ± 0.018
24 Feb 2013	00:20:03	0.029 ± 0.013	0.028 ± 0.012	0.002 ± 0.018
24 Feb 2013	00:27:38	0.020 ± 0.012	0.013 ± 0.012	0.008 ± 0.017
24 Feb 2013	00:35:13	0.028 ± 0.012	-0.020 ± 0.012	0.049 ± 0.017

Note: These data are plotted in Figure 3.11.
[a] Times have been corrected for light travel time between the object and the observer.

Table C.7: 3317 Paris: $V-I$ Color Variation for Partial Light Curve

Date	Time[a] (UT)	V (Relative)	I (Interpolated)	$V-I$
27 June 2011	07:23:17	-0.010 ± 0.014	-0.022 ± 0.015	0.012 ± 0.020
27 June 2011	07:32:02	-0.007 ± 0.013	-0.011 ± 0.014	0.004 ± 0.019
27 June 2011	07:35:49	-0.011 ± 0.013	-0.012 ± 0.014	0.001 ± 0.019
27 June 2011	07:39:35	-0.004 ± 0.013	-0.001 ± 0.014	-0.003 ± 0.019
27 June 2011	07:43:21	0.010 ± 0.013	-0.005 ± 0.017	0.015 ± 0.021
27 June 2011	07:47:09	0.001 ± 0.013	0.006 ± 0.014	-0.005 ± 0.019
27 June 2011	07:50:55	-0.017 ± 0.015	0.013 ± 0.014	-0.030 ± 0.021
27 June 2011	07:54:41	0.008 ± 0.014	0.026 ± 0.014	-0.018 ± 0.020
27 June 2011	07:58:28	0.005 ± 0.013	0.035 ± 0.014	-0.030 ± 0.019
27 June 2011	08:02:14	0.022 ± 0.014	0.040 ± 0.014	-0.019 ± 0.020
27 June 2011	08:06:01	0.045 ± 0.014	0.045 ± 0.014	0.000 ± 0.020
27 June 2011	08:14:16	0.052 ± 0.014	0.040 ± 0.014	0.011 ± 0.020
27 June 2011	08:18:03	0.048 ± 0.014	0.038 ± 0.014	0.010 ± 0.020
27 June 2011	08:21:49	0.047 ± 0.014	0.031 ± 0.014	0.016 ± 0.020
27 June 2011	08:25:36	0.047 ± 0.014	0.030 ± 0.014	0.017 ± 0.020
27 June 2011	08:29:23	0.022 ± 0.014	0.014 ± 0.014	0.008 ± 0.020
27 June 2011	08:33:09	0.025 ± 0.014	0.023 ± 0.014	0.002 ± 0.020
27 June 2011	08:36:55	0.020 ± 0.013	0.026 ± 0.014	-0.006 ± 0.019
27 June 2011	08:40:42	0.020 ± 0.014	0.017 ± 0.014	0.003 ± 0.020
27 June 2011	08:44:27	0.007 ± 0.014	0.012 ± 0.014	-0.005 ± 0.020
27 June 2011	08:48:14	0.007 ± 0.014	0.002 ± 0.014	0.005 ± 0.020
27 June 2011	08:53:13	0.003 ± 0.013	-0.011 ± 0.014	0.013 ± 0.019
27 June 2011	08:57:00	-0.002 ± 0.013	-0.010 ± 0.013	0.008 ± 0.018
27 June 2011	09:00:46	-0.011 ± 0.013	-0.013 ± 0.014	0.002 ± 0.019

Continued on next page

Table C.7 – continued from previous page

Date	Time[a] (UT)	V (Relative)	I (Interpolated)	$V-I$
27 June 2011	09:04:32	-0.018 ± 0.013	-0.028 ± 0.013	0.010 ± 0.018
27 June 2011	09:08:18	-0.018 ± 0.013	-0.036 ± 0.013	0.018 ± 0.018
27 June 2011	09:12:04	-0.018 ± 0.013	-0.036 ± 0.013	0.018 ± 0.018
27 June 2011	09:15:50	-0.028 ± 0.013	-0.039 ± 0.013	0.011 ± 0.018
27 June 2011	09:19:36	-0.029 ± 0.013	-0.028 ± 0.013	-0.001 ± 0.018
27 June 2011	09:23:23	-0.027 ± 0.013	-0.035 ± 0.013	0.008 ± 0.018
27 June 2011	09:27:08	-0.033 ± 0.013	-0.034 ± 0.013	0.001 ± 0.018
27 June 2011	09:42:31	-0.023 ± 0.013	-0.024 ± 0.013	0.001 ± 0.018
27 June 2011	09:46:17	-0.013 ± 0.013	-0.017 ± 0.013	0.004 ± 0.018
27 June 2011	09:50:04	-0.017 ± 0.013	-0.018 ± 0.013	0.001 ± 0.018
27 June 2011	09:53:49	-0.015 ± 0.013	-0.005 ± 0.013	-0.010 ± 0.018
27 June 2011	09:57:36	-0.028 ± 0.013	-0.010 ± 0.014	-0.018 ± 0.019
27 June 2011	10:01:22	-0.018 ± 0.013	-0.004 ± 0.014	-0.014 ± 0.019
27 June 2011	10:05:08	-0.028 ± 0.013	0.002 ± 0.015	-0.030 ± 0.020
27 June 2011	10:08:55	-0.016 ± 0.014	0.008 ± 0.017	-0.024 ± 0.022
27 June 2011	10:12:40	0.013 ± 0.015	0.006 ± 0.019	0.007 ± 0.024
27 June 2011	10:16:26	-0.005 ± 0.016	0.003 ± 0.021	-0.008 ± 0.026
9 Aug 2011	08:16:09	-0.023 ± 0.023	-0.005 ± 0.027	-0.018 ± 0.035
9 Aug 2011	08:20:24	-0.026 ± 0.024	-0.010 ± 0.027	-0.016 ± 0.036
9 Aug 2011	08:23:12	-0.024 ± 0.023	-0.012 ± 0.027	-0.012 ± 0.035
9 Aug 2011	08:26:00	-0.012 ± 0.023	-0.011 ± 0.027	-0.001 ± 0.035
9 Aug 2011	08:28:47	-0.028 ± 0.023	-0.017 ± 0.027	-0.011 ± 0.035
9 Aug 2011	08:31:35	-0.014 ± 0.023	-0.021 ± 0.027	0.007 ± 0.035
9 Aug 2011	08:34:24	-0.022 ± 0.024	-0.016 ± 0.026	-0.006 ± 0.036
9 Aug 2011	08:37:13	-0.015 ± 0.024	-0.017 ± 0.027	0.002 ± 0.036
9 Aug 2011	08:40:01	-0.022 ± 0.024	-0.023 ± 0.027	0.001 ± 0.036
9 Aug 2011	08:42:50	-0.022 ± 0.024	-0.019 ± 0.027	-0.003 ± 0.036
9 Aug 2011	08:45:38	-0.022 ± 0.024	-0.013 ± 0.027	-0.009 ± 0.036
9 Aug 2011	08:48:27	-0.016 ± 0.023	-0.015 ± 0.027	-0.001 ± 0.035
9 Aug 2011	08:51:14	-0.027 ± 0.024	-0.012 ± 0.027	-0.015 ± 0.036
9 Aug 2011	08:54:02	-0.014 ± 0.024	-0.012 ± 0.027	-0.002 ± 0.036
9 Aug 2011	08:56:50	-0.007 ± 0.024	-0.015 ± 0.027	0.008 ± 0.036
9 Aug 2011	08:59:38	0.012 ± 0.024	-0.008 ± 0.027	0.020 ± 0.036
9 Aug 2011	09:02:26	0.004 ± 0.024	-0.003 ± 0.027	0.007 ± 0.036
9 Aug 2011	09:12:32	0.002 ± 0.024	-0.001 ± 0.027	0.003 ± 0.036
9 Aug 2011	09:15:21	0.012 ± 0.024	-0.002 ± 0.027	0.014 ± 0.036
9 Aug 2011	09:18:10	0.009 ± 0.024	-0.001 ± 0.028	0.010 ± 0.037
9 Aug 2011	09:20:58	-0.005 ± 0.024	-0.005 ± 0.027	0.000 ± 0.036
9 Aug 2011	09:23:46	-0.007 ± 0.024	-0.009 ± 0.027	0.002 ± 0.036
9 Aug 2011	09:26:34	-0.008 ± 0.024	-0.013 ± 0.027	0.005 ± 0.036
9 Aug 2011	09:29:23	-0.018 ± 0.024	-0.008 ± 0.027	-0.010 ± 0.036
9 Aug 2011	09:32:11	0.002 ± 0.024	0.004 ± 0.027	-0.002 ± 0.036
9 Aug 2011	09:34:59	-0.004 ± 0.024	0.008 ± 0.027	-0.012 ± 0.036
9 Aug 2011	09:37:48	0.009 ± 0.025	0.007 ± 0.027	0.002 ± 0.037
9 Aug 2011	09:40:36	0.010 ± 0.025	0.008 ± 0.028	0.002 ± 0.037
9 Aug 2011	09:43:25	0.027 ± 0.025	0.014 ± 0.028	0.013 ± 0.038
9 Aug 2011	09:46:13	0.019 ± 0.025	0.020 ± 0.028	-0.001 ± 0.038
9 Aug 2011	09:49:02	0.037 ± 0.026	0.031 ± 0.028	0.006 ± 0.038
9 Aug 2011	09:51:50	0.055 ± 0.026	0.047 ± 0.029	0.008 ± 0.039
9 Aug 2011	09:54:38	0.083 ± 0.027	0.054 ± 0.029	0.029 ± 0.040
9 Aug 2011	09:59:10	0.080 ± 0.028	0.050 ± 0.031	0.030 ± 0.041
9 Aug 2011	10:01:58	0.051 ± 0.031	0.042 ± 0.033	0.009 ± 0.045
9 Aug 2011	10:04:47	0.000 ± 0.033	0.025 ± 0.036	-0.025 ± 0.049

Continued on next page

Table C.7 – continued from previous page

Date	Time[a] (UT)	V (Relative)	I (Interpolated)	$V-I$
9 Aug 2011	10:07:34	-0.032 ± 0.036	-0.019 ± 0.041	-0.013 ± 0.055
9 Aug 2011	10:10:23	-0.048 ± 0.044	-0.087 ± 0.047	0.039 ± 0.064

Note: These data are plotted in Figure 3.13.
[a] Times have been corrected for light travel time between the object and the observer.

Table C.8: 3451 Mentor: $V-I$ Color Variation for Partial Light Curve

Date	Time[a] (UT)	V (Relative)	I (Interpolated)	$V-I$
14 Aug 2011	04:47:27	0.010 ± 0.025	0.072 ± 0.021	-0.062 ± 0.033
14 Aug 2011	04:52:54	-0.011 ± 0.025	-0.018 ± 0.021	0.007 ± 0.033
14 Aug 2011	04:55:40	-0.030 ± 0.025	-0.026 ± 0.021	-0.004 ± 0.033
14 Aug 2011	05:26:19	-0.090 ± 0.024	-0.150 ± 0.020	0.060 ± 0.031
14 Aug 2011	05:29:05	-0.094 ± 0.023	-0.136 ± 0.019	0.042 ± 0.030
14 Aug 2011	05:31:51	-0.129 ± 0.022	-0.168 ± 0.019	0.040 ± 0.029
14 Aug 2011	05:34:38	-0.109 ± 0.022	-0.175 ± 0.018	0.067 ± 0.028
14 Aug 2011	05:37:24	-0.134 ± 0.021	-0.176 ± 0.018	0.043 ± 0.028
14 Aug 2011	05:40:10	-0.195 ± 0.021	-0.205 ± 0.018	0.011 ± 0.028
14 Aug 2011	05:42:57	-0.187 ± 0.021	-0.228 ± 0.018	0.042 ± 0.028
14 Aug 2011	05:45:42	-0.184 ± 0.021	-0.208 ± 0.018	0.025 ± 0.028
14 Aug 2011	05:48:29	-0.193 ± 0.021	-0.210 ± 0.018	0.017 ± 0.028
14 Aug 2011	05:51:15	-0.221 ± 0.021	-0.219 ± 0.018	-0.002 ± 0.028
14 Aug 2011	05:54:01	-0.211 ± 0.021	-0.216 ± 0.018	0.006 ± 0.028
14 Aug 2011	05:56:47	-0.209 ± 0.021	-0.215 ± 0.018	0.006 ± 0.028
14 Aug 2011	05:59:32	-0.221 ± 0.021	-0.219 ± 0.018	-0.002 ± 0.028
14 Aug 2011	06:02:19	-0.195 ± 0.021	-0.203 ± 0.018	0.008 ± 0.028
14 Aug 2011	06:05:04	-0.201 ± 0.021	-0.222 ± 0.018	0.021 ± 0.028
14 Aug 2011	06:07:50	-0.207 ± 0.021	-0.195 ± 0.018	-0.011 ± 0.028
14 Aug 2011	06:10:43	-0.194 ± 0.021	-0.208 ± 0.018	0.014 ± 0.028
14 Aug 2011	06:13:28	-0.182 ± 0.022	-0.176 ± 0.018	-0.006 ± 0.028
14 Aug 2011	06:16:14	-0.169 ± 0.022	-0.171 ± 0.018	0.002 ± 0.028
14 Aug 2011	06:19:01	-0.165 ± 0.021	-0.161 ± 0.019	-0.004 ± 0.028
14 Aug 2011	06:21:47	-0.167 ± 0.022	-0.153 ± 0.018	-0.014 ± 0.029
14 Aug 2011	06:24:33	-0.123 ± 0.022	-0.162 ± 0.021	0.040 ± 0.030
14 Aug 2011	06:27:19	-0.137 ± 0.023	-0.109 ± 0.026	-0.027 ± 0.035
14 Aug 2011	06:30:04	-0.170 ± 0.030	-0.124 ± 0.024	-0.046 ± 0.038
14 Aug 2011	06:32:50	-0.116 ± 0.027	-0.111 ± 0.019	-0.005 ± 0.033
14 Aug 2011	06:35:35	-0.064 ± 0.022	-0.091 ± 0.019	0.028 ± 0.029
14 Aug 2011	06:38:21	-0.060 ± 0.023	-0.062 ± 0.019	0.002 ± 0.030
14 Aug 2011	06:41:07	-0.027 ± 0.023	-0.045 ± 0.020	0.019 ± 0.030
14 Aug 2011	06:43:53	0.015 ± 0.023	-0.015 ± 0.020	0.030 ± 0.030
14 Aug 2011	06:46:39	-0.009 ± 0.024	0.001 ± 0.020	-0.010 ± 0.031
14 Aug 2011	06:49:25	0.058 ± 0.024	0.031 ± 0.021	0.027 ± 0.032
14 Aug 2011	06:52:11	0.066 ± 0.024	0.058 ± 0.021	0.008 ± 0.032
14 Aug 2011	06:55:08	0.094 ± 0.024	0.083 ± 0.021	0.011 ± 0.032
14 Aug 2011	06:57:55	0.120 ± 0.024	0.095 ± 0.021	0.025 ± 0.032
14 Aug 2011	07:00:40	0.130 ± 0.025	0.141 ± 0.022	-0.011 ± 0.033
14 Aug 2011	07:03:27	0.155 ± 0.026	0.165 ± 0.023	-0.010 ± 0.035
14 Aug 2011	07:06:12	0.194 ± 0.026	0.152 ± 0.022	0.042 ± 0.034
14 Aug 2011	07:08:58	0.194 ± 0.026	0.199 ± 0.023	-0.004 ± 0.035
14 Aug 2011	07:11:44	0.215 ± 0.026	0.213 ± 0.023	0.002 ± 0.035
14 Aug 2011	07:14:30	0.222 ± 0.026	0.257 ± 0.024	-0.034 ± 0.035

Continued on next page

Table C.8 – continued from previous page

Date	Time[a] (UT)	V (Relative)	I (Interpolated)	$V-I$
14 Aug 2011	07:17:16	0.244 ± 0.027	0.271 ± 0.025	-0.027 ± 0.037
14 Aug 2011	07:20:02	0.291 ± 0.028	0.308 ± 0.025	-0.017 ± 0.038
14 Aug 2011	07:22:48	0.288 ± 0.027	0.314 ± 0.025	-0.026 ± 0.037
14 Aug 2011	07:25:34	0.322 ± 0.028	0.331 ± 0.025	-0.009 ± 0.038
14 Aug 2011	07:28:21	0.352 ± 0.029	0.373 ± 0.026	-0.021 ± 0.039
14 Aug 2011	07:31:07	0.352 ± 0.029	0.390 ± 0.027	-0.038 ± 0.040
14 Aug 2011	07:33:52	0.389 ± 0.030	0.398 ± 0.027	-0.009 ± 0.040
14 Aug 2011	07:36:38	0.411 ± 0.029	0.417 ± 0.027	-0.006 ± 0.040
14 Aug 2011	07:40:41	0.387 ± 0.030	0.420 ± 0.027	-0.033 ± 0.040
14 Aug 2011	07:43:26	0.395 ± 0.030	0.428 ± 0.027	-0.033 ± 0.040
14 Aug 2011	07:46:12	0.377 ± 0.030	0.426 ± 0.027	-0.049 ± 0.040
14 Aug 2011	07:48:58	0.406 ± 0.030	0.425 ± 0.027	-0.019 ± 0.040
14 Aug 2011	07:51:44	0.436 ± 0.030	0.418 ± 0.027	0.018 ± 0.040
14 Aug 2011	07:54:30	0.373 ± 0.029	0.413 ± 0.027	-0.040 ± 0.040
14 Aug 2011	07:57:17	0.383 ± 0.030	0.376 ± 0.027	0.008 ± 0.040
14 Aug 2011	08:00:04	0.368 ± 0.030	0.386 ± 0.027	-0.017 ± 0.040
14 Aug 2011	08:02:55	0.364 ± 0.029	0.362 ± 0.026	0.002 ± 0.039
14 Aug 2011	08:05:40	0.315 ± 0.028	0.313 ± 0.025	0.003 ± 0.038
14 Aug 2011	08:08:27	0.311 ± 0.028	0.281 ± 0.025	0.030 ± 0.038
14 Aug 2011	08:24:05	0.083 ± 0.026	0.103 ± 0.022	-0.019 ± 0.034
14 Aug 2011	08:26:51	0.040 ± 0.026	0.049 ± 0.022	-0.009 ± 0.034
14 Aug 2011	08:29:36	0.007 ± 0.026	0.054 ± 0.022	-0.047 ± 0.034
14 Aug 2011	08:32:22	0.046 ± 0.026	0.030 ± 0.021	0.017 ± 0.033
14 Aug 2011	08:35:08	0.020 ± 0.025	0.011 ± 0.021	0.009 ± 0.033
14 Aug 2011	08:37:54	0.030 ± 0.025	-0.013 ± 0.021	0.043 ± 0.033
14 Aug 2011	08:40:41	-0.044 ± 0.024	-0.025 ± 0.020	-0.018 ± 0.031
14 Aug 2011	08:43:27	-0.045 ± 0.024	-0.038 ± 0.020	-0.007 ± 0.031
14 Aug 2011	08:46:13	-0.084 ± 0.024	-0.066 ± 0.020	-0.017 ± 0.031
14 Aug 2011	08:48:59	-0.081 ± 0.024	-0.058 ± 0.020	-0.022 ± 0.031
14 Aug 2011	08:51:44	-0.094 ± 0.024	-0.079 ± 0.020	-0.014 ± 0.031
14 Aug 2011	08:54:30	-0.081 ± 0.024	-0.106 ± 0.019	0.025 ± 0.031
14 Aug 2011	08:57:16	-0.128 ± 0.024	-0.096 ± 0.020	-0.032 ± 0.031
14 Aug 2011	09:00:02	-0.096 ± 0.024	-0.095 ± 0.019	-0.001 ± 0.031
14 Aug 2011	09:02:48	-0.103 ± 0.024	-0.125 ± 0.019	0.022 ± 0.031
14 Aug 2011	09:05:34	-0.147 ± 0.024	-0.137 ± 0.019	-0.009 ± 0.031
14 Aug 2011	09:10:50	-0.130 ± 0.023	-0.175 ± 0.019	0.045 ± 0.030
14 Aug 2011	09:13:36	-0.130 ± 0.023	-0.173 ± 0.019	0.044 ± 0.030
14 Aug 2011	09:16:22	-0.165 ± 0.023	-0.191 ± 0.019	0.026 ± 0.030
14 Aug 2011	09:19:08	-0.152 ± 0.024	-0.204 ± 0.018	0.053 ± 0.030
14 Aug 2011	09:21:54	-0.158 ± 0.023	-0.220 ± 0.018	0.062 ± 0.029
14 Aug 2011	09:24:40	-0.182 ± 0.023	-0.211 ± 0.019	0.030 ± 0.030
14 Aug 2011	09:27:26	-0.234 ± 0.024	-0.220 ± 0.018	-0.014 ± 0.030
14 Aug 2011	09:30:12	-0.217 ± 0.023	-0.230 ± 0.018	0.013 ± 0.029
14 Aug 2011	09:32:58	-0.234 ± 0.024	-0.232 ± 0.019	-0.002 ± 0.031
14 Aug 2011	09:35:45	-0.208 ± 0.024	-0.235 ± 0.019	0.028 ± 0.031
14 Aug 2011	09:38:31	-0.229 ± 0.024	-0.234 ± 0.018	0.005 ± 0.030
14 Aug 2011	09:41:17	-0.258 ± 0.024	-0.228 ± 0.018	-0.030 ± 0.030
14 Aug 2011	09:44:03	-0.257 ± 0.025	-0.229 ± 0.019	-0.028 ± 0.031
14 Aug 2011	09:46:49	-0.245 ± 0.026	-0.215 ± 0.020	-0.029 ± 0.033
14 Aug 2011	09:49:35	-0.219 ± 0.027	-0.173 ± 0.023	-0.045 ± 0.036
14 Aug 2011	09:52:21	-0.163 ± 0.032	-0.131 ± 0.026	-0.031 ± 0.041
30 Sept 2012	06:38:21	-0.066 ± 0.022	-0.067 ± 0.010	0.001 ± 0.024
30 Sept 2012	06:43:25	-0.090 ± 0.023	-0.079 ± 0.010	-0.012 ± 0.025

Continued on next page

Table C.8 – continued from previous page

Date	Time[a] (UT)	V (Relative)	I (Interpolated)	$V-I$
30 Sept 2012	06:48:30	-0.104 ± 0.023	-0.087 ± 0.010	-0.018 ± 0.025
30 Sept 2012	06:53:34	-0.134 ± 0.023	-0.119 ± 0.010	-0.016 ± 0.025
30 Sept 2012	06:58:39	-0.117 ± 0.024	-0.143 ± 0.010	0.025 ± 0.026
30 Sept 2012	07:03:44	-0.131 ± 0.024	-0.155 ± 0.010	0.024 ± 0.026
30 Sept 2012	07:12:54	-0.160 ± 0.024	-0.183 ± 0.010	0.022 ± 0.026
30 Sept 2012	07:17:58	-0.171 ± 0.025	-0.179 ± 0.010	0.008 ± 0.027
30 Sept 2012	07:23:03	-0.169 ± 0.024	-0.198 ± 0.010	0.028 ± 0.026
30 Sept 2012	07:28:07	-0.195 ± 0.025	-0.214 ± 0.010	0.018 ± 0.027
30 Sept 2012	07:33:12	-0.220 ± 0.023	-0.211 ± 0.010	-0.010 ± 0.025
30 Sept 2012	07:38:16	-0.235 ± 0.023	-0.207 ± 0.010	-0.028 ± 0.025
30 Sept 2012	07:46:50	-0.222 ± 0.024	-0.220 ± 0.010	-0.003 ± 0.026
30 Sept 2012	07:51:55	-0.251 ± 0.024	-0.228 ± 0.010	-0.024 ± 0.026
30 Sept 2012	07:57:00	-0.220 ± 0.023	-0.228 ± 0.011	0.007 ± 0.025
30 Sept 2012	08:02:04	-0.206 ± 0.024	-0.229 ± 0.010	0.022 ± 0.026
30 Sept 2012	08:07:09	-0.212 ± 0.025	-0.226 ± 0.011	0.014 ± 0.027
30 Sept 2012	08:12:14	-0.219 ± 0.026	-0.214 ± 0.011	-0.006 ± 0.028
30 Sept 2012	08:20:36	-0.177 ± 0.025	-0.198 ± 0.012	0.020 ± 0.028
30 Sept 2012	08:25:41	-0.184 ± 0.026	-0.179 ± 0.012	-0.006 ± 0.029
30 Sept 2012	08:30:45	-0.134 ± 0.027	-0.154 ± 0.011	0.019 ± 0.029
30 Sept 2012	08:35:50	-0.124 ± 0.025	-0.135 ± 0.012	0.011 ± 0.028
30 Sept 2012	08:40:54	-0.111 ± 0.024	-0.112 ± 0.011	0.001 ± 0.027
30 Sept 2012	08:45:59	-0.090 ± 0.025	-0.100 ± 0.012	0.009 ± 0.028
30 Sept 2012	08:54:18	-0.047 ± 0.029	-0.059 ± 0.015	0.011 ± 0.033
30 Sept 2012	08:59:22	-0.044 ± 0.032	-0.030 ± 0.019	-0.014 ± 0.037
30 Sept 2012	09:04:26	-0.004 ± 0.041	-0.016 ± 0.024	0.011 ± 0.048
3 Oct 2012	08:07:54	-0.074 ± 0.021	-0.054 ± 0.013	-0.020 ± 0.025
3 Oct 2012	08:12:12	-0.069 ± 0.021	-0.068 ± 0.013	-0.001 ± 0.025
3 Oct 2012	08:16:30	-0.086 ± 0.022	-0.071 ± 0.013	-0.015 ± 0.026
3 Oct 2012	08:20:49	-0.089 ± 0.022	-0.081 ± 0.014	-0.008 ± 0.026
3 Oct 2012	08:25:07	-0.071 ± 0.024	-0.092 ± 0.014	0.021 ± 0.028
3 Oct 2012	08:32:05	-0.116 ± 0.021	-0.108 ± 0.015	-0.008 ± 0.026
3 Oct 2012	08:36:23	-0.143 ± 0.024	-0.114 ± 0.014	-0.029 ± 0.028
3 Oct 2012	08:40:42	-0.097 ± 0.021	-0.121 ± 0.013	0.024 ± 0.025
3 Oct 2012	08:45:00	-0.122 ± 0.021	-0.113 ± 0.013	-0.009 ± 0.025
3 Oct 2012	08:49:18	-0.078 ± 0.022	-0.104 ± 0.013	0.026 ± 0.026
3 Oct 2012	08:56:00	-0.070 ± 0.024	-0.102 ± 0.015	0.032 ± 0.028
3 Oct 2012	09:00:20	-0.132 ± 0.027	-0.122 ± 0.018	-0.011 ± 0.032
3 Oct 2012	09:04:39	-0.150 ± 0.035	-0.151 ± 0.021	0.001 ± 0.041

Note: These data are plotted in Figure 3.15.
[a] Times have been corrected for light travel time between the object and the observer.

Table C.9: 3793 Leonteus: $V-I$ Color Variation for Partial Light Curve

Date	Time[a] (UT)	V (Relative)	I (Interpolated)	$V-I$
15 Nov 2011	07:00:28	-0.019 ± 0.010	-0.007 ± -0.004	-0.012 ± 0.011
15 Nov 2011	07:07:59	-0.054 ± 0.011	-0.030 ± 0.005	-0.025 ± 0.012
15 Nov 2011	07:12:46	-0.022 ± 0.016	-0.044 ± 0.011	0.021 ± 0.020
15 Nov 2011	07:17:32	-0.019 ± 0.022	-0.042 ± 0.018	0.022 ± 0.028
15 Nov 2011	07:22:19	0.023 ± 0.017	-0.023 ± 0.020	0.045 ± 0.027
15 Nov 2011	07:27:06	0.019 ± 0.025	-0.019 ± 0.013	0.037 ± 0.028
15 Nov 2011	07:31:53	0.075 ± 0.053	0.027 ± 0.025	0.048 ± 0.059

Continued on next page

Table C.9 – continued from previous page

Date	Time[a] (UT)	V (Relative)	I (Interpolated)	$V-I$
11 Dec 2011	06:13:06	0.001 ± 0.036	0.039 ± 0.033	-0.038 ± 0.049
11 Dec 2011	06:15:24	0.005 ± 0.034	0.046 ± 0.035	-0.041 ± 0.048
11 Dec 2011	06:17:41	0.043 ± 0.040	0.015 ± 0.036	0.028 ± 0.054
11 Dec 2011	06:19:59	-0.023 ± 0.037	-0.023 ± 0.036	0.000 ± 0.052
11 Dec 2011	06:22:16	0.043 ± 0.036	-0.033 ± 0.034	0.076 ± 0.050
11 Dec 2011	06:24:34	0.002 ± 0.034	-0.042 ± 0.032	0.044 ± 0.047
11 Dec 2011	06:26:52	-0.035 ± 0.032	-0.041 ± 0.031	0.006 ± 0.045
11 Dec 2011	06:29:09	-0.030 ± 0.033	-0.050 ± 0.031	0.020 ± 0.045
11 Dec 2011	06:31:26	-0.081 ± 0.032	-0.085 ± 0.031	0.004 ± 0.044
11 Dec 2011	06:33:45	-0.037 ± 0.033	-0.097 ± 0.030	0.060 ± 0.045
11 Dec 2011	06:36:08	-0.045 ± 0.032	-0.123 ± 0.029	0.079 ± 0.043
11 Dec 2011	06:38:26	-0.144 ± 0.030	-0.177 ± 0.028	0.033 ± 0.041
11 Dec 2011	06:40:43	-0.150 ± 0.029	-0.192 ± 0.028	0.042 ± 0.040
11 Dec 2011	06:43:00	-0.154 ± 0.029	-0.181 ± 0.028	0.027 ± 0.040
11 Dec 2011	06:45:18	-0.195 ± 0.028	-0.189 ± 0.028	-0.006 ± 0.040
11 Dec 2011	06:47:35	-0.162 ± 0.029	-0.192 ± 0.028	0.030 ± 0.040
11 Dec 2011	06:49:52	-0.197 ± 0.028	-0.185 ± 0.028	-0.012 ± 0.040
11 Dec 2011	06:52:10	-0.178 ± 0.028	-0.197 ± 0.029	0.019 ± 0.040
11 Dec 2011	06:54:27	-0.205 ± 0.031	-0.198 ± 0.032	-0.007 ± 0.045
11 Dec 2011	06:56:45	-0.160 ± 0.031	-0.185 ± 0.031	0.025 ± 0.044
11 Dec 2011	06:59:19	-0.167 ± 0.029	-0.171 ± 0.028	0.004 ± 0.040
11 Dec 2011	07:01:37	-0.157 ± 0.030	-0.158 ± 0.028	0.001 ± 0.041
11 Dec 2011	07:03:54	-0.150 ± 0.029	-0.125 ± 0.029	-0.025 ± 0.041
11 Dec 2011	07:06:11	-0.071 ± 0.031	-0.067 ± 0.031	-0.003 ± 0.044
11 Dec 2011	07:08:30	-0.083 ± 0.031	-0.030 ± 0.033	-0.053 ± 0.045
11 Dec 2011	07:10:46	-0.006 ± 0.034	-0.001 ± 0.034	-0.005 ± 0.048
11 Dec 2011	07:13:03	0.012 ± 0.035	0.029 ± 0.036	-0.016 ± 0.050
11 Dec 2011	07:15:22	0.005 ± 0.045	0.044 ± 0.035	-0.039 ± 0.057
11 Dec 2011	07:17:40	0.042 ± 0.035	0.053 ± 0.036	-0.011 ± 0.050
11 Dec 2011	07:19:56	0.039 ± 0.036	0.064 ± 0.036	-0.025 ± 0.051
11 Dec 2011	07:22:19	0.052 ± 0.037	0.066 ± 0.035	-0.014 ± 0.051
11 Dec 2011	07:24:36	0.039 ± 0.035	0.080 ± 0.035	-0.041 ± 0.050
11 Dec 2011	07:26:54	0.117 ± 0.037	0.116 ± 0.036	0.002 ± 0.052
11 Dec 2011	07:29:11	0.089 ± 0.036	0.139 ± 0.037	-0.050 ± 0.052
11 Dec 2011	07:31:28	0.090 ± 0.037	0.145 ± 0.038	-0.055 ± 0.053
11 Dec 2011	07:33:46	0.126 ± 0.037	0.138 ± 0.038	-0.012 ± 0.053
11 Dec 2011	07:36:03	0.092 ± 0.037	0.161 ± 0.038	-0.069 ± 0.053
11 Dec 2011	07:38:21	0.150 ± 0.038	0.178 ± 0.040	-0.028 ± 0.055
11 Dec 2011	07:40:39	0.193 ± 0.041	0.175 ± 0.040	0.018 ± 0.057
11 Dec 2011	07:42:56	0.188 ± 0.041	0.175 ± 0.039	0.014 ± 0.057
11 Dec 2011	07:45:19	0.197 ± 0.041	0.178 ± 0.039	0.019 ± 0.057
11 Dec 2011	07:47:35	0.202 ± 0.041	0.200 ± 0.040	0.003 ± 0.058
11 Dec 2011	07:49:54	0.176 ± 0.041	0.209 ± 0.041	-0.033 ± 0.058
11 Dec 2011	07:52:12	0.254 ± 0.043	0.192 ± 0.041	0.062 ± 0.059
11 Dec 2011	07:54:30	0.265 ± 0.044	0.201 ± 0.041	0.064 ± 0.060
23 Feb 2013	01:45:54	-0.126 ± 0.015	-0.120 ± 0.016	-0.005 ± 0.022
23 Feb 2013	01:53:39	-0.112 ± 0.015	-0.125 ± 0.015	0.014 ± 0.021
23 Feb 2013	02:01:23	-0.111 ± 0.017	-0.105 ± 0.018	-0.006 ± 0.024
23 Feb 2013	02:09:08	-0.048 ± 0.015	-0.099 ± 0.021	0.052 ± 0.026
23 Feb 2013	02:16:54	-0.082 ± 0.026	-0.089 ± 0.019	0.008 ± 0.033
23 Feb 2013	02:24:38	0.091 ± 0.029	0.008 ± 0.049	0.083 ± 0.057
23 Feb 2013	02:40:08	0.073 ± 0.027	0.143 ± 0.063	-0.070 ± 0.068
23 Feb 2013	02:55:26	0.163 ± 0.069	0.163 ± 0.074	0.000 ± 0.101

Continued on next page

Table C.9 – continued from previous page

Date	Time[a] (UT)	V (Relative)	I (Interpolated)	$V-I$
23 Feb 2013	03:04:01	0.085 ± 0.032	0.113 ± 0.055	-0.027 ± 0.063
23 Feb 2013	03:12:36	0.181 ± 0.069	0.173 ± 0.065	0.008 ± 0.094
23 Feb 2013	05:58:49	0.084 ± 0.016	0.073 ± 0.018	0.012 ± 0.024
23 Feb 2013	06:07:24	0.075 ± 0.023	0.063 ± 0.024	0.012 ± 0.033
23 Feb 2013	06:15:59	0.012 ± 0.019	0.045 ± 0.019	-0.032 ± 0.027
23 Feb 2013	06:24:33	-0.019 ± 0.019	0.023 ± 0.021	-0.042 ± 0.028
23 Feb 2013	06:37:41	0.048 ± 0.018	0.002 ± 0.027	0.046 ± 0.032
23 Feb 2013	06:46:16	-0.002 ± 0.017	0.009 ± 0.029	-0.010 ± 0.034
23 Feb 2013	06:54:50	-0.055 ± 0.026	-0.007 ± 0.023	-0.048 ± 0.035
23 Feb 2013	07:03:25	-0.032 ± 0.009	-0.057 ± 0.011	0.026 ± 0.014
23 Feb 2013	07:16:26	-0.093 ± 0.008	-0.114 ± 0.011	0.021 ± 0.014
23 Feb 2013	07:25:01	-0.092 ± 0.010	-0.109 ± 0.010	0.017 ± 0.014
23 Feb 2013	07:33:35	-0.061 ± 0.012	-0.107 ± 0.010	0.047 ± 0.016
23 Feb 2013	07:42:10	-0.084 ± 0.012	-0.112 ± 0.010	0.029 ± 0.016
23 Feb 2013	07:55:10	-0.058 ± 0.008	-0.088 ± 0.009	0.031 ± 0.012
23 Feb 2013	08:03:44	-0.017 ± 0.008	-0.064 ± 0.010	0.047 ± 0.012
23 Feb 2013	08:12:19	-0.007 ± 0.011	-0.025 ± 0.011	0.019 ± 0.016
23 Feb 2013	08:20:53	0.072 ± 0.013	0.037 ± 0.015	0.036 ± 0.020
23 Feb 2013	08:33:56	0.102 ± 0.024	0.098 ± 0.064	0.004 ± 0.068

Note: These data are plotted in Figure 3.17.
[a] Times have been corrected for light travel time between the object and the observer.

Table C.10: 4709 Ennomos: $V-I$ Color Variation for Partial Light Curve

Date	Time[a] (UT)	V (Relative)	I (Interpolated)	$V-I$
5 Sept 2011	04:55:52	0.030 ± 0.017	0.043 ± 0.007	-0.013 ± 0.018
5 Sept 2011	05:03:40	0.035 ± 0.006	0.024 ± 0.006	0.011 ± 0.008
5 Sept 2011	05:11:13	0.031 ± 0.006	0.025 ± 0.006	0.006 ± 0.008
5 Sept 2011	05:18:41	0.015 ± 0.006	-0.021 ± 0.006	0.036 ± 0.008
5 Sept 2011	05:26:42	-0.005 ± 0.005	-0.042 ± 0.006	0.038 ± 0.008
5 Sept 2011	05:34:02	-0.034 ± 0.005	-0.059 ± 0.006	0.025 ± 0.008
5 Sept 2011	05:41:42	-0.048 ± 0.005	-0.070 ± 0.006	0.022 ± 0.008
5 Sept 2011	05:48:45	-0.064 ± 0.005	-0.074 ± 0.006	0.011 ± 0.008
5 Sept 2011	05:57:17	-0.066 ± 0.005	-0.079 ± 0.006	0.014 ± 0.008
5 Sept 2011	06:06:10	-0.040 ± 0.005	-0.054 ± 0.007	0.014 ± 0.009
5 Sept 2011	06:13:14	-0.057 ± 0.007	-0.035 ± 0.011	-0.022 ± 0.013
5 Sept 2011	06:20:19	-0.012 ± 0.006	-0.008 ± 0.010	-0.004 ± 0.012
5 Sept 2011	06:27:43	-0.019 ± 0.009	0.008 ± 0.011	-0.027 ± 0.014
5 Sept 2011	06:45:11	0.041 ± 0.025	0.026 ± 0.010	0.016 ± 0.027
5 Sept 2011	06:59:34	0.020 ± 0.007	0.034 ± 0.009	-0.014 ± 0.011
5 Sept 2011	07:07:07	0.024 ± 0.006	0.085 ± 0.013	-0.061 ± 0.014
5 Sept 2011	07:16:43	0.062 ± 0.014	0.093 ± 0.015	-0.030 ± 0.021
5 Sept 2011	07:23:22	0.082 ± 0.012	0.133 ± 0.026	-0.051 ± 0.029
7 Nov 2013	10:55:37	0.106 ± 0.007	0.026 ± 0.008	0.081 ± 0.011
7 Nov 2013	11:01:15	0.086 ± 0.007	0.014 ± 0.008	0.072 ± 0.011
7 Nov 2013	11:06:54	0.068 ± 0.007	-0.005 ± 0.008	0.073 ± 0.011
7 Nov 2013	11:12:33	0.057 ± 0.007	-0.003 ± 0.008	0.060 ± 0.011
7 Nov 2013	11:18:11	0.032 ± 0.007	-0.018 ± 0.008	0.051 ± 0.011
7 Nov 2013	11:23:49	0.019 ± 0.007	-0.023 ± 0.008	0.043 ± 0.011
7 Nov 2013	11:29:28	0.011 ± 0.007	-0.025 ± 0.008	0.036 ± 0.011
7 Nov 2013	11:35:07	-0.003 ± 0.007	-0.034 ± 0.008	0.031 ± 0.011

Continued on next page

Table C.10 – continued from previous page

Date	Time[a] (UT)	V (Relative)	I (Interpolated)	$V-I$
7 Nov 2013	11:40:45	-0.006 ± 0.007	-0.036 ± 0.008	0.031 ± 0.011
7 Nov 2013	11:46:24	-0.024 ± 0.007	-0.027 ± 0.008	0.004 ± 0.011
7 Nov 2013	11:52:02	-0.032 ± 0.007	-0.032 ± 0.008	-0.000 ± 0.011
7 Nov 2013	11:57:40	-0.041 ± 0.007	-0.020 ± 0.009	-0.020 ± 0.011
7 Nov 2013	12:12:58	-0.050 ± 0.008	0.022 ± 0.009	-0.072 ± 0.012
7 Nov 2013	12:18:37	-0.051 ± 0.009	0.023 ± 0.011	-0.073 ± 0.014
7 Nov 2013	12:24:21	-0.074 ± 0.012	0.047 ± 0.014	-0.121 ± 0.018
7 Nov 2013	12:29:59	-0.103 ± 0.018	0.081 ± 0.018	-0.184 ± 0.025
8 Nov 2013	10:58:56	0.149 ± 0.005	0.019 ± 0.008	0.130 ± 0.009
8 Nov 2013	11:09:34	0.088 ± 0.005	0.004 ± 0.007	0.084 ± 0.009
8 Nov 2013	11:20:12	0.052 ± 0.005	0.015 ± 0.007	0.037 ± 0.009
8 Nov 2013	11:30:51	0.005 ± 0.007	0.008 ± 0.009	-0.003 ± 0.011
8 Nov 2013	11:41:29	-0.019 ± 0.005	-0.026 ± 0.007	0.007 ± 0.009
8 Nov 2013	11:52:07	-0.061 ± 0.004	-0.037 ± 0.005	-0.024 ± 0.006
8 Nov 2013	12:08:40	-0.097 ± 0.005	-0.008 ± 0.006	-0.089 ± 0.007
8 Nov 2013	12:19:18	-0.117 ± 0.006	0.021 ± 0.006	-0.138 ± 0.009

Note: These data are plotted in Figure 3.19.
[a] Times have been corrected for light travel time between the object and the observer.

Table C.11: 4833 Meges: $V-I$ Color Variation for Partial Light Curve

Date	Time[a] (UT)	V (Relative)	I (Interpolated)	$V-I$
8 Feb 2015	07:15:38	-0.008 ± 0.015	-0.063 ± 0.011	0.055 ± 0.019
8 Feb 2015	07:36:16	-0.039 ± 0.013	-0.070 ± 0.011	0.031 ± 0.017
8 Feb 2015	07:56:56	-0.090 ± 0.013	-0.086 ± 0.011	-0.004 ± 0.017
8 Feb 2015	08:17:47	-0.112 ± 0.012	-0.109 ± 0.010	-0.003 ± 0.016
8 Feb 2015	08:38:27	-0.109 ± 0.011	-0.087 ± 0.010	-0.022 ± 0.015
8 Feb 2015	08:59:07	-0.100 ± 0.011	-0.050 ± 0.010	-0.050 ± 0.015
8 Feb 2015	09:20:05	-0.059 ± 0.011	-0.016 ± 0.010	-0.043 ± 0.015
8 Feb 2015	09:40:58	-0.045 ± 0.011	-0.017 ± 0.010	-0.028 ± 0.015
8 Feb 2015	10:01:37	-0.025 ± 0.011	-0.011 ± 0.010	-0.014 ± 0.015
8 Feb 2015	10:22:17	0.032 ± 0.012	0.042 ± 0.011	-0.010 ± 0.016
8 Feb 2015	10:42:57	0.054 ± 0.012	0.055 ± 0.011	-0.001 ± 0.016
8 Feb 2015	11:03:48	0.066 ± 0.012	0.054 ± 0.011	0.011 ± 0.016
8 Feb 2015	11:24:55	0.110 ± 0.012	0.085 ± 0.012	0.025 ± 0.017
8 Feb 2015	11:45:34	0.120 ± 0.012	0.105 ± 0.012	0.015 ± 0.017
8 Feb 2015	12:06:13	0.101 ± 0.012	0.091 ± 0.012	0.010 ± 0.017
8 Feb 2015	12:26:52	0.106 ± 0.013	0.072 ± 0.014	0.034 ± 0.019
9 Feb 2015	06:44:53	-0.020 ± 0.014	0.008 ± 0.013	-0.028 ± 0.019
9 Feb 2015	07:05:32	-0.028 ± 0.014	-0.049 ± 0.012	0.021 ± 0.019
9 Feb 2015	07:26:11	0.005 ± 0.013	0.019 ± 0.012	-0.014 ± 0.018
9 Feb 2015	07:46:51	0.028 ± 0.013	0.078 ± 0.012	-0.050 ± 0.018
9 Feb 2015	08:07:29	0.062 ± 0.013	0.106 ± 0.012	-0.045 ± 0.018
9 Feb 2015	08:28:07	0.047 ± 0.012	0.127 ± 0.012	-0.081 ± 0.017
9 Feb 2015	08:48:59	0.068 ± 0.012	0.108 ± 0.012	-0.040 ± 0.017
9 Feb 2015	09:09:38	0.080 ± 0.012	0.094 ± 0.012	-0.014 ± 0.017
9 Feb 2015	09:30:16	0.051 ± 0.011	0.059 ± 0.011	-0.008 ± 0.016
9 Feb 2015	09:51:15	0.047 ± 0.011	0.040 ± 0.011	0.007 ± 0.016
9 Feb 2015	10:11:53	0.036 ± 0.011	0.025 ± 0.011	0.010 ± 0.015
9 Feb 2015	10:32:32	-0.010 ± 0.010	0.009 ± 0.010	-0.020 ± 0.014
9 Feb 2015	10:53:11	-0.016 ± 0.010	-0.006 ± 0.010	-0.010 ± 0.014

Continued on next page

Table C.11 – continued from previous page

Date	Time[a] (UT)	V (Relative)	I (Interpolated)	$V-I$
9 Feb 2015	11:13:50	-0.030 ± 0.010	-0.089 ± 0.009	0.059 ± 0.014
9 Feb 2015	11:34:28	-0.060 ± 0.009	-0.146 ± 0.009	0.086 ± 0.013
9 Feb 2015	11:55:07	-0.064 ± 0.009	-0.129 ± 0.009	0.064 ± 0.013
9 Feb 2015	12:15:46	-0.095 ± 0.009	-0.115 ± 0.009	0.020 ± 0.013
9 Feb 2015	12:36:37	-0.093 ± 0.011	-0.114 ± 0.015	0.021 ± 0.019
16 Feb 2015	06:33:37	0.088 ± 0.006	0.061 ± 0.010	0.027 ± 0.011
16 Feb 2015	06:54:16	0.044 ± 0.006	0.045 ± 0.009	-0.000 ± 0.011
16 Feb 2015	07:14:55	0.006 ± 0.006	0.014 ± 0.009	-0.008 ± 0.010
16 Feb 2015	07:35:45	-0.006 ± 0.005	-0.015 ± 0.008	0.010 ± 0.009
16 Feb 2015	07:56:24	-0.036 ± 0.005	-0.030 ± 0.008	-0.005 ± 0.009
16 Feb 2015	08:17:04	-0.038 ± 0.005	-0.029 ± 0.008	-0.008 ± 0.009
16 Feb 2015	08:37:44	-0.038 ± 0.005	-0.021 ± 0.008	-0.016 ± 0.009
16 Feb 2015	08:58:23	-0.026 ± 0.005	-0.027 ± 0.008	0.001 ± 0.009
16 Feb 2015	09:19:02	-0.021 ± 0.005	-0.020 ± 0.008	-0.001 ± 0.010
16 Feb 2015	09:41:04	0.002 ± 0.005	-0.011 ± 0.009	0.014 ± 0.010
16 Feb 2015	10:01:43	0.027 ± 0.005	0.004 ± 0.009	0.023 ± 0.011
16 Feb 2015	10:22:22	0.018 ± 0.005	0.003 ± 0.010	0.016 ± 0.011
16 Feb 2015	10:43:00	-0.023 ± 0.005	-0.037 ± 0.010	0.015 ± 0.011
17 Feb 2015	06:46:28	-0.092 ± 0.006	-0.050 ± 0.009	-0.042 ± 0.011
17 Feb 2015	07:07:07	-0.059 ± 0.006	-0.027 ± 0.008	-0.032 ± 0.010
17 Feb 2015	07:27:46	-0.035 ± 0.006	-0.007 ± 0.008	-0.028 ± 0.010
17 Feb 2015	07:48:25	-0.012 ± 0.006	0.024 ± 0.008	-0.036 ± 0.010
17 Feb 2015	08:09:04	0.024 ± 0.006	0.055 ± 0.008	-0.031 ± 0.010
17 Feb 2015	08:29:43	0.066 ± 0.006	0.081 ± 0.008	-0.015 ± 0.010
17 Feb 2015	08:50:21	0.083 ± 0.006	0.099 ± 0.009	-0.016 ± 0.011
17 Feb 2015	09:11:00	0.114 ± 0.006	0.120 ± 0.009	-0.006 ± 0.011
17 Feb 2015	09:31:39	0.106 ± 0.006	0.136 ± 0.010	-0.030 ± 0.012
17 Feb 2015	09:52:18	0.120 ± 0.006	0.128 ± 0.009	-0.008 ± 0.011
17 Feb 2015	10:12:57	0.116 ± 0.006	0.112 ± 0.009	0.004 ± 0.011
17 Feb 2015	10:33:36	0.108 ± 0.006	0.086 ± 0.009	0.022 ± 0.011
17 Feb 2015	10:54:27	0.080 ± 0.006	0.042 ± 0.009	0.038 ± 0.011
17 Feb 2015	11:15:06	0.050 ± 0.006	0.024 ± 0.009	0.026 ± 0.011
17 Feb 2015	11:35:45	0.032 ± 0.006	0.010 ± 0.008	0.022 ± 0.010
17 Feb 2015	11:56:23	0.005 ± 0.005	-0.022 ± 0.008	0.027 ± 0.009
17 Feb 2015	12:17:02	-0.026 ± 0.006	-0.038 ± 0.009	0.012 ± 0.010

Note: These data are plotted in Figure 3.21.

[a] Times have been corrected for light travel time between the object and the observer.

Table C.12: 5144 Achates: $V-I$ Color Variation for Partial Light Curve

Date	Time[a] (UT)	V (Relative)	I (Interpolated)	$V-I$
26 June 2011	04:12:44	0.004 ± 0.005	-0.006 ± 0.007	0.010 ± 0.008
26 June 2011	04:17:23	0.022 ± 0.004	0.019 ± 0.006	0.003 ± 0.007
26 June 2011	04:22:06	0.040 ± 0.004	0.035 ± 0.006	0.006 ± 0.007
26 June 2011	04:26:46	0.054 ± 0.004	0.035 ± 0.006	0.020 ± 0.007
26 June 2011	04:31:30	0.039 ± 0.004	0.040 ± 0.005	-0.000 ± 0.007
26 June 2011	04:36:09	0.052 ± 0.004	0.047 ± 0.006	0.006 ± 0.007
26 June 2011	04:40:49	0.051 ± 0.004	0.056 ± 0.005	-0.004 ± 0.006
26 June 2011	04:45:29	0.039 ± 0.004	0.049 ± 0.005	-0.009 ± 0.006
26 June 2011	04:50:08	0.029 ± 0.004	0.040 ± 0.005	-0.011 ± 0.006
26 June 2011	04:54:51	0.031 ± 0.004	0.040 ± 0.005	-0.008 ± 0.006

Continued on next page

Table C.12 – continued from previous page

Date	Time[a] (UT)	V (Relative)	I (Interpolated)	$V-I$
26 June 2011	05:27:05	0.008 ± 0.004	0.016 ± 0.005	-0.008 ± 0.006
26 June 2011	05:31:44	0.003 ± 0.004	0.015 ± 0.005	-0.012 ± 0.006
26 June 2011	05:36:27	0.013 ± 0.004	0.017 ± 0.005	-0.003 ± 0.006
26 June 2011	05:41:04	0.002 ± 0.004	0.016 ± 0.005	-0.014 ± 0.006
26 June 2011	05:45:43	0.008 ± 0.005	0.020 ± 0.005	-0.012 ± 0.007
26 June 2011	05:50:21	0.015 ± 0.004	0.019 ± 0.005	-0.004 ± 0.006
26 June 2011	05:55:00	0.017 ± 0.004	0.028 ± 0.005	-0.011 ± 0.007
26 June 2011	05:59:42	0.009 ± 0.004	0.036 ± 0.006	-0.026 ± 0.007
26 June 2011	06:04:19	0.000 ± 0.004	0.001 ± 0.005	-0.001 ± 0.006
26 June 2011	06:08:56	-0.006 ± 0.004	-0.004 ± 0.005	-0.002 ± 0.006
26 June 2011	06:37:54	-0.063 ± 0.004	-0.058 ± 0.005	-0.004 ± 0.006
26 June 2011	06:42:30	-0.066 ± 0.004	-0.064 ± 0.005	-0.001 ± 0.006
26 June 2011	06:47:13	-0.077 ± 0.004	-0.069 ± 0.005	-0.008 ± 0.006
26 June 2011	06:51:49	-0.077 ± 0.004	-0.069 ± 0.005	-0.007 ± 0.006
26 June 2011	06:56:29	-0.089 ± 0.004	-0.071 ± 0.005	-0.017 ± 0.006
26 June 2011	07:01:05	-0.070 ± 0.004	-0.081 ± 0.005	0.012 ± 0.007
26 June 2011	07:05:44	-0.068 ± 0.004	-0.072 ± 0.006	0.005 ± 0.007
26 June 2011	07:10:24	-0.059 ± 0.004	-0.067 ± 0.005	0.008 ± 0.006
26 June 2011	07:15:08	-0.055 ± 0.004	-0.052 ± 0.005	-0.002 ± 0.006
26 June 2011	07:19:47	-0.036 ± 0.004	-0.037 ± 0.005	0.002 ± 0.006
26 June 2011	07:24:51	-0.025 ± 0.005	-0.030 ± 0.005	0.005 ± 0.007
26 June 2011	07:29:29	-0.003 ± 0.005	-0.019 ± 0.005	0.017 ± 0.007
26 June 2011	07:34:11	0.007 ± 0.004	-0.011 ± 0.007	0.018 ± 0.008
26 June 2011	07:38:48	0.042 ± 0.004	0.004 ± 0.007	0.039 ± 0.008
26 June 2011	07:43:26	0.043 ± 0.006	0.037 ± 0.007	0.006 ± 0.009
26 June 2011	07:48:04	0.058 ± 0.005	0.037 ± 0.009	0.021 ± 0.011
26 June 2011	07:52:45	0.076 ± 0.005	0.036 ± 0.008	0.040 ± 0.010
26 June 2011	07:57:25	0.097 ± 0.004	0.069 ± 0.005	0.028 ± 0.007
26 June 2011	08:02:05	0.092 ± 0.005	0.066 ± 0.006	0.026 ± 0.008
26 June 2011	08:06:43	0.086 ± 0.004	0.067 ± 0.007	0.019 ± 0.008
26 June 2011	08:15:25	0.063 ± 0.005	0.080 ± 0.005	-0.017 ± 0.007
26 June 2011	08:20:03	0.052 ± 0.005	0.067 ± 0.006	-0.015 ± 0.008
26 June 2011	08:24:44	0.060 ± 0.005	0.059 ± 0.006	0.002 ± 0.008
26 June 2011	08:29:21	0.044 ± 0.004	0.061 ± 0.006	-0.017 ± 0.007
26 June 2011	08:34:03	0.025 ± 0.004	0.051 ± 0.006	-0.026 ± 0.007
26 June 2011	08:38:41	0.025 ± 0.004	0.021 ± 0.006	0.004 ± 0.007
26 June 2011	08:43:18	0.009 ± 0.004	0.023 ± 0.005	-0.013 ± 0.007
26 June 2011	08:53:04	0.001 ± 0.004	0.003 ± 0.006	-0.001 ± 0.007
26 June 2011	08:57:45	-0.017 ± 0.004	-0.003 ± 0.006	-0.013 ± 0.007
26 June 2011	09:02:23	-0.026 ± 0.004	-0.000 ± 0.005	-0.025 ± 0.006
26 June 2011	09:07:01	-0.037 ± 0.004	-0.017 ± 0.005	-0.019 ± 0.006
26 June 2011	09:11:44	-0.047 ± 0.004	-0.020 ± 0.005	-0.027 ± 0.007
26 June 2011	09:16:22	-0.048 ± 0.004	-0.028 ± 0.006	-0.019 ± 0.007
26 June 2011	09:21:04	-0.064 ± 0.004	-0.055 ± 0.005	-0.008 ± 0.006
26 June 2011	09:25:43	-0.058 ± 0.004	-0.060 ± 0.005	0.003 ± 0.006
26 June 2011	09:30:21	-0.071 ± 0.004	-0.059 ± 0.005	-0.011 ± 0.006
26 June 2011	09:34:59	-0.065 ± 0.004	-0.066 ± 0.005	0.002 ± 0.006
26 June 2011	09:40:42	-0.058 ± 0.004	-0.068 ± 0.005	0.010 ± 0.006
26 June 2011	09:45:19	-0.042 ± 0.004	-0.062 ± 0.005	0.021 ± 0.006
26 June 2011	09:49:59	-0.050 ± 0.004	-0.061 ± 0.005	0.012 ± 0.007
26 June 2011	09:54:36	-0.027 ± 0.005	-0.059 ± 0.006	0.032 ± 0.008
26 June 2011	09:59:14	-0.021 ± 0.004	-0.037 ± 0.005	0.016 ± 0.006
26 June 2011	10:03:59	-0.003 ± 0.004	-0.019 ± 0.005	0.017 ± 0.006

Continued on next page

Table C.12 – continued from previous page

Date	Time[a] (UT)	V (Relative)	I (Interpolated)	$V-I$
26 June 2011	10:08:44	0.003 ± 0.004	-0.004 ± 0.005	0.008 ± 0.006
26 June 2011	10:13:24	0.022 ± 0.004	0.014 ± 0.005	0.008 ± 0.006
26 June 2011	10:18:02	0.014 ± 0.005	0.014 ± 0.005	0.001 ± 0.007
26 June 2011	10:22:41	0.046 ± 0.006	0.007 ± 0.006	0.040 ± 0.009

Note: These data are plotted in Figure 3.23.
[a] Times have been corrected for light travel time between the object and the observer.

D Full Anchises Light Curve Data

Table D.1: Observations of 1173 Anchises

Date	Time[a] (UT)	Phase[b]	Filter[c]	Relative[d] Magnitude
8 Aug 2011	23:05:35	0.299	V	0.214 ± 0.023
8 Aug 2011	23:09:19	0.304	I	0.217 ± 0.032
8 Aug 2011	23:15:00	0.312	V	0.251 ± 0.022
8 Aug 2011	23:20:58	0.321	I	0.232 ± 0.022
8 Aug 2011	23:22:22	0.323	V	0.240 ± 0.020
8 Aug 2011	23:23:47	0.325	I	0.238 ± 0.022
8 Aug 2011	23:25:11	0.327	V	0.223 ± 0.020
8 Aug 2011	23:26:36	0.329	I	0.224 ± 0.021
8 Aug 2011	23:28:00	0.331	V	0.198 ± 0.020
8 Aug 2011	23:29:24	0.333	I	0.237 ± 0.021
8 Aug 2011	23:30:49	0.335	V	0.205 ± 0.019
8 Aug 2011	23:32:13	0.337	I	0.203 ± 0.021
8 Aug 2011	23:33:37	0.339	V	0.208 ± 0.021
8 Aug 2011	23:35:00	0.341	I	0.211 ± 0.022
8 Aug 2011	23:36:24	0.343	V	0.200 ± 0.022
8 Aug 2011	23:37:49	0.345	I	0.247 ± 0.052
8 Aug 2011	23:39:13	0.347	V	0.169 ± 0.034
8 Aug 2011	23:40:37	0.349	I	0.201 ± 0.031
8 Aug 2011	23:42:01	0.351	V	0.175 ± 0.028
8 Aug 2011	23:43:26	0.353	I	0.174 ± 0.027
8 Aug 2011	23:44:50	0.355	V	0.197 ± 0.022
8 Aug 2011	23:46:14	0.357	I	0.198 ± 0.030
8 Aug 2011	23:47:38	0.359	V	0.188 ± 0.038
8 Aug 2011	23:49:02	0.361	I	0.232 ± 0.038
8 Aug 2011	23:50:26	0.363	V	0.185 ± 0.048
8 Aug 2011	23:51:50	0.365	I	0.210 ± 0.046
8 Aug 2011	23:53:15	0.367	V	0.173 ± 0.035
8 Aug 2011	23:54:39	0.369	I	0.182 ± 0.026
8 Aug 2011	23:56:03	0.371	V	0.149 ± 0.037
8 Aug 2011	23:57:27	0.373	I	0.271 ± 0.092
9 Aug 2011	00:00:14	0.377	I	0.161 ± 0.110
9 Aug 2011	00:01:38	0.379	V	0.148 ± 0.026
9 Aug 2011	00:03:02	0.381	I	0.176 ± 0.038
9 Aug 2011	00:04:26	0.383	V	0.143 ± 0.036
9 Aug 2011	00:08:14	0.389	I	0.136 ± 0.030
9 Aug 2011	00:09:38	0.391	V	0.179 ± 0.026
9 Aug 2011	00:11:02	0.393	I	0.157 ± 0.028
9 Aug 2011	00:12:26	0.395	V	0.141 ± 0.021

Continued on next page

Table D.1 – continued from previous page

Date	Time[a] (UT)	Phase[b]	Filter[c]	Relative[d] Magnitude
9 Aug 2011	00:13:51	0.397	I	0.161 ± 0.026
9 Aug 2011	00:15:14	0.399	V	0.114 ± 0.024
9 Aug 2011	00:18:04	0.403	V	0.153 ± 0.018
9 Aug 2011	00:20:51	0.407	V	0.149 ± 0.018
9 Aug 2011	00:22:15	0.409	I	0.138 ± 0.020
9 Aug 2011	00:23:40	0.411	V	0.142 ± 0.020
9 Aug 2011	00:25:03	0.413	I	0.130 ± 0.026
9 Aug 2011	00:26:27	0.415	V	0.146 ± 0.021
9 Aug 2011	00:27:51	0.417	I	0.137 ± 0.019
9 Aug 2011	00:29:16	0.419	V	0.119 ± 0.016
9 Aug 2011	00:30:41	0.421	I	0.135 ± 0.018
9 Aug 2011	00:32:04	0.423	V	0.138 ± 0.016
9 Aug 2011	00:33:28	0.425	I	0.118 ± 0.018
9 Aug 2011	00:34:53	0.427	V	0.116 ± 0.016
9 Aug 2011	00:36:17	0.429	I	0.103 ± 0.018
9 Aug 2011	00:37:41	0.431	V	0.098 ± 0.016
9 Aug 2011	00:39:06	0.433	I	0.102 ± 0.018
9 Aug 2011	00:40:31	0.435	V	0.084 ± 0.015
9 Aug 2011	00:41:55	0.437	I	0.103 ± 0.018
9 Aug 2011	00:43:19	0.439	V	0.065 ± 0.015
9 Aug 2011	00:46:08	0.443	V	0.064 ± 0.017
9 Aug 2011	00:47:32	0.445	I	0.053 ± 0.020
9 Aug 2011	00:48:56	0.447	V	0.034 ± 0.017
9 Aug 2011	00:50:21	0.449	I	0.037 ± 0.019
9 Aug 2011	00:51:46	0.451	V	0.043 ± 0.017
9 Aug 2011	00:53:29	0.454	I	0.019 ± 0.021
9 Aug 2011	00:54:54	0.456	V	0.018 ± 0.023
9 Aug 2011	00:56:19	0.458	I	0.016 ± 0.038
9 Aug 2011	00:57:42	0.460	V	0.011 ± 0.036
9 Aug 2011	00:59:07	0.462	I	-0.037 ± 0.053
9 Aug 2011	01:00:31	0.464	V	-0.056 ± 0.124
9 Aug 2011	01:01:55	0.466	I	-0.007 ± 0.050
9 Aug 2011	01:03:19	0.468	V	-0.050 ± 0.016
9 Aug 2011	01:04:44	0.470	I	-0.054 ± 0.017
9 Aug 2011	01:06:08	0.472	V	-0.045 ± 0.014
9 Aug 2011	01:07:32	0.474	I	-0.059 ± 0.015
9 Aug 2011	01:08:56	0.476	V	-0.055 ± 0.013
9 Aug 2011	01:10:21	0.478	I	-0.052 ± 0.016
9 Aug 2011	01:11:45	0.480	V	-0.051 ± 0.014
9 Aug 2011	01:13:09	0.482	I	-0.085 ± 0.016
9 Aug 2011	01:14:32	0.484	V	-0.080 ± 0.014
9 Aug 2011	01:15:55	0.486	I	-0.093 ± 0.017
9 Aug 2011	01:17:20	0.488	V	-0.091 ± 0.016
9 Aug 2011	01:18:45	0.490	I	-0.127 ± 0.021
9 Aug 2011	01:20:09	0.492	V	-0.095 ± 0.024
9 Aug 2011	01:21:32	0.494	I	-0.051 ± 0.034
9 Aug 2011	01:22:56	0.496	V	-0.062 ± 0.053
9 Aug 2011	01:24:20	0.498	I	-0.098 ± 0.074
9 Aug 2011	01:28:32	0.504	V	-0.128 ± 0.063
9 Aug 2011	01:29:57	0.506	I	-0.108 ± 0.037
9 Aug 2011	01:31:21	0.508	V	-0.097 ± 0.037
9 Aug 2011	01:32:45	0.510	I	-0.147 ± 0.086
9 Aug 2011	01:34:08	0.512	V	-0.135 ± 0.102

Continued on next page

Table D.1 – continued from previous page

Date	Time[a] (UT)	Phase[b]	Filter[c]	Relative[d] Magnitude
9 Aug 2011	01:36:57	0.516	V	-0.098 ± 0.054
9 Aug 2011	01:38:34	0.518	I	-0.131 ± 0.029
9 Aug 2011	01:39:58	0.520	V	-0.161 ± 0.019
9 Aug 2011	01:41:23	0.522	I	-0.158 ± 0.022
9 Aug 2011	01:42:47	0.524	V	-0.161 ± 0.021
9 Aug 2011	01:44:11	0.527	I	-0.174 ± 0.021
9 Aug 2011	01:45:35	0.529	V	-0.163 ± 0.016
9 Aug 2011	01:46:59	0.531	I	-0.184 ± 0.020
9 Aug 2011	01:48:23	0.533	V	-0.160 ± 0.017
9 Aug 2011	01:49:47	0.535	I	-0.166 ± 0.023
9 Aug 2011	01:51:10	0.537	V	-0.183 ± 0.022
9 Aug 2011	01:52:34	0.539	I	-0.164 ± 0.027
9 Aug 2011	01:53:58	0.541	V	-0.160 ± 0.033
9 Aug 2011	01:55:23	0.543	I	-0.171 ± 0.049
9 Aug 2011	01:56:46	0.545	V	-0.183 ± 0.043
9 Aug 2011	01:58:09	0.547	I	-0.105 ± 0.074
9 Aug 2011	01:59:34	0.549	V	-0.171 ± 0.043
9 Aug 2011	02:00:58	0.551	I	-0.196 ± 0.036
9 Aug 2011	02:02:22	0.553	V	-0.202 ± 0.021
9 Aug 2011	02:03:46	0.555	I	-0.177 ± 0.026
9 Aug 2011	02:05:10	0.557	V	-0.216 ± 0.020
9 Aug 2011	02:06:34	0.559	I	-0.208 ± 0.017
9 Aug 2011	02:07:58	0.561	V	-0.246 ± 0.016
9 Aug 2011	02:09:23	0.563	I	-0.221 ± 0.016
9 Aug 2011	02:10:47	0.565	V	-0.237 ± 0.015
9 Aug 2011	02:12:11	0.567	I	-0.217 ± 0.015
9 Aug 2011	02:13:36	0.569	V	-0.219 ± 0.015
9 Aug 2011	02:15:00	0.571	I	-0.209 ± 0.014
9 Aug 2011	02:16:24	0.573	V	-0.225 ± 0.012
9 Aug 2011	02:17:49	0.575	I	-0.210 ± 0.013
9 Aug 2011	02:19:13	0.577	V	-0.202 ± 0.012
9 Aug 2011	02:20:37	0.579	I	-0.232 ± 0.014
9 Aug 2011	02:22:01	0.581	V	-0.197 ± 0.012
9 Aug 2011	02:24:55	0.585	V	-0.212 ± 0.012
9 Aug 2011	02:26:19	0.587	I	-0.234 ± 0.013
9 Aug 2011	02:27:43	0.589	V	-0.210 ± 0.012
9 Aug 2011	02:29:07	0.591	I	-0.225 ± 0.014
9 Aug 2011	02:30:31	0.593	V	-0.204 ± 0.012
9 Aug 2011	02:31:56	0.595	I	-0.236 ± 0.014
9 Aug 2011	02:33:19	0.597	V	-0.206 ± 0.014
9 Aug 2011	02:34:44	0.599	I	-0.235 ± 0.014
9 Aug 2011	02:36:08	0.601	V	-0.214 ± 0.012
9 Aug 2011	02:38:56	0.605	V	-0.199 ± 0.012
9 Aug 2011	02:40:20	0.607	I	-0.233 ± 0.013
9 Aug 2011	02:41:45	0.609	V	-0.206 ± 0.011
9 Aug 2011	02:43:09	0.611	I	-0.245 ± 0.012
9 Aug 2011	02:44:32	0.613	V	-0.188 ± 0.011
9 Aug 2011	02:45:57	0.615	I	-0.235 ± 0.013
9 Aug 2011	02:47:21	0.617	V	-0.192 ± 0.013
9 Aug 2011	02:48:46	0.619	I	-0.238 ± 0.013
9 Aug 2011	02:50:10	0.621	V	-0.187 ± 0.012
9 Aug 2011	02:51:34	0.623	I	-0.231 ± 0.013
9 Aug 2011	02:52:59	0.625	V	-0.191 ± 0.011

Continued on next page

Table D.1 – continued from previous page

Date	Time[a] (UT)	Phase[b]	Filter[c]	Relative[d] Magnitude
9 Aug 2011	02:54:23	0.627	I	-0.227 ± 0.013
9 Aug 2011	02:55:46	0.629	V	-0.197 ± 0.013
9 Aug 2011	02:57:11	0.631	I	-0.228 ± 0.013
9 Aug 2011	02:58:35	0.633	V	-0.187 ± 0.012
9 Aug 2011	03:00:00	0.635	I	-0.231 ± 0.013
9 Aug 2011	03:01:24	0.637	V	-0.183 ± 0.012
9 Aug 2011	03:02:48	0.639	I	-0.224 ± 0.014
9 Aug 2011	03:04:13	0.641	V	-0.177 ± 0.012
9 Aug 2011	03:07:01	0.645	V	-0.178 ± 0.012
9 Aug 2011	03:08:37	0.648	I	-0.204 ± 0.014
9 Aug 2011	03:10:02	0.650	V	-0.175 ± 0.012
9 Aug 2011	03:11:26	0.652	I	-0.205 ± 0.014
9 Aug 2011	03:12:51	0.654	V	-0.165 ± 0.012
9 Aug 2011	03:14:15	0.656	I	-0.198 ± 0.013
9 Aug 2011	03:15:40	0.658	V	-0.149 ± 0.012
9 Aug 2011	03:17:03	0.660	I	-0.185 ± 0.013
9 Aug 2011	03:18:28	0.662	V	-0.153 ± 0.012
9 Aug 2011	03:19:53	0.664	I	-0.194 ± 0.013
9 Aug 2011	03:21:16	0.666	V	-0.143 ± 0.012
9 Aug 2011	03:22:40	0.668	I	-0.171 ± 0.013
9 Aug 2011	03:24:05	0.670	V	-0.132 ± 0.012
9 Aug 2011	03:25:29	0.672	I	-0.181 ± 0.013
9 Aug 2011	03:26:53	0.674	V	-0.149 ± 0.012
9 Aug 2011	04:00:11	0.722	V	-0.009 ± 0.012
9 Aug 2011	04:01:36	0.724	I	0.009 ± 0.015
9 Aug 2011	04:03:00	0.726	V	0.000 ± 0.013
9 Aug 2011	04:04:24	0.728	I	0.003 ± 0.019
9 Aug 2011	04:05:49	0.730	V	0.007 ± 0.017
9 Aug 2011	04:07:13	0.732	I	0.036 ± 0.022
9 Aug 2011	04:08:36	0.734	V	0.022 ± 0.018
9 Aug 2011	04:10:01	0.736	I	0.037 ± 0.028
9 Aug 2011	04:11:25	0.738	V	0.022 ± 0.020
9 Aug 2011	04:12:49	0.740	I	0.042 ± 0.021
9 Aug 2011	04:14:13	0.742	V	0.044 ± 0.019
9 Aug 2011	04:15:37	0.744	I	0.072 ± 0.019
9 Aug 2011	04:17:01	0.746	V	0.040 ± 0.013
9 Aug 2011	04:18:26	0.748	I	0.065 ± 0.016
9 Aug 2011	04:19:50	0.750	V	0.069 ± 0.015
9 Aug 2011	04:21:13	0.752	I	0.071 ± 0.022
9 Aug 2011	04:22:38	0.754	V	0.083 ± 0.015
9 Aug 2011	04:24:02	0.756	I	0.106 ± 0.019
9 Aug 2011	04:25:26	0.758	V	0.112 ± 0.014
9 Aug 2011	04:26:49	0.760	I	0.118 ± 0.017
9 Aug 2011	04:28:13	0.762	V	0.130 ± 0.014
9 Aug 2011	04:29:37	0.764	I	0.131 ± 0.016
9 Aug 2011	04:31:02	0.766	V	0.144 ± 0.014
9 Aug 2011	04:32:26	0.768	I	0.143 ± 0.017
9 Aug 2011	04:33:50	0.770	V	0.177 ± 0.016
9 Aug 2011	04:35:14	0.772	I	0.157 ± 0.024
9 Aug 2011	04:36:39	0.774	V	0.184 ± 0.017
9 Aug 2011	04:38:03	0.776	I	0.167 ± 0.018
9 Aug 2011	04:39:27	0.778	V	0.152 ± 0.015
9 Aug 2011	04:41:13	0.781	I	0.159 ± 0.017

Continued on next page

Table D.1 – continued from previous page

Date	Time[a] (UT)	Phase[b]	Filter[c]	Relative[d] Magnitude
9 Aug 2011	04:42:36	0.783	V	0.168 ± 0.014
9 Aug 2011	04:44:00	0.785	I	0.165 ± 0.017
9 Aug 2011	04:45:24	0.787	V	0.172 ± 0.015
9 Aug 2011	04:46:49	0.789	I	0.166 ± 0.017
9 Aug 2011	04:48:12	0.791	V	0.176 ± 0.015
9 Aug 2011	04:49:36	0.793	I	0.170 ± 0.017
9 Aug 2011	04:51:01	0.795	V	0.202 ± 0.015
9 Aug 2011	04:52:25	0.797	I	0.176 ± 0.017
9 Aug 2011	04:53:49	0.799	V	0.213 ± 0.016
9 Aug 2011	04:55:14	0.801	I	0.187 ± 0.017
9 Aug 2011	04:56:38	0.803	V	0.225 ± 0.016
9 Aug 2011	04:58:02	0.805	I	0.189 ± 0.017
9 Aug 2011	04:59:26	0.807	V	0.225 ± 0.015
9 Aug 2011	05:00:50	0.809	I	0.199 ± 0.017
9 Aug 2011	05:02:15	0.811	V	0.229 ± 0.015
9 Aug 2011	05:03:39	0.813	I	0.208 ± 0.017
9 Aug 2011	05:05:03	0.815	V	0.227 ± 0.015
9 Aug 2011	05:06:27	0.817	I	0.206 ± 0.018
9 Aug 2011	05:07:52	0.819	V	0.234 ± 0.016
9 Aug 2011	05:09:16	0.821	I	0.186 ± 0.018
9 Aug 2011	05:10:40	0.823	V	0.222 ± 0.016
9 Aug 2011	05:12:04	0.825	I	0.201 ± 0.018
9 Aug 2011	05:13:29	0.827	V	0.225 ± 0.017
9 Aug 2011	05:14:53	0.829	I	0.203 ± 0.018
9 Aug 2011	05:16:16	0.831	V	0.219 ± 0.015
9 Aug 2011	05:17:40	0.833	I	0.195 ± 0.018
9 Aug 2011	05:19:04	0.835	V	0.228 ± 0.016
9 Aug 2011	05:20:28	0.837	I	0.189 ± 0.017
9 Aug 2011	05:21:52	0.839	V	0.206 ± 0.015
9 Aug 2011	05:23:16	0.841	I	0.210 ± 0.020
9 Aug 2011	05:24:40	0.843	V	0.223 ± 0.016
9 Aug 2011	05:27:25	0.847	I	0.212 ± 0.018
9 Aug 2011	05:28:49	0.849	V	0.216 ± 0.017
9 Aug 2011	05:30:14	0.851	I	0.219 ± 0.025
9 Aug 2011	05:31:38	0.853	V	0.184 ± 0.041
9 Aug 2011	05:33:03	0.855	I	0.206 ± 0.035
9 Aug 2011	05:34:27	0.857	V	0.210 ± 0.023
9 Aug 2011	05:35:51	0.859	I	0.200 ± 0.027
9 Aug 2011	05:37:16	0.861	V	0.231 ± 0.016
9 Aug 2011	05:38:40	0.863	I	0.216 ± 0.021
9 Aug 2011	05:40:04	0.865	V	0.243 ± 0.031
9 Aug 2011	05:41:28	0.867	I	0.204 ± 0.023
9 Aug 2011	05:42:52	0.869	V	0.219 ± 0.037
9 Aug 2011	05:44:16	0.871	I	0.239 ± 0.045
9 Aug 2011	05:45:40	0.873	V	0.220 ± 0.038
9 Aug 2011	05:47:04	0.875	I	0.258 ± 0.032
9 Aug 2011	05:48:29	0.877	V	0.216 ± 0.026
9 Aug 2011	05:49:53	0.879	I	0.246 ± 0.054
9 Aug 2011	05:51:17	0.881	V	0.238 ± 0.062
9 Aug 2011	05:54:04	0.885	V	0.209 ± 0.041
9 Aug 2011	05:55:30	0.887	I	0.246 ± 0.047
9 Aug 2011	05:56:55	0.889	V	0.218 ± 0.046
9 Aug 2011	05:59:43	0.893	V	0.189 ± 0.025

Continued on next page

Table D.1 – continued from previous page

Date	Time[a] (UT)	Phase[b]	Filter[c]	Relative[d] Magnitude
9 Aug 2011	06:01:07	0.895	I	0.202 ± 0.022
9 Aug 2011	06:02:32	0.897	V	0.195 ± 0.018
9 Aug 2011	06:03:55	0.899	I	0.202 ± 0.022
9 Aug 2011	06:05:19	0.901	V	0.165 ± 0.022
9 Aug 2011	06:06:44	0.903	I	0.179 ± 0.029
9 Aug 2011	06:08:08	0.905	V	0.192 ± 0.022
9 Aug 2011	06:09:31	0.907	I	0.186 ± 0.022
9 Aug 2011	06:10:55	0.909	V	0.168 ± 0.019
9 Aug 2011	06:12:25	0.912	I	0.175 ± 0.024
9 Aug 2011	06:13:49	0.914	V	0.161 ± 0.016
9 Aug 2011	06:15:13	0.916	I	0.148 ± 0.017
9 Aug 2011	06:16:37	0.918	V	0.145 ± 0.014
9 Aug 2011	06:18:01	0.920	I	0.129 ± 0.016
9 Aug 2011	06:19:25	0.922	V	0.131 ± 0.014
9 Aug 2011	06:20:50	0.924	I	0.130 ± 0.016
9 Aug 2011	06:22:14	0.926	V	0.125 ± 0.014
9 Aug 2011	06:23:38	0.928	I	0.116 ± 0.016
9 Aug 2011	06:25:02	0.930	V	0.116 ± 0.014
9 Aug 2011	06:26:26	0.932	I	0.122 ± 0.017
9 Aug 2011	06:27:50	0.934	V	0.100 ± 0.015
9 Aug 2011	06:29:14	0.936	I	0.081 ± 0.017
9 Aug 2011	06:30:38	0.938	V	0.095 ± 0.030
9 Aug 2011	06:32:02	0.940	I	0.115 ± 0.037
9 Aug 2011	06:33:27	0.942	V	0.052 ± 0.018
9 Aug 2011	06:34:51	0.944	I	0.079 ± 0.019
9 Aug 2011	06:36:15	0.946	V	0.057 ± 0.014
9 Aug 2011	06:37:41	0.948	I	0.045 ± 0.020
9 Aug 2011	06:39:05	0.950	V	0.037 ± 0.018
9 Aug 2011	06:40:30	0.952	I	0.038 ± 0.020
9 Aug 2011	06:41:55	0.954	V	0.047 ± 0.028
9 Aug 2011	06:43:19	0.956	I	0.025 ± 0.031
9 Aug 2011	06:44:43	0.958	V	0.037 ± 0.027
9 Aug 2011	06:46:07	0.960	I	0.006 ± 0.022
9 Aug 2011	06:47:31	0.962	V	-0.013 ± 0.017
9 Aug 2011	06:48:55	0.964	I	0.013 ± 0.025
9 Aug 2011	06:50:19	0.966	V	-0.014 ± 0.015
9 Aug 2011	06:53:07	0.970	V	-0.030 ± 0.014
9 Aug 2011	06:54:31	0.972	I	-0.028 ± 0.016
9 Aug 2011	06:55:55	0.974	V	-0.048 ± 0.013
9 Aug 2011	06:57:22	0.976	I	-0.039 ± 0.015
9 Aug 2011	06:58:45	0.978	V	-0.066 ± 0.012
9 Aug 2011	07:01:33	0.982	V	-0.081 ± 0.012
9 Aug 2011	07:02:58	0.984	I	-0.100 ± 0.014
9 Aug 2011	07:04:22	0.986	V	-0.090 ± 0.012
9 Aug 2011	07:05:46	0.988	I	-0.123 ± 0.014
9 Aug 2011	07:07:11	0.990	V	-0.100 ± 0.012
9 Aug 2011	07:08:35	0.992	I	-0.124 ± 0.014
9 Aug 2011	07:09:59	0.994	V	-0.128 ± 0.012
9 Aug 2011	07:11:22	0.996	I	-0.133 ± 0.014
9 Aug 2011	07:12:46	0.998	V	-0.135 ± 0.012
9 Aug 2011	07:15:34	0.002	V	-0.136 ± 0.012
9 Aug 2011	07:18:21	0.006	V	-0.148 ± 0.012
9 Aug 2011	07:19:45	0.008	I	-0.171 ± 0.013

Continued on next page

Table D.1 – continued from previous page

Date	Time[a] (UT)	Phase[b]	Filter[c]	Relative[d] Magnitude
9 Aug 2011	07:21:09	0.010	V	-0.153 ± 0.012
9 Aug 2011	07:22:33	0.012	I	-0.169 ± 0.014
9 Aug 2011	07:23:57	0.014	V	-0.163 ± 0.012
9 Aug 2011	07:25:20	0.016	I	-0.186 ± 0.013
9 Aug 2011	07:26:44	0.018	V	-0.176 ± 0.011
9 Aug 2011	07:28:08	0.020	I	-0.182 ± 0.014
9 Aug 2011	07:29:33	0.022	V	-0.178 ± 0.011
9 Aug 2011	07:30:57	0.024	I	-0.189 ± 0.013
9 Aug 2011	07:32:21	0.026	V	-0.189 ± 0.011
9 Aug 2011	07:33:45	0.028	I	-0.177 ± 0.014
9 Aug 2011	07:35:09	0.030	V	-0.197 ± 0.011
9 Aug 2011	07:36:33	0.032	I	-0.194 ± 0.014
9 Aug 2011	07:37:56	0.034	V	-0.194 ± 0.011
9 Aug 2011	07:39:21	0.036	I	-0.197 ± 0.014
9 Aug 2011	07:40:45	0.038	V	-0.207 ± 0.011
9 Aug 2011	07:42:11	0.040	I	-0.193 ± 0.013
9 Aug 2011	07:43:35	0.042	V	-0.216 ± 0.011
9 Aug 2011	07:45:00	0.045	I	-0.196 ± 0.013
9 Aug 2011	07:46:24	0.047	V	-0.217 ± 0.011
9 Aug 2011	07:47:47	0.049	I	-0.194 ± 0.013
9 Aug 2011	07:49:12	0.051	V	-0.217 ± 0.011
9 Aug 2011	07:50:36	0.053	I	-0.209 ± 0.013
9 Aug 2011	07:52:00	0.055	V	-0.218 ± 0.011
9 Aug 2011	07:53:24	0.057	I	-0.215 ± 0.013
9 Aug 2011	07:54:48	0.059	V	-0.228 ± 0.011
9 Aug 2011	07:56:12	0.061	I	-0.227 ± 0.013
9 Aug 2011	07:57:37	0.063	V	-0.232 ± 0.011
9 Aug 2011	07:59:00	0.065	I	-0.218 ± 0.013
9 Aug 2011	08:00:24	0.067	V	-0.239 ± 0.011
9 Aug 2011	08:03:14	0.071	V	-0.234 ± 0.011
9 Aug 2011	08:04:37	0.073	I	-0.228 ± 0.013
9 Aug 2011	08:06:02	0.075	V	-0.230 ± 0.011
9 Aug 2011	08:07:26	0.077	I	-0.232 ± 0.013
9 Aug 2011	08:08:51	0.079	V	-0.237 ± 0.011
30 Sept 2012	01:08:27	0.745	I	-0.064 ± 0.017
30 Sept 2012	01:10:59	0.748	V	-0.033 ± 0.017
30 Sept 2012	01:13:32	0.752	I	-0.030 ± 0.017
30 Sept 2012	01:18:36	0.759	I	-0.033 ± 0.017
30 Sept 2012	01:21:09	0.763	V	-0.014 ± 0.017
30 Sept 2012	01:23:41	0.767	I	-0.006 ± 0.017
30 Sept 2012	01:28:45	0.774	I	-0.013 ± 0.017
30 Sept 2012	01:33:50	0.781	I	0.019 ± 0.017
30 Sept 2012	01:36:22	0.785	V	-0.020 ± 0.017
30 Sept 2012	01:43:46	0.795	I	-0.007 ± 0.017
30 Sept 2012	01:46:18	0.799	V	-0.015 ± 0.016
30 Sept 2012	01:48:51	0.803	I	-0.009 ± 0.016
30 Sept 2012	01:51:23	0.806	V	0.025 ± 0.017
30 Sept 2012	01:53:55	0.810	I	-0.004 ± 0.016
30 Sept 2012	01:56:28	0.814	V	0.028 ± 0.017
30 Sept 2012	01:59:00	0.817	I	0.019 ± 0.016
30 Sept 2012	02:01:33	0.821	V	0.065 ± 0.017
30 Sept 2012	02:04:05	0.825	I	0.024 ± 0.016
30 Sept 2012	02:06:38	0.828	V	0.060 ± 0.017

Continued on next page

Table D.1 – continued from previous page

Date	Time[a] (UT)	Phase[b]	Filter[c]	Relative[d] Magnitude
30 Sept 2012	02:09:10	0.832	I	0.025 ± 0.016
30 Sept 2012	02:11:43	0.836	V	0.054 ± 0.017
30 Sept 2012	02:18:25	0.845	I	0.046 ± 0.016
30 Sept 2012	02:20:57	0.849	V	0.068 ± 0.017
30 Sept 2012	02:23:29	0.852	I	0.089 ± 0.016
30 Sept 2012	02:26:01	0.856	V	0.066 ± 0.017
30 Sept 2012	02:28:34	0.860	I	0.073 ± 0.016
30 Sept 2012	02:31:06	0.863	V	0.048 ± 0.016
30 Sept 2012	02:33:38	0.867	I	0.078 ± 0.016
30 Sept 2012	02:36:10	0.871	V	0.070 ± 0.016
30 Sept 2012	02:38:43	0.874	I	0.069 ± 0.016
30 Sept 2012	02:41:15	0.878	V	0.078 ± 0.016
30 Sept 2012	02:43:48	0.882	I	0.084 ± 0.016
30 Sept 2012	02:46:20	0.885	V	0.051 ± 0.016
30 Sept 2012	02:53:07	0.895	I	0.075 ± 0.014
30 Sept 2012	02:55:39	0.899	V	0.094 ± 0.016
30 Sept 2012	02:58:11	0.902	I	0.076 ± 0.016
30 Sept 2012	03:00:44	0.906	V	0.076 ± 0.016
30 Sept 2012	03:03:16	0.910	I	0.082 ± 0.016
30 Sept 2012	03:05:49	0.913	V	0.079 ± 0.016
30 Sept 2012	03:08:21	0.917	I	0.070 ± 0.016
30 Sept 2012	03:10:53	0.921	V	0.078 ± 0.016
30 Sept 2012	03:13:25	0.924	I	0.070 ± 0.014
30 Sept 2012	03:15:57	0.928	V	0.034 ± 0.016
30 Sept 2012	03:18:30	0.931	I	0.035 ± 0.016
30 Sept 2012	03:21:02	0.935	V	0.066 ± 0.016
30 Sept 2012	03:28:09	0.945	I	0.045 ± 0.014
30 Sept 2012	03:30:41	0.949	V	0.059 ± 0.016
30 Sept 2012	03:33:13	0.953	I	0.047 ± 0.014
30 Sept 2012	03:35:45	0.956	V	0.039 ± 0.016
30 Sept 2012	03:38:18	0.960	I	0.044 ± 0.015
30 Sept 2012	03:40:50	0.964	V	0.040 ± 0.016
30 Sept 2012	03:43:22	0.967	I	0.037 ± 0.015
30 Sept 2012	03:45:54	0.971	V	0.029 ± 0.016
30 Sept 2012	03:48:27	0.974	I	0.026 ± 0.014
30 Sept 2012	03:50:59	0.978	V	0.021 ± 0.015
30 Sept 2012	03:53:31	0.982	I	0.009 ± 0.014
30 Sept 2012	03:56:03	0.985	V	0.011 ± 0.016
30 Sept 2012	04:06:12	1.000	I	-0.017 ± 0.014
30 Sept 2012	04:11:17	0.007	I	-0.021 ± 0.014
30 Sept 2012	04:13:49	0.011	V	-0.023 ± 0.016
30 Sept 2012	04:16:22	0.015	I	-0.047 ± 0.014
30 Sept 2012	04:18:53	0.018	V	-0.033 ± 0.015
30 Sept 2012	04:21:26	0.022	I	-0.033 ± 0.014
30 Sept 2012	04:23:58	0.025	V	-0.052 ± 0.016
30 Sept 2012	04:26:30	0.029	I	-0.047 ± 0.014
30 Sept 2012	04:29:02	0.033	V	-0.059 ± 0.015
30 Sept 2012	04:31:35	0.036	I	-0.064 ± 0.014
30 Sept 2012	04:34:07	0.040	V	-0.055 ± 0.016
30 Sept 2012	04:40:24	0.049	I	-0.077 ± 0.014
30 Sept 2012	04:42:56	0.053	V	-0.067 ± 0.015
30 Sept 2012	04:45:28	0.056	I	-0.077 ± 0.014
30 Sept 2012	04:48:01	0.060	V	-0.078 ± 0.016

Continued on next page

Table D.1 – continued from previous page

Date	Time[a] (UT)	Phase[b]	Filter[c]	Relative[d] Magnitude
30 Sept 2012	04:50:33	0.064	I	-0.069 ± 0.014
30 Sept 2012	04:53:05	0.067	V	-0.069 ± 0.015
30 Sept 2012	04:55:37	0.071	I	-0.080 ± 0.014
30 Sept 2012	04:58:09	0.075	V	-0.085 ± 0.015
30 Sept 2012	05:00:42	0.078	I	-0.090 ± 0.014
30 Sept 2012	05:03:14	0.082	V	-0.080 ± 0.015
30 Sept 2012	05:05:47	0.085	I	-0.078 ± 0.014
30 Sept 2012	05:08:19	0.089	V	-0.078 ± 0.016
30 Sept 2012	05:14:44	0.098	I	-0.086 ± 0.014
30 Sept 2012	05:17:16	0.102	V	-0.081 ± 0.016
30 Sept 2012	05:19:49	0.106	I	-0.090 ± 0.014
30 Sept 2012	05:22:21	0.109	V	-0.088 ± 0.016
30 Sept 2012	05:24:53	0.113	I	-0.066 ± 0.014
30 Sept 2012	05:27:25	0.117	V	-0.086 ± 0.016
30 Sept 2012	05:29:57	0.120	I	-0.095 ± 0.014
30 Sept 2012	05:32:30	0.124	V	-0.089 ± 0.016
30 Sept 2012	05:35:02	0.127	I	-0.075 ± 0.014
30 Sept 2012	05:37:34	0.131	V	-0.082 ± 0.016
30 Sept 2012	05:40:06	0.135	I	-0.076 ± 0.014
30 Sept 2012	05:42:39	0.138	V	-0.063 ± 0.016
30 Sept 2012	05:49:01	0.148	I	-0.064 ± 0.014
30 Sept 2012	05:51:33	0.151	V	-0.059 ± 0.016
30 Sept 2012	05:54:06	0.155	I	-0.068 ± 0.014
30 Sept 2012	05:56:38	0.158	V	-0.067 ± 0.016
30 Sept 2012	05:59:10	0.162	I	-0.048 ± 0.014
30 Sept 2012	06:01:42	0.166	V	-0.040 ± 0.017
30 Sept 2012	06:04:15	0.169	I	-0.042 ± 0.014
30 Sept 2012	06:06:47	0.173	V	-0.060 ± 0.016
30 Sept 2012	06:09:19	0.177	I	-0.040 ± 0.014
30 Sept 2012	06:11:52	0.180	V	-0.051 ± 0.017
30 Sept 2012	06:14:24	0.184	I	-0.034 ± 0.015
30 Sept 2012	06:16:56	0.188	V	-0.016 ± 0.018
6 Oct 2012	23:28:01	0.072	I	-0.039 ± 0.016
6 Oct 2012	23:33:30	0.080	V	-0.049 ± 0.015
6 Oct 2012	23:39:06	0.088	I	-0.043 ± 0.022
6 Oct 2012	23:44:35	0.096	V	-0.040 ± 0.016
6 Oct 2012	23:50:12	0.104	I	-0.044 ± 0.018
6 Oct 2012	23:55:41	0.112	V	-0.069 ± 0.015
7 Oct 2012	00:08:22	0.130	I	-0.053 ± 0.016
7 Oct 2012	00:13:52	0.138	V	-0.060 ± 0.013
7 Oct 2012	00:19:27	0.146	I	-0.058 ± 0.014
7 Oct 2012	00:24:06	0.153	V	-0.024 ± 0.013
7 Oct 2012	00:28:52	0.159	I	-0.030 ± 0.013
7 Oct 2012	00:33:31	0.166	V	-0.042 ± 0.013
7 Oct 2012	00:49:51	0.189	I	-0.065 ± 0.013
7 Oct 2012	00:52:50	0.194	V	-0.062 ± 0.013
7 Oct 2012	00:55:55	0.198	I	-0.047 ± 0.013
7 Oct 2012	00:58:54	0.202	V	-0.042 ± 0.013
7 Oct 2012	01:23:38	0.238	I	-0.011 ± 0.013
7 Oct 2012	01:26:36	0.242	V	0.004 ± 0.013
7 Oct 2012	01:29:41	0.247	I	0.012 ± 0.013
7 Oct 2012	01:32:40	0.251	V	0.016 ± 0.013
7 Oct 2012	01:35:46	0.255	I	0.011 ± 0.014

Continued on next page

Table D.1 – continued from previous page

Date	Time[a] (UT)	Phase[b]	Filter[c]	Relative[d] Magnitude
7 Oct 2012	01:38:45	0.260	V	0.017 ± 0.013
7 Oct 2012	01:41:51	0.264	I	0.031 ± 0.014
7 Oct 2012	01:44:49	0.268	V	0.029 ± 0.013
7 Oct 2012	01:47:56	0.273	I	0.042 ± 0.014
7 Oct 2012	01:50:55	0.277	V	0.038 ± 0.014
7 Oct 2012	01:57:22	0.286	I	0.047 ± 0.014
7 Oct 2012	02:00:21	0.291	V	0.049 ± 0.013
7 Oct 2012	02:03:27	0.295	I	0.051 ± 0.013
7 Oct 2012	02:06:25	0.299	V	0.048 ± 0.013
7 Oct 2012	02:09:31	0.304	I	0.050 ± 0.013
7 Oct 2012	02:12:30	0.308	V	0.053 ± 0.013
7 Oct 2012	02:15:36	0.313	I	0.068 ± 0.013
7 Oct 2012	02:18:35	0.317	V	0.054 ± 0.013
7 Oct 2012	02:21:40	0.321	I	0.061 ± 0.013
7 Oct 2012	02:24:39	0.326	V	0.069 ± 0.013
7 Oct 2012	02:31:02	0.335	I	0.067 ± 0.013
7 Oct 2012	02:34:01	0.339	V	0.071 ± 0.013
7 Oct 2012	02:37:07	0.343	I	0.069 ± 0.013
7 Oct 2012	02:40:05	0.348	V	0.070 ± 0.013
7 Oct 2012	02:43:11	0.352	I	0.070 ± 0.013
7 Oct 2012	02:46:10	0.356	V	0.064 ± 0.013
7 Oct 2012	02:49:16	0.361	I	0.069 ± 0.013
7 Oct 2012	02:52:15	0.365	V	0.067 ± 0.013
7 Oct 2012	02:55:20	0.370	I	0.073 ± 0.013
7 Oct 2012	02:58:18	0.374	V	0.068 ± 0.013
7 Oct 2012	03:04:26	0.383	I	0.067 ± 0.013
7 Oct 2012	03:07:24	0.387	V	0.071 ± 0.013
7 Oct 2012	03:10:30	0.391	I	0.072 ± 0.013
7 Oct 2012	03:13:29	0.396	V	0.067 ± 0.013
7 Oct 2012	03:16:35	0.400	I	0.066 ± 0.013
7 Oct 2012	03:19:34	0.404	V	0.064 ± 0.013
7 Oct 2012	03:22:39	0.409	I	0.067 ± 0.013
7 Oct 2012	03:25:38	0.413	V	0.067 ± 0.013
7 Oct 2012	03:28:44	0.418	I	0.070 ± 0.013
7 Oct 2012	03:31:43	0.422	V	0.065 ± 0.013
7 Oct 2012	03:38:19	0.431	I	0.070 ± 0.013
7 Oct 2012	03:41:18	0.436	V	0.071 ± 0.013
7 Oct 2012	03:44:24	0.440	I	0.072 ± 0.013
7 Oct 2012	03:47:23	0.444	V	0.070 ± 0.013
7 Oct 2012	03:50:29	0.449	I	0.066 ± 0.013
7 Oct 2012	03:53:28	0.453	V	0.064 ± 0.013
7 Oct 2012	03:56:33	0.458	I	0.053 ± 0.013
7 Oct 2012	03:59:32	0.462	V	0.047 ± 0.013
7 Oct 2012	04:02:38	0.466	I	0.054 ± 0.013
7 Oct 2012	04:05:37	0.471	V	0.045 ± 0.013
7 Oct 2012	04:11:34	0.479	I	0.043 ± 0.013
7 Oct 2012	04:14:33	0.483	V	0.052 ± 0.013
7 Oct 2012	04:17:39	0.488	I	0.037 ± 0.013
7 Oct 2012	04:20:38	0.492	V	0.041 ± 0.013
7 Oct 2012	04:23:44	0.497	I	0.035 ± 0.013
7 Oct 2012	04:26:43	0.501	V	0.036 ± 0.013
7 Oct 2012	04:29:48	0.505	I	0.025 ± 0.013
7 Oct 2012	04:32:47	0.510	V	0.018 ± 0.013

Continued on next page

Table D.1 – continued from previous page

Date	Time[a] (UT)	Phase[b]	Filter[c]	Relative[d] Magnitude
7 Oct 2012	04:35:53	0.514	I	0.023 ± 0.013
7 Oct 2012	04:38:52	0.518	V	0.022 ± 0.013
7 Oct 2012	04:44:43	0.527	I	0.011 ± 0.013
7 Oct 2012	04:47:41	0.531	V	0.007 ± 0.013
7 Oct 2012	04:50:47	0.535	I	-0.004 ± 0.013
7 Oct 2012	04:53:46	0.540	V	-0.009 ± 0.013
7 Oct 2012	04:56:52	0.544	I	-0.009 ± 0.013
7 Oct 2012	04:59:51	0.548	V	-0.012 ± 0.013
7 Oct 2012	05:02:56	0.553	I	-0.014 ± 0.013
7 Oct 2012	05:05:55	0.557	V	-0.016 ± 0.013
7 Oct 2012	05:09:01	0.562	I	-0.026 ± 0.013
7 Oct 2012	05:12:00	0.566	V	-0.019 ± 0.013
7 Oct 2012	05:17:54	0.574	I	-0.035 ± 0.013
7 Oct 2012	05:20:53	0.579	V	-0.037 ± 0.013
7 Oct 2012	05:23:59	0.583	I	-0.026 ± 0.013
7 Oct 2012	05:26:57	0.587	V	-0.026 ± 0.013
7 Oct 2012	05:30:03	0.592	I	-0.030 ± 0.013
7 Oct 2012	05:33:02	0.596	V	-0.035 ± 0.013
7 Oct 2012	05:36:08	0.600	I	-0.037 ± 0.013
20 Sept 2013	03:31:02	0.989	V	0.062 ± 0.035
20 Sept 2013	03:36:14	0.997	I	-0.626 ± 0.034
20 Sept 2013	03:41:26	0.004	V	0.023 ± 0.032
20 Sept 2013	03:46:38	0.012	I	0.028 ± 0.030
20 Sept 2013	03:51:50	0.019	V	-0.090 ± 0.031
20 Sept 2013	03:57:02	0.026	I	0.057 ± 0.030
20 Sept 2013	04:02:14	0.034	V	0.007 ± 0.031
20 Sept 2013	04:07:26	0.041	I	0.077 ± 0.030
20 Sept 2013	04:12:38	0.049	V	-0.078 ± 0.031
20 Sept 2013	04:17:49	0.056	I	0.124 ± 0.030
20 Sept 2013	04:27:46	0.071	V	-0.044 ± 0.031
20 Sept 2013	04:32:57	0.078	I	-0.097 ± 0.030
20 Sept 2013	04:38:09	0.086	V	0.016 ± 0.031
20 Sept 2013	04:43:21	0.093	I	0.039 ± 0.030
20 Sept 2013	04:48:33	0.100	V	-0.058 ± 0.030
20 Sept 2013	04:53:45	0.108	I	0.005 ± 0.030
20 Sept 2013	04:58:56	0.115	V	-0.024 ± 0.030
20 Sept 2013	05:04:08	0.123	I	0.065 ± 0.030
20 Sept 2013	05:09:20	0.130	V	-0.033 ± 0.030
20 Sept 2013	05:14:32	0.138	I	0.041 ± 0.030
20 Sept 2013	05:23:58	0.151	V	-0.050 ± 0.030
20 Sept 2013	05:29:09	0.159	I	-0.077 ± 0.030
20 Sept 2013	05:34:22	0.166	V	-0.018 ± 0.030
20 Sept 2013	05:39:33	0.174	I	-0.076 ± 0.030
20 Sept 2013	05:44:45	0.181	V	-0.023 ± 0.030
20 Sept 2013	05:49:56	0.189	I	0.010 ± 0.030
20 Sept 2013	05:55:09	0.196	V	-0.004 ± 0.030
20 Sept 2013	06:00:20	0.204	I	-0.015 ± 0.030
20 Sept 2013	06:05:33	0.211	V	0.018 ± 0.030
20 Sept 2013	06:10:44	0.218	I	0.054 ± 0.030
20 Sept 2013	06:19:41	0.231	V	0.004 ± 0.030
20 Sept 2013	06:24:53	0.239	I	0.040 ± 0.030
20 Sept 2013	06:30:06	0.246	V	0.044 ± 0.030
20 Sept 2013	06:35:17	0.254	I	0.130 ± 0.030

Continued on next page

Table D.1 – continued from previous page

Date	Time[a] (UT)	Phase[b]	Filter[c]	Relative[d] Magnitude
20 Sept 2013	06:40:30	0.261	V	0.051 ± 0.030
20 Sept 2013	06:45:41	0.269	I	0.114 ± 0.030
20 Sept 2013	06:50:54	0.276	V	0.055 ± 0.030
20 Sept 2013	06:56:06	0.284	I	0.061 ± 0.030
20 Sept 2013	07:01:18	0.291	V	0.039 ± 0.030
20 Sept 2013	07:06:29	0.299	I	0.130 ± 0.030
20 Sept 2013	07:15:16	0.311	V	0.042 ± 0.030
20 Sept 2013	07:20:28	0.319	I	0.109 ± 0.030
20 Sept 2013	07:25:40	0.326	V	0.066 ± 0.030
20 Sept 2013	07:30:52	0.334	I	0.105 ± 0.030
20 Sept 2013	07:36:04	0.341	V	0.052 ± 0.030
20 Sept 2013	07:41:16	0.348	I	0.032 ± 0.030
20 Sept 2013	07:46:28	0.356	V	0.062 ± 0.030
20 Sept 2013	07:51:40	0.363	I	0.020 ± 0.030
20 Sept 2013	08:02:04	0.378	I	-0.296 ± 0.030
20 Sept 2013	08:14:43	0.396	I	-0.492 ± 0.030
20 Sept 2013	08:25:08	0.411	I	-0.192 ± 0.030
20 Sept 2013	08:35:31	0.426	I	0.134 ± 0.030
20 Sept 2013	08:40:43	0.434	V	0.030 ± 0.030
20 Sept 2013	08:45:55	0.441	I	0.074 ± 0.030
20 Sept 2013	08:51:06	0.449	V	0.049 ± 0.030
20 Sept 2013	08:56:18	0.456	I	0.157 ± 0.030
20 Sept 2013	09:03:48	0.467	V	-0.008 ± 0.030
20 Sept 2013	09:09:00	0.474	I	-0.024 ± 0.030
20 Sept 2013	09:14:12	0.482	V	0.039 ± 0.030
20 Sept 2013	09:19:24	0.489	I	0.038 ± 0.030
20 Sept 2013	09:24:36	0.497	V	0.009 ± 0.030
20 Sept 2013	09:29:48	0.504	I	-0.001 ± 0.030
20 Sept 2013	09:35:01	0.512	V	-0.004 ± 0.030
20 Sept 2013	09:40:12	0.519	I	0.082 ± 0.030
20 Sept 2013	09:45:24	0.527	V	-0.005 ± 0.030
20 Sept 2013	09:50:36	0.534	I	0.060 ± 0.030
20 Sept 2013	09:58:21	0.545	V	-0.049 ± 0.030
20 Sept 2013	10:03:33	0.553	I	0.019 ± 0.030
20 Sept 2013	10:08:45	0.560	V	-0.026 ± 0.030
20 Sept 2013	10:13:57	0.568	I	-0.005 ± 0.030
20 Sept 2013	10:19:09	0.575	V	-0.035 ± 0.030
20 Sept 2013	10:24:21	0.583	I	-0.027 ± 0.030
20 Sept 2013	10:29:33	0.590	V	-0.032 ± 0.030
20 Sept 2013	10:34:45	0.597	I	-0.015 ± 0.030
20 Sept 2013	10:39:57	0.605	V	-0.038 ± 0.030
20 Sept 2013	10:45:08	0.612	I	0.007 ± 0.030
20 Sept 2013	10:53:23	0.624	V	-0.063 ± 0.030
20 Sept 2013	10:58:35	0.632	I	-0.048 ± 0.030
20 Sept 2013	11:03:46	0.639	V	-0.046 ± 0.030
20 Sept 2013	11:08:58	0.647	I	-0.043 ± 0.030
20 Sept 2013	11:14:10	0.654	V	-0.036 ± 0.030
20 Sept 2013	11:19:23	0.662	I	-0.056 ± 0.030
20 Sept 2013	11:24:36	0.669	V	-0.083 ± 0.030
20 Sept 2013	11:29:47	0.676	I	0.046 ± 0.030
20 Sept 2013	11:35:00	0.684	V	-0.026 ± 0.030
20 Sept 2013	11:40:11	0.691	I	0.032 ± 0.030
25 Sept 2013	03:09:28	0.295	V	0.052 ± 0.030

Continued on next page

Table D.1 – continued from previous page

Date	Time[a] (UT)	Phase[b]	Filter[c]	Relative[d] Magnitude
25 Sept 2013	03:14:39	0.302	I	-0.103 ± 0.030
25 Sept 2013	03:24:22	0.316	V	0.062 ± 0.030
25 Sept 2013	03:29:33	0.324	I	-0.021 ± 0.030
25 Sept 2013	03:34:45	0.331	V	0.036 ± 0.030
25 Sept 2013	03:39:57	0.339	I	-0.030 ± 0.030
25 Sept 2013	03:45:09	0.346	V	0.009 ± 0.030
25 Sept 2013	03:50:20	0.354	I	-0.226 ± 0.030
25 Sept 2013	04:00:43	0.369	I	-0.290 ± 0.030
25 Sept 2013	04:56:51	0.449	I	-0.090 ± 0.030
25 Sept 2013	05:02:03	0.457	V	-0.018 ± 0.030
25 Sept 2013	05:07:15	0.464	I	-0.228 ± 0.030
25 Sept 2013	05:16:09	0.477	V	0.038 ± 0.030
25 Sept 2013	05:21:21	0.484	I	-0.045 ± 0.030
25 Sept 2013	05:26:33	0.492	V	-0.006 ± 0.030
25 Sept 2013	05:31:44	0.499	I	-0.053 ± 0.030
25 Sept 2013	05:36:56	0.507	V	-0.005 ± 0.030
25 Sept 2013	05:42:09	0.514	I	0.005 ± 0.030
25 Sept 2013	05:47:21	0.522	V	-0.037 ± 0.030
25 Sept 2013	05:52:32	0.529	I	-0.005 ± 0.030
25 Sept 2013	05:57:44	0.537	V	-0.035 ± 0.030
25 Sept 2013	06:02:56	0.544	I	0.060 ± 0.030
25 Sept 2013	06:11:19	0.556	V	0.006 ± 0.030
25 Sept 2013	06:16:31	0.563	I	0.141 ± 0.030
25 Sept 2013	06:21:42	0.571	V	-0.090 ± 0.030
25 Sept 2013	06:26:53	0.578	I	-0.014 ± 0.030
25 Sept 2013	06:32:05	0.586	V	-0.060 ± 0.030
25 Sept 2013	06:37:16	0.593	I	-0.023 ± 0.030
25 Sept 2013	06:42:28	0.601	V	-0.030 ± 0.030
25 Sept 2013	06:47:40	0.608	I	0.087 ± 0.030
25 Sept 2013	06:52:52	0.616	V	-0.075 ± 0.030
25 Sept 2013	06:58:03	0.623	I	0.086 ± 0.030
25 Sept 2013	07:06:28	0.635	V	-0.067 ± 0.030
25 Sept 2013	07:11:39	0.643	I	-0.138 ± 0.030
25 Sept 2013	07:16:51	0.650	V	-0.047 ± 0.030
25 Sept 2013	07:22:03	0.658	I	-0.121 ± 0.030
25 Sept 2013	07:27:14	0.665	V	-0.058 ± 0.030
25 Sept 2013	07:32:26	0.673	I	-0.072 ± 0.030
25 Sept 2013	07:37:37	0.680	V	-0.051 ± 0.030
25 Sept 2013	07:42:49	0.687	I	-0.051 ± 0.030
25 Sept 2013	07:48:01	0.695	V	-0.043 ± 0.030
25 Sept 2013	07:53:13	0.702	I	0.050 ± 0.030
25 Sept 2013	08:01:07	0.714	V	-0.082 ± 0.030
25 Sept 2013	08:06:19	0.721	I	0.053 ± 0.030
25 Sept 2013	08:11:30	0.729	V	-0.023 ± 0.030
25 Sept 2013	08:16:41	0.736	I	0.051 ± 0.030
25 Sept 2013	08:21:53	0.743	V	-0.015 ± 0.030
25 Sept 2013	08:27:05	0.751	I	-0.014 ± 0.030
25 Sept 2013	08:32:16	0.758	V	0.033 ± 0.030
25 Sept 2013	08:37:28	0.766	I	0.131 ± 0.030
25 Sept 2013	08:42:40	0.773	V	-0.037 ± 0.030
25 Sept 2013	08:47:52	0.781	I	0.038 ± 0.030
25 Sept 2013	08:55:20	0.792	V	0.014 ± 0.030
25 Sept 2013	09:00:32	0.799	I	0.070 ± 0.030

Continued on next page

Table D.1 – continued from previous page

Date	Time[a] (UT)	Phase[b]	Filter[c]	Relative[d] Magnitude
25 Sept 2013	09:05:44	0.806	V	0.045 ± 0.030
25 Sept 2013	09:10:55	0.814	I	0.086 ± 0.030
25 Sept 2013	09:16:07	0.821	V	-0.005 ± 0.030
25 Sept 2013	09:21:19	0.829	I	0.049 ± 0.030
25 Sept 2013	09:26:30	0.836	V	0.078 ± 0.030
25 Sept 2013	09:31:42	0.844	I	0.066 ± 0.030
25 Sept 2013	09:36:54	0.851	V	0.040 ± 0.030
25 Sept 2013	09:42:06	0.859	I	0.123 ± 0.030
25 Sept 2013	09:49:57	0.870	V	0.024 ± 0.030
25 Sept 2013	09:55:09	0.877	I	0.064 ± 0.030
25 Sept 2013	10:00:21	0.885	V	0.079 ± 0.030
25 Sept 2013	10:05:32	0.892	I	0.015 ± 0.030
25 Sept 2013	10:10:43	0.900	V	0.035 ± 0.030
25 Sept 2013	10:15:55	0.907	I	-0.001 ± 0.030
25 Sept 2013	10:21:06	0.915	V	0.043 ± 0.030
25 Sept 2013	10:26:18	0.922	I	0.053 ± 0.030
25 Sept 2013	10:31:30	0.930	V	0.016 ± 0.030
25 Sept 2013	10:36:41	0.937	I	0.014 ± 0.030
25 Sept 2013	10:44:31	0.948	V	0.001 ± 0.030
25 Sept 2013	10:49:42	0.956	I	0.005 ± 0.030
25 Sept 2013	10:54:54	0.963	V	0.037 ± 0.030
25 Sept 2013	11:00:06	0.971	I	0.024 ± 0.030
25 Sept 2013	11:05:18	0.978	V	-0.046 ± 0.030
25 Sept 2013	11:10:29	0.986	I	0.074 ± 0.030
25 Sept 2013	11:15:41	0.993	V	-0.005 ± 0.030
25 Sept 2013	11:20:52	0.000	I	0.100 ± 0.030
25 Sept 2013	11:26:04	0.008	V	-0.020 ± 0.030
25 Sept 2013	11:31:16	0.015	I	0.053 ± 0.030
25 Sept 2013	11:41:04	0.029	V	-0.012 ± 0.030
25 Sept 2013	11:46:15	0.037	I	-0.182 ± 0.030
8 Feb 2015	01:59:25	0.008	I	-0.104 ± 0.027
8 Feb 2015	02:07:32	0.019	V	-0.116 ± 0.026
8 Feb 2015	02:20:57	0.039	I	-0.120 ± 0.027
8 Feb 2015	02:28:26	0.049	V	-0.137 ± 0.026
8 Feb 2015	02:41:03	0.067	I	-0.129 ± 0.027
8 Feb 2015	02:48:21	0.078	V	-0.143 ± 0.026
8 Feb 2015	03:00:02	0.095	I	-0.123 ± 0.027
8 Feb 2015	03:07:18	0.105	V	-0.127 ± 0.026
8 Feb 2015	03:19:01	0.122	I	-0.120 ± 0.027
8 Feb 2015	03:26:18	0.132	V	-0.117 ± 0.026
8 Feb 2015	03:38:00	0.149	I	-0.099 ± 0.027
8 Feb 2015	03:45:17	0.160	V	-0.080 ± 0.027
8 Feb 2015	03:56:59	0.176	I	-0.082 ± 0.027
8 Feb 2015	04:04:16	0.187	V	-0.061 ± 0.027
8 Feb 2015	04:15:57	0.204	I	-0.045 ± 0.027
8 Feb 2015	04:23:14	0.214	V	0.018 ± 0.027
8 Feb 2015	04:35:37	0.232	I	0.031 ± 0.027
8 Feb 2015	04:42:55	0.242	V	0.077 ± 0.027
8 Feb 2015	04:54:37	0.259	I	0.032 ± 0.027
8 Feb 2015	05:01:53	0.270	V	0.123 ± 0.027
8 Feb 2015	05:13:36	0.286	I	0.088 ± 0.027
8 Feb 2015	05:20:52	0.297	V	0.132 ± 0.027
8 Feb 2015	05:32:34	0.314	I	0.115 ± 0.027

Continued on next page

Table D.1 – continued from previous page

Date	Time[a] (UT)	Phase[b]	Filter[c]	Relative[d] Magnitude
8 Feb 2015	05:39:51	0.324	V	0.169 ± 0.028
8 Feb 2015	05:51:33	0.341	I	0.172 ± 0.028
8 Feb 2015	05:58:50	0.351	V	0.151 ± 0.030
8 Feb 2015	06:10:32	0.368	I	0.156 ± 0.027
8 Feb 2015	06:17:49	0.379	V	0.136 ± 0.028
9 Feb 2015	01:23:24	0.023	I	-0.116 ± 0.027
9 Feb 2015	01:32:52	0.037	V	-0.126 ± 0.027
9 Feb 2015	01:42:22	0.050	I	-0.129 ± 0.027
9 Feb 2015	01:51:52	0.064	V	-0.132 ± 0.026
9 Feb 2015	02:01:21	0.078	I	-0.124 ± 0.027
9 Feb 2015	02:10:50	0.091	V	-0.130 ± 0.026
9 Feb 2015	02:19:32	0.104	I	-0.125 ± 0.027
9 Feb 2015	02:28:11	0.116	V	-0.108 ± 0.026
9 Feb 2015	02:36:50	0.129	I	-0.118 ± 0.027
9 Feb 2015	02:45:29	0.141	V	-0.103 ± 0.026
9 Feb 2015	02:54:10	0.154	I	-0.094 ± 0.027
9 Feb 2015	03:02:49	0.166	V	-0.074 ± 0.027
9 Feb 2015	03:11:46	0.179	I	-0.064 ± 0.027
9 Feb 2015	03:20:26	0.191	V	-0.039 ± 0.027
9 Feb 2015	03:29:05	0.204	I	-0.020 ± 0.027
9 Feb 2015	03:37:44	0.216	V	0.005 ± 0.027
9 Feb 2015	03:46:24	0.229	I	0.016 ± 0.027
9 Feb 2015	03:55:03	0.241	V	0.062 ± 0.027
9 Feb 2015	04:04:09	0.254	I	0.063 ± 0.027
9 Feb 2015	04:12:48	0.266	V	0.102 ± 0.027
9 Feb 2015	04:21:27	0.279	I	0.098 ± 0.027
9 Feb 2015	04:30:06	0.291	V	0.133 ± 0.027
9 Feb 2015	04:38:46	0.304	I	0.114 ± 0.027
9 Feb 2015	04:47:25	0.316	V	0.152 ± 0.027
9 Feb 2015	04:56:38	0.329	I	0.128 ± 0.027
9 Feb 2015	05:05:16	0.342	V	0.158 ± 0.027
9 Feb 2015	05:13:56	0.354	I	0.106 ± 0.027
9 Feb 2015	05:22:35	0.367	V	0.148 ± 0.027
9 Feb 2015	05:31:15	0.379	I	0.138 ± 0.027
9 Feb 2015	05:39:54	0.391	V	0.150 ± 0.027
9 Feb 2015	05:48:38	0.404	I	0.111 ± 0.027
9 Feb 2015	05:57:17	0.416	V	0.124 ± 0.027
9 Feb 2015	06:06:02	0.429	I	0.059 ± 0.028
9 Feb 2015	06:14:41	0.441	V	0.105 ± 0.027
16 Feb 2015	01:30:57	0.506	I	-0.029 ± 0.027
16 Feb 2015	01:39:37	0.518	V	-0.065 ± 0.027
16 Feb 2015	01:48:16	0.530	I	-0.055 ± 0.027
16 Feb 2015	01:56:55	0.543	V	-0.094 ± 0.027
16 Feb 2015	02:05:47	0.556	I	-0.091 ± 0.027
16 Feb 2015	02:14:26	0.568	V	-0.099 ± 0.027
16 Feb 2015	02:23:05	0.580	I	-0.092 ± 0.027
16 Feb 2015	02:31:43	0.593	V	-0.133 ± 0.027
16 Feb 2015	02:41:21	0.607	I	-0.115 ± 0.027
16 Feb 2015	02:50:00	0.619	V	-0.154 ± 0.027
16 Feb 2015	02:58:39	0.631	I	-0.129 ± 0.027
16 Feb 2015	03:07:18	0.644	V	-0.153 ± 0.027
16 Feb 2015	03:15:58	0.656	I	-0.112 ± 0.027
16 Feb 2015	03:24:37	0.669	V	-0.141 ± 0.027

Continued on next page

Table D.1 – continued from previous page

Date	Time[a] (UT)	Phase[b]	Filter[c]	Relative[d] Magnitude
16 Feb 2015	03:33:16	0.681	I	-0.073 ± 0.027
16 Feb 2015	03:41:56	0.694	V	-0.100 ± 0.027
16 Feb 2015	03:50:38	0.706	I	-0.037 ± 0.027
16 Feb 2015	03:59:17	0.718	V	-0.074 ± 0.027
16 Feb 2015	04:07:57	0.731	I	0.024 ± 0.027
16 Feb 2015	04:16:37	0.743	V	-0.030 ± 0.027
16 Feb 2015	04:25:16	0.756	I	0.029 ± 0.027
16 Feb 2015	04:33:55	0.768	V	-0.033 ± 0.027
16 Feb 2015	04:42:35	0.781	I	0.006 ± 0.027
16 Feb 2015	04:51:15	0.793	V	-0.048 ± 0.027
16 Feb 2015	05:00:01	0.806	I	0.017 ± 0.027
16 Feb 2015	05:08:40	0.818	V	0.049 ± 0.027
16 Feb 2015	05:17:20	0.831	I	0.082 ± 0.027
16 Feb 2015	05:26:00	0.843	V	0.052 ± 0.027
16 Feb 2015	05:34:40	0.855	I	0.150 ± 0.027
16 Feb 2015	05:43:19	0.868	V	0.096 ± 0.027
16 Feb 2015	05:51:59	0.880	I	0.173 ± 0.027
16 Feb 2015	06:00:38	0.893	V	0.101 ± 0.027
17 Feb 2015	01:09:48	0.543	V	-0.045 ± 0.058
17 Feb 2015	01:17:03	0.553	I	-0.128 ± 0.028
17 Feb 2015	01:27:22	0.568	V	-0.124 ± 0.027
17 Feb 2015	01:37:41	0.583	I	-0.114 ± 0.027
17 Feb 2015	01:48:12	0.598	V	-0.140 ± 0.026
17 Feb 2015	01:58:33	0.612	I	-0.129 ± 0.027
17 Feb 2015	02:08:52	0.627	V	-0.149 ± 0.027
17 Feb 2015	02:19:12	0.642	I	-0.123 ± 0.027
17 Feb 2015	02:29:31	0.657	V	-0.087 ± 0.027
17 Feb 2015	02:39:51	0.672	I	-0.085 ± 0.027
17 Feb 2015	02:50:21	0.687	V	-0.115 ± 0.027
17 Feb 2015	03:00:41	0.702	I	-0.081 ± 0.027
17 Feb 2015	03:11:00	0.717	V	-0.080 ± 0.027
17 Feb 2015	03:21:21	0.731	I	-0.046 ± 0.027
17 Feb 2015	03:31:40	0.746	V	-0.015 ± 0.027
17 Feb 2015	03:42:00	0.761	I	0.010 ± 0.027
17 Feb 2015	03:52:19	0.776	V	0.029 ± 0.027
17 Feb 2015	04:02:39	0.791	I	0.063 ± 0.027
17 Feb 2015	04:12:57	0.805	V	0.088 ± 0.027
17 Feb 2015	04:23:17	0.820	I	0.107 ± 0.027
17 Feb 2015	04:33:36	0.835	V	0.094 ± 0.027
17 Feb 2015	04:43:57	0.850	I	0.099 ± 0.027
17 Feb 2015	04:54:16	0.865	V	0.112 ± 0.027
17 Feb 2015	05:04:36	0.880	I	0.163 ± 0.027
17 Feb 2015	05:14:55	0.894	V	0.175 ± 0.027
17 Feb 2015	05:25:15	0.909	I	0.129 ± 0.027
17 Feb 2015	05:35:46	0.924	V	0.139 ± 0.027
17 Feb 2015	05:46:06	0.939	I	0.099 ± 0.028
17 Feb 2015	05:56:25	0.954	V	0.063 ± 0.027
17 Feb 2015	06:06:45	0.969	I	0.144 ± 0.028
17 Feb 2015	06:17:03	0.984	V	0.094 ± 0.027

Continued on next page

Table D.1 – continued from previous page

Date	Time[a] (UT)	Phase[b]	Filter[c]	Relative[d] Magnitude

Note: Information about specific observing runs can be found in Table 4.2.

[a] Times have been corrected for light travel time between the object and the observer.

[b] The phase as calculated for Figure 4.1 and Figure 4.4.

[c] *Johnson-Cousins*

[d] The magnitude given is relative to the mean of 4th order Fourier fit to the data as described in Section 2.5.

E Anchises Color Data

Table E.1: $V - I$ Color Variation for 1173 Anchises

Date	Time[a] (UT)	Phase[b]	Relative[c] $V - I$ (mag)
8 Aug 2011	23:05:35	0.299	-0.001 ± 0.042
8 Aug 2011	23:15:00	0.312	0.024 ± 0.035
8 Aug 2011	23:22:22	0.323	0.002 ± 0.030
8 Aug 2011	23:25:11	0.327	-0.011 ± 0.029
8 Aug 2011	23:28:00	0.331	-0.035 ± 0.029
8 Aug 2011	23:30:49	0.335	-0.018 ± 0.028
8 Aug 2011	23:33:37	0.339	-0.002 ± 0.030
8 Aug 2011	23:36:24	0.343	-0.032 ± 0.043
8 Aug 2011	23:39:13	0.347	-0.058 ± 0.054
8 Aug 2011	23:42:01	0.351	-0.016 ± 0.040
8 Aug 2011	23:44:50	0.355	0.008 ± 0.036
8 Aug 2011	23:47:38	0.359	-0.030 ± 0.051
8 Aug 2011	23:50:26	0.363	-0.039 ± 0.064
8 Aug 2011	23:53:15	0.367	-0.026 ± 0.050
8 Aug 2011	23:56:03	0.371	-0.080 ± 0.070
9 Aug 2011	00:01:38	0.379	-0.023 ± 0.078
9 Aug 2011	00:04:26	0.383	-0.025 ± 0.051
9 Aug 2011	00:09:38	0.391	0.029 ± 0.039
9 Aug 2011	00:12:26	0.395	-0.021 ± 0.034
9 Aug 2011	00:15:14	0.399	-0.046 ± 0.035
9 Aug 2011	00:18:04	0.403	0.001 ± 0.029
9 Aug 2011	00:20:51	0.407	0.004 ± 0.028
9 Aug 2011	00:23:40	0.411	0.005 ± 0.031
9 Aug 2011	00:26:27	0.415	0.010 ± 0.031
9 Aug 2011	00:29:16	0.419	-0.020 ± 0.024
9 Aug 2011	00:32:04	0.423	0.008 ± 0.024
9 Aug 2011	00:34:53	0.427	0.003 ± 0.024
9 Aug 2011	00:37:41	0.431	-0.007 ± 0.024
9 Aug 2011	00:40:31	0.435	-0.021 ± 0.023
9 Aug 2011	00:43:19	0.439	-0.028 ± 0.024
9 Aug 2011	00:46:08	0.443	-0.004 ± 0.026
9 Aug 2011	00:48:56	0.447	-0.014 ± 0.026
9 Aug 2011	00:51:46	0.451	0.011 ± 0.026
9 Aug 2011	00:54:54	0.456	-0.002 ± 0.037
9 Aug 2011	00:57:42	0.460	0.018 ± 0.058
9 Aug 2011	01:00:31	0.464	-0.037 ± 0.134
9 Aug 2011	01:03:19	0.468	-0.022 ± 0.037

Continued on next page

Table E.1 – continued from previous page

Date	Time[a] (UT)	Phase[b]	Relative[c] $V-I$ (mag)
9 Aug 2011	01:06:08	0.472	0.009 ± 0.021
9 Aug 2011	01:08:56	0.476	-0.002 ± 0.020
9 Aug 2011	01:11:45	0.480	0.015 ± 0.021
9 Aug 2011	01:14:32	0.484	0.006 ± 0.022
9 Aug 2011	01:17:20	0.488	0.016 ± 0.025
9 Aug 2011	01:20:09	0.492	-0.009 ± 0.037
9 Aug 2011	01:22:56	0.496	0.010 ± 0.076
9 Aug 2011	01:28:32	0.504	-0.025 ± 0.078
9 Aug 2011	01:31:21	0.508	0.028 ± 0.072
9 Aug 2011	01:34:08	0.512	0.005 ± 0.125
9 Aug 2011	01:36:57	0.516	0.035 ± 0.070
9 Aug 2011	01:39:58	0.520	-0.020 ± 0.032
9 Aug 2011	01:42:47	0.524	0.002 ± 0.030
9 Aug 2011	01:45:35	0.529	0.013 ± 0.026
9 Aug 2011	01:48:23	0.533	0.012 ± 0.027
9 Aug 2011	01:51:10	0.537	-0.021 ± 0.033
9 Aug 2011	01:53:58	0.541	0.005 ± 0.050
9 Aug 2011	01:56:46	0.545	-0.048 ± 0.075
9 Aug 2011	01:59:34	0.549	-0.023 ± 0.070
9 Aug 2011	02:02:22	0.553	-0.018 ± 0.037
9 Aug 2011	02:05:10	0.557	-0.026 ± 0.029
9 Aug 2011	02:07:58	0.561	-0.034 ± 0.023
9 Aug 2011	02:10:47	0.565	-0.021 ± 0.022
9 Aug 2011	02:13:36	0.569	-0.009 ± 0.021
9 Aug 2011	02:16:24	0.573	-0.018 ± 0.018
9 Aug 2011	02:19:13	0.577	0.016 ± 0.018
9 Aug 2011	02:22:01	0.581	0.033 ± 0.018
9 Aug 2011	02:24:55	0.585	0.019 ± 0.018
9 Aug 2011	02:27:43	0.589	0.017 ± 0.018
9 Aug 2011	02:30:31	0.593	0.024 ± 0.018
9 Aug 2011	02:33:19	0.597	0.027 ± 0.020
9 Aug 2011	02:36:08	0.601	0.018 ± 0.018
9 Aug 2011	02:38:56	0.605	0.032 ± 0.018
9 Aug 2011	02:41:45	0.609	0.030 ± 0.017
9 Aug 2011	02:44:32	0.613	0.049 ± 0.017
9 Aug 2011	02:47:21	0.617	0.042 ± 0.018
9 Aug 2011	02:50:10	0.621	0.045 ± 0.018
9 Aug 2011	02:52:59	0.625	0.035 ± 0.017
9 Aug 2011	02:55:46	0.629	0.028 ± 0.018
9 Aug 2011	02:58:35	0.633	0.040 ± 0.018
9 Aug 2011	03:01:24	0.637	0.042 ± 0.018
9 Aug 2011	03:04:13	0.641	0.039 ± 0.018
9 Aug 2011	03:07:01	0.645	0.029 ± 0.018
9 Aug 2011	03:10:02	0.650	0.027 ± 0.018
9 Aug 2011	03:12:51	0.654	0.034 ± 0.018
9 Aug 2011	03:15:40	0.658	0.040 ± 0.018
9 Aug 2011	03:18:28	0.662	0.034 ± 0.018
9 Aug 2011	03:21:16	0.666	0.037 ± 0.018
9 Aug 2011	03:24:05	0.670	0.041 ± 0.018
9 Aug 2011	03:26:53	0.674	0.022 ± 0.018
9 Aug 2011	04:00:11	0.722	-0.013 ± 0.019
9 Aug 2011	04:03:00	0.726	-0.008 ± 0.021
9 Aug 2011	04:05:49	0.730	-0.015 ± 0.027

Continued on next page

Table E.1 – continued from previous page

Date	Time[a] (UT)	Phase[b]	Relative[c] $V-I$ (mag)
9 Aug 2011	04:08:36	0.734	-0.017 ± 0.031
9 Aug 2011	04:11:25	0.738	-0.020 ± 0.032
9 Aug 2011	04:14:13	0.742	-0.016 ± 0.028
9 Aug 2011	04:17:01	0.746	-0.031 ± 0.022
9 Aug 2011	04:19:50	0.750	-0.001 ± 0.024
9 Aug 2011	04:22:38	0.754	-0.008 ± 0.025
9 Aug 2011	04:25:26	0.758	-0.002 ± 0.023
9 Aug 2011	04:28:13	0.762	0.003 ± 0.022
9 Aug 2011	04:31:02	0.766	0.005 ± 0.022
9 Aug 2011	04:33:50	0.770	0.025 ± 0.026
9 Aug 2011	04:36:39	0.774	0.020 ± 0.027
9 Aug 2011	04:39:27	0.778	-0.014 ± 0.023
9 Aug 2011	04:42:36	0.783	0.004 ± 0.022
9 Aug 2011	04:45:24	0.787	0.004 ± 0.023
9 Aug 2011	04:48:12	0.791	0.006 ± 0.023
9 Aug 2011	04:51:01	0.795	0.027 ± 0.023
9 Aug 2011	04:53:49	0.799	0.029 ± 0.023
9 Aug 2011	04:56:38	0.803	0.035 ± 0.023
9 Aug 2011	04:59:26	0.807	0.029 ± 0.023
9 Aug 2011	05:02:15	0.811	0.023 ± 0.023
9 Aug 2011	05:05:03	0.815	0.018 ± 0.023
9 Aug 2011	05:07:52	0.819	0.036 ± 0.024
9 Aug 2011	05:10:40	0.823	0.026 ± 0.024
9 Aug 2011	05:13:29	0.827	0.021 ± 0.025
9 Aug 2011	05:16:16	0.831	0.018 ± 0.023
9 Aug 2011	05:19:04	0.835	0.034 ± 0.024
9 Aug 2011	05:21:52	0.839	0.004 ± 0.024
9 Aug 2011	05:24:40	0.843	0.010 ± 0.025
9 Aug 2011	05:28:49	0.849	-0.002 ± 0.027
9 Aug 2011	05:31:38	0.853	-0.031 ± 0.051
9 Aug 2011	05:34:27	0.857	0.005 ± 0.039
9 Aug 2011	05:37:16	0.861	0.020 ± 0.029
9 Aug 2011	05:40:04	0.865	0.031 ± 0.038
9 Aug 2011	05:42:52	0.869	-0.005 ± 0.050
9 Aug 2011	05:45:40	0.873	-0.031 ± 0.054
9 Aug 2011	05:48:29	0.877	-0.038 ± 0.050
9 Aug 2011	05:51:17	0.881	-0.010 ± 0.081
9 Aug 2011	05:54:04	0.885	-0.039 ± 0.064
9 Aug 2011	05:56:55	0.889	-0.019 ± 0.061
9 Aug 2011	05:59:43	0.893	-0.026 ± 0.038
9 Aug 2011	06:02:32	0.897	-0.009 ± 0.028
9 Aug 2011	06:05:19	0.901	-0.028 ± 0.034
9 Aug 2011	06:08:08	0.905	0.007 ± 0.034
9 Aug 2011	06:10:55	0.909	-0.015 ± 0.030
9 Aug 2011	06:13:49	0.914	-0.003 ± 0.026
9 Aug 2011	06:16:37	0.918	0.004 ± 0.022
9 Aug 2011	06:19:25	0.922	-0.001 ± 0.021
9 Aug 2011	06:22:14	0.926	-0.000 ± 0.021
9 Aug 2011	06:25:02	0.930	-0.005 ± 0.022
9 Aug 2011	06:27:50	0.934	-0.004 ± 0.023
9 Aug 2011	06:30:38	0.938	-0.005 ± 0.040
9 Aug 2011	06:33:27	0.942	-0.047 ± 0.033
9 Aug 2011	06:36:15	0.946	-0.008 ± 0.024

Continued on next page

Table E.1 – continued from previous page

Date	Time[a] (UT)	Phase[b]	Relative[c] $V-I$ (mag)
9 Aug 2011	06:39:05	0.950	-0.007 ± 0.027
9 Aug 2011	06:41:55	0.954	0.013 ± 0.038
9 Aug 2011	06:44:43	0.958	0.019 ± 0.038
9 Aug 2011	06:47:31	0.962	-0.025 ± 0.029
9 Aug 2011	06:50:19	0.966	-0.019 ± 0.027
9 Aug 2011	06:53:07	0.970	-0.015 ± 0.023
9 Aug 2011	06:55:55	0.974	-0.017 ± 0.020
9 Aug 2011	06:58:45	0.978	-0.014 ± 0.019
9 Aug 2011	07:01:33	0.982	0.001 ± 0.019
9 Aug 2011	07:04:22	0.986	0.019 ± 0.018
9 Aug 2011	07:07:11	0.990	0.021 ± 0.018
9 Aug 2011	07:09:59	0.994	-0.002 ± 0.018
9 Aug 2011	07:12:46	0.998	0.002 ± 0.018
9 Aug 2011	07:15:34	0.002	0.014 ± 0.018
9 Aug 2011	07:18:21	0.006	0.014 ± 0.018
9 Aug 2011	07:21:09	0.010	0.015 ± 0.018
9 Aug 2011	07:23:57	0.014	0.012 ± 0.018
9 Aug 2011	07:26:44	0.018	0.006 ± 0.017
9 Aug 2011	07:29:33	0.022	0.005 ± 0.017
9 Aug 2011	07:32:21	0.026	-0.008 ± 0.017
9 Aug 2011	07:35:09	0.030	-0.014 ± 0.018
9 Aug 2011	07:37:56	0.034	-0.001 ± 0.018
9 Aug 2011	07:40:45	0.038	-0.014 ± 0.017
9 Aug 2011	07:43:35	0.042	-0.024 ± 0.017
9 Aug 2011	07:46:24	0.047	-0.024 ± 0.017
9 Aug 2011	07:49:12	0.051	-0.018 ± 0.017
9 Aug 2011	07:52:00	0.055	-0.008 ± 0.017
9 Aug 2011	07:54:48	0.059	-0.009 ± 0.017
9 Aug 2011	07:57:37	0.063	-0.012 ± 0.017
9 Aug 2011	08:00:24	0.067	-0.021 ± 0.017
9 Aug 2011	08:03:14	0.071	-0.011 ± 0.017
9 Aug 2011	08:06:02	0.075	-0.002 ± 0.017
9 Aug 2011	08:08:51	0.079	-0.005 ± 0.017
30 Sept 2012	01:10:59	0.748	0.013 ± 0.024
30 Sept 2012	01:21:09	0.763	0.005 ± 0.024
30 Sept 2012	01:36:22	0.785	-0.033 ± 0.024
30 Sept 2012	01:46:18	0.799	-0.008 ± 0.023
30 Sept 2012	01:51:23	0.806	0.031 ± 0.023
30 Sept 2012	01:56:28	0.814	0.020 ± 0.023
30 Sept 2012	02:01:33	0.821	0.043 ± 0.023
30 Sept 2012	02:06:38	0.828	0.035 ± 0.023
30 Sept 2012	02:11:43	0.836	0.022 ± 0.023
30 Sept 2012	02:20:57	0.849	-0.000 ± 0.023
30 Sept 2012	02:26:01	0.856	-0.016 ± 0.023
30 Sept 2012	02:31:06	0.863	-0.028 ± 0.023
30 Sept 2012	02:36:10	0.871	-0.004 ± 0.023
30 Sept 2012	02:41:15	0.878	0.001 ± 0.023
30 Sept 2012	02:46:20	0.885	-0.031 ± 0.023
30 Sept 2012	02:55:39	0.899	0.018 ± 0.022
30 Sept 2012	03:00:44	0.906	-0.004 ± 0.022
30 Sept 2012	03:05:49	0.913	0.002 ± 0.022
30 Sept 2012	03:10:53	0.921	0.007 ± 0.022
30 Sept 2012	03:15:57	0.928	-0.019 ± 0.022

Continued on next page

Table E.1 – continued from previous page

Date	Time[a] (UT)	Phase[b]	Relative[c] $V-I$ (mag)
30 Sept 2012	03:21:02	0.935	0.028 ± 0.022
30 Sept 2012	03:30:41	0.949	0.012 ± 0.021
30 Sept 2012	03:35:45	0.956	-0.007 ± 0.022
30 Sept 2012	03:40:50	0.964	-0.001 ± 0.022
30 Sept 2012	03:45:54	0.971	-0.003 ± 0.021
30 Sept 2012	03:50:59	0.978	0.003 ± 0.021
30 Sept 2012	03:56:03	0.985	0.006 ± 0.021
30 Sept 2012	04:13:49	0.011	0.010 ± 0.021
30 Sept 2012	04:18:53	0.018	0.006 ± 0.020
30 Sept 2012	04:23:58	0.025	-0.013 ± 0.021
30 Sept 2012	04:29:02	0.033	-0.004 ± 0.021
30 Sept 2012	04:34:07	0.040	0.012 ± 0.021
30 Sept 2012	04:42:56	0.053	0.009 ± 0.021
30 Sept 2012	04:48:01	0.060	-0.006 ± 0.021
30 Sept 2012	04:53:05	0.067	0.005 ± 0.021
30 Sept 2012	04:58:09	0.075	-0.001 ± 0.021
30 Sept 2012	05:03:14	0.082	0.003 ± 0.021
30 Sept 2012	05:08:19	0.089	0.001 ± 0.021
30 Sept 2012	05:17:16	0.102	0.006 ± 0.021
30 Sept 2012	05:22:21	0.109	-0.011 ± 0.021
30 Sept 2012	05:27:25	0.117	-0.006 ± 0.021
30 Sept 2012	05:32:30	0.124	-0.005 ± 0.021
30 Sept 2012	05:37:34	0.131	-0.007 ± 0.021
30 Sept 2012	05:42:39	0.138	0.009 ± 0.021
30 Sept 2012	05:51:33	0.151	0.006 ± 0.022
30 Sept 2012	05:56:38	0.158	-0.010 ± 0.022
30 Sept 2012	06:01:42	0.166	0.004 ± 0.022
30 Sept 2012	06:06:47	0.173	-0.020 ± 0.022
30 Sept 2012	06:11:52	0.180	-0.015 ± 0.022
30 Sept 2012	06:16:56	0.188	0.017 ± 0.023
6 Oct 2012	23:33:30	0.080	-0.009 ± 0.024
6 Oct 2012	23:44:35	0.096	0.003 ± 0.025
6 Oct 2012	23:55:41	0.112	-0.023 ± 0.023
7 Oct 2012	00:13:52	0.138	-0.005 ± 0.020
7 Oct 2012	00:24:06	0.153	0.019 ± 0.019
7 Oct 2012	00:33:31	0.166	-0.005 ± 0.018
7 Oct 2012	00:52:50	0.194	-0.007 ± 0.018
7 Oct 2012	00:58:54	0.202	0.000 ± 0.018
7 Oct 2012	01:26:36	0.242	0.003 ± 0.018
7 Oct 2012	01:32:40	0.251	0.004 ± 0.019
7 Oct 2012	01:38:45	0.260	-0.005 ± 0.019
7 Oct 2012	01:44:49	0.268	-0.008 ± 0.019
7 Oct 2012	01:50:55	0.277	-0.006 ± 0.020
7 Oct 2012	02:00:21	0.291	-0.001 ± 0.019
7 Oct 2012	02:06:25	0.299	-0.003 ± 0.018
7 Oct 2012	02:12:30	0.308	-0.007 ± 0.018
7 Oct 2012	02:18:35	0.317	-0.011 ± 0.019
7 Oct 2012	02:24:39	0.326	0.005 ± 0.018
7 Oct 2012	02:34:01	0.339	0.002 ± 0.018
7 Oct 2012	02:40:05	0.348	-0.000 ± 0.018
7 Oct 2012	02:46:10	0.356	-0.006 ± 0.018
7 Oct 2012	02:52:15	0.365	-0.005 ± 0.018
7 Oct 2012	02:58:18	0.374	-0.004 ± 0.018

Continued on next page

Table E.1 – continued from previous page

Date	Time[a] (UT)	Phase[b]	Relative[c] $V-I$ (mag)
7 Oct 2012	03:07:24	0.387	0.001 ± 0.018
7 Oct 2012	03:13:29	0.396	-0.003 ± 0.018
7 Oct 2012	03:19:34	0.404	-0.003 ± 0.018
7 Oct 2012	03:25:38	0.413	-0.002 ± 0.018
7 Oct 2012	03:31:43	0.422	-0.006 ± 0.018
7 Oct 2012	03:41:18	0.436	-0.001 ± 0.018
7 Oct 2012	03:47:23	0.444	0.000 ± 0.018
7 Oct 2012	03:53:28	0.453	0.004 ± 0.018
7 Oct 2012	03:59:32	0.462	-0.007 ± 0.018
7 Oct 2012	04:05:37	0.471	-0.006 ± 0.018
7 Oct 2012	04:14:33	0.483	0.011 ± 0.018
7 Oct 2012	04:20:38	0.492	0.004 ± 0.018
7 Oct 2012	04:26:43	0.501	0.005 ± 0.018
7 Oct 2012	04:32:47	0.510	-0.007 ± 0.018
7 Oct 2012	04:38:52	0.518	0.002 ± 0.018
7 Oct 2012	04:47:41	0.531	0.002 ± 0.018
7 Oct 2012	04:53:46	0.540	-0.003 ± 0.018
7 Oct 2012	04:59:51	0.548	-0.001 ± 0.018
7 Oct 2012	05:05:55	0.557	0.003 ± 0.018
7 Oct 2012	05:12:00	0.566	0.009 ± 0.018
7 Oct 2012	05:20:53	0.579	-0.007 ± 0.018
7 Oct 2012	05:26:57	0.587	0.001 ± 0.018
7 Oct 2012	05:33:02	0.596	-0.002 ± 0.018
20 Sept 2013	03:31:02	0.989	1.023 ± 0.050
20 Sept 2013	03:41:26	0.004	0.330 ± 0.045
20 Sept 2013	03:51:50	0.019	-0.125 ± 0.043
20 Sept 2013	04:02:14	0.034	-0.052 ± 0.043
20 Sept 2013	04:12:38	0.049	-0.171 ± 0.043
20 Sept 2013	04:27:46	0.071	-0.015 ± 0.043
20 Sept 2013	04:38:09	0.086	0.053 ± 0.043
20 Sept 2013	04:48:33	0.100	-0.072 ± 0.043
20 Sept 2013	04:58:56	0.115	-0.051 ± 0.043
20 Sept 2013	05:09:20	0.130	-0.078 ± 0.043
20 Sept 2013	05:23:58	0.151	-0.007 ± 0.042
20 Sept 2013	05:34:22	0.166	0.066 ± 0.042
20 Sept 2013	05:44:45	0.181	0.018 ± 0.042
20 Sept 2013	05:55:09	0.196	0.006 ± 0.042
20 Sept 2013	06:05:33	0.211	0.006 ± 0.042
20 Sept 2013	06:19:41	0.231	-0.033 ± 0.042
20 Sept 2013	06:30:06	0.246	-0.033 ± 0.042
20 Sept 2013	06:40:30	0.261	-0.063 ± 0.042
20 Sept 2013	06:50:54	0.276	-0.025 ± 0.042
20 Sept 2013	07:01:18	0.291	-0.049 ± 0.042
20 Sept 2013	07:15:16	0.311	-0.067 ± 0.042
20 Sept 2013	07:25:40	0.326	-0.033 ± 0.042
20 Sept 2013	07:36:04	0.341	-0.009 ± 0.042
20 Sept 2013	07:46:28	0.356	0.044 ± 0.042
20 Sept 2013	08:40:43	0.434	-0.066 ± 0.042
20 Sept 2013	08:51:06	0.449	-0.059 ± 0.042
20 Sept 2013	09:03:48	0.467	-0.050 ± 0.042
20 Sept 2013	09:14:12	0.482	0.040 ± 0.042
20 Sept 2013	09:24:36	0.497	-0.002 ± 0.042
20 Sept 2013	09:35:01	0.512	-0.037 ± 0.042

Continued on next page

Table E.1 – continued from previous page

Date	Time[a] (UT)	Phase[b]	Relative[c] $V-I$ (mag)
20 Sept 2013	09:45:24	0.527	-0.068 ± 0.042
20 Sept 2013	09:58:21	0.545	-0.077 ± 0.042
20 Sept 2013	10:08:45	0.560	-0.025 ± 0.042
20 Sept 2013	10:19:09	0.575	-0.011 ± 0.042
20 Sept 2013	10:29:33	0.590	-0.003 ± 0.042
20 Sept 2013	10:39:57	0.605	-0.026 ± 0.042
20 Sept 2013	10:53:23	0.624	-0.028 ± 0.042
20 Sept 2013	11:03:46	0.639	0.007 ± 0.042
20 Sept 2013	11:14:10	0.654	0.021 ± 0.042
20 Sept 2013	11:24:36	0.669	-0.070 ± 0.042
20 Sept 2013	11:35:00	0.684	-0.057 ± 0.042
25 Sept 2013	03:09:28	0.295	0.163 ± 0.043
25 Sept 2013	03:24:22	0.316	0.119 ± 0.042
25 Sept 2013	03:34:45	0.331	0.069 ± 0.042
25 Sept 2013	03:45:09	0.346	0.145 ± 0.042
25 Sept 2013	05:02:03	0.457	0.149 ± 0.042
25 Sept 2013	05:16:09	0.477	0.158 ± 0.042
25 Sept 2013	05:26:33	0.492	0.051 ± 0.042
25 Sept 2013	05:36:56	0.507	0.027 ± 0.042
25 Sept 2013	05:47:21	0.522	-0.029 ± 0.042
25 Sept 2013	05:57:44	0.537	-0.055 ± 0.042
25 Sept 2013	06:11:19	0.556	-0.096 ± 0.042
25 Sept 2013	06:21:42	0.571	-0.146 ± 0.042
25 Sept 2013	06:32:05	0.586	-0.034 ± 0.042
25 Sept 2013	06:42:28	0.601	-0.054 ± 0.042
25 Sept 2013	06:52:52	0.616	-0.154 ± 0.042
25 Sept 2013	07:06:28	0.635	-0.007 ± 0.042
25 Sept 2013	07:16:51	0.650	0.090 ± 0.042
25 Sept 2013	07:27:14	0.665	0.046 ± 0.042
25 Sept 2013	07:37:37	0.680	0.018 ± 0.042
25 Sept 2013	07:48:01	0.695	-0.035 ± 0.042
25 Sept 2013	08:01:07	0.714	-0.126 ± 0.042
25 Sept 2013	08:11:30	0.729	-0.067 ± 0.042
25 Sept 2013	08:21:53	0.743	-0.026 ± 0.042
25 Sept 2013	08:32:16	0.758	-0.018 ± 0.042
25 Sept 2013	08:42:40	0.773	-0.114 ± 0.042
25 Sept 2013	08:55:20	0.792	-0.035 ± 0.042
25 Sept 2013	09:05:44	0.806	-0.025 ± 0.042
25 Sept 2013	09:16:07	0.821	-0.065 ± 0.042
25 Sept 2013	09:26:30	0.836	0.028 ± 0.042
25 Sept 2013	09:36:54	0.851	-0.047 ± 0.042
25 Sept 2013	09:49:57	0.870	-0.056 ± 0.042
25 Sept 2013	10:00:21	0.885	0.047 ± 0.042
25 Sept 2013	10:10:43	0.900	0.036 ± 0.042
25 Sept 2013	10:21:06	0.915	0.025 ± 0.042
25 Sept 2013	10:31:30	0.930	-0.010 ± 0.042
25 Sept 2013	10:44:31	0.948	0.000 ± 0.042
25 Sept 2013	10:54:54	0.963	0.030 ± 0.042
25 Sept 2013	11:05:18	0.978	-0.087 ± 0.042
25 Sept 2013	11:15:41	0.993	-0.084 ± 0.042
25 Sept 2013	11:26:04	0.008	-0.089 ± 0.042
25 Sept 2013	11:41:04	0.029	0.097 ± 0.042
8 Feb 2015	02:07:32	0.019	-0.001 ± 0.038

Continued on next page

Table E.1 – continued from previous page

Date	Time[a] (UT)	Phase[b]	Relative[c] $V-I$ (mag)
8 Feb 2015	02:28:26	0.049	-0.008 ± 0.037
8 Feb 2015	02:48:21	0.078	-0.011 ± 0.037
8 Feb 2015	03:07:18	0.105	0.000 ± 0.038
8 Feb 2015	03:26:18	0.132	0.000 ± 0.038
8 Feb 2015	03:45:17	0.160	0.018 ± 0.038
8 Feb 2015	04:04:16	0.187	0.012 ± 0.038
8 Feb 2015	04:23:14	0.214	0.040 ± 0.038
8 Feb 2015	04:42:55	0.242	0.051 ± 0.038
8 Feb 2015	05:01:53	0.270	0.075 ± 0.038
8 Feb 2015	05:20:52	0.297	0.039 ± 0.039
8 Feb 2015	05:39:51	0.324	0.037 ± 0.039
8 Feb 2015	05:58:50	0.351	-0.010 ± 0.041
8 Feb 2015	06:17:49	0.379	-0.013 ± 0.039
9 Feb 2015	01:32:52	0.037	0.002 ± 0.038
9 Feb 2015	01:51:52	0.064	-0.000 ± 0.037
9 Feb 2015	02:10:50	0.091	-0.000 ± 0.037
9 Feb 2015	02:28:11	0.116	0.019 ± 0.038
9 Feb 2015	02:45:29	0.141	0.008 ± 0.038
9 Feb 2015	03:02:49	0.166	0.010 ± 0.038
9 Feb 2015	03:20:26	0.191	0.008 ± 0.038
9 Feb 2015	03:37:44	0.216	0.012 ± 0.038
9 Feb 2015	03:55:03	0.241	0.028 ± 0.038
9 Feb 2015	04:12:48	0.266	0.027 ± 0.038
9 Feb 2015	04:30:06	0.291	0.032 ± 0.038
9 Feb 2015	04:47:25	0.316	0.036 ± 0.038
9 Feb 2015	05:05:16	0.342	0.046 ± 0.038
9 Feb 2015	05:22:35	0.367	0.031 ± 0.039
9 Feb 2015	05:39:54	0.391	0.031 ± 0.039
9 Feb 2015	05:57:17	0.416	0.044 ± 0.039
9 Feb 2015	06:14:41	0.441	0.051 ± 0.039
16 Feb 2015	01:39:37	0.518	-0.018 ± 0.038
16 Feb 2015	01:56:55	0.543	-0.016 ± 0.038
16 Feb 2015	02:14:26	0.568	-0.003 ± 0.038
16 Feb 2015	02:31:43	0.593	-0.025 ± 0.038
16 Feb 2015	02:50:00	0.619	-0.027 ± 0.038
16 Feb 2015	03:07:18	0.644	-0.028 ± 0.038
16 Feb 2015	03:24:37	0.669	-0.044 ± 0.038
16 Feb 2015	03:41:56	0.694	-0.040 ± 0.038
16 Feb 2015	03:59:17	0.718	-0.063 ± 0.038
16 Feb 2015	04:16:37	0.743	-0.052 ± 0.038
16 Feb 2015	04:33:55	0.768	-0.046 ± 0.038
16 Feb 2015	04:51:15	0.793	-0.055 ± 0.038
16 Feb 2015	05:08:40	0.818	0.004 ± 0.038
16 Feb 2015	05:26:00	0.843	-0.059 ± 0.038
16 Feb 2015	05:43:19	0.868	-0.061 ± 0.038
16 Feb 2015	06:00:38	0.893	-0.065 ± 0.038
17 Feb 2015	01:09:48	0.543	0.086 ± 0.065
17 Feb 2015	01:27:22	0.568	0.002 ± 0.038
17 Feb 2015	01:48:12	0.598	-0.013 ± 0.038
17 Feb 2015	02:08:52	0.627	-0.018 ± 0.038
17 Feb 2015	02:29:31	0.657	0.022 ± 0.038
17 Feb 2015	02:50:21	0.687	-0.027 ± 0.038
17 Feb 2015	03:11:00	0.717	-0.011 ± 0.038

Continued on next page

Table E.1 – continued from previous page

Date	Time[a] (UT)	Phase[b]	Relative[c] $V-I$ (mag)
17 Feb 2015	03:31:40	0.746	0.008 ± 0.038
17 Feb 2015	03:52:19	0.776	-0.002 ± 0.038
17 Feb 2015	04:12:57	0.805	0.008 ± 0.038
17 Feb 2015	04:33:36	0.835	-0.004 ± 0.038
17 Feb 2015	04:54:16	0.865	-0.014 ± 0.038
17 Feb 2015	05:14:55	0.894	0.034 ± 0.038
17 Feb 2015	05:35:46	0.924	0.030 ± 0.038
17 Feb 2015	05:56:25	0.954	-0.053 ± 0.039
17 Feb 2015	06:17:03	0.984	-0.067 ± 0.039

Note: Information about specific observing runs can be found in Table 4.2.

[a] Times have been corrected for light travel time between the object and the observer. The times given here correspond to the V Filter observations in Table D.1.

[b] The phase as calculated for Figure 4.1 and Figure 4.4.

[c] The magnitude given is *Johnson-Cousins* V minus the I magnitude interpolated to the time of the V observations found in Table D.1 and relative to the mean of the epoch.